Synthesis of Metal Nanoparticles and Their Application in Degradation of Textile Dyes by Advanced Oxidation Process

A thesis
Submitted for the Award of the

Doctor of Philosophy

Degree in

CHEMISTRY

(Faculty in Science)

to the
University of Kota, Kota

by
Niharika Nagar

Under the supervision of
Dr. (Mrs.) Vijay Devra
Associate Professor

Department of Chemistry
J.D.B. Govt. Girls College, Kota

UNIVERSITY OF KOTA, KOTA
2018

CERTIFICATE

I feel great pleasure in certifying that the thesis entitled "**Synthesis of Metal Nanoparticles and Their Application in Degradation of Textile Dyes by Advanced Oxidation Process**" by **Niharika Nagar** under my guidance. She has completed the following requirements as per Ph.D. regulations of the University.

(a) Course work as per the university rules.

(b) Residential requirements of the university (**200 days**).

(c) Regularly submitted annual progress report. (d) Presented his work in the departmental committee.

(e) Published/accepted minimum of one research paper in a referred research journal, I recommend the submission of thesis.

Date:

Dr. (Mrs.) Vijay Devra

Supervisor

ANTI-PLAGIARISM CERTIFICATE

It is certified that Ph.D. thesis entitled "**Synthesis of Metal Nanoparticles and Their Application in Degradation of Textile Dyes by Advanced Oxidation Process**" by **Niharika Nagar** has been examined by us with the following anti-plagiarism tools. We undertake the follows:

a. Thesis has significant new work/knowledge as compared already published or are under consideration to be published elsewhere. No sentence, equation, diagram, table, paragraph or section has been copied verbatim from previous work unless it is placed under quotation marks and duly referenced.
b. The work presented is original and own work of the author (i.e. there is no plagiarism). No ideas, processes, results or words of others have been presented as author's own work.
c. There is no fabrication of data or results which have been compiled and analysed.
d. There is no falsification by manipulating research materials, equipment or processes, or changing or omitting data or results such that the research is not accurately represented in the research record.
e. The thesis has been checked using SMALL SAE TOOLS – Plagiarism checker website and found within limits as per HEC plagiarism policy and instructions issued from time to time.

(Name & Signature of Research Scholar)	(Name & Signature and seal of Research Supervisor)
Place: Kota	Place: Kota
Date:	Date:

ABSTRACT

In recent years, the development of competent green chemistry methods for synthesis of metal nanoparticles have become a main limelight of researchers in the field of nanotechnology. The utilization of secondary metabolites from plant leaf broth has emerged as a novel technology for the synthesis of various nanoparticles. Water pollution due to discharge of textile effluents from textile dyeing mills are one of the major environmental problem, in the world today. Color effluents are responsible for the receiving aquatic ecosystem poses aesthetic problem and serious ecological problems. Therefore a numbers of techniques aimed at preferential removal dyes from wastewater have been developed. The advanced oxidation technology is the most effective chemical oxidation method and currently gaining significant application in water treatment process.

The present study includes brief discussion about metal nanoparticles, properties of nanoparticles, nanocatalysis and different synthesis method of nanoparticles. The review also gives a concise discussion of azo dyes, degradation method of dyes and applications of metal nanoparticles in different environmental remediation process. The experimental section gives depiction of several instruments, characterization, analytical techniques and also describing the details of the reagents, chemicals, their solutions with other specifications in the kinetic study of the degradation of dyes.

The current research work describes, silver nanoparticles (AgNPs) and copper nanoparticles (CuNPs) were synthesized by the leaf broth of *Azadirachta indica* and effect of different reaction parameters such as precursor salt concentration, leaf broth percentage and temperature on the conversion rate and morphology of the AgNPs and CuNPs were analyzed. The plant biomolecules induce the reduction of Ag^{+} ions to AgNPs and Cu^{2+} ions to CuNPs also act as a stabilizing agent. The formation of AgNPs and CuNPs was monitored by absorbance spectra of UV-visible spectrophotometer at different stages during the synthesis process. The biosynthesized AgNPs and CuNPs were characterized by different instrumental techniques. The study also explain synthesized AgNPs and

CuNPs were effectively catalyzed the degradation process of Methyl Orange (MO), Orange G (OG) and wastewater samples in presence of peroxodisulphate (PDS) or peroxomonosulphate (PMS). It was observed that the synthesized Nano-catalyst could effectively decompose oxidant to generate sulphate radicals (SRs) and degrade dye in aqueous solution by advanced oxidation process (AOP). Sulphate radicals (SRs) ($SO_4^{\bullet -}$) were identified as oxidative species using specific alcohols. The increasing concentration of nanocatalyst, size of nanocatalyst, peroxosulphates, Dye, initial pH and high temperature rapidly promoted the degradation kinetics of dye. Furthermore, Chemical oxygen demand (COD) and Biochemical oxygen demand (BOD) of wastewater were also determined. The results implies that the advanced oxidation process enhance the biodegradability of the wastewater. Liquid chromatography-mass spectrometry (LC-MS) analysis and UV-Visible spectral changes were used to analyse the structure of intermediate and end products during degradation process of dye in nanocatalyst/Peroxosulphate system. Addition of neutral salts has no or retarding effect on degradation of dye.

Candidate's Declaration

I, hereby, certify that the work, which is being presented in the thesis, entitled "**Synthesis of Metal Nanoparticles and Their Application in Degradation of Textile Dyes by Advanced Oxidation Process**" in partial fulfillment of the requirement for the award of the Degree of Doctor of Philosophy, carried under the supervision of Associate Professor **Dr. (Mrs.) Vijay Devra** and submitted to the (**Department of Chemistry** /University Research Center), University of Kota, Kota represents my ideas in my own words and where others ideas or words have been included. I have adequately cited and referenced the original sources. The work presented in this thesis has not been submitted elsewhere for the award of any other degree or diploma from any Institutions. I also declare that I have adhered to all principles of academic honesty and integrity and have not misrepresented or fabricated or falsified any idea/data/fact/source in my submission. I understand that any violation of the above will cause for disciplinary action by the University and can also evoke penal action from the sources which have thus not been properly cited or from whom proper permission has not been taken when needed.

Date: **Niharika Nagar**

Research Scholar

This is to certify that the above statement made by **Niharika Nagar** (Enrolment No. 2015/000109, Registration No. RS/1777/16) is correct to the best of my knowledge.

Date: **Dr. (Mrs.) Vijay Devra**

Supervisor

ACKNOWLEDGEMENT

First and foremost I would like to bow down my head in front of Almighty "**दादा गुरु श्री गंगाई नाथ जी, गुरुदेव राम लाल जी सियाग और गुरु माँ**" who are continuous source of inspiration and power, most beneficent and merciful for making this task reaches its completion.

No words can express my profound and deep sense of gratitude to my supervisor, **Dr. (Mrs.) Vijay Devra**, Associate professor, Department of Chemistry, J. D. B. Govt. Girls College, Kota, supported me in all stages of this work. She always gave me constant encouragement and advice, despite his busy agenda. Without a coherent and illuminating instruction, this thesis would not have reached its present form. I will not forget our very frequent teleconferences during which she gave me advice and encouragement.

I would like to expand my thanks to **Dr. (Mrs.) Reeta Gulati,** Principal; **Dr. (Mrs.) Laxmi Bhal,** Head, Department of Chemistry, and **all faculty members** of J. D. B. Govt. Girls College, Kota, for their inspiring guidance and generous support.

I express my heart-felt gratitude to **Prof. Ashu Rani** (Professor, Department of Pure and Applied Chemistry, University of Kota, Kota), **Dr. Naveen Mittal**, **Dr. Arti Shah** and **Dr. Manju Bala Yadav,** who have been very kind enough to extend their help at various phases of this research. It is an honour for me to convey my special regards to **Dr. Pankaj Kachhawah,** for his sincere interest, continuous encouragement and enthusiastic support. I would also like to extend my thanks to **Pranav Kachhawah** for his scientific inputs.

My heartfelt thanks to my seniors **Dr. Shanu Mathur, Dr. Renu Hada, Dr. Khushboo Shrivastava, Dr. Shikha Jain, Dr. Ankita Jain and Dr. Dhan Raj** for their guidance and moral support. In my daily work I have been blessed with a friendly and cheerful group of fellow students. I would like to thank my fellow researchers **Rashmi Gupta** and **Mahima Sharma** for her support. I also express my worm thanks to **Gajala Tazwar** that I had the pleasure to work with her.

Her wise advice, invaluable help and very deeply appreciated friendship, always encouraged me and rendered this period a more enjoyable experience.

Without the support of all members of my family, I would never complete this work and I would never find the courage to overcome all these difficulties during this work. My thanks go to my parents, my **docile** father **Shri Bhanwar Lal nagar** and my mother **Smt. Sita Nagar** for their confidence and their love during all these years. I would especially like to express my gratitude to my elder brother **Gagan**, who has always been a source of inspiration for me and has been one of my best counselors. I am highly thankful to him for all of the advice and wise words provided me over the last several years and all of the incredible strength he've forced me to see in myself. Thank you for being my rock when I needed it the most and for supporting me through every decision I made.

I gratefully acknowledge the **University Grants Commission, New Delhi** through a **Junior Research Fellowship** for financial support. I would also like to thanks **Department of Science and Technology, India sponsored FIST Laboratory** of our institution for experimental work. I wish to express my sincere thanks to **SAIF/CIL (Panjab University, Chandigarh), MRC Department (MNIT Jaipur), IIT Ropar** for sample analysis and characterization. I wish to express my gratitude to those who may have contributed to my work directly or indirectly even though they remain anonymous.

Niharika Nagar

Contents **Page No.**

LIST OF TABLES

LIST OF FIGURES

LIST OF SCHEMES

LIST OF ABBREVIATIONS

A. Indica	*Azadirachta indica*
AgNPs	Silver Nanoparticles
AOP	Advanced Oxidation Process
API	Atmospheric Pressure Ionization
APCI	Atmospheric Pressure Chemical Ionization
BOD	Biological Oxygen Demand
COD	Chemical Oxygen Demand
CuNPs	Copper Nanoparticles
DLS	Dynamic Light Scattering
EDS	Energy Dispersive X-ray Spectroscopy
ESI	Electrospray Ionization
EtOH	Ethanol
FCC	Face Centered Cubic
FT-IR	Fourier Transform Infrared Spectrophotometer
HPLC	High Pressure Liquid Chromatography
JCPDA	Joint Committee for Powder Diffraction Standard
LC-MS	Liquid Chromatography-Mass Spectroscopy
MO	Methyl Orange
NPs	Nanoparticles
OG	Orange G
PDS	Peroxodisulphate
PMS	Peroxomonosulphate
SAED	Selected Area Electron diffraction
SEM	Scanning Electron Microscopy
SPR	Surface Plasma Resonance
SRs	Sulphate Radicles
TBA	*t*-Butyl alcohol
TEM	Transmission Electron Microscopy
UV-Vis	Ultraviolet-Visible Spectrophotometer
XRD	X-Ray Diffractometer

Chapter – 1

Introduction

1.1. Chemical Kinetics

Chemical kinetics is the branch of chemical science and the study of chemical reactions with respect to reaction rates, the effect of various variables, re-arrangement of atoms, formation of intermediates etc. The study of motion is called kinetics, from Greek kinesis, meaning movement. In this study chemists and chemical engineers describe the mathematical models which provide information about chemical reaction kinetics, to better understand and describe chemical processes and the complex chemistry of reactions. This model also provides an idea to make predictions about reactions and to develop, design or modification of chemical reactors to optimize product yield, more efficiently separate products, and eliminate environmentally harmful by-products. Hence, Chemical kinetics is not just a part of physical chemistry but it is a consolidated discipline covering the whole of chemistry, many aspects of biochemistry and textile industries waste treatment.

In this research work chemical kinetic apply as to determine the metal nanoparticles effect in dye effluents degradation reaction. Metal nanoparticles use as a catalyst in degradation process, catalytic reactions progressed by a different pathway of lower activation energy whereas noncatalytic reactions adopted regular degradation pathways.

Degradation pathway defines intermediate, free radicals, which bonds are broken, and which are formed. A whole degradation pathway must also describe the reason for the reactants and catalyst used products and the amount of each. A kinetics experiment is used to determine the change in concentration of a species over time and experiments are done under controlled conditions so that measurements are made at regular time intervals. Either a reactant (decreasing concentration with time) or a product (increasing concentration with time) is that species. If more than one reactant or products are involved, it is important that the concentration of only one reactant or product change with time.

The present research work basically contains degradation of azo dye in presence of nanocatalyst and study will useful in wastewater treatment. Degradation of azo dyes viz. methyl orange, orange (acid orange 10) is studied by peroxomonosulphate, and peroxodisulphate in the presence of silver and copper nanoparticles as a catalyst in an aqueous medium. A Review of silver and copper nanoparticles as a catalyst, peroxomonosulphate, and peroxodisulphate as oxidants, and degradation of dye is presented in this chapter.

1.2. Metal Nanoparticles

Nanotechnology mentions to the subdivision of science and engineering keen to materials [1]. Nanoscience is the study of the phenomena at 1-100 nm particle size and nanomaterials are those which have structured components with at least one dimension less than 100 nm [2]. Nanomaterials derived from nanoparticles since the past decade nanoparticles have grown as a separate class of materials. Due to the high conductivity of metal nanoparticles, it has received a great scientific interest as compared to metal oxides nanoparticles [3]. Metal nanoparticles do not represent a metal-metal chemical bond and defined as isolated particles between 1-100 nm size. Metal nanoparticles (NPs) have extraordinary different properties as compared to their bulk metal that mostly contains a degenerated density of energy states and a large surface to volume ratio along with the sizes in the nanometer scale [4-6]. Therefore they show high chemical activity and specificity as compared to bulk metals so that they are attractive to use as catalysts [7, 8]. The high surface-to-volume ratio along with size effects (quantum effects) gives metal nanoparticles distinctively different properties (chemical, electronic, optical, magnetic and mechanical) from those of bulk metal [9-13].

Researchers have achieved considerable attention in nanomaterials because of their unique properties and various applications in different areas [14, 15]. In past two decades, nanoparticles exhibit many fascinating applications in a wide variety of fields including conductors [16], electronics [17-19], sensors [20-22], photovoltaic devices [23], drug delivery [24], catalysis [25-27], fuel cells

[28], light-emitting diodes [29], industrial lithography [30], quantum dots [31], quantum wires [32], quantum devices [33], optical and biological devices [34-37] etc. due to their unique properties, which vary from molecular or bulk materials. Incredible properties of nanoparticles intensely depend on the distinct shape and diminutive size of nanoparticles, surrounding media, and their fabrication method. So, scientists take interest in targeting fabrication of metal nanoparticles [38-40]. Different shape and size of metal nanoparticles allow exploring their applications in fields includes catalysis, electronics, sensor, and optical device [41-43].

1.3. Synthesis of Metal Nanoparticles

There are two approaches for the synthesis of nanoparticles one is "Top-down" approach and another is "Bottom-up" approach [44]. In top-down approach size reduction from a suitable starting material is used for the synthesis of nanoparticles [45]. Various physical and chemical treatments are used to achieve reduces the size (**Figure 1.1**). Imperfections are introduced by a top-down approach in the surface structure of the nanoparticles and this is a major limitation because the surface chemistry and the other physical properties of nanoparticles are highly dependent on the surface structure [46]. In bottom-up synthesis, smaller entities are joined each other and fabricated the nanoparticles [47]. In this approach first smaller entities are formed after that these entities are assembled to produce the final particles and particles size are in nanometer range [46]. Chemical and biological methods are used to achieve the bottom-up approach.

Chemical and physical methods for synthesis of nanoparticles are performed in eco-hazardous, energy-intensive conditions and toxic chemicals are used, whereas biological methods are performed in eco-friendly conditions and consume very less energy. Though the time needed for synthesis of metal nanoparticles is longer in biological methods compared to chemical methods, the time has been decreased with verdict appropriate microorganisms or organism [48]. Hence, the benefits of biological methods over chemical and physical methods are cost effective, eco-friendly, single step process for the large-scale

synthesis of nanoparticles, and no need of high pressure, energy, temperature and toxic chemicals which are harmful to the health of living entities [49].

In the biological methods, the synthesis of nanoparticles from microorganisms has been widely reported [49-57]. Microbial synthesis of nanoparticles is readily scalable, environmental friendly and compatible with the use of the nanoparticles for medical applications, but the creation and handling of microorganisms are more expensive than the plant extracts. Synthesis of plant mediated metal nanoparticles is very cost effective, therefore can be used as an economic and valuable alternative for the large-scale production of metal nanoparticles [58, 59]. Plant extracts may act both as reducing and capping agents in nanoparticles synthesis, biomolecules found in plant extracts are responsible for the reduction of metal ions and stabilizer for metal nanoparticles [60-66]. The plant Neem belongs to meliaceae family and botanical name *is Azadirachta Indica*. Neem is a very famous and found abundantly in India and in nearby subcontinents. It is one of the most versatile medicinal plant since many years ago; biological activity of neem is in wide spectrum. Every part of neem plant like leaves, stem, fruits etc. has been used as a medicine for household remedy against various human diseases such as anti-inflammatory, antipyretic, antitumor, antibacterial as well as pesticidal activities [67]. The biomolecules such as Terpenoids, nimbaflavone, sugars etc. are present in neem leaves extract which are responsible for metal ion reduction with capping agents [68]. Neem is a cheap and easily available source, hence we select neem leaf extract for synthesis of nanoparticles.

1.4. Physicochemical Properties of Metal Nanoparticles

Various physicochemical properties such as high surface to volume ratio, mechanically strong, optically active and chemically reactive create nanoparticles exclusive and suitable applicants for different applications. Some of their remarkable properties are given below.

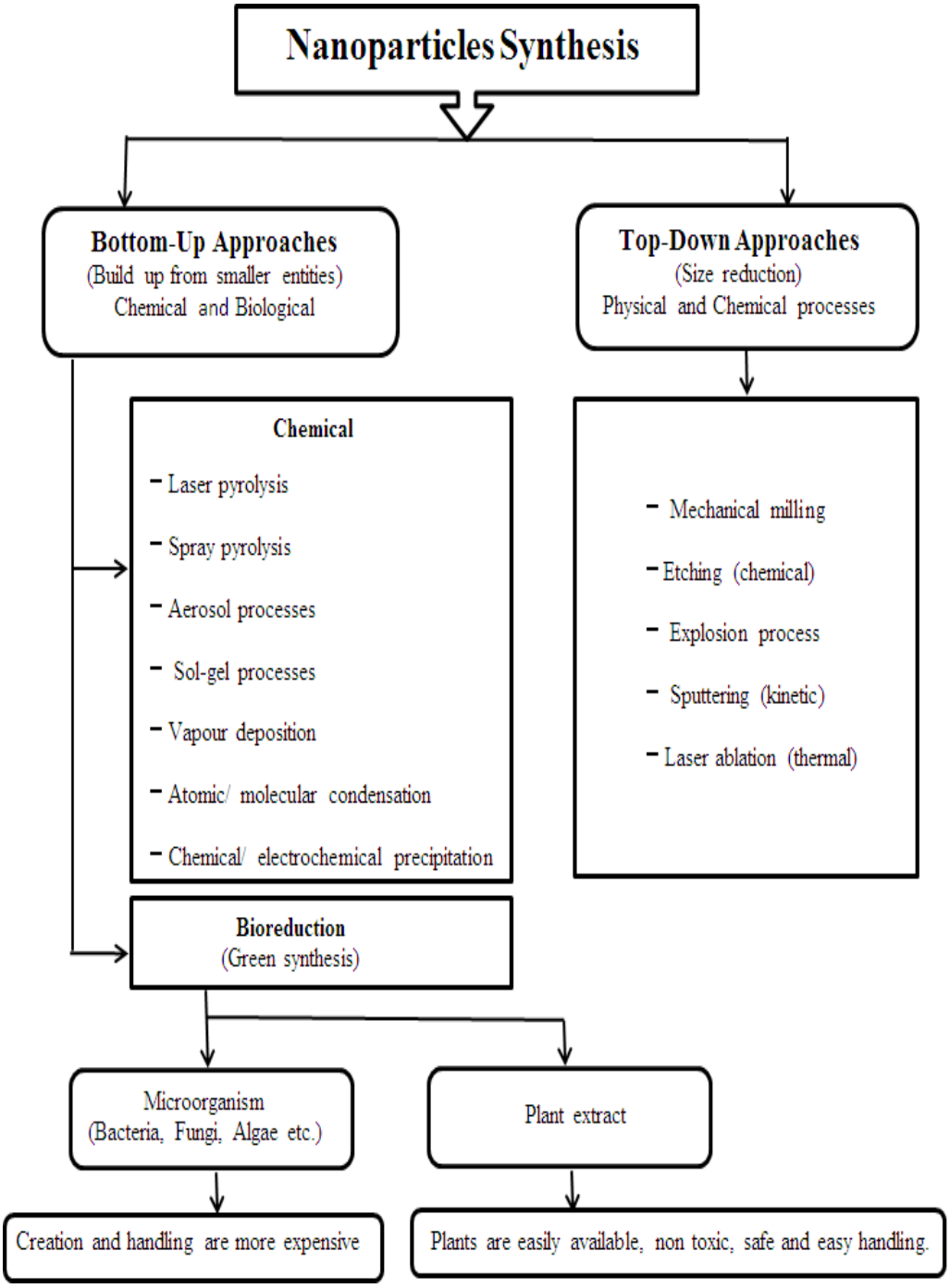

Figure 1.1: Various approaches for fabrication of Metal Nanoparticles.

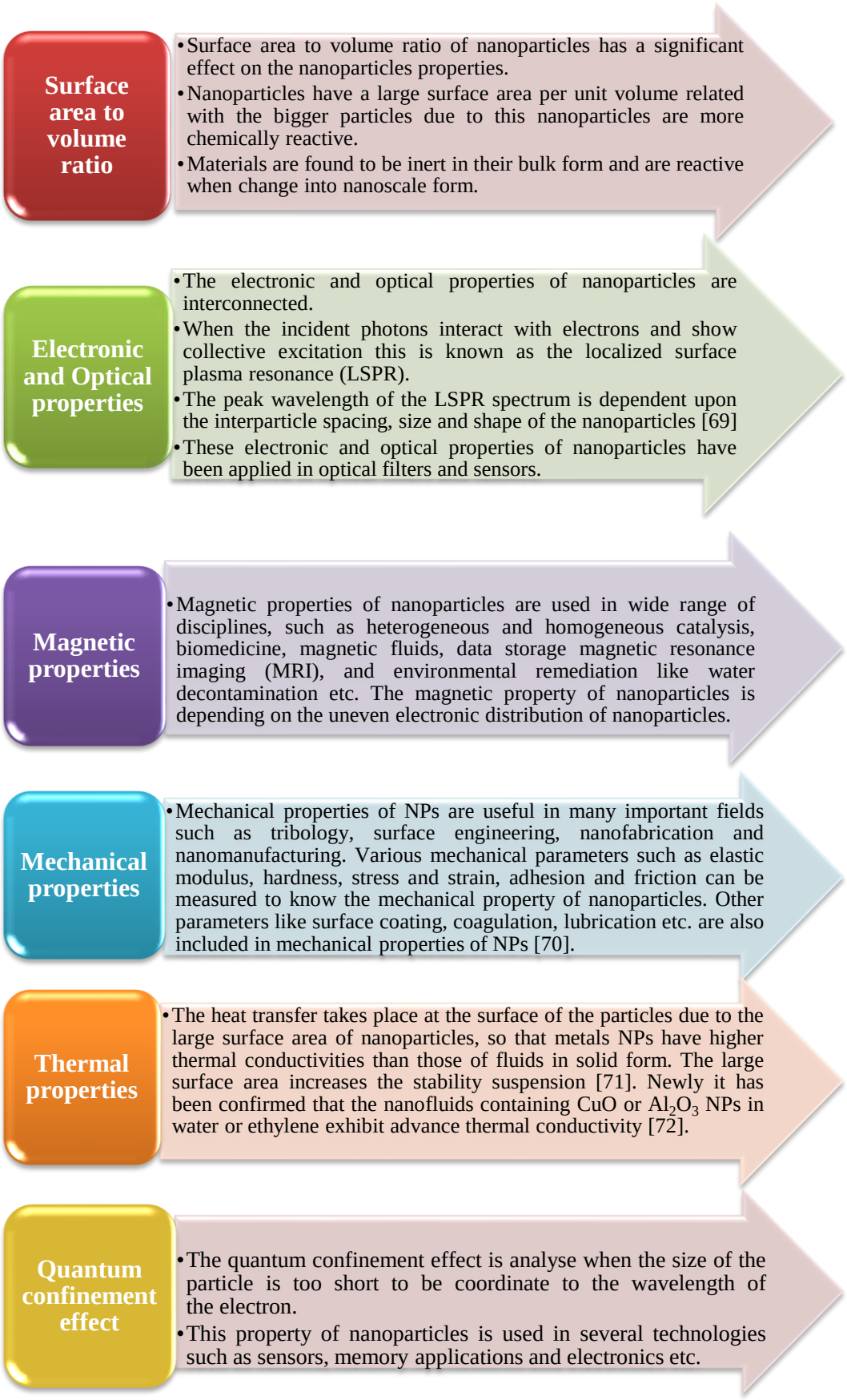
Surface area to volume ratio
•Surface area to volume ratio of nanoparticles has a significant effect on the nanoparticles properties.
•Nanoparticles have a large surface area per unit volume related with the bigger particles due to this nanoparticles are more chemically reactive.
•Materials are found to be inert in their bulk form and are reactive when change into nanoscale form.
Electronic and Optical properties
•The electronic and optical properties of nanoparticles are interconnected.
•When the incident photons interact with electrons and show collective excitation this is known as the localized surface plasma resonance (LSPR).
•The peak wavelength of the LSPR spectrum is dependent upon the interparticle spacing, size and shape of the nanoparticles [69]
•These electronic and optical properties of nanoparticles have been applied in optical filters and sensors.
Magnetic properties
•Magnetic properties of nanoparticles are used in wide range of disciplines, such as heterogeneous and homogeneous catalysis, biomedicine, magnetic fluids, data storage magnetic resonance imaging (MRI), and environmental remediation like water decontamination etc. The magnetic property of nanoparticles is depending on the uneven electronic distribution of nanoparticles.
Mechanical properties
•Mechanical properties of NPs are useful in many important fields such as tribology, surface engineering, nanofabrication and nanomanufacturing. Various mechanical parameters such as elastic modulus, hardness, stress and strain, adhesion and friction can be measured to know the mechanical property of nanoparticles. Other parameters like surface coating, coagulation, lubrication etc. are also included in mechanical properties of NPs [70].
Thermal properties
•The heat transfer takes place at the surface of the particles due to the large surface area of nanoparticles, so that metals NPs have higher thermal conductivities than those of fluids in solid form. The large surface area increases the stability suspension [71]. Newly it has been confirmed that the nanofluids containing CuO or Al_2O_3 NPs in water or ethylene exhibit advance thermal conductivity [72].
Quantum confinement effect
•The quantum confinement effect is analyse when the size of the particle is too short to be coordinate to the wavelength of the electron.
•This property of nanoparticles is used in several technologies such as sensors, memory applications and electronics etc.

1.5. Nanocatalysis

From the past decade, the field of nanocatalysis has undergone an explosive growth [73-76], due to the large surface area of nanoparticles they show a positive effect on reaction rate. The catalytic activity of nanomaterial is depending on the structure, shape-based properties, nanoscale size and composition of nanoparticles. Nanostructure catalysts have numerous potential benefits, which have considerable academic and industrial research attention (**Figure 1.2**).

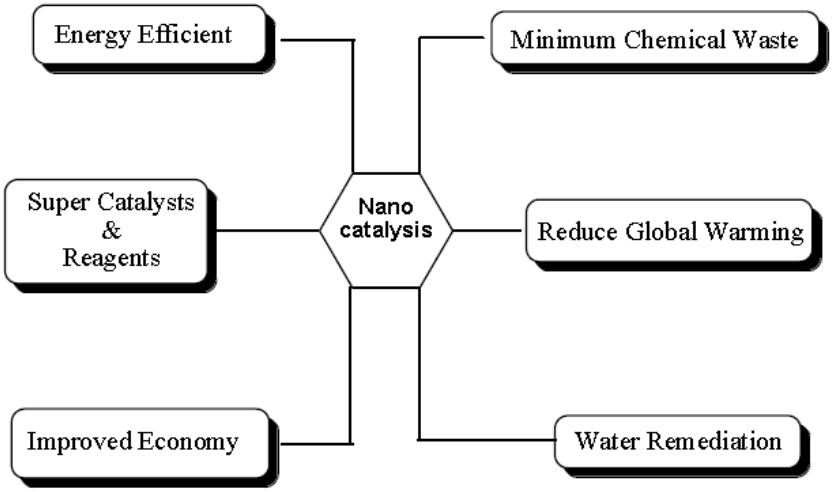

Figure 1.2: Advantage of Nanocatalysis [77].

Nanocatalysis one classified as, homogeneous type catalysis in colloidal solution [78-85] and heterogeneous type supported nanoparticles catalysis in gas-phase reactions [86-98]. The nano-catalyst in heterogeneous system may be generally a solid or immobilized on a solid inert matrix. In solution phase reaction a heterogeneous catalyst may very well serve as a catalytic reservoir or 'resting state', due to this molecular catalytic species are liberated for catalysis, and re-deposited subsequently the completion of a catalytic cycle [99]. Example includes copper, ruthenium; silver, rhodium, gold, palladium, iron, platinum and nickel nanoparticles supported onto clays, silica, alumina and zeolite or biowaste materials, carbon fibres. Heterogeneous catalysts are easy to recover but have some drawbacks, such as the drastic conditions they require to be effective and the

mass transport difficulties. However, they often have poor catalytic activity and selectivity compared to many homogeneous catalysts [100-102]. The nano-catalyst in homogeneous system means a solution or suspension of nanoparticles in a solvent. In this system it must be consider how to prevent its aggregation when designing a nano-catalyst for use in a solution. Nanoparticles have a characteristic to agglomerate and will cluster together to form larger particles, if it is not prevent appropriately, nanoparticles drop their large surface area, catalytic activity and other significance. Biomolecules-based stabilization of nano-particles to prevent its aggregation is recognized as most effective and green way to stabilize nanoparticles in solution.

Metal colloids are very capable catalysts because a large number of atoms are existent on the surface of the nanoparticles. This catalytic system is often called "quasi-homogeneous" nanoparticle catalysts. The solution of colloidal nanoparticles must prevent aggregation of nanoparticles for stabilization and also be good potential recyclable catalysts. The Quasi-homogeneous catalysts are promising catalysts for industrial application because they have benefits of both homogeneous and heterogeneous catalysts, like high activity, selectivity and easy separation for re-use. 'Quasi-homogeneous catalysis', a classification that has mostly been accepted by the catalysis community, and this catalysis is used to define catalytic processes, which is create an interface between homogeneous and heterogeneous catalysis [99].

1.6. Azo Dyes

Azo dye is a large and commercially important group of synthetic dyes. **Azo dyes** are organic compounds which contain the azo bond −N=N−, which is known as a chromophore in azo dyes. –OH, -NH_2, -NHR etc auxochromes groups are present in azo dyes. Azo dyes are broadly used to give textiles, leather articles, and some foods. Azo dyes are divided into two parts according to their number of azo group present in dye after that division is based on application (**Figure 1.3**).

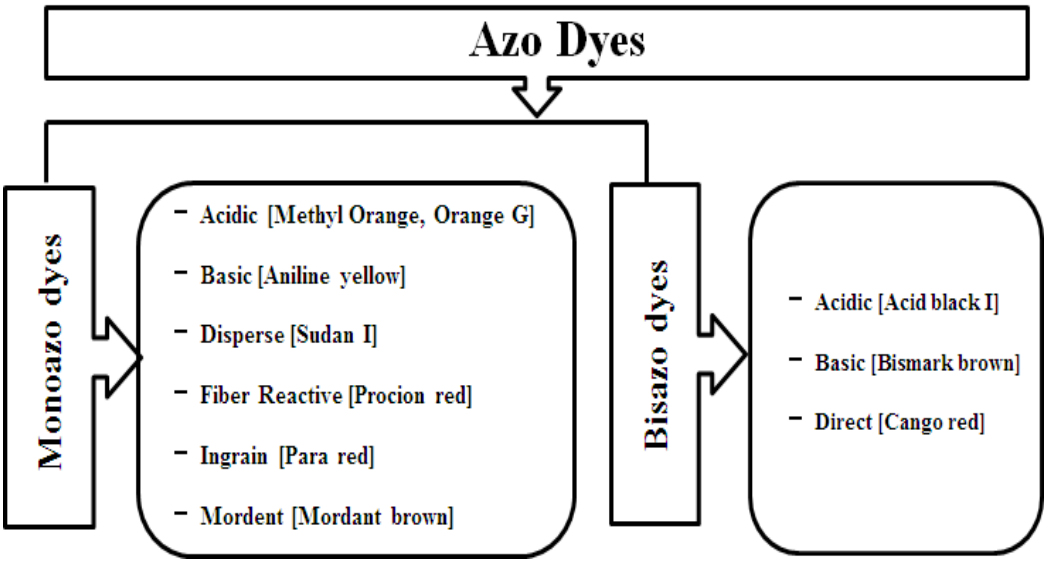

Figure 1.3: Classification of Azo Dyes.

Methyl Orange and Orange G acidic monoazo dyes are used as a targeted compound in this presented research work. Methyl orange does not have a full spectrum of the color change but has a sharper end point. Methyl orange shows red color in acidic medium (pH < 3.1) and yellow color in basic medium (pH > 4.4). It is used as a pH-indicator in 0.1% aqueous solution for the titration of mineral acids (not organic acids) and strong bases. Methyl orange is also used in dyeing and printing textiles as a dyestuff [103] (**Figure 1.4 A**). Orange G belongs to the hydrosoluble phenylazonaphthol dyes. It is widely used in histology in many staining formulations, dying of textiles, food, in weaving, tanning and paper industries (**Figure 1.4 B**) [104].

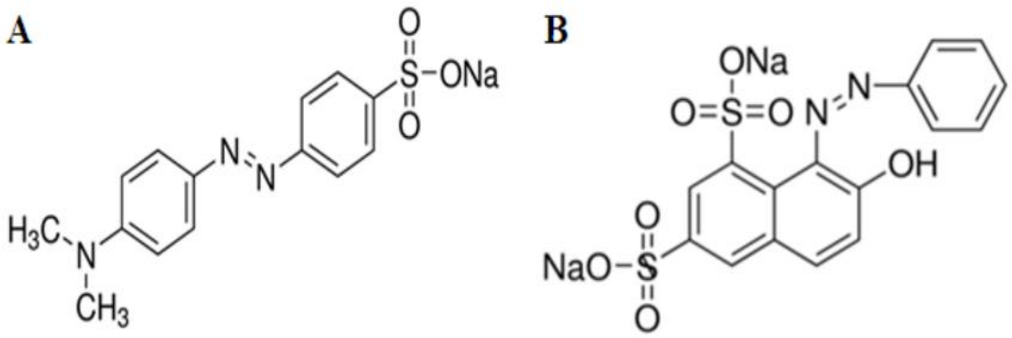

Figure 1.4: (A) Structure of Methyl Orange. (B) Structure of Orange G.

1.7. Degradation of Dyes

The textile dyeing industry has generated massive pollution problem as it is one of the most chemically intensive industries on earth, and the number one pollutant of water (after agriculture) [105]. Only 80 percent of the dyestuffs stay on the fabric and rest go down the trench. The liberation of waste waters having synthetic dyes tends to reason serious damage to aquatic biota, with direct effects on photosynthesis and oxygenation. Usual toxicity of these compounds and resistance to natural degradation like light, acid, base and oxygen due to this the color of the dye becomes permanent [106]. The majority azo dyes are water-soluble and are therefore easy for the body to absorb, and this takes place through inhalation and swallowing of dust as well as through skin contact due to this these dyes are the cause of mutagen and cancer [107]. Azo dyes may also be toxic to aquatic organisms and cause long-term adverse effects in the aquatic environment (**Figure 1.5**).

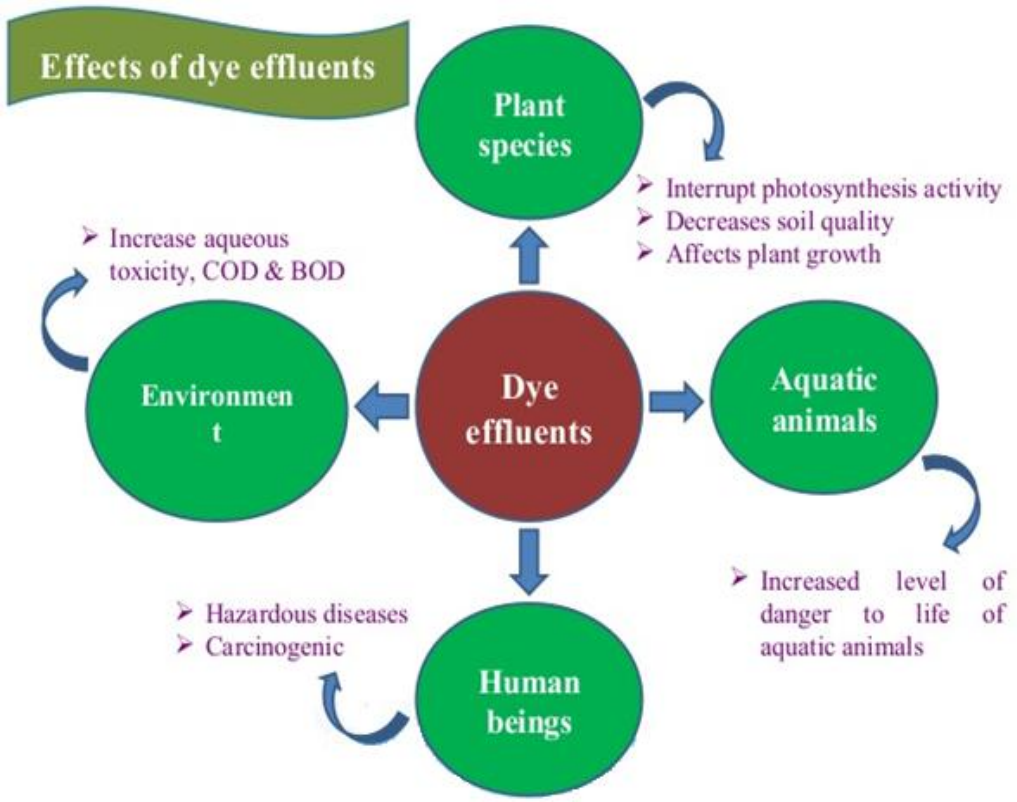

Figure 1.5: Effect of textile dye effluents on the environment [108].

Azo dyes are used in dyeing industries and the river and groundwater which are nearby these industries are contaminated by azo dyes [109]. Dyes contributed to overall toxicity at all treatment stages. Furthermore, dye baths might have a high level of BOD/COD (Biological oxygen demand / Chemical oxygen demand) [110, 111], color, toxicity, surfactants, fibers and turbidity, and may have heavy metals [112]. When BOD levels are high in the untreated wastewater can cause fast reduction of dissolved oxygen (DO). High COD levels are toxic to the biological life [113]. Dyes effluents are decreasing light absorption may considerably affect photosynthesis of aquatic life and may be toxic due to the presence of aromatic compounds or heavy metals [114-117]. Dye degradation is a process in which the dye molecules are degraded into smaller molecules. As the result, harmless products are H_2O, CO_2, and mineral byproducts are obtained.

During the past two decades, various physical and chemical treatment techniques can be employed to eliminate color from the dye containing wastewaters [118-125]. Various physical treatment processes like stripping, sedimentation, filtering, flotation, reverse osmosis, ion exchange, and adsorption [126-128], removed many dissolve and non-dissolve organic pollutants without necessarily changing their chemical structures. The main disadvantage of the physical method is the sludge formation, chemical coagulation and flocculation add a large amount of chemical and the obtained sludge contain hazardous materials and the sludge removal remains as a problem [129]. The disadvantage of adsorption technique is that the dye is absorbed by absorbent and need to be regenerated regularly so that this technique is associated with additional costs. Membrane technologies like ultrafiltration, nanofiltration and reverse osmosis have been used for the complete treatment and recycle of water [124], but these processes have many operative problems with high capital costs. Chemical treatment processes are chemical precipitation, Chemical oxidation or reduction etc., among these chemical methods, the oxidation methods are effective and are appropriate for large-scale treatment of dye effluent. The conventional chemical oxidation process by air and oxygen is also occurring but these are no longer

enough for highly polluted effluent. As the result of this, the Advanced Oxidation Processes (AOPs) used for the effluent treatment and this method is used in this research work.

1.8. Advanced Oxidation Process

Advanced oxidation processes (AOPs) are considered to be efficient wastewater treatment methods. Powerful oxidizing radical intermediates such as hydroxyl radicals ($^{\bullet}OH$) and sulphate radicals ($SO_4^{\bullet-}$) are involved in AOPs, leading to the elimination of target compound. Sulphate radicals have higher standard reduction potential (2.5- 3.1 V) than hydroxyl radicals at neutral pH [130] and acting as a more selective oxidising agent than hydroxyl radicals in acidic medium. Electron transfer, hydrogen abstracting, hydrogen addition mechanisms are obtained by sulphate and hydroxyl radicals [131]. Sulphate radicals have better selectivity than hydroxyl radicals because $SO_4^{\bullet-}$ having longer life span than $^{\bullet}OH$. Due to the above advantage of $SO_4^{\bullet-}$ radicals, sulphate radical based AOPs are playing important role in wastewater treatment. Sulphate radicals are generated by peroxomonosulphate and peroxodisulphate. Both oxidants show relatively slow consumption rate due to their stability at room temperature. But with the help of thermal, photolytic or transition metal activated decomposition of both oxidants was done and generated sulphate radicals [132-137].

1.8.1. Peroxosulphate Oxidants

Peroxosulphate oxidants are known as the sulphate derivatives of hydrogen peroxide (H_2O_2). Peroxomonosulphate (PMS) and peroxydisulphate (PDS), these oxidants are increased vital significance due to their application as auxiliary reagents in organic reactions. The peroxosulphate oxidants are highly reactive because of weak peroxobond (-O-O-). The bond is very sensitive towards trace amount of catalysts and promoters for generating sulphate radicals.

1.8.1.1. Peroxomonosulphate (PMS)

Oxone is a commercial name of peroxomonosulfate (PMS) and it is a potassium triple salt containing potassium peroxomonosulfate, as an effective oxidant used in numerous organic transformation reactions (**Figure 1.6**) [138]. Peroxomonosulphate is a sulphonate derivative of hydrogen peroxide (H-O-O-H), replacing one of the hydrogen atoms in H_2O_2 by sulphate group. Infra-red spectroscopy studies of PMS and H_2O_2 indicates that the stretching frequency of O-O bond is higher in PMS than H_2O_2 so that the two -OH groups are chemically and spectroscopically different [139]. Therefore, PMS exists as HSO_5^- at pH 4.0.

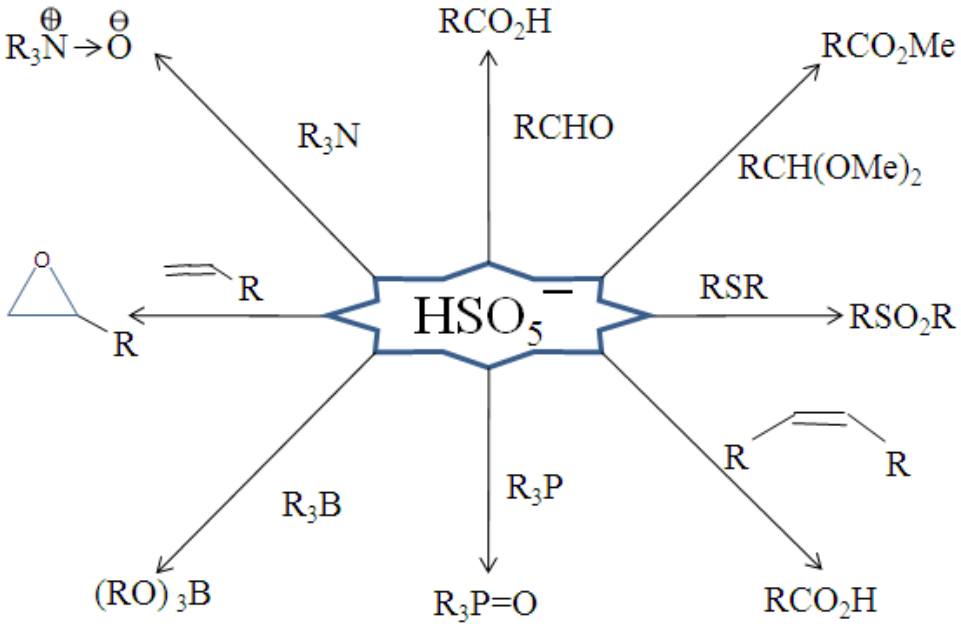

Figure 1.6: Various organic reactions with Peroxomonosulphate[138].

Peroxomonosulphate has high oxidation potential (2.5-3.1V) [140] and generate sulphate radicals ($SO_4^{\bullet-}$) by radiation excitation [141], heat [142], ultrasound [143] and transition metals excitation [144, 145]. PMS shows radical based mechanism and generated sulphate radicals are used in various organic reactions. Therefore, PMS plays a significant role in the oxidation of organic compounds by the advanced oxidation process. PMS possess high reactivity due to the electrostatic effect and weak peroxo bond. The characteristic of oxone such

as stability, ease of transport, nontoxic nature, nonpolluting byproducts, grow rapidly as efficient oxidant.

1.8.1.2. Peroxodisulphate (PDS)

Peroxodisulfate (PDS) is the common peroxygens of sulfurate, which can be derived from hydrogen peroxide (H_2O_2) by the replacement of both the hydrogen atoms by sulfonate group. Peroxodisulphate is the most chemically active reagent and has great utility in a variety of chemical processes. Chemical abstract used peroxodisulphate and the international union of pure and applied chemistry (IUPAC) has recommended the term peroxodisulphate, another name is persulphate [146, 147]. In aqueous solution peroxodisulphate ion ($S_2O_8^{2-}$) shows strong oxidizing properties and standard reduction potential is 2.01 V in (**Equation 1**).

$$S_2O_8^{2-} + 2e^- \rightarrow 2SO_4^{2-} \qquad (1)$$

Figure 1.7 shows the structure of PDS which have two sulphate groups linked by a covalent bond between two oxygen atoms, the distance between these two oxygen atoms is 1.46 A^o, the distance S-O is 1.50 A^o, while S-O-O- inter bond angle is 128^o and the axis of symmetry is pass through the mid-point between the central oxygen atoms. These parameters of the structure were approved by the results of Raman spectra of sodium and ammonium peroxodisulphate [148]**.**

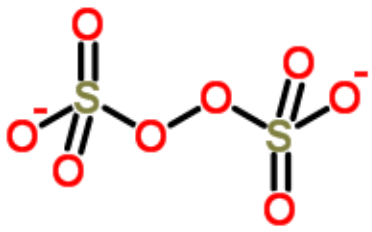

Figure 1.7: Structure of peroxodisulphate group.

Reactions of peroxodisulphate ion are generally slow at ordinary temperatures but are catalysed by adding transition metal ions and metal

nanoparticles [149-160]. In recent years the kinetics and mechanism of the oxidation of inorganic and organic compounds by peroxodisulphate under catalysed and uncatalyzed conditions have taken considerable attention [146, 161]. Peroxodisulphate is a vital oxidizing agent because their products and by-products pose little or no threat to the environment [162]. PDS used as oxidant in degradation of wide range of organic pollutants like tetracycline [163], bisphenol A [164], acid orange 7 [165], basic red 46 [166] the PDS activated by photons, heat, transition metal ions and generate SRs. SRs are active species which are attack on organic pollutants and convert them in harmless end products. A detailed literature survey reported here (Table 1.1) on nanomaterials assisted degradation of dye containing effluents by advanced oxidation process.

1.9. Catalytic application of green synthesized metal nanoparticles

Nanomaterials possess high surface area to volume ratio so they are widely applied as catalyst in various fields. Metal nanoparticles play a role of catalyst, shows greater efficiency and selectivity towards oxidants to achieve selective products. Many recent studies have indicated the catalytic potential of metal NPs for environmental remediation such as degradation of organic dyes, organic pollutants and removal of heavy metals.

Singh et al. [174] employed ascorbic acid and gum acacia synthesis of silver nanoparticles to catalyse degradation of methylene blue dye. The catalytic activity of pseudo-spherical silver nanoparticles (size 11–15 nm) exhibit greater than rod- and thread-shaped silver nanoparticles (size 40–54 nm). The size and shape of the NPs seems to play a significant role in controlling the catalytic activity. Similarly, the reactivity of AgNPs synthesized by aqueous *Terminalia chebula* (*T. chebula*) fruit extract was tested for degradation of dye methylene blue by Edison et al. [175]. The presence of AgNPs acts as a redox catalyst, which is often termed as electron relay effect (**Figure 1.8**). They also reported the

TABLE: 1.1

Nanomaterials Assisted Degradation of Dyes by Advanced Oxidation Process.

S. No.	Catalyst	Oxidant	Dye Employed	Comments	Ref.
1	Zero valent iron (ZVI) Nanoparticles	Persulfate	Orange G	Oxidation pathway was proposed for the oxidation of Orange G with iron activated Persulfate based. According to this pathway, final products like Phthalic acid, oxalic acid and aromatic intermediates were obtained by oxidation of OG.	167
2	$Co_xFe_{3-x}O_4$ Nanoparticles	Oxone	Rhodamine B	The Chemical oxygen demand removal rate of Rhodamine B was observed in the $Co_xFe_{3-x}O_4$/Oxone system, which reached to nearly 54.4% within 40 min and was corresponding to 99% decolourization rate.	168
3	Nano-Co_3O_4	Peroxymonosulfate	Acid Orange 7	The observed results show that the key step of Acid orange 7 degradation was the cleavage of N–N and C=N bonds and obtained final products were CO_2 and H_2O.	169
4	Au-TiO_2 Nanoparticles	Peroxomonosulphate, Peroxodisulphate	Acid red 88	The rate constant observed 4–5 fold increase in Au–TiO_2 nanoparticles with PMS and PDS. It is due to the immediate trapping of the generated electrons by the electron acceptors (PMS and PDS), which in turn decreases the recombination of electron–hole pairs there by increasing the oxidation competence of the organic dye molecules by the holes. Further, greater activity in the presence of PMS due to the oxidizing nature of both $^{\bullet}OH$ and $SO_4^{\bullet-}$ radicals, which are generated by PMS.	170

5	Co_3O_4 Nanoparticles	Persulphate, Sodium Persulphate, Peroxomonosulphate	Orange G	Nano-Co_3O_4 exhibited good heterogeneous activity in nano- Co_3O_4/ Persulphate system and low dissolved Co ions especially at neutral or alkaline conditions. The reactivity discrepancy of Persulphate (PS), Sodium Persulphate (NaPS) and PMS followed the order of nano-Co_3O_4/PMS > nano- Co_3O_4/PS > nano- Co_3O_4/NaPS.	171
6	Magnetite nanoparticles (Fe_3O_4)	Peroxymonosulfate	Orange G	The catalytic treatment of azo dye was evaluated by NH_2OH enhanced Fe_3O_4/PMS process. The presence of NH_2OH with Fe_3O_4/PMS process greatly accelerated the cycle of $Fe_{(III)}/Fe_{(II)}$ on the surface of Fe_3O_4 and the generation of reactive radicals, i.e. $SO_4^{\bullet-}$ and $^{\bullet}OH$.The end degradation products of NH_2OH were N_2, N_2O, NO_2^- and NO_3^- in NH_2OH / Fe_3O_4/PMS process, while the eco-friendly N_2 was the major product.	172
7	$MnFe_2O_4$-SAC Nanocomposites	Persulfate	Orange G	Magnetically separable $MnFe_2O_4$-SAC hybrid catalyst has been successfully synthesized using a facile solvothermal method. The $MnFe_2O_4$-SAC catalyst exhibited excellent catalytic activity in Persulfate activation for OG degradation, in the meantime, the as-prepared catalyst maintained high catalytic performance after repeated five runs, and the degradation efficiency of OG could still be more than 94%.	173

photocatalytic activity of AgNPs fabricated by using *Morinda tinctoria* leaf extract for degradation of methylene blue [176].

In another report, *Trigonella foenum-graecum* seeds synthesized AgNPs were employed for catalytic degradation rate of hazardous dyes, methyl orange, methylene blue and eosin Y in presence of $NaBH_4$. The result indicate that complete removal of MO. MB and eosin Y from water at a concentration of 5 x 10^{-5} mol dm^{-3} green synthesized NPs proved that reaction takes time higher with increase in particle size [177]. Alzahrani et al. [178] reported, different ratios of tangerine peel extract (2:1, 1:1, 1:2) synthesised AgNPs, different size of AgNPs with average size 30.29 nm, 16.68 nm, 25.85 nm were obtained. The catalytic activity of synthesized NPs at synthesized three different ratios was evaluated in presence H_2O_2 or $NaBH_4$ for degradation of MO. The results indicates highest MO removal rate obtained at 1:2 ratio of tangerine peel extract and $AgNO_3$ solution select for synthesis of NPs.

Ramkrishna et al. [179] used two different brown algae *Turbinaria conoides* and *Sargassum tenerrimum* for synthesis of gold nanoparticles (AuNPs) to evaluate catalytic activity in degradation of dye Rhodamine B, Sulforhodamine 101 and nitro compounds. From experiments, it was observed that synthesized AuNPs from *T. conoides* with average size 27.5 nm (**Figure 1.9a**) more catalysed than *S. tenerrimum* synthesized AuNPs (**Figure 1.9b**) with average size 35 nm, the reduced size are more effective due to the higher surface volume ratio. Whereas, Mata et al. [61] also reported at different percentage (1% and 5%) of *Plumeria alba* flower extract (PAFE) fabricated AuNPs show different catalytic activity for degradation six hazardous dyes (methylene blue, eosin Y, 4-nitrophenol, methyl red, Congo red and ethidium bromide). The highest degradation rate was activated at higher percentage (5%) of PAFE and was attributed to small size (15.6 nm) of synthesized AuNPs.

Ganapuram et al. [180] used salmalia malabarica gum for synthesis of AuNPs further employed to degrade methylene blue and congo red. The results

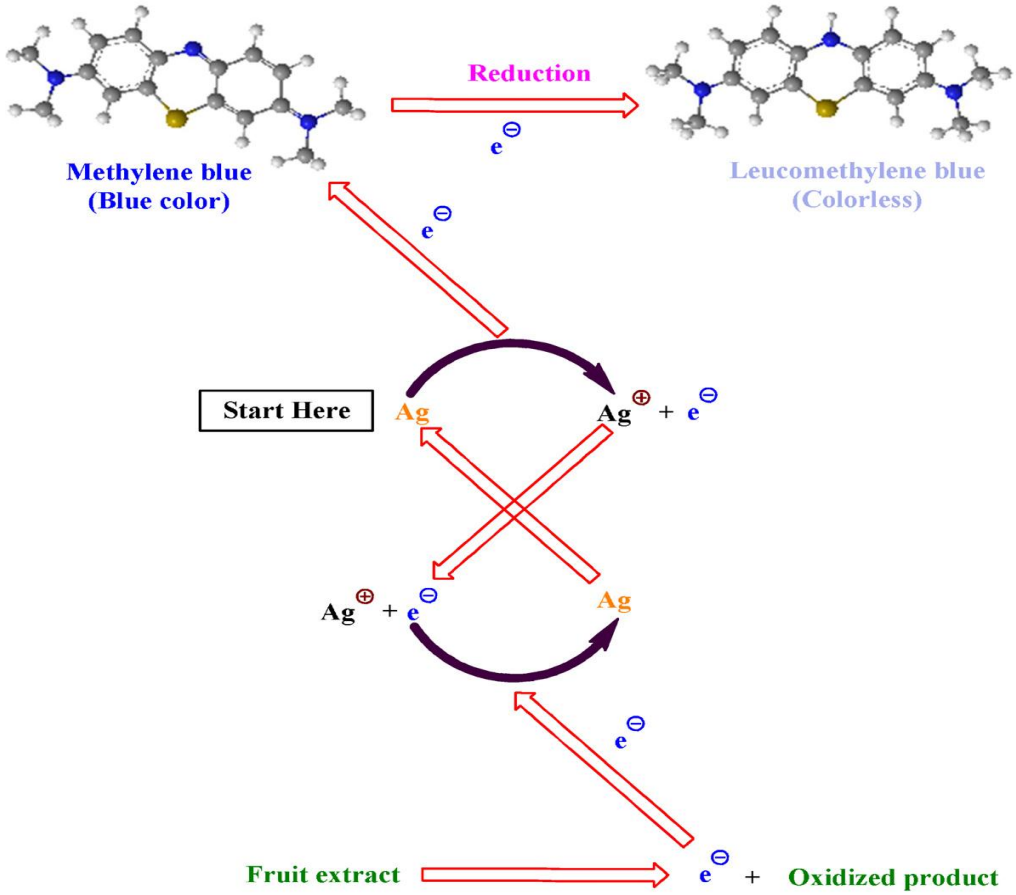

Figure 1.8: Role of T. chebula fruit extract and catalytic action of AgNPs in degradation of methylene blue (electron relay effect) [175].

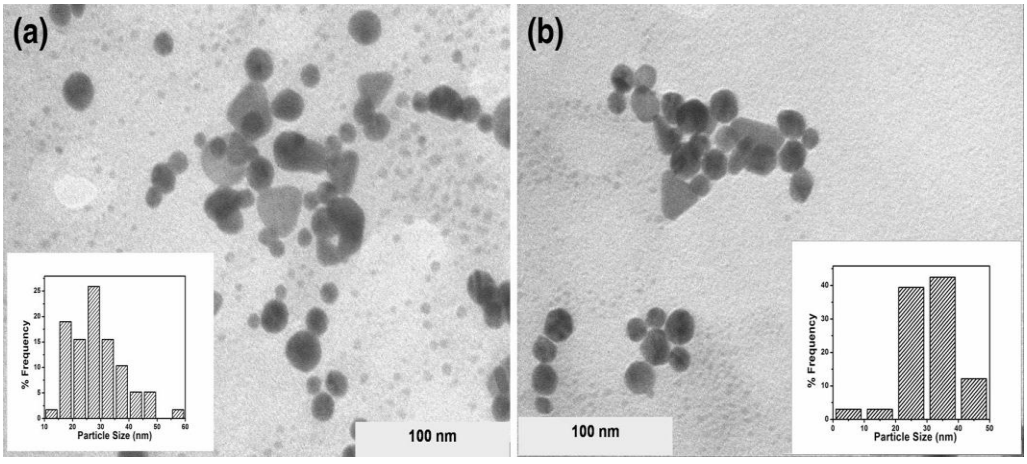

Figure 1.9: TEM images and size distribution of particles histogram (inset) of AuNPs synthesized from (a) T. conoides and (b) S. tenerrimum[179].

also showed that: First, polysaccharide D-galacturonic acid, D-galactose, L-arabinose in salmalia malabarica gum acted as both reducing and capping agent in synthesis of AuNPs, leading to reduced aggregation and to increased reactivity of AuNPs, second, AuNPs proved to be efficient catalyst in degradation of MB and congo red. In another report xanthan gum reduced and stabilized PdNPs also exhibited good catalytic activity in reduction of 4-nitrophenol to 4-aminophenol [181].

Hoag et al. [182] employed green tea (GT) synthesised iron nanoparticles (FeNPs) to catalyse hydrogen peroxide for the degradation of the bromothymol blue. The catalytic activity of green synthesised zero-valent iron was more than that of Fe-EDTA and Fe-EDDS. From experiments, it was observed that by increasing concentrations of FeNPs, enhance concentration of catalyse hydrogen peroxide, which ultimately increased the degradation of bromothymol blue (BB). Similarly, the reactivity of FeNPs synthesised by sorghum bran extracts was employed for degradation of dye (BB) by Njagi et al. [183]. In presence of iron nanoparticles and H_2O_2, Bromothymol blue degrades rapidly, suggesting that the FeNPs catalyses the reaction for generated free radicals from H_2O_2. The catalysis of H_2O_2 enhancing the rate of reaction ultimately increases the rate of degradation of bromothymol blue [183].

Shahwan et al. [184] reported that green tea synthesised iron nanoparticles were employed for catalytic degradation of methylene blue (MB) and methyl orange (MO) dyes. The results illustrate the complete removal of methylene blue (MB) and methyl orange (MO) dyes from water was obtained at a concentration of 10–200 mg/L. The removal of MB was 80% within 5 min whereas MO dye removed after 1 h of reaction. Green tea fabricated iron nanoparticles proved to be more effective as a Fenton-like catalyst both in terms of kinetics and percentage removal compared to iron nanoparticles synthesized by borohydride reduction.

In another report, oolong tea extract employed for synthesis of iron nanoparticles, which were used for catalytic degradation of degrade malachite green (MG) [185]. In the study, polyphenols/caffeine in oolong tea extract acted as both reducing and capping agents in synthesis of Fe nanoparticles. Synthesize FeNPs proved to be efficient in the degradation of MG, resulting in 75.5% of MG (50 mg/L) being removed. Kuang et al. [186] used extracts of three different teas i.e., green tea (GT), oolong tea (OT), and black tea (BT) separately for synthesis of iron nanoparticles, were used as a catalyst for Fenton-like oxidation of monochlorobenzene (MCB). The result showed that highest degradation rate was achieved by green tea synthesised Fe NPs due to high polyphenol present in extract. In 180 min of reaction 69% degradation was observed for GT-FeNPs while 53% by OT-FeNPs and 39% by BT-FeNPs.

Plant mediated FeNPs act as Fenton-catalyst with H_2O_2. The oxidation depends on the activity of hydroxyl radicles ($OH^{\bullet}$), which generate in aqueous solution and due to reaction with Fe^{+2} and hydrogen peroxide (H_2O_2).

$$Fe^{+2} + H_2O_2 \rightarrow Fe^{+3} + HO^- + OH^{\bullet} \quad (2)$$

$$Fe^{+3} + H_2O_2 \rightarrow Fe^{+2} + OOH^{\bullet} + H^+ \quad (3)$$

However, reaction pathway may be different for varied catalysts or may depend on dye molecule as well as chemical nature of the catalyst.

Iron polyphenol nanoparticles (Fe-P NPs) synthesized by three different plants i.e., *E. tereticornis, M. nesophila* and *R. officinalis* were compared for degradation of dye by Wang et al. [187]. About 100% of Acid black dye was degraded, and 87% removal of total organic carbon (TOC) was achieved in presence of Fe-P NPs. E. tereticornis Fe-P NPs showed good activity for dye degradation as compared to other nanoparticles and attributed to small size and good dispersibility of synthesized particles.

Gupta et al. [188] studied the synthesis different metal nanoparticles such as gold, silver, platinum using tannic acid to catalyse degradation of methyl orange. The result conclude that catalytic effect of synthesized NPs for degradation rate are $k_{AgNPs} > k_{AuNPs} > k_{PtNPs} > k_{uncatalyzed}$ reaction. The greater

catalytic activity of AgNPs has been obtained due to its low value of work function as compared to AuNPs and PtNPs.

Nasrollahzadeh et al. [189] reports the synthesis of sodium borosilicate glass supported CuNPs by *Acalypha indica* L. leaf extract play a role of reducing and stabilizing agent. Supported CuNPs exhibits excellent catalytic activity for the reduction of the 4-nitrophenol (4-NP), 2, 4-dinitrophenilhydrazine (2, 4-DNPH), Congo red (CR), methylene blue (MB) and methyl orange (MO) by using $NaBH_4$ in aqueous medium. To the best of our knowledge, this is the first study to report on without supported neem leaf synthesized CuNPs utilized for remediation of waste water. Hence, the above studies shows that the plant mediated metal NPs were significantly effective for the degradation of various types of dyes under different experimental conditions.

1.10 Objective of Present Work

Our main aim of present research is to develop environmental friendly, cost effective and simple synthesis method for the metal nanoparticle. For the synthesis of metal nanoparticles biomolecules present in plant extract used as a reducing as well as the stabilizing agent. Optimize the conditions of synthesis of nanoparticles, for enhance the catalytic activity and for increase stability of nanoparticles. The characterization of metal nanoparticles will done by different instrumental techniques like UV-Visible spectroscopy, Fourier transform infrared (FT-IR), X-Ray diffractometer (XRD), Scanning electron microscope (SEM), Transmission electron microscope (TEM) and Zetasizer. The work also includes application of synthesized nanoparticles as catalyst in dye containing wastewater treatment. The size dependant catalytic activity of synthesized nanoparticles will also check in degradation study as will as compare the degradation rate in presence of different oxidants. The degradation product will identified by different instrumental techniques.

1.11 References

[1] O. Salata, ***J. Nanobiotechnol.***, 2 (2004) 3.

[2] R. Luque, R. S. Varma, ***Sustainable Preparation of Metal Nanoparticles Methods and Applications, Royal Society of Chemistry, Cambridge (UK)***, ***2013.***

[3] L. N. Lewis, ***Chem. Rev.,*** 93 (1993) 2693.

[4] G. A. Ozin, A. C. Arsenault, L. Cademartiri, ***Nanochemistry: A Chemical Approach to Nanomaterials, Royal Society of Chemistry, Cambridge, UK***, ***2000.***

[5] (a) C. A. Mirkin, ***Small***, 1 (2005) 14; (b) J. Grunes, J. Zhu, G. A. Somorjai, ***Chem. Commun.***, (2003) 2257.

[6] M. Chen, Y. Cai, Z. Yan, D. W. Goodman, ***J. Am. Chem. Soc.***, 128 (2006) 6341.

[7] A. S. Bruss, M. A. Gelesky, G. Machado, J. Dupont, ***J. of Molecular Catalysis A***, 252 (2006) 212.

[8] A. A. Firooz, A. R. Mahjoub, and A. A. Khodadadi, ***World Academy of Science, Engineering and Technology,*** 76 (2011) 138.

[9] M. A. El-Sayed, ***Accounts of Chemical Research,*** 34 (2001) 257.

[10] M. C. Daniel, D. Astruc, ***Chemical Reviews***, 104 (2004) 293.

[11] C. Burda, X. B. Chen, R. Narayanan, M. A. El-Sayed, ***Chemical Reviews***, 105 (2005)1025.

[12] M. A. El-Sayed, ***Accounts of Chemical Research,*** 37 (2004) 326.

[13] A. P. Alivisatos, ***Journal of Physical Chemistry***, 100 (1996) 13226.

[14] A. Tiwari, S. K. Shukla, (Ed.), ***In Advanced Carbon Materials and Technology, WILEY-Scrivener Publishing LLC, USA, 2014;*** A. Tiwari, ***Adv. Mat. Lett.,*** 3 (2012) 1.

[15] P. Singh, A. Katyal, R. Kalra, R. Chandra, ***Tetrahedron Lett.,*** 49 (2008) 727; A. Tiwari, A. K. Mishra, H. Kobayashi, A. P. F. Turner, ***In Intelligent Nanomaterials, WILEY-Scrivener Publishing LLC, USA, 2012.***

[16] W. Pan, Z. R. Dai, Z. L. Wang, ***Science***, 291 (2001) 1947.

[17] B. K. Park, D. Kim, S. Jeong, J. Moon, J. S. Kim, ***Thin Solid Films,*** 515 (2007) 7706.

[18] N. A. Luechinger, E. K. Athanassiou, W. J. Stark, ***Nanotechnology,*** 19 (2008) 445201.

[19] Y. Lee, J. Choi, K. J. Lee, N. E. Stott, D. Kim, ***Nanotechnology,*** 19 (2008) 415604.

[20] R. Elghanian, J. J. Storhoff, R. C. Mucic, R. L. Letsinger, C. A. Mirkin, ***Science***, 277 (1997) 1078.

[21] J. N. Anker, W. P. Hall, O. Lyandres, N. C. Shah, J. Zhao, R. P. V. Duyne, ***Nature Mater.***, 7 (2008) 442.

[22] E. K. Athanassiou, R. N. Grass, W. J. Stark, ***Nanotechnology,*** 17 (2006) 1668.

[23] M. Law, L. E. Greene, J. C. Johnson, R. Saykally, P. Yang, ***Nature Mater.***, 4 (2005) 455.

[24] D. A. Lavan, T. McGuire, R. Langer, ***Nature Biotechnol.***, 21 (2003) 1184.

[25] D. Astruc, F. Lu, J. R. Aranzaes, ***Angew. Chem., Int. Ed.,*** 44 (2005) 7852.

[26] A. Sarkar, T. Mukherjee, S. Kapoor, ***J. Phys. Chem. C,*** 112 (2008) 3334.

[27] B. C. Ranu, A. Saha, R. Jana, ***Adv. Synth. Catal.,*** 349 (2007) 2690.

[28] S. H. Joo, S. J. Choi, I. Oh, J. Kwak, Z. Liu, O. Terasaki, R. Ryoo, ***Nature***, 412 (2001) 169.

[29] V. L. Colvin, M. C. Schlamp, A. P. Alivisatos, ***Nature***, 370 (1994) 354.

[30] M. T. Reetz, M. Winter, G. Dumpich, J. Lohau, S. Friedrichowski, ***J. Am. Chem. Soc.***, 119 (1997) 4539.

[31] C. B. Murray, C. R. Kagan, M. G. Bawendi, ***Science***, 270 (1995) 1335.

[32] S. J. Tans, M. H. Devoret, H. J. Dai, A. Thess, R. E. Smalley, L. J. Geerligs, C. Dekker, ***Nature***, 386 (1997) 474.

[33] M. Antonietti, C. Goltner, ***Angew. Chem. Int. Ed. Engl.***, 36 (1997) 910.

[34] Y. Leroux, J. C. Lacroix, C. Fave, G. Trippe, N. Felidj, J. Aubard, A. Hohenau, J. R. Krenn, ***ACS Nano,*** 2 (2008) 728.

[35] N. Cioffi, L. Torsi, N. Ditaranto, G. Tantillo, L. Ghibelli, L. Sabbatini, T. B. Zacheo, M.D. Alessio, P. G. Zambonin, E. Traversa, ***Chem. Mater.,*** 17 (2005) 5255.

[36] X. Zhang, G. Wang, X. Liu, H. Wu, B. Fang, ***Cryst. Growth Des.,*** 8 (2008) 1430.

[37] P. S. Ghosh, C. K. Kim, G. Han, N. S. Forbes, V. M. Rotello, ***ACS Nano,*** 2 (2008) 2213.

[38] K. Mallick, M. J. Witcomb, M. S. Scurrell, ***Materials Science and Engineering: B***, 123 (2005) 181.

[39] R. Das, S. S. Nath, R. Bhattacharjee, ***Journal of Luminescence***, 131 (2011) 2703.

[40] M. Abdulla-al-mamun, Y. Kusumoto, M. Muruganandham, ***Materials Letters,*** 63 (2009) 2007.

[41] B. R.Cuenya, ***Thin Solid Films,*** 518 (2010) 3127.

[42] Y. Li, F. Qian, J. Xiang and M. L. Charles, ***Material Today,*** 9 (2006) 18.

[43] D. L. Feldheim, C. A. Foss, ***Marcel Dekker Incorporated, New York, USA, 2002.***

[44] S. Sepeur, ***Nanotechnology: technical basics and applications. Hannover: Vincentz, 2008***.

[45] M. A. Meyers, A. Mishra, D. J. Benson, ***Prog. Mater Sci.***, 51 (2006) 427.

[46] K. N. Thakkar, S. S. Mhatre, R. Y. Parikh, ***Nanomed. Nanotechnol. Biol. Med.***, 6 (2010) 257.

[47] P. Mukherjee, A. Ahmad, D. Mandal, S. Senapati, S. R. Sainkar, M. I. Khan, ***Nano Lett.***, 1 (2001) 515.

[48] H. R. Ghorbani, A. A. Safekordi, H. Attar, S. M. R. Sorkhabadi, ***Chem. Biochem. Eng. Q.***, 25 (2011) 317.

[49] M. Sastry, A. Ahmad, M. I. Khan, R. Kumar, ***Curr. Sci.***, 85 (2003) 162.

[50] G. S. Dhillon, S. K. Brar, S. Kaur, M. Verma, ***Crit. Rev. Biotechnol.***, 32 (2012) 49.

[51] M. Gericke, A. Pinches, ***Hydrometallurgy***, 83 (2006) 132.

[52] A. Kaler, R. Nankar, M. S. Bhattacharyya, U. C. Banerjee, ***J. Bionanosci.***, 5 (2011) 53.

[53] H. Korbekandi, S. Iravani, S. Abbasi, ***Crit. Rev. Biotechnol.***, 29 (2009) 279.

[54] X. Li, H. Xu, Z. S. Chen, G. Chen, ***J. Nanomater.***, 2011 (2011) 270974.

[55] T. Luangpipat, I. R. Beattie, Y. Chisti, R. G. Haverkamp, ***J. Nanopart. Res.***, 13 (2011) 6439.

[56] P. Mohanpuria, N. K. Rana, S. K. Yadav, ***J. Nanopart. Res.***, 10 (2008) 507.

[57] R. Sanghi, P. Verma, ***Green Chem. Environ. Sustainable***, 15 (2010) 315.

[58] J. L. Gardea-Torresdey, E. Gomez, J. R. Peralta-Videa, J. G. Parsons, H. Troiani, M. Jose-Yacaman, ***Langmuir***, 19 (2003) 1357.

[59] Y. Park, Y. N. Hong, A. Weyers, Y. S. Kim, R. J. Linhardt, ***IET Nanobiotechnol***., 5 (2011) 69.

[60] T. Wang, X. Jin, Z. Chen, M. Megharaj, R. Naidu, ***Sci. Total Environ.***, 466–467 (2014) 210.

[61] R. Mata, A. Bhaskaran, S. R. Sadras, ***Particuology***, 24 (2016) 78.

[62] B. K. Bindhani, A. K. Panigrahi, ***Int. J. Adv. Biotechnol. Res.,*** 5 (2014) 457.

[63] M. Pattanayak, P. L. Nayak, ***World J. Nano. Sci. Technol.,*** 2 (2013) 6.

[64] A. Thirumurugan, P. Aswitha, C. Kiruthika, S. Nagarajan, A. N. Christy, ***Mater. Lett.,*** 170 (2016) 175.

[65] A. Krishnasamy, M. Sundaresan, P. Velan, ***Int. J. Chem.Tech. Res.,*** 8 (2015) 2047.

[66] D. Gnanasangeetha, D. T. Sarala, ***Int. J. Pharm. Sci. Res.,*** 5 (2014) 2866.

[67] O. Koul, M. B. Isman, C. M. Ketkar, ***Can. J. Bot***., 68 (1990) 1.

[68] B. S. Siddiqui, F. Afshan, Ghiasuddin, S. Faizi, S. N. H. Naqvi, R. M. Tariq, ***Phytochemistry***, 53 (2000) 371.

[69] S. Eustis, M. A. El-Sayed, ***Chem. Soc. Rev.***, 35 (2006) 209.

[70] D. Guo, G. Xie, J. Luo, ***J. Phys. D. Appl. Phys.***, 47 (2014) 13001.

[71] S. Lee, S. U. -S. Choi, S. Li, J. A. Eastman, ***J. Heat Transfer***, 121 (1999) 280.

[72] Y. C. Cao, ***Science***, 297 (2002) 1536.

[73] E. Bayram, J. C. Linehan, J. L. Fulton, J. A. S. Roberts, N. K. Szymczak, T. D. Smurthwaite, S. Ozkar, M. Balasubramanian, R. G. Finke, ***J. Am. Chem. Soc.,*** 133 (2011) 18889.

[74] V. Artero, M. Fontecave, ***Chem. Soc. Rev.,*** 42 (2013) 2338.

[75] N. Yan, Y. Yuan, P. J. Dyson, ***Dalton Trans.,*** 42 (2013) 13294.

[76] R. H. Crabtree, ***Chem. Rev.,*** 112 (2012) 1536.

[77] S. B. Singh, P. K. Tandon, ***JEECE***, 2 (2014) 106.

[78] J. S. Bradley, ***Cluster Colloids,*** 00 (1994) 459.

[79] D. G. Duff, A. Baiker, ***Stud. Surf. Sci. Catal.,*** 91 (1995) 505.

[80] N. Toshima, ***NATO ASI Ser.,*** 12 (1996) 371.

[81] H. Boennemann, G. Braun, G. B. Brijoux, R. Brinkman, A. S. Tilling, S. K. Schulze, K. Siepen, ***J. Organomet. Chem.,*** 520 (1996) 143.

[82] K. Fugami, ***Organomet. News,*** 1 (2000) 25.

[83] A. B. R. Mayer, ***Polym. AdV. Technol.***, 12 (2001) 96.

[84] H. Bonnemann, R. Richards, ***Synth. Methods Organomet. Inorg. Chem.***, 10 (2002) 209.

[85] I. I. Moiseev, M. N. Vargaftik, ***Russ. J. Chem.,*** 72 (2002) 512.

[86] N. Toshima, T. Yonezawa, ***New J. Chem.***, 22 (1998) 1179.

[87] A. Eppler, G. Rupprechter, L. Guczi, G. A. Somorjai, ***J. Phys. Chem. B,*** 101 (1997) 9973.

[88] G. Schmid, ***Met. Cluster Chem.,*** 3 (1999) 1325.

[89] R. J. Puddephatt, ***Met. Cluster Chem.,*** 2 (1999) 605.

[90] C. R. Henry***, Appl. Surf. Sci.,*** 164 (2000) 252.

[91] T. P. St. Clair, D. W. Goodman, ***Top. Catal.,*** 13 (2000) 5.

[92] M. Kralik, B. Corain, M. Zecca, ***Chem. Pap.,*** 54 (2000) 254.

[93] C. C. Chusuei, X. Lai, K. Luo, D. W. Goodman, ***Top. Catal.,*** 14 (2001) 71.

[94] M. Bowker, R. A. Bennett, A. Dickinson, D. James,; R. D. Smith, P. Stone, ***Stud. Surf. Sci. Catal.,*** 133 (2001) 3.

[95] M. Kralik, A. Biffis, ***J. Mol. Catal. A: Chem.,*** 177 (2001)113.

[96] J. M. Thomas, R. Raja, ***Chem. Rec.,*** 1 (2001) 448.

[97] C. Mohr, P. Claus, ***Sci. Prog.,*** 84 (2001) 311.

[98] J. M. Thomas, B. F. G. Johnson, R. Raja, G. Sankar, P. A. Midgley, ***Acc. Chem. Res.,*** 36 (2003) 20.

[99] J. F. Sonnenberg, R. H. Morris, ***Catal. Sci. Technol.,*** 4 (2014) 3426.

[100] R. Nishio, M. Sugiura, and S. Kobayashi, ***Org. Lett.,*** 7 (2005) 4831.

[101] S. Gloggler, A. M. Grunfeld, Y. N. Ertas, J. McCormick, S. Wagner, P. P. M. Schleker, L. S. Bouchard, ***Angew. Chem. Int. Ed.,*** 54 (2015) 2452.

[102] B. Yoon, H. Kim, and C. M. Wai, ***Chem. Comm.,*** 00 (2003) 1040.

[103] M. B. Alqaragully, ***IJACSA***, 1 (2014) 48.

[104] X. Y. Chen, J. W. Chen, X. L. Qiao, D. G. Wang, X. Y. Cai, ***Appl. Catal. B: Environ.***, 80 (2008) 116.

[105] R. Kant, ***Natural Science***, 4 (2012) 22.

[106] M. N. Chong, B. Jin, C. W. K. Chow, C. Saint, ***Water Res.***, 44 (2010) 2997.

[107] M. A. Brown, S. C. DeVito, ***Grit. Rev. Env. Sci. Tec.***, 23 (1993) 249.

[108] https://www.slideshare.net/Shameem_Byadgi/decolourization-of-textile-dye-effluents, visited **March, 2018.**

[109] J. Riu, I. Schonsee, D. Barcelo, ***J. Mass Spect.***, 33 (1998) 653.

[110] R. G. Saratale, G. D. Saratale, J. S. Chang, S. P. Govindwar, ***Bioresour. Technol.***, 100b (2009) 2493.

[111] U. Pagga, D. Brown, ***Chemosphere***, 15 (1986) 479.

[112] AEPA (Australian Environmental Protection Authority), ***Environmental guidelines for the textile dyeing and finishing industry, State government of Victoria, Melbourne, Victoria, Australia, 1998.***

[113] B. G. Uzo, E. O. Edward, A. L. Fredrick, D. O. Lawerence, ***J. Pure. AppL. Sci.***, 12 (2006) 69.

[114] M. Banat, P. Nigam, D. Singh, R. Marchant, ***Biores. Technol.***, 58 (1996) 217.

[115] Y. M. Slokar, A. M. Le Marechal, ***Dyes Pig.***, 37 (1998) 335.

[116] M. V. B. Zanoni, P. A. Carneiro, ***Ciencia Hoje.***,99 (2001) 61.

[117] A. Kunz, P. Peralta-Zamora, S. G. de Moraes, N. Duran, ***Quimica Nova.***, 25 (2002) 78.

[118] P. Cooper, ***J. Soc. Dyers Col.***, 109 (1993) 97.

[119] P. Grau, ***Water Sci. Technol.***, 24 (1991) 97.

[120] O. J. Hao, H. Kim, P. C. Chiang, ***Crit. Rev. Env. Sci. Tech.***, 30 (2000) 449.

[121] J. E. F. F. Judkins Jr, ***J. Water Pollut. Control Fed.***, 56 (1984) 642.

[122] T. G. Southern, ***Technical solutions to the color problem: a critical review, in Color in dyehouse effluent, P. Cooper, Society of Dyers and Colorists: Bradford, England. 1995.***

[123] O. Tunay, I. Kabdasli, G. Eremektar, D. Orhon, ***Water Sci. Technol.***, 34 (1996) 9.

[124] P. C. Vandevivere, R. Bianchi, V. Weaver, ***J. Chem. Technol. Biotechnol.***, 72 (1998) 289.

[125] A. Pala, E. Toket, ***Water Res.***, 36 (2002) 2920.

[126] Y. Fu, T. Viraraghavan, ***Bioresource. Technol.***, 79 (2001) 251.

[127] O. Abdelwahab, A. El-Nemr, A. El-Sikaily, A. Khaled, ***Chem. Ecol.***, 22 (2006) 253.

[128] G. Akkaya, I. Üzun, F. Guzel, ***Dyes Pigm.***, 73 (2007) 168.

[129] S. K. Yesiladali, G. Pekin, H. Bermek, I. A. Alaton, D. Orhon, C. Tamerler, ***World J. Microbiol. Biotechnol.***, 22 (2006) 1027.

[130] K. H. Chan, W. Chu, ***Water Res.***, 43 (2009) 2513.

[131] P. Neta, V. Madhavan, H. Zemel, R. W. Fessenden, ***JACS***, 99 (1977) 163.

[132] R. L. Johanson, P. G. Tratnyek, R. O. Johnson, ***Enviro. Sci. Technol.***, 42 (2008) 9350.

[133] C. J. Liang, H. W. Su, ***Ind. Eng. Chem. Res.***, 48 (2009), 5558.

[134] L. Dogliotti, E. Hayon, ***J. Phy. Chem.***, 71 (1967) 2511.

[135] V. Dulman, M. Ungureanu, G. Nemtoi, V. I. Popa, ***Cellul. Chem. Technol.***, 38 (2004) 353.

[136] G. P. Anipsitakis, D. D. Dionysiou, ***Enviro. Sci. Technol.***, 37 (2003) 4790.

[137] E. Hayon, A. Treinin, J. Wilf, ***JACS***, 94 (1972) 47.

[138] B. R. Travis, M. Sivakumar, G. O. Hollist, B. Borhan, ***Org. Lett.***, 5 (2003) 1013.

[139] J. L. Arnau, P. A. Giguere, ***Can. J. Chem.,*** 48 (1970) 3903.

[140] P. Neta, R. E. Huie, A. B. Ross, ***J. Phys. Chem. Ref. Data.***, 17 (1988) 1027.

[141] Y. H. Guan, J. Ma, X. C. Li, J. Y. Fang, L. W. Chen, ***Environ. Sci. Technol.***, 45 (2011) 9308.

[142] S. Y. Yang, P. Wang, X.Yang, L. Shan, W. Y. Zhang, X. T. Shao, R. Niu, ***J. Hazard. Mater.***, 179 (2010) 552.

[143] S. N. Su, W. L. Guo, C. L. Yi, Y. Q. Leng, Z. M. Ma, ***Ultrason. Sonochem.***, 19 (2012) 469.

[144] G. P. Anipsitakis, D. D. Dionysiou, ***Environ. Sci. Technol.***, 38 (2004) 3705.

[145] M. Murugavelu, P. Andal, S. Shailaja, M. S. Ramachandran, ***J. Mol. Catal. A – Chem.***, 306 (2009) 1.

[146] M. Ahmad, A. L. Teel, R. J. Watts, ***Journal of Contaminant Hydrology,*** 115 (2010) 34.

[147] D. A. House, ***Chemical Review,*** 62 (1962) 185.

[148] P. Durrant, B. Durrent, ***Introduction to Inorganic Chemistry, Longman, 1962***.

[149] J. M. Anderson, J. K. Kochi, ***J. Am. Chem. Soc.,*** 92 (1970) 1651.

[150] C. Walling, D. M. Camaioni, ***J. Org. Chem.,*** 43 (1978) 3266.

[151] C. Arnoldi, A. Citterio, F. Minisci, ***J. Chem. Soc., Perkin Trans.,*** 2 (1983) 531.

[152] A. Citterio, C. Arnoldi***, J. Chem. Soc. Perkin Trans.,*** 1 (1983) 891.

[153] C. Giordano, A. Belli, A. Citterio, F. Minisci, ***J. Org. Chem.,*** 44 (1979) 2314.

[154] C. Giordano, A. Belli, A. Citterio, F. Minisci, ***J. Chem. Soc., Perkin Trans***., 1 (1981) 1574.

[155] S. Yamazaki, Y. Yamazaki, ***Chem. Lett.,*** 00 (1989) 1361.

[156] C. I. Nikishin, I. E. Troyansky, I. Lazareva, ***Tetrahedron Lett.,*** 25 (1984) 4987.

[157] S. Tyrlik, I. Woiochowicz, ***Bull. Soc. Chim. Fr.,*** 00 (1973) 2147.

[158] J. E. McMurry, M. P. Fleming, ***J. Am. Chem. Soc.,*** 96 (1974) 4708.

[159] H. Wynberg, K. Lammertsma, L. A. Hulshof, ***Tetrahedron Lett.,*** 16 (1975) 3749.

[160] R. F. Langler, T. T. Tidwell, ***Tetrahedron Lett.,*** 16 (1975) 777.

[161] W. M. Latimert, ***The oxidation states of the elements and their potentials in aqueous solution, Prentice Hall, Englewood Cliffs, New York. N.Y. 1952.***

[162] Usepa, ***Fed. Reg.,*** 63 (1998) 69389.

[163] L. Hou, H. Zhang, X. Xue, ***Sep. Purif. Technol.,*** 84 (2012) 147.

[164] H. Lin, J. Wu, H. Zhang, ***Sep. Purif. Technol.,*** 117 (2013) 18.

[165] J. Wu, H. Zhang, J. Qiu, ***J. Hazard. Mater.,*** 215-216 (2012) 138.

[166] M. H. Rasoulifard, R. Marandi, H. Majidzadeh, I. Bagheri, ***Environ. Eng. Sci.,*** 28 (2011) 229.

[167] S. Rodriguez, L. Vasquez, D. Costa, A. Romero, A. Santos, ***Chemosphere***, 101 (2014) 86.

[168] S. Su, W. Guo, Y. Leng, C. Yi, Z. Ma, ***J. Hazard. Mater.***, 244– 245 (2013) 736.

[169] X. Chen, J. Chen, X. Qiao, D. Wang, X. Cai, ***Appl. Catal. B: Environ.***, 80 (2008) 116.

[170] P. S. S. Kumar, R. Sivakumar, S. Anandan, J. Madhavan, P. Maruthamuthu, M. Ashokkumar, ***Water Res.***, 42 (2008) 4878.

[171] J. Zhang, M. Chen, L. Zhu, ***RSC Adv.***, 6 (2016) 758.

[172] J. Zhang, M. Chen, L. Zhu, ***RSC Adv.***, 6 (2016) 47562.

[173] Y. Li, Z. Yang, H. Zhang, X. Tong, J. Feng, ***Colloids Surf. A: Physicochem. Eng. Asp.***, 529 (2017) 856.

[174] T. D. Singh, S. D. Henam, T. G. Singh, ***Green Materials***, 5 (2017) 165.

[175] T. J. I. Edison, M.G. Sethuraman, ***Process Biochem.***, 47 (2012) 1351.

[176] R. Vinayagam, T. Varadavenkatesan, R. Selvaraj, ***Green Process Synth.***, 7 (2017) 30.

[177] V. K. Vidhu, D. Philip, ***Micron***, 56 (2014) 54.

[178] E. Alzahrani, ***World Journal of Nano Science and Engineering***, 5 (2015) 10.

[179] M. Ramkrishna, D. R. Babu, R. M. Gengan, S. Chandra, G. N. Rao, ***J. Nanostruct. Chem.***, 6 (2016) 1.

[180] B. R. Ganapuram, M. Alle, R. Dadigala, A. Dasari, V. Maragoni, V. Guttena, ***Int. Nano Lett.***, 5 (2015) 215.

[181] A. S. Kumari, M. Venkatesham, D. Ayodhya, G. Veerabhadram, ***Appl. Nanosci.***, 5 (2015) 315.

[182] G. E. Hoag, J. B. Collins, J. L. Holcomb, J. R. Hoag, M. N. Nadagouda, R. S. Varma, ***J. Mater. Chem.***, 19 (2009) 8671.

[183] E. C. Njagi, H. Huang, L. Stafford, H. Genuino, H. M. Galindo, J. B. Collins, G. E. Hoag, S. L. Suib, ***Langmuir***, 27 (2011) 264.

[184] T. Shahwana, S. A. Sirriah, M. Nairat, E. Boyacı, A. E. Erolu, T.B. Scott, K. R. Hallam, ***Chem. Eng. J.***, 172 (2011) 258.

[185] L. Huang, X. Weng, Z. Chen, M. Megharaj, R. Naidu, ***Spectrochim. Acta A***, 117 (2013) 801.

[186] Y. Kuang, Q. Wang, Z. Chen, M. Megharaj, R. Naidu, ***J. Colloid Interface Sci.***, 410 (2013) 67.

[187] Z. Wang, C. Fang, M. Megharaj, ***ACS Sustainable Chem. Eng***., 2 (2014) 1022.

[188] N. Gupta, H. P. Singh, R. K. Sharma, ***J. Mol. Catal. A: Chem.***, 335 (2011) 248.

[189] M. Nasrollahzadeh, M. Sajjadi, H. R. Dasmeh, S. M. Sajadi, ***J. Alloy Compd.***, 763 (2018) 1024.

Chapter – 2

Instrumentation and Materials

The present chapter illustrates the detail of the instruments of all the characterization and analytic tools, information of the chemicals, reagents and their solutions with other details of specifications employed in the degradation processes and kinetic study. Two sections are existent in this chapter:

Section I

2.1. Instrumental Techniques

This section includes the basic principles and theories of the main analytical approaches and characterization techniques. This section of this chapter also concerns with the details of different instrumental techniques such as electron microscopy, XRD, Zetasizer, LC-MS, FT-IR spectroscopy, UV-Visible spectroscopy etc. adopted for characterization of nanoparticles and studies the degradation of dyes in the presence of nanocatalysts.

2.1.1. Ultraviolet-Visible Spectrophotometer

Ultraviolet–visible spectroscopy (UV-Vis or UV/Vis) is an absorption spectroscopy or reflectance spectroscopy. It uses light in the ultraviolet and visible range. The absorption or reflectance in the visible range directly affects the colour of the chemicals involved. In this region of the electromagnetic spectrum, atoms and molecules undergo electronic transitions. Fluorescence spectroscopy is opposite to absorption spectroscopy, in the fluorescence electrons transitions from the excited state to the ground state, while in absorption electrons transitions from the ground state to the excited state.

Molecules having π-electrons or non-bonding electrons (n-electrons) which are excited in higher anti-bonding molecular orbitals may absorb the energy in the form of ultraviolet or visible light. There are four possible types of transitions (π-π*, n-π*, σ-σ*, and n-σ*), and they can be ordered as follows: σ-σ* > n-σ* > π-π* > n-π* [1].

In analytical chemistry UV-Visible spectroscopy is used for the quantitative determination of different analytes, such as transition metal ions,

highly conjugated organic compounds, and biological macromolecules and this technique readily allows determining the concentrations of substances, to study the rates of reactions, to determine rate equations for reactions, with the help of these a mechanism can be suggested. Generally, spectroscopic analysis is carried out in liquid solutions but solids and gasses may also be studied [1].

UV-Vis spectroscopy is useful for analysis metal nanoparticles dispersed in a solvent or embedded in the insulator matrix. In this analysis, absorption of incident radiation takes place due to surface plasmon resonance (SPR) of the metal nanoparticles. Surface plasmon resonance is essentially the light waves that are trapped on the surface because of their interaction with the free electrons of the metal [2].

For the kinetic study of reaction, occurring in solution must present colour or brightness shifts from reactants to products. The rate constant of a degradation of dye can be determined by measuring the UV-Vis absorbance spectrum at specific time intervals. If the reaction is first order, it would have the integral first order rate law: $\ln [A](\text{time } t) = -kt + \ln[A](\text{initial})$. Then, plot the graph of natural log (ln) of the concentration [A] versus time obtained a line with slope –k, which is negative the rate constant. According to the mechanism of the reaction different rate orders have different integrated rate laws. The degradation of dye was observed by changes in absorbance is useful in the kinetics study.

The kinetic study of the degradation of dye and optical characterization of the synthesized metallic nanoparticles was observed in this research work with the help of a double beam 3000^{+} LABINDIA, UV-Vis spectrophotometer and a cell of 1.0 cm path length in the spectral range 200-800 nm. Effect of temperature on kinetic study of reaction was studied by a Peltier accessory (temperature-Controller) model PTC-2 is linked with the UV-Visible spectrophotometer. Two lamp combinations are used in double beam spectrophotometer one is deuterium lamp used for UV part and second is tungsten lamp used for the visible part. Sample cell is made by Quartz and light beam travels a distance of 1 cm through

the sample. For obtained UV spectra of our sample first done baseline by reference so that other reagent peaks were nullified, after that obtain the spectra of reaction mixture. Spectra were plotted between wavelength v/s absorbance [3, 4].

2.1.2. Centrifuge

Centrifugation is a technique that advantages to separate mixtures by applying centrifugal force. A centrifuge is a device, generally driven by an electric motor that puts an object, like a rotor, in a rotational movement around a fixed axis. Sedimentation is the principle of centrifuge: Under the effect of gravitational force (g-force), materials separate according to their density.

In present research work Centrifuge (Remi C-854/6 Laboratory) with 8x15 swings out heads were used. For the preparation of metal nanoparticles purified pellets, nanoparticles were put in tubes and these tubes centrifuged at 3500 rpm for 15 minutes then pellets were re-dispersed in deionized water. This process (centrifugation and re-dispersion) was repeated three times to confirm better separation of free entities from the metal nanoparticles. Purified pellets were separate out by Whatman filter paper and then dried for further use in FT-IR and XRD.

2.1.3. Vacuum Oven

Centrifuged samples dried in vacuum oven at 70 °C for 2 hours (LABPRO INTERNATIONAL). The oven consist double wall with chambers size is 250 x 250 mm and 12 L capacity, inner round chamber made of stainless steel, exterior made of mild steel duly finished in white stoving enamel/powder coated paint with mat finished colour combinations. The oven work on temperature range 50 °C to 150 °C ± 3 °C. The body capable of withstanding the vacuum of 760 mm Hg, workable on 220 VAC 50 Hz single phase and dried samples were used for further characterization.

2.1.4. X-Ray Diffractometer

X-ray diffraction (XRD) is an analytical technique mainly used for phase determination of a crystalline material and give knowledge about unit cell dimensions. The analysed material is finely grind, homogenized, and average bulk composition is determined.

X-ray diffraction is depending on constructive interference of monochromatic X-rays and a crystalline sample. These X-rays are produced by a cathode ray tube and then filtered to produce monochromatic radiation, collimated to concentrate, and focussed toward the sample. The collaboration of the incident rays with the sample generates constructive interference when situations satisfy Bragg's Law ($n\lambda = 2d \sin \theta$). This law shows the relation among the wavelength of electromagnetic radiation, the diffraction angle and the lattice spacing present in a crystalline sample. These diffracted X-rays are detected, processed and counted. 2θ angles range is used for scanning the sample, all possible diffraction angles of the lattice should be achieved because of the random orientation of the powdered material. Change of the diffraction peaks to d-spacings permits identification of the mineral as each mineral has a set of unique d-spacings. Usually, this is gained by comparison of d-spacings with standard reference patterns [5].

X-ray diffractometers contain of three basic elements like an X-ray tube, a sample holder, and an X-ray detector. For X-rays are generated in a cathode ray tube by heating a filament to produce electrons, accelerating the electrons directed towards a target by applying a voltage, and bombarding the target material with electrons. When electrons have sufficient energy to remove inner shell electrons of the target material, characteristic X-ray spectra are produced. These spectra consist of several components, the most common being K_α and K_β.

X-ray powder diffraction is most broadly used to determine of unknown crystalline materials. Identification of unknown solids is serious to studies in geology, environmental science, material science, engineering and biology [6].

XRD analysis was done by X'PERT PRO Panalytical Instrument (SAIF/CIL, Panjab University, Chandigarh). In this instrument copper used as an anode, 2θ range starts from 10.0 to 89.9. For analysis, centrifuged and dried samples (2 g) were grind in mortar and pestle then powdered sample keeps into samples holder. The powder was pressed by glass slide for the powder to "stick" in well. Enter sample into XRD machine to identify unit cell dimensions [7].

2.1.5. Fourier Transform Infrared Spectrophotometer

Fourier Transform Infrared Spectroscopy (FTIR) is useful technique for identifying chemical bond in molecules. It can be utilized to know some components of an unknown mixture and for the analysis of solids, liquids, and gasses. In the Fourier Transform Infrared Spectroscopy, data is collected and converted from an interference pattern to a spectrum. It is a powerful tool for identifying types of chemical bonds in a molecule by producing an infrared absorption spectrum that is like a molecular "fingerprint". The wavelength of light absorbed is characteristic of the chemical bond as can be seen in IR spectrum [8].

Bonds are present in molecules are vibrate at several frequencies which is depend on the elements are present in molecule and the type of bonds. Any bond vibrates on several specific frequencies. Quantum mechanics illustrate that these frequencies related to the ground state (lowest frequency) and many excited states (higher frequencies). One way to cause the frequency of a molecular vibration to increase is to excite the bond due to absorb light energy. Transition between given two states, the energy equal to the difference in the energy between the ground state and the excited state [9].

For getting spectra between wavelength and transmittance ALPHA-T model, Bruker, Germany spectrometer was used range is 400-4000 cm^{-1} and resolution is 4 cm^{-1}. For preparation of pellet of sample first pellet holder, pestle, mortar, dies etc. were washing with alcohol and then 1:4 ratio centrifuged dried sample and KBr grind with a pestle and mortar. Place just enough grinded sample to cover the bottom in pellet dies and press at 0-10 Tones. Then carefully remove

the pressed sample from die and place in the FTIR sample holder for FTIR analysis. The pressed disc should be nearly clear if properly made [10, 11].

2.1.6. Ultrasonic Processor

The ultrasonic processor works on principle that ultrasound waves transfer energy into the sample, causing turbulence and friction in the liquid so that clear sample were prepared.

The ultrasonic processor was used to prepare the nanoparticles samples for characterization by the electron microscopy (Transmission Electron Microscopy (TEM), Scanning Electron Microscopy (SEM)) and Zetasizer analysis. The dispersed nanoparticles were sonicated in Ultrasonic processor (model -Ultramet 2005 (Buehler), USA) (115 VAC, 60 Hz) with a 9.5 L capacity quickly cleans samples to prepare for the next preparation step and 0- 60 minute is timer range.

2.1.7. Transmission Electron Microscopy

Transmission Electron Microscopy is a major analytical technique in physics, chemistry, and biological sciences. In nanotechnology the results of TEM analysis plays a most important role in imaging morphology and distribution of nanomaterial with high resolution and provide information about the structure, crystallography nature is studied by the diffraction mode.

The basic principle of TEM is based on Light Microscope, uses electrons instead of light and electromagnetic lenses to focus the electrons into a very thin beam rather than glass lenses focus the light. TEM use electrons as “Light source” and their lower wavelength, high energy makes it possible to get thousand times better resolution than Light Microscope [12]. Electron source present at the top of the microscope emits electrons that travel through a vacuum in the column of the microscope then travels through the specimen to form an image. The specimen is most often an ultrathin section less than 100 nm thick or a suspension on a grid at the bottom of the microscope the unscattered electrons hit a fluorescent screen.

This screen gives rise to a "Shadow image" of the specimen with its different parts displayed in varied darkness according to their density [12].

In TEM analysis at first electrons emits by electron gum (these electrons accelerate and have a potential difference in the range 40-200 kV) and operates under vacuum because electrons are easily scattered at atmospheric pressure [13]. Electron gun below electron on two or more condenser lenses. These lenses are electromagnetic lenses. An aperture is present between the condenser lenses to control electron beam diameter as it hits the specimen. Now electron beam interacts with the specimen and unscattered beam passes through the objective lens. The work of the objective lens is either image or diffraction pattern made of the specimen. To identify the crystallographic structure of the material electron diffraction patterns is used. After beam passes through objective lenses, produced 50-100 times magnified image [13]. This is further magnified by a series of intermediate lenses and finally projected on to the fluorescent screen.

The TEM analysis results presented in this thesis, transmission electron microscope Model- Tecnai G^2 20 (FEI) S-Twin with 200 kV energy has been used. The Tecnai G^2 supports a wide range of techniques including high resolution scanning STEM diffraction and chemical analysis with on BF/DF axis detectors provide the Z-contrast imaging. The high angle, annular dark field detector generates atomic resolution dark field STEM images. The equipment provides a point resolution of 0.24 nm, line resolution of 0.14 nm and STEM resolution of 1.0 nm. EDAX gives the elemental composition of the material and the facility available in Malaviya National Institute of Technology Jaipur, Jaipur (Rajasthan).

For TEM characterization the sample were prepared as follows: the drops of the sonicated sample were mounted on the copper grid using a micropipette, thin sections of material are sufficiently robust to spread out over the grid without additional support. This copper grid was allowed to stand for 2 minutes, the extra

solution was removed using a blotting paper and the grid allowed to dry prior to TEM analysis [14].

2.1.8. Scanning Electron Microscopy

The scanning electron microscope (SEM) analysis is same as the transmission electron microscope (TEM) analysis because both have a beam of electrons focussed at the specimen. The certain features, such as the electron gun, condenser lenses and vacuum system, are same in both instruments, though the ways in which the images are produced and magnified are totally different. The TEM analysis gives information about the internal structure of thin specimens whereas the SEM analysis is used to study the surface, or near the surface, the structure of specimens [13].

In the SEM instrument includes an electron source; a condenser lens; a deflector; an aberration correction device; a convergence aperture; and a detector [15]. In this technique, an electron beam is thermionically emitted from an electron gun. The electron beam, which has an energy ranging from 0.2 keV to 40 keV, is directed by one or two condenser lenses to a spot about 0.4 nm to 0.5 nm in breadth. In the final lance this beam passes over pairs of scanning coils or pairs of deflector plates in the electron column, typically in the final lens, which are responsible for deflection of the beam in the *x* and *y*-axes so that it scans in a raster fashion over the sample surface [16].

Accelerated electrons in an SEM carry significant amounts of kinetic energy, and this energy is dissipated as a variety of signals produced by electron-sample interactions when the incident electrons are decelerated in the sample. These signals include secondary electrons, backscattered electrons, diffracted backscattered electrons, X-Ray, visible light, and heat. Secondary electrons and backscattered electrons are commonly used for imaging samples: secondary electrons are most valuable for showing morphology and topography on samples and backscattered electrons are most valuable for illustrating contrasts in the

composition in multiphase samples. X-Ray is used for elemental and crystalline structure analysis [17].

Nova Nano FE-SEM 450 (FEI) instrument used for SEM analysis in the laboratory of Malaviya National Institute of Technology Jaipur, Rajasthan. Ultra-high resolution provied by the instrument for characterization and analysis giving precise, true nanometer scale information. Advanced optics and detection, including beam deceleration, in lens ETD (SE), TLD (custom), a lens mounted DBS & LVD offer the best selection of information and image optimization. Beam landing energy can go down from 30 keV to 50 eV. It gives a resolution of 1.4 nm at 1 kV (TLD-SE) & 1 nm at 15 kV (TLD-SE). The FE-SEM is coupled to EDAX detector for measuring the elemental chemical composition of materials. For SEM analysis the samples were prepared as follows: 30µl aliquots of sonicated sample extracted and deposited on the glass slide or carbon tap by micropipette. The stub was dried and keeps it on the sample holder for SEM analysis [18].

2.1.9. Zetasizer

The Zetasizer Nano range of instruments provides the ability to measure two characteristics of particles or molecules in a liquid medium that is particles size and Zeta potential. This technique is work over a wide range of concentrations of solutions.

Size of particle determined by measuring the random changes in the intensity of light scattered due to their random motion from a suspension or solution. This technique is called as dynamic light scattering (DLS). Random motion of particles related to their size so smaller particles move faster than larger particles. The speed of Brownian motion is also determined by the temperature, therefore precision temperature control is essential for accurate size measurement. To measure the diffusion speed, the speckle pattern produced by illuminating the particles with a laser is observed. The intensity changes are analyzed with a digital

autocorrelator which generates a correlation function and curve gives the information about size and the size distribution [19].

The Zetasizer Nano series calculates the zeta potential by determining the Electrophoretic Mobility with applying the Henry equation. The development of a net charge at the particle surface affects the distribution of ions in the surrounding interfacial region, resulting in an increased concentration of counter ions to the surface. Thus an electrical double layer exists around each particle and the potential exists at this boundary is known as the Zeta potential. The magnitude of the zeta potential gives an indication of the potential stability of the colloidal system. If the particles present in suspension have a large negative or positive zeta potential then they will tend to repel each other and there is no tendency to flocculate. However, if the particles have low zeta potential values then there is no force to prevent the particles coming together and flocculating [19].

In this research work Zetasizer ver. 7.11 (Malvern), UK was used to analyze the average size and zeta potential of the colloidal solution of metal nanoparticles. This analysis was done in the laboratory of Malaviya National Institute of Technology Jaipur, Jaipur (Rajasthan). For this analysis, sonicated sample poured in the disposable folded capillary cell then the cell was placed in the zetasizer instrument and obtained the electronic output of average size. To determine zeta potential value, the sonicated sample pour in dip cell of the instrument [20].

2.1.10. Liquid Chromatography – Mass Spectroscopy

Liquid chromatography-mass spectrometry (LC-MS) is an analytical chemistry technique which is based on the combinations of the physical separation abilities of liquid chromatography with the mass analysis capabilities of mass spectrometry (MS). The typical LC-MS system is a combination of HPLC with MS using interface (ionization source). The sample is separated by LC, and the separated sample species are sprayed into the atmospheric pressure ion source, to ions converted in the gas phase. The mass analyser is used to categorise ions

according to their mass to charge ratio. The separated ion identifies and quantifies directed to a photo or electron multiplier tube detector amplifies the signal generated from each ion. Result of mass spectrum (a plot of the ion signal as a function of the mass-to-charge ratio) is generated, which is used to determine the elemental nature of a sample, the masses of particles of molecules, and to elucidate the chemical structures of molecules [21, 22].

The advantages of this technology like sensitivity, specificity, and precision as analysis is done at the molecular level. This technique can be capable to analyse inorganic compounds, organic compounds and biochemical compounds commonly found in complex samples of environmental and biological origin [22].

An interface is present in LC-MS that efficiently transfers the separated components from the LC column into the MS ion source. While the mobile phase in an LC system is a pressurized liquid, the MS analysers commonly operate under vacuum. Therefore, the eluate directly pumped from the LC column into the MS source is not possible. LC-MS interfaces are grounded on atmospheric pressure ionization (API) strategies such as electrospray ionization (ESI), atmospheric pressure chemical ionization (APCI), and atmospheric pressure photo-ionization (APPI) [23].

Intermediates and end products obtained during dye degradation process were detected by LC-MS technique. Mass/charge ratio is used to determine the molecular ions of unknown products. When fragmentation voltage of LC-MS increases more fragments are observed to facilitate product determination. This study, for LC-ESI-MS analysis Waters, Micromass Q-TOF micro was used with parting Module: Waters Alliance 2795; LC Column: Unisol YVR C18; Ionization: Electro spray Positive (ES+); Acquisition: MRM, unit resolution; Injection Volume: 20 micro liters; Flow rate: 0.5 ml per min and for Mass spectrometer, Desolvation Gas: 550 Lts/Hr; Cone Gas: 30 Lts/Hr; Desolvation Temperature: 300 °C; Source Temperature: 110 °C; Capillary Voltage: 3000 V; Cone Voltage: 30 V; Collision energy 4 ev; Gases used N_2 and Argon; Mobile Phase used:

20/80:H_2O: MeOH; 6-7 bar (90-100 psi) pressure is used for N_2 supply and fro Argon is 5-6 bar etc. parameters were used. LC-MS characterization was done from SAIF/CIL, Panjab University, Chandigarh [24].

2.1.11. Chemical Oxygen Demand (COD) and Biological Oxygen Demand (BOD)

To determine the COD, BOD the Winkler method with azide modification was used.

Chemical Oxygen Demand (COD) is the total measurement of all chemicals (organics and inorganics) in the water samples.

Twenty ml sample was diluted to 40 ml with distilled water then add pumice stone, 10 ml $K_2Cr_2O_7$, 30 ml H_2SO_4 containing Ag_2SO_4. Now the flask of the mixture connected to condensor and reflux for minimum 2 h. After that cool the mixture and titrate excess $K_2Cr_2O_7$ with ferrous ammonium sulphate using ferroin indicator and sharp colour change from blue green to wine red indicates end-point. The same process was applied for the blank sample using distilled water instead of sample.

Calculation:

$$COD\ mg/l\ = \frac{(a-b)\ x\ N\ x\ 8000}{ml\ of\ \ Sample\ taken}$$

Where:
a = ml. of Ferrous ammonium sulphate used for titration of blank
b = ml. of Ferrous ammonium sulphate used for titration of sample
N = normality of $(NH_4)_2Fe(SO_4)_2$ (Ferrous ammonium sulphate)

Biochemical Oxygen Demand (BOD) is a measure of, the amount of oxygen that require for the microorganism to degrade the organic components present in water samples.

Preparation of dilution water: First aerate the required volume of distilled water in a container by bubbling compressed air for 1-2 days and maintain the temperature near 20 °C. Then add 1 ml each of phosphate buffer, magnesium

sulphate, calcium chloride and ferric chloride solution for each liter of dilution water.

Dilution of sample: First neutralize the sample, and then remove chlorine content by using Na_2SO_4. Take four BOD bottles and add 10 ml sample in two bottles, then fill the remaining volume with dilution water. Remaining two BOD bottles fill with dilution water for blank experiment, immediately close the bottles to avoid the air bubble in the bottles and shifted to the incubator (Labline Incubator Sun Instruments Pvt. Ltd. Ahmedabad (India)) at 20 °C for 5 days. Analyse dissolve oxygen immediately and after 5 days incubation.

Test of dissolved oxygen: In BOD bottles add 2 ml manganous sulfate ($MnSO_4.H_2O$) solution followed by 2 ml of the alkali-iodide-azide reagent and allow reacting the solution with the present oxygen in the sample. When precipitates are settled down at the bottom add 2 ml of concentrate sulfuric acid, mix well to dissolve the precipitates. Take sample from BOD bottle into an Erlenmeyer flask, titrate immediately with sodium thiosulfate solution using starch indicator until blue color disappear.

Calculation:

Blank correction = B.R. for blank at D_0 – B.R. for blank at D_5

BOD mg/l = [(B.R. for sample at D_0 –D_5)– blank correction] x dilution factor

$$Dilution\ factor = \frac{Bottle\ volume\ (300\ ml)}{Sample\ volume}$$

Where:
B.R. = burette reading
D_0 = Initial
D_5 = Day five after incubation

BOD and COD measurments done from Rajasthan state pollution control board, Kota, Rajasthan.

2.1.12. Electronic Balance

Citizen electronic balance (model- CX 220) was used for weighing reagents. The weighing range of balance is 0.0001 mg and 220 g respectively.

2.1.13. pH – Meter

To determine the pH of the synthesized nanoparticles and the reaction mixtures, Systronic digital pH meter. Model MAC (MSW-552) was used with maximum uncertainty in pH of ±0.01 unit. To determine the pH of solution first calibrate the pH meter using buffer solutions of different pH such as 7.0, 4.0, 9.2. Thoroughly wash the pH electrode between measurements with distilled water to avoid carryover impurity of the tested solutions. Softly blot the electrode on a tissue paper to remove the excess rinse water and do not rub the bulb to avoid build-up static charge.

2.1.14. Magnetic Stirrer with Hot Plate

Magnetic stirrer with the hot plate was used for the synthesis of nanoparticles (MSW-313, MAC) at 600 rpm (range 0-1200 rpm), stirrer work on 220/230 volts AC supply and temperature 0-100 °C. The synthesis process of nanoparticles and size of nanoparticles are also affected by speed of stirring and reaction temperature.

Section II

2.2. Materials

The section deals with the details of all reagents employed in this study and the details regarding methods of preparation of various solutions. Chromic acid and doubly distilled water was used for cleaning glassware, which were used for handling chemicals in practical work and double distilled water also used for preparing all solutions.

2.2.1. Silver Nitrate

Silver nitrate is an inorganic compound and colourless crystalline solid. Lunar caustic is another name of silver nitrate. A solution of silver nitrate (E.

Merck) was prepared by dissolving an required amount of $AgNO_3$ with the addition of double distilled water. Prepare solution were kept in dark bottle to avoid the photodecomposition and also kept the solution 4 °C temperature so that it do not show any other decomposition for appreciable longer period.

2.2.2. Copper(II) Chloride Dihydrate

Copper(II) chloride dihydrate (Cupric Chloride) is a blue-green crystalline solid. A fresh solution of copper chloride dihydrate (E. Merck) was prepared by dissolving an appropriate amount of $CuCl_2.2H_2O$ with the addition of double distilled water, make up to required volume in a volumetric flask.

2.2.3. Neem Leaf Broth

The plant *Azadirachta indica* (neem) was selected from Kota (Rajasthan) India, on the basis of cost-effective, easily available and medicinal property. Collected fresh and healthy leaves and rinsed thoroughly first with tap water followed by deionized water to remove all the dust and unwanted particles, leaves were dried in an oven for 15 minutes at 50 °C temperature and cut into small pieces. 10 g of finely incised leaves was transferred into 250 ml beaker containing 100 ml deionized water and stirred on magnetic stirrer at 80 °C for 20 minutes. The extract was then filtered twice through Whatman filter paper, then refrigerated (4 °C) in Erlenmeyer flasks for further experiments. In each and every step of the experiment, sterile conditions were maintained for the effectiveness and accuracy in results.

2.2.4. Methyl Orange

Methyl Orange is a mono-azo, water-soluble dye. Methyl orange is widely used in the textile, printing, paper manufacturing, pharmaceutical, food industries and also in research laboratories. This dye is mainly used as an acid-base indicator in the analytical chemistry laboratories [25]. The solutions of required concentration of this dye were prepared by dissolving the requisite amount of methyl orange (Sigma-Aldrich) in the known volume of double distilled water.

2.2.5. Orange G (Acid Orange 10)

Orange G is a synthetic anionic mono-azo dye used in dying of textile, food, paper industry, preparation of colour marker, and in many staining formulations [26]. Solutions of required concentration of orange G were prepared by dissolving the requisite amount of orange G (Sigma-Aldrich) in a known volume of double distilled water.

2.2.6. Peroxomonosulphate Solution

Peroxomonosulphate (PMS) was purchased from Sigma Aldrich by the name "Oxone". The solution of peroxomonosulphate (Sigma-Aldrich) was prepared by dissolving the requisite amount of its potassium salt in doubly distilled water and was kept in the black volumetric flask to avoid the photo-decomposition. It is a triple salt with the composition of $2KHSO_5 \cdot KHSO_4 \cdot K_2SO_4$ and form with higher stability. PMS is found to be 96% pure when analyzed by both ceremetrically and iodometrically [27]. This reagent was used without further purification because permanganate tests showed the absence of free hydrogen peroxide. However, tests for free H_2O_2 were negative. Freshly prepared solution of the peracid always used in kinetics as well as analytical studies.

2.2.7. Peroxodisulphate Solution

The peroxodisulphate (PDS) is a white powder. A fresh solution of PDS (Sigma-Aldrich) was prepared by dissolving an appropriate amount of PDS with the addition of double distilled water, make up to required volume in a volumetric flask.

2.2.8. Sodium Hydroxide

Sodium hydroxide solution was prepared by dissolving approximately weighed pellets of NaOH (BDH Analar) in double distilled water and solution was standardized by titration the known aliquot sample against the standard oxalic acid solution using phenolphthalein indicator [28, 29]. However, sodium

hydroxide solution was always used after standardizing because these solutions decline on standing at ambient temperature.

2.2.9. Sulfuric Acid Solution

For preparation of sulphuric acid (Merck) solution first dissolves the requisite volume of sulfuric acid in double distilled water and second, the solution was standardized against pre standardized solution of sodium hydroxide employing phenolphthalein as an indicator. The standardized solution was kept stoppered as a stock solution.

2.2.10. Ethanol (EtOH)

Ethanol is miscible with water and is a good general purpose solvent. Ethanol (E. Merck) is a volatile, colourless liquid that has a slight odour. It was used for testing free radicals formed in reaction mixture.

All other reagents such as hydrochloric acid, potassium bromide etc. were either of (BDH AnalaR) grade or (E. Merck) guaranteed grade and used as supplied. Double distilled water, second distillation being from alkaline permanganate solution in a glass assembly, was employed in all the solution preparations and kinetic studies. All glass vessels were used for storing the chemicals solutions and for kinetic studies of degradation process were either of pyrex or borosil makes. Synthesis process of nanoparticles and kinetic procedure and analysis of results were discussed in concerned chapters.

2.3 Reference

[1] H. Förster, ***Mol. Sieves***, 4 (2004) 337.

[2] W. L. Brans, A. Dereux, T. W. Ebbesen, ***Nature***, 424 (2003) 824.

[3] https://www.chemguide.co.uk/analysis/uvvisible/spectrometer.html, visited in ***May, 2018.***

[4] X. Xiong, B. Sun, J. Zhang, N. Gao, J. Shen, J. Li, X. Guan, ***Water Res.***, 62 (2014) 53.

[5] B. E. Warren, ***X-Ray Diffraction, Addison-Wesley, Reading, MA, 1969***.

[6] E. N. Maslen, A. G. Fox, M. A. O'Keefe, ***X-ray Scattering, in: E. Prince (Ed), International Tables for Crystallography, Kluwer Academic, Dordrecht, 2004***.

[7] H. Yang, J. Ouyang, A. Tang, Y. Xiao, X. Li, X. Dong, Y. Yu, ***Mater. Res. Bull.***, 41 (2006) 1310.

[8] W. M. Doyle, B. C. McIntosh, W. L. Clarke, ***Appl. Spectrosc.***, 34 (1980) 599.

[9] K.-P. Möllmann, M. Vollmer, ***Eur. J. Phys.***, 34 (2013) S123.

[10] http://web.mst.edu/~tbone/Subjects/TBone/chem224/FTIR%20Procedure.pdf, visited in ***May, 2018.***

[11] T. Zhang, Y. Chen, Y. Wang, J. L. Roux, Y. Yang, J. -P. Croue, ***Environ. Sci. Technol.***, 48 (2014) 5868.

[12] https://www.nobelprize.org/educational/physic/microscopes/tem, visited in ***Feb, 2018.***

[13] P. J. Goodhew, J. Humphreys, R. Beanland, ***Electron Microscopy and Analysis, Taylor and Francis, London and New York, 2001.***

[14] D. B. Williams, C. B. Carter, ***Transmission Electron Microscopy, A Textbook for Materials Science, Springer, New York***, 2009.

[15] K. Nakamura, H. Inada, ***Scanning transmission electron microscope and axial adjustment method thereof, US 2013/0112875 A1, May 9, 2013.***

[16] https://en.wikipedia.org/wiki/Scanning_electron_microscope, visited in ***Feb, 2018.***

[17] https://serc.carleton.edu/research_education/geochemsheets/techniques/SEM.html, visited in ***Feb, 2018.***

[18] J. Anuradha, A. Tasneem, S. A. Abbasi, ***Res. J. Biotech.***, 6 (2011) 69.

[19] http://149.171.168.221/partcat/wp-content/uploads/Malvern-Zetasizer-LS.pdf, visited in ***Feb, 2018.***

[20] file:///C:/Users/pc-4/Downloads/Zetasizer%20range.pdf, visited in ***May, 2018***.

[21] W. M. A. Niessen, A. P. Tinke, ***J. Chromatogr. A***, 703 (1995) 37.

[22] S. Parasuraman, R. Anish, S. Balamurugan, S. Muralidharan, K. J. Kumar, V. Vijayan, ***Pharmaceutical Methods***, 5 (2014) 47.

[23] J. J. Pitt, ***Clin. Biochem. Rev.***, 30 (2009) 19.

[24] A. J. Watkinson, E. J. Murby, S. D. Costanzo, ***Water Res.***, 41 (2007) 4164.

[25] A. Mittal, A. Malviya, D. Kaur, J. Mittal, L. Kurup, ***J. Hazard. Mater.***, 148 (2007), 229.

[26] X. Y. Chen, J. W. Chen, X. L. Qiao, D. G. Wang, X. Y. Cai, ***Appl. Catal. B***, 80 (2008) 116.

[27] K. Bottger, W. Bottger, ***Z. Anal. Chem.***, 70 (1927) 225.

[28] A. I. Vogel, ***A Text Book of Quantitative Inorganic Analysis, Longmans, UK***, 2 (1961) 240.

[29] C. J. Battaglia, J. O. Edwards, ***Inorg. Chem.***, 4 (1965) 552.

Chapter – 3

Experimental Investigation on The Synthesis of Metal Nanoparticles

3.1. Introduction

Nanoparticles (NPs) are being considered to be the fundamental building blocks of nanotechnology. Nanotechnology branch is interdisciplinary which includes physics, biology, chemistry, medicines and material science. Presently, synthesis of metal NPs has been reported by many physical and chemical means [1-4]. All reported chemical methods and energy-intensive routes, which make these choices eco-hazardous and preclude their applications in biology, medicine, and clinical field. Therefore developing environmental friendly protocols are the need of the hour in nanomaterial synthesis [5-7]. A focused integration of bio and nano-techniques for biosynthesis of NPs, known as biotechnology has emerged from nanotechnology [8-10]. These nano-products are unique not only in their treatment methodology but also due to their exclusivity in particle size, physical, biochemical, chemical properties and broad range of application as well. The current developing field of nanotechnology is at the primary stage of growth due to lack of implementation in large industrial scale. Hence there is need to design an economic, nontoxic and eco-friendly route of synthesis of metal nanoparticles in order to meet its growing demand in diverse fields. Synthesis of metal nanoparticles can be achieved through different methods such as chemical [11], electrochemical [12], radiation [13] and photochemical [14]. Chemical approach is the most popular method for the synthesis of nanoparticles. Though, some chemical methods cannot avoid the use of lethal chemicals in the synthesis protocol. Since metal nanoparticles are extensively applied to human contacting areas, there is rising need to develop environmental friendly process of nanoparticles synthesis that does not use toxic chemicals. Biosynthesis of nanoparticles using microorganism [15, 16, 17], enzyme [18] and plant extract [19] have been recommended as possible eco-friendly alternative to physical and chemical methods.

The biosynthesis of NPs has been mainly focused on noble metal NPs like silver, gold, platinum [20-25] and their alloys. Nobel metal nanoparticles such as gold, silver and platinum are well recognized to have significant applications in electronics, catalysis, environmental and biotechnology [26-28]. One such

important number of nobel metal nanoparticles is silver nanoparticles. Silver has long been recognized as having an inhibitory effect towards many bacterial strain and microorganism commonly present in medical and industrial processes [29]**.** The most widely use and known applications of silver and silver nanoparticles are in the medical and pharmaceutical products and are hence directly encountered by human system [30, 31]**.** Earlier the antifungal properties of silver were well incorporated in the field of medical science. Existing study also reports successful synthesis of silver nanoparticles through a green route where the reducing and capping agent selected was the leaf extract of Aloe Vera [32], *Acalypha indica* [33], *Garcinia mangostana* [34].

Amongst Nobel metal, Copper nanoparticles (CuNPs) are of great interest because of low cost, easy availability and properties possessed are similar to that of other metallic NPs [35-37]. CuNPs finds applications in heat transfer fluids, sensors, antimicrobial and catalysis [38-41]. Current literature also reports successful synthesis of CuNPs through a green route where *T. arjuna* bark broth [7], *Capparious zeylanica* leaf broth [42], *Ocimum sanctum* leaf broth [43, 44], *Syzygium aromaticum* (cloves) aqueous extract [45] and *vitis vinifera* leaf broth [46] as well as numerous other plant extract were used as reducing and capping agent. In fact, pure metallic CuNPs in an aqueous phase still challenge for the researcher. Furthermore, it is of interest to obtain monodispersed CuNPs by a simple and green route.

Indian greeneries are the major and economical source of medicinal plants and plant products. Usually medicinal plants have been widely utilized in Ayurveda. Recently many such plants have been gaining importance due to their unique properties and their multipurpose applicability in various developing fields of research and development. Though the medicinal importance of numerous plants was known, but the plant mediated metal nano-product is a relatively newer concept. Characteristics of nanoparticles influenced by the source of the plant extract [19] because each plant extract contain unique concentration and combination of organic reducing agents [47]. The invention of these new

biological sources for the synthesis of metal NPs is more valuable than chemical and physical methods as these sources are abundantly available, cost-effective and conveniently applicable. The plant extracts often contain flavonoids, proteins, terpenoids, polyphenols etc., these biomolecules act as reducing agent for metal ion and capping agents to minimize the agglomeration of NPs, thus improves the biological potential.

Here, we have developed a rapid, eco-friendly and convenient green route for the synthesis of metal nanoparticles such as AgNPs and CuNPs from their salt using leaf broth of Indian medicinal plant namely *A. indica*. *A. Indica* commonly known as neem belongs to meliaceae family and is well known in India and its neighbouring countries for more than 200 years as one of the most versatile medicinal plant having a wide spectrum of biological activity [48]. The influence of different parameters on the course of reaction such as reactant concentration, temperature, and pH were examined. The plant-mediated synthesized nanoparticles were characterized by different instrumental techniques and studied in details with all of their properties significant to prevailing technologies.

3.2. Bioreduction Method for Synthesis of Nanoparticles

Metal nanoparticles have been synthesized by physical and chemical methods for a long back time. However, biological synthesis of metal nanoparticles has been explored very recently. Plant extract used as biological reducing agent for metal ions has been known since the early 1900s. Though, the reduction products have not been studied. The synthesis of metal nanoparticles using natural products and chemical or physical methods has been shown similar results. The application of plant extracts for the green synthesis of metal nanoparticles has expanded considerable importance due to the boost of the chemical, physical biological and medicinal properties of particles synthesized by this method. Metal nanoparticles used as heat transfer fluids, conductors, sensors, electronics, and catalysis has great importance for their exceptional morphology (size and shape) dependent properties. Metal nanoparticles are noticeable due to

their simple synthesis process, variations in size as well as shape distribution [49, 50]. The biosynthesis of metal NPs has well-known huge consideration because of the awful requirement for environmentally recognized technologies in material synthesis. Hence, to develop environment-friendly routes for nanoparticle synthesis without using lethal chemicals is the rising need of the day [49, 50]. The environmentally maintainable synthesis of metal nanoparticles has managed to a few novel approaches. The fundamental steps in the biosynthesis of nanoparticles are first: bioreduction of nanoparticles, second: growth of nanoparticles and last third: stabilization of nanoparticles (**Figure 3.1**). Green synthesized metal nanoparticles, with microorganisms, plant extracts and natural compounds, has been led for many causes, containing eco-friendly ease of maintaining and cost effectiveness. Additional, it is also bigger by removing the processes of handling microbial cultures and can also be appropriately set up for large-scale nanoparticle synthesis [51, 52]. Many recent reports on the biosynthesis of metal nanoparticles using various natural products like extracts from the leaves have been successfully reported like Aloe Vera [32], *Acalypha indica* [33], *Garcinia mangostana* [34], *Capparious zeylanica* leaf broth [42], *Ocimum sanctum* leaf broth [43, 44] etc.

In specific, naturally developed plant species, which are a dynamic source of phytochemicals, may aid as environmentally benign pools for the production of metallic nanoparticles. **Figure 3.2** shows graphical representation of synthesis of metal nanoparticles by plant extract. Further, it minimizes hectic processes and does not need elaborate processes, multiple purification steps and maintenance of microbial cell cultures [53]. An imperative branch of the biosynthesis of nanoparticles is the potential of plant extracts in the biosynthesis reaction.

The possible equations for synthesis of metal nanoparticles are —

$$M^{+n}_{(aq)} + A.indica \text{ leaf broth} \xrightarrow[\text{at optimal temperature}]{stirring} [Ag / A.indica \text{ leaf broth}]^{+n} \quad (1)$$

$$[M / A.indica \text{ leaf broth}]^{+n} \xrightarrow[\text{at optimal temperature}]{stirring} [M / A.indica \text{ leaf broth}] \quad (2)$$

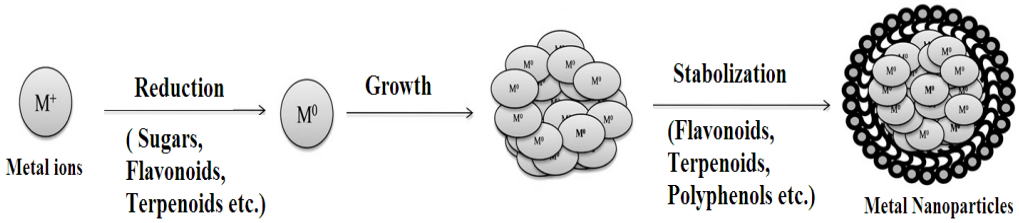

Figure 3.1: Biosynthesis of metal nanoparticles.

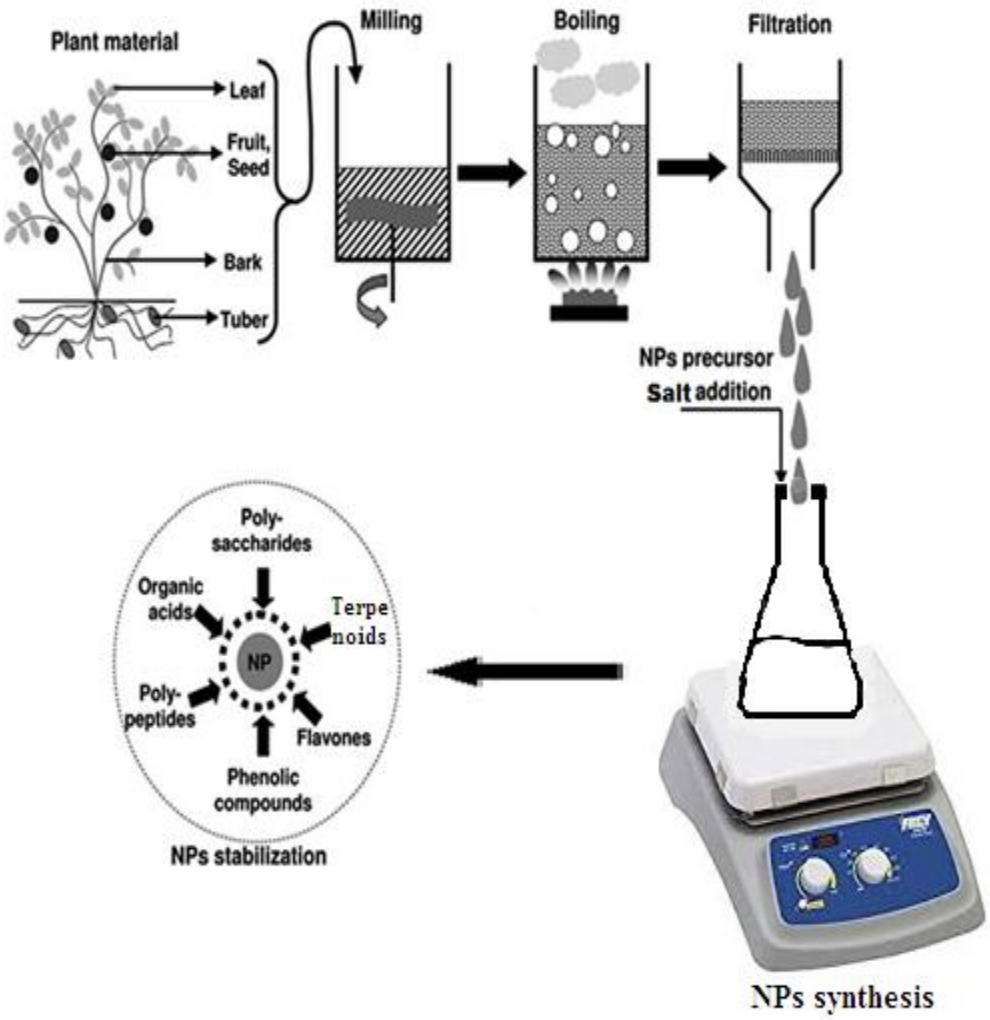

Figure 3.2: Graphical representation of synthesis of metal nanoparticles using plant extract.

When *A. indica* leaf broth was added in metal salt solution, the leaf broth reacts with $M^{+n}_{(aq)}$ and form [M/ *A. indica* leaf broth]$^{+n}$ complex (Equation 1). Further complex bioreduced into metal nanoparticles capped by biomolecules of leaf broth (Equation 2).

3.3. Preparation of leaf broth

Neem (*Azadirachta Indica*) (*A. Indica*) leaves were collected from Kota (Rajasthan) India, fresh and healthy 20 g leaves with 100 ml H_2O stirred on a magnetic stirrer at 80 °C for 20 minutes. The prepared extract was filtered twice through Whatman paper and stored at 4 °C temperature further experiments. Deionized water was employed throughout the study. A detail of preparation of leaf broth is given in chapter 2 (Instrumentation and Materials).

3.4. Green Synthesis of Silver nanoparticles

Aqueous solution 1.0 x 10^{-3} M of silver nitrate ($AgNO_3$) was prepared in 250 ml Erlenmeyer flask and 10 % leaf broth was added for reduction of Ag^+ ions. The complete mixture was kept on magnetic stirring at 30 ^{0}C temperature. Time and colour change were recorded along with periodic sampling and scanning by UV-visible spectrophotometer. Suitable controls were maintained all through the conditions of experiments. Complete reduction of Ag^+ ions was confirmed by the change in colour from light or faint to yellowish colloidal brown. The colloidal solution kept aside for 24 hour for complete bio-reduction and saturation denoted by UV-visible spectrophotometric scanning. The solution was sealed and stored properly for further use. The formation of silver nanoparticles was further confirmed by different spectrophotometric analysis.

3.4.1. Characterization

Different spectrophotometric techniques like UV-visible, SEM, TEM, EDS, XRD, FTIR, and Zetasizer analysis were used for investigating the morphology, elemental composition, crystalline nature, functional group and

stability of synthesized AgNPs. Details of these techniques are given in chapter 2 (Instrumentation and Materials).

3.4.2. Result and Discussion

Synthesis of metal nanoparticles by reduction of the aqueous metal ions during reaction to the broth of *Azadirachta indica* leaves were studied by UV-visible spectroscopy. Silver nanoparticles appear yellowish brown colour in aqueous medium as a result of surface plasma resonance [33]. As the leaf broth were added to silver nitrate solution, the colour of the solution changed from light or faint to yellowish colloidal brown indicating silver nanoparticles formation (**Figure 3.3**). Similar colour changes have also been observed in previous studies [19, 21, 54-56].

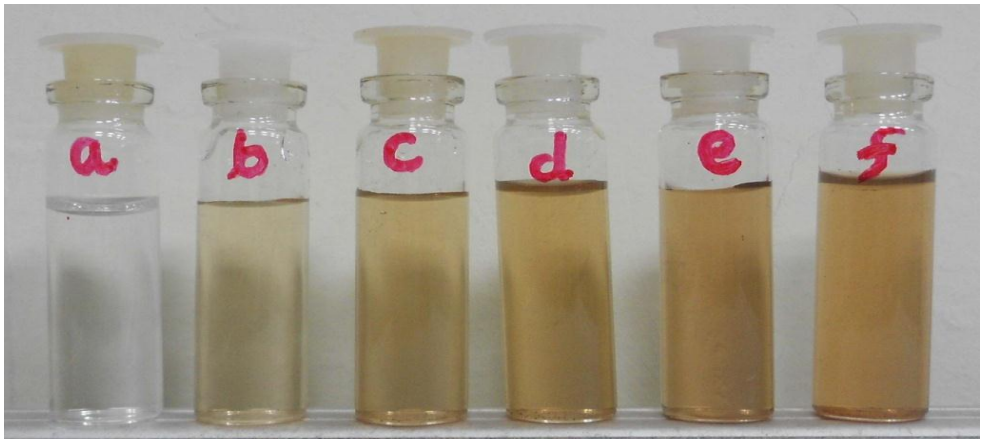

Figure 3.3: Observation of colour change during synthesis of silver nanoparticles at different time interval (a) 0 minutes (b) 30 minutes (c) 60 minutes (d) 90 minutes (e) 120 minutes (f) 24 hour.

The UV-visible spectra recorded after different time intervals from the initiation of reaction as shown in (**Figure 3.4**). It is observed that absorption spectra of synthesized silver nanoparticles show the maxima at wavelength 433 nm. The reduction of the metal ions occurs fairly rapidly within 30 minutes addition of neem leaf broth to metal ion solution and steadily increase in intensity as function of time of reaction without any shift in the peak wavelength. After 24

hours there are no increases in the absorbance due to the depletion of the silver ions (**Figure 3.4 inset**). In earlier studies the synthesis of silver nanoparticles using bacteria [57], fungi [58], requires time for completion of reaction is 24 to 120 hours and is thus rather slow.

TEM analysis results shows the synthesized silver nanoparticles are spherical in shape with average size 9 nm (**Figure 3.5 A**). It has been reported that biosynthesized silver nanoparticles are surrounded by a thin layer of some capping organic material of plant leaf broth and are thus stable in solution up to four weeks after synthesis [19, 59]. **Figure 3.5 B** shows the selected area electron diffraction (SAED) pattern recorded of the silver nanoparticles; the ring like diffraction indicates that the particles are crystalline. Similar SAED pattern was obtained with silver nanoparticles synthesis using *Diopyras kaki* leaf broth by Jae Yong Song [60].

Elemental analysis of silver was measured by Energy-dispersive X-ray spectroscopy **(**EDS). EDS spectra reveals strong signals in the silver region 3 Kev and confirmed the formation of nano silver in its elemental nature (**Figure 3.6**). This signal was appears due to the excitation of surface plasma resonance (SPR) of silver nanoparticles.

Figure 3.7 shows the XRD pattern of the dried nanoparticles at 70 ^{0}C in vacuum for 12 h. In this pattern four sharp peaks observed at 2θ = 37.63, 44.70, 64.39 and 77.20 corresponding to (111), (200), (220) and (311) representing the face centred cubic (FCC) structure. These results are correlates with JCPDS No. 89-3722 and it is confirmed that synthesized AgNPs are pure and crystalline in nature [61-63]. The average size (9 nm) of AgNPs was calculated by Debye-Scherrer formula.

Nanoparticles size distribution is also confirmed by Dynamic light scattering (DLS) (**Figure 3.8**). DLS results indicate the size of AgNPs situated in between 5 to 48 nm range with an average particle size 9 nm of AgNPs.

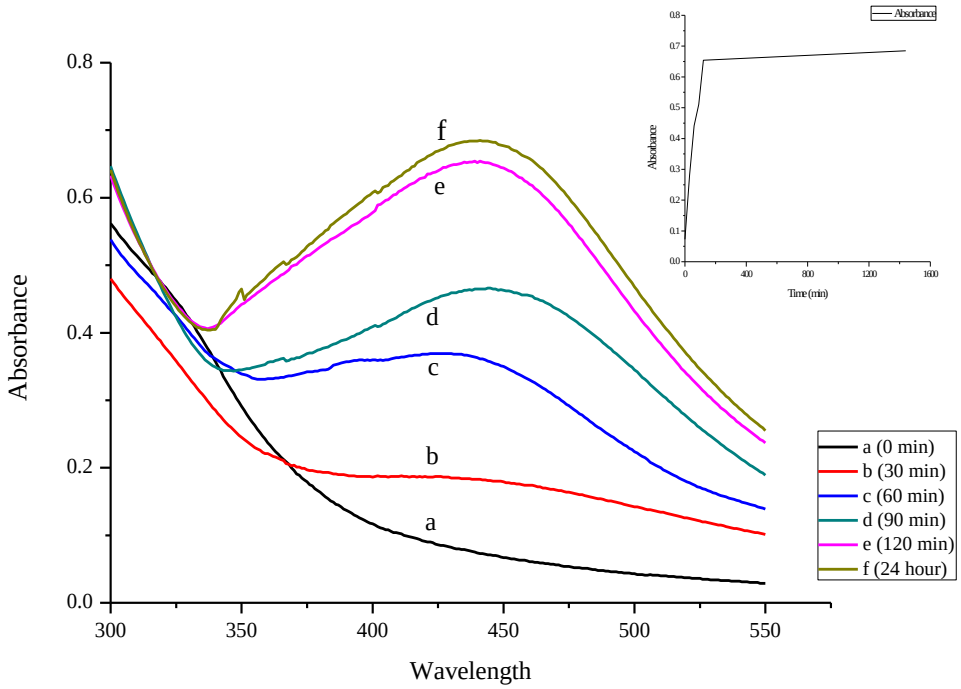

Figure 3.4: UV-visible spectra recorded as a function of reaction at different wavelength versus absorbance during synthesis of silver nanoparticles at different time interval (in inset Respective plot of absorbance at λ_{max} = 433 nm versus time).

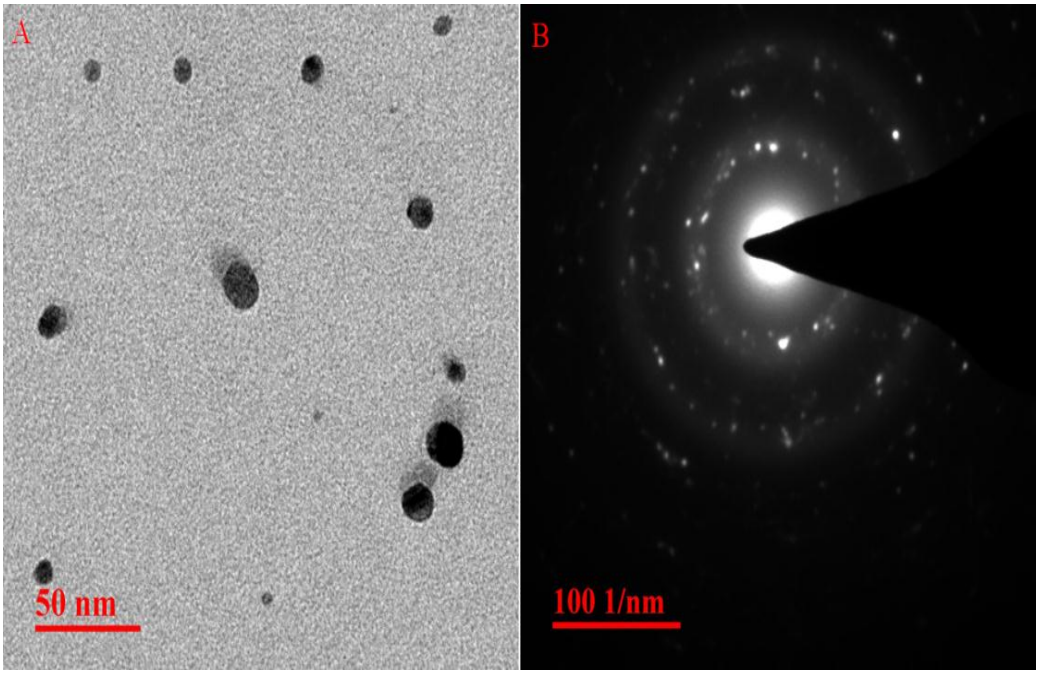

Figure 3.5: (A) TEM image of synthesized Silver Nanoparticles, (B) SAED pattern of Silver Nanoparticles.

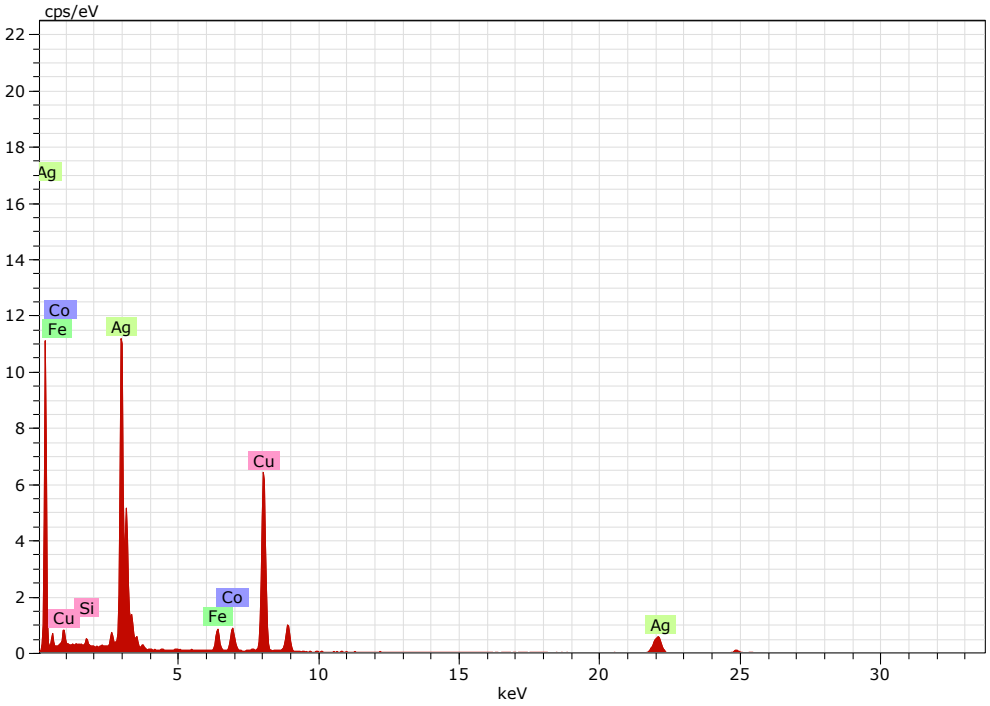

Figure 3.6: Spot profile EDS spectra of synthesized silver nanoparticles.

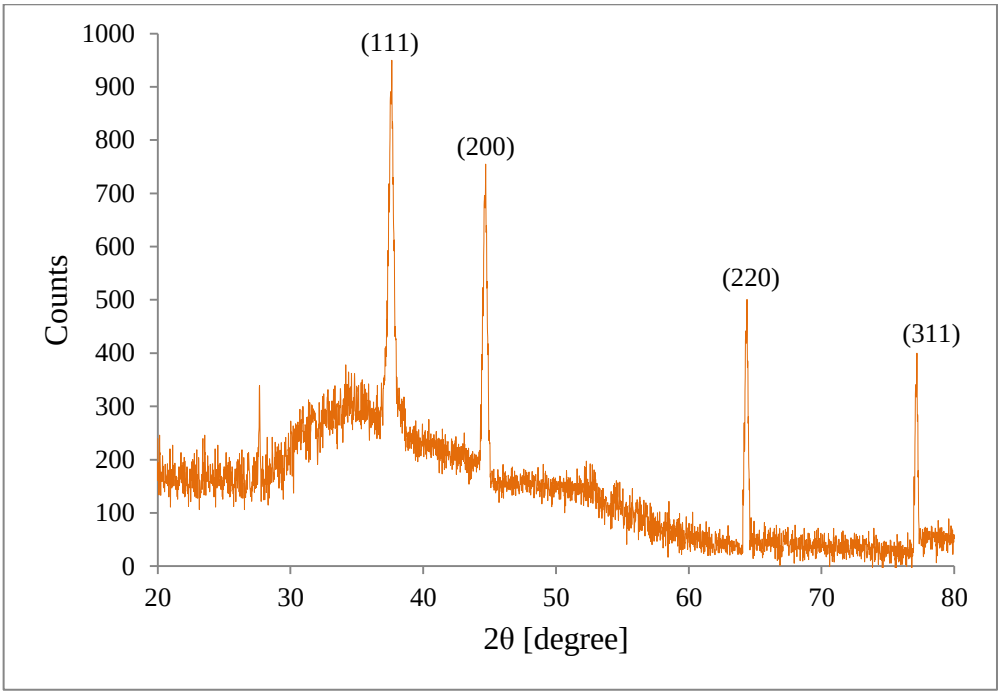

Figure 3.7: XRD of biosynthesized Silver Nanoparticles.

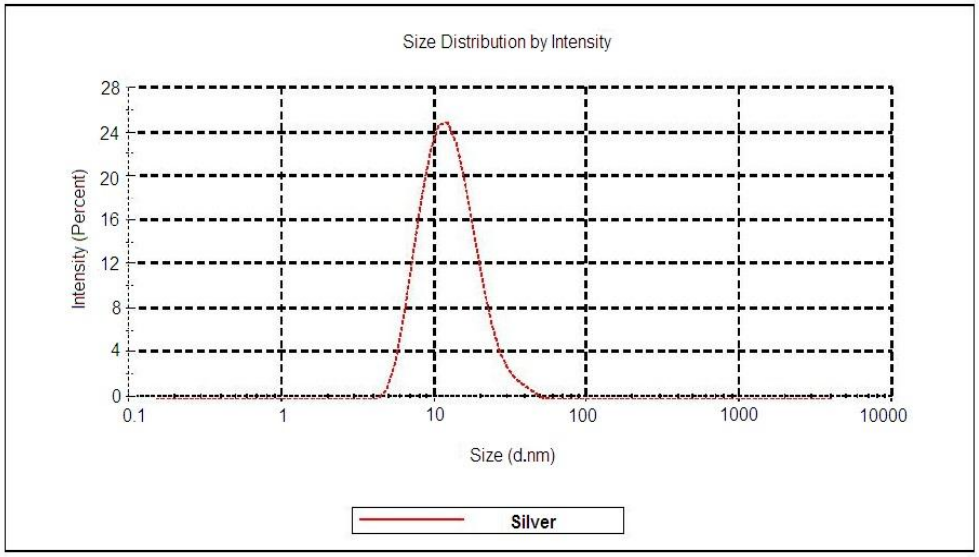

Figure 3.8: Particles size distribution of synthesized Silver Nanoparticles.

3.4.2.1. Effect of leaf Broth Percentage

The effect of different concentration of leaf broth on synthesis rate and particle size of synthesized nanoparticles was also investigated. **Figure 3.9** shows the time course of silver nanoparticles formation with different neem leaf broth percentage (5 % to 15 %) and 1.0 x 10^{-3} M concentration of $AgNO_3$ at 30 ºC temperature. When low percentage (5 %) of leaf broth was used, a weak absorption peak at 433 nm was observed, due to insufficient reduction of Ag^+ ions so relatively low concentration of silver nanoparticles were produced. It is well known that UV-visible absorption peak give information on the degree of dispersion of silver nanoparticles [59]. Percentage of leaf broth increases up to 10 % the intensity of absorption peak increases at 433 nm after that absorption peak become lowers, indicating the aggregation of silver nanoparticles at high percentage of leaf broth. However the maximum absorption peak was obtained at 10 % neem leaf broth, suggesting that the optimum percentage of leaf broth for synthesis of silver nanoparticles.

The result of TEM analysis and histograms of synthesised silver nanoparticles with size distribution are also presented in (**Figure 3.10**) at the different percentage of leaf broth. The histogram reveals an increase in leaf broth percentage up to 10 %, the particle size decreases from 20 to 9 nm after that size of nanoparticles was increases (56 nm) with increases in percentage of leaf broth (15 %), suggesting that too many reducing agents cause aggregation of the synthesized silver particles. It is possible due to the interaction between capping molecules bound to the surface of particles and secondary reduction process on the surface of the performed nuclei. Similar aggregation of nanoparticles was earlier reported by Vanaja et al. [64] using the extract of *Morindat inctoria* in the reduction of Ag^+ ions. The results are well consistent with UV-visible spectra in (**Figure 3.10**).

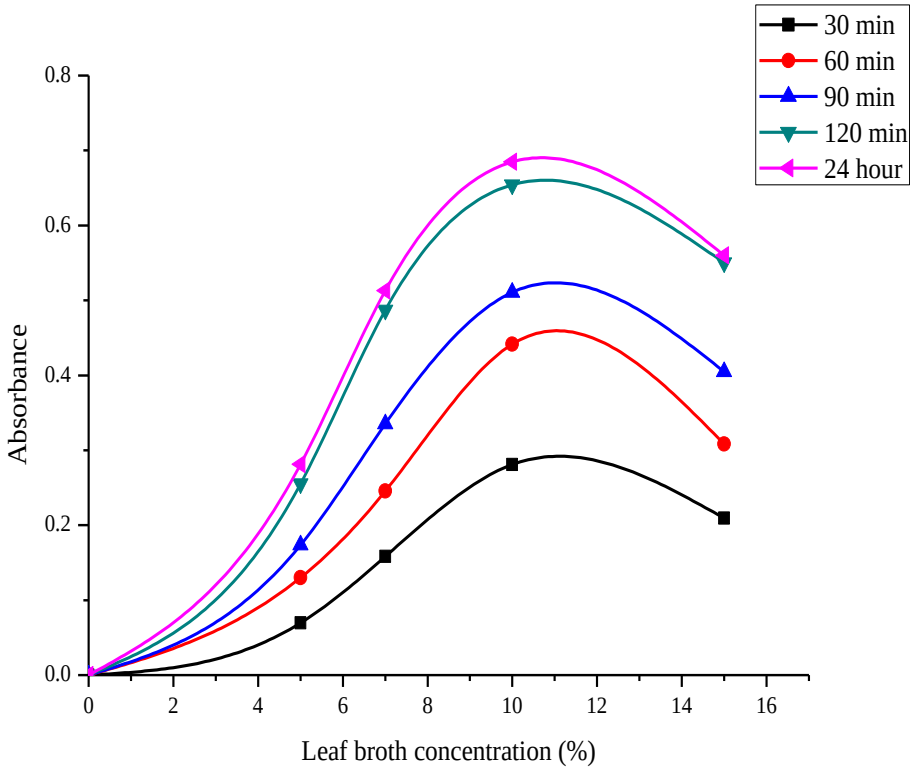

Figure 3.9: Time course of silver nanoparticles synthesis with different leaf broth concentration (5 % to 15 %), [$AgNO_3$] = 1.0 x 10^{-3} M and Temperature = 30 °C.

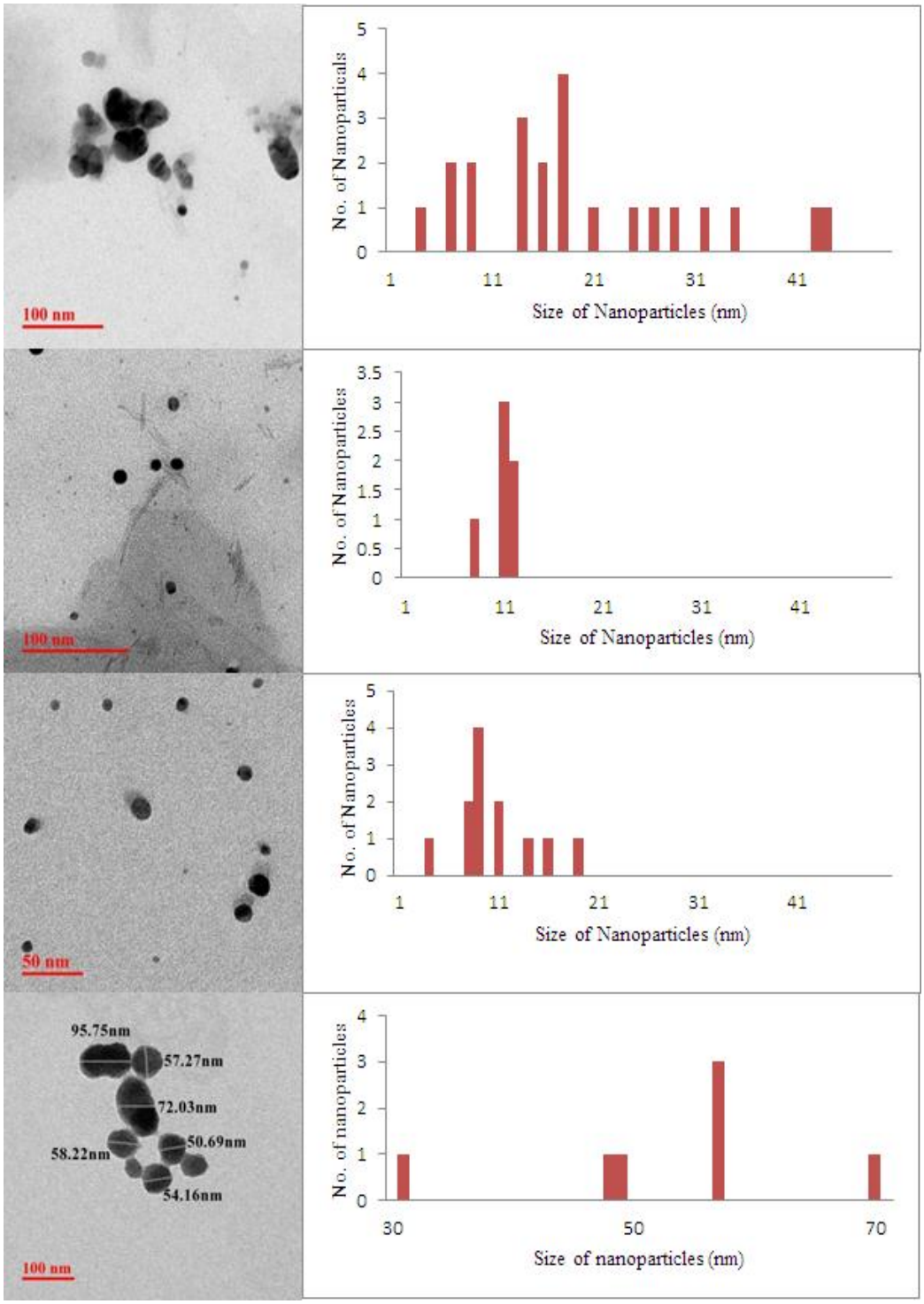

Figure 3.10: TEM images with histogram of synthesized silver nanoparticles at different percentage of leaf broth (A) 5 %, d = 20 nm, (B) 7 %, d =11nm, (C) 10 %, d = 9 nm, (D) 15 %, d = 56 nm.

3.4.2.2. Effect of Initial Precursor Salt Concentration

The effect of initial concentration of $AgNO_3$ on the formation of silver nanoparticles was studied between 5.0 x 10^{-4} to 2.0 x 10^{-3} M at fixed other reactant concentration and conditions. There are two stages when silver nanoparticles formed in the solution, the first stage to generate silver nuclei and second stage is the growth of silver nuclei [65], so it is important to control synthesis process that silver nuclei must generate faster and grow up slower which requires optimum concentration of $AgNO_3$. **Figure 3.11** shows the UV-visible spectra recorded as a function of reaction at different concentration of $AgNO_3$ versus absorbance during synthesis of silver nanoparticles at different time interval. It was observed that the highest absorbance was obtained when the concentration of $AgNO_3$ is 1.0 x 10^{-3} M. This confirmed that the synthesis process can be affected by initial concentration of $AgNO_3$ and suggest that reaction rate increases with the increasing amount of silver nuclei rises and smaller particle size are obtained correspondingly. The SEM images of synthesized silver nanoparticles at different initial concentration of $AgNO_3$ are shown in **Figure 3.12**. The results indicate that an excess number of nuclei will be generated when the Ag^+ ions concentration is too high i.e. 2.0 x 10^{-3} M, thus results in the agglomeration of the nuclei and growing particle size. So the optimal concentration of $AgNO_3$ is 1.0 x 10^{-3} M for synthesis of monodispersed and average size 9 nm silver nanoparticles.

3.4.2.3. Effect of Temperature

Figure 3.13 has shown the time course of silver nanoparticles formation at different reaction temperature (25 ^{0}C to 40 ^{0}C) and fixed other reactant concentration and conditions. As the reaction temperature increases, synthesis rate of silver nanoparticles also increases. Jae Yona Song [60] reported that *Diopyros kaki* leaf broth assisted reduction of Ag^+ ions increases with increase in the reaction temperature. The results of TEM images of synthesized nanoparticles at different temperature (**Figure 3.14)** indicates as reaction temperature increases 25 ^{0}C to 30 ^{0}C the particle size decreases 20 to 9 nm respectively but the size grows up when increase in after certain temperature, which is due to at high temperature (40 ^{0}C) the nanoparticles were agglomerated while at 30 ^{0}C nanoparticles are well

dispersed which as average size about 9 nm. Basically, the reduction of Ag^+ ions increases by increasing the reaction temperature. Therefore at high temperature the synthesis rate is too high to control particle size. When reducing agent (Neem broth) added in silver nitrate solution at 40 ^{0}C, nucleation as well as growth of silver nanoparticles accelerated almost coincidently, resultant higher averaged size of silver nanoparticles were agglomerated. Therefore moderate temperature 30 ^{0}C should be selected for synthesis of silver nanoparticles with appropriate controlling on size.

3.4.2.4. The Stability of Synthesized Silver Nanoparticles

FTIR measurements were carried out to identify the potential functional groups of the bio-molecules in the leaf broth of *Azadirachta indica* (neem) which are responsible for the reduction of silver ions into silver nanoparticles. Comparison with FTIR of green synthesized silver nanoparticles (**Figure 3.15 A)** and leaf broth of pure neem (**Figure 3.15 B**) the observed peak at 1609 cm^{-1}, 1381cm^{-1}, 1077 cm^{-1} in **Figure 3.15 A** are more characteristic of flavanones and terpenoids that are abundant in neem plant broth [66, 67]. The peak observed at 1609 cm^{-1} indicating C=C groups, 1381 cm^{-1} occurring to the germinal methyls and 1077 cm^{-1} are shows ether linkages, suggest the presence of flavanones or terpenoids adsorbed on the surface of silver nanoparticles. These reducing sugars could be responsible for the reduction of silver ions in to silver nanoparticles. Currently the mechanism of biological nanoparticles synthesis is not fully understood. Terpenoids are believed to be the surface active molecules stabilizing the nanoparticles and reduction of the metal ions is possible facilitated by reducing sugars or terpenoids present in neem leaf broth is reported in [19].

Stability of AgNPs also confirms by the instrument of zeta potential. The zeta potential of biosynthesized AgNPs is obtained -22.4 mV (**Figure 3.16**). The value of zeta potential suggesting that the AgNPs was negatively charged in dispersed so; particles repel each other which prevent from aggregation.

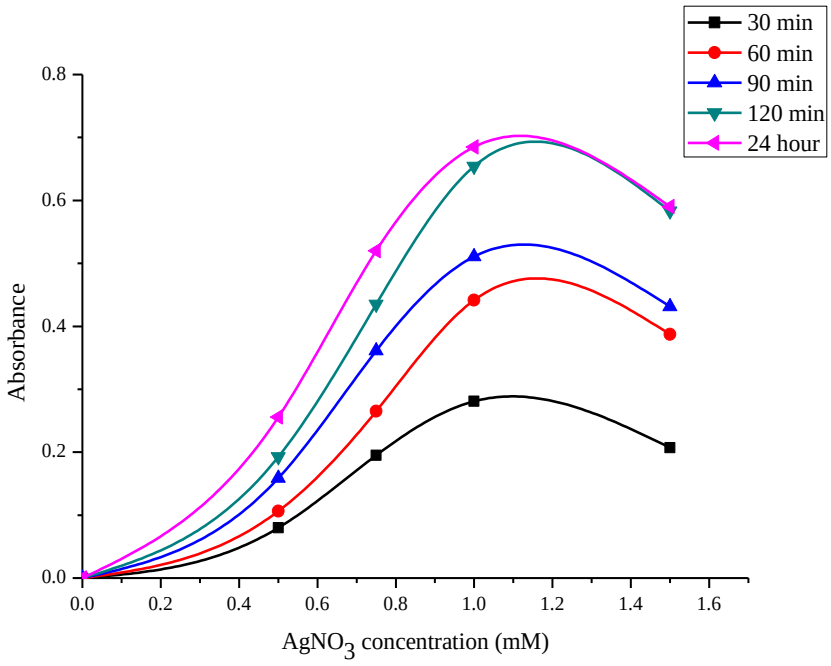

Figure 3.11: Time course of silver nanoparticles synthesis with different initial concentration of $AgNO_3$ (5.0×10^{-4} to 2.0×10^{-3} M), leaf broth =10 % and Temperature = 30 °C.

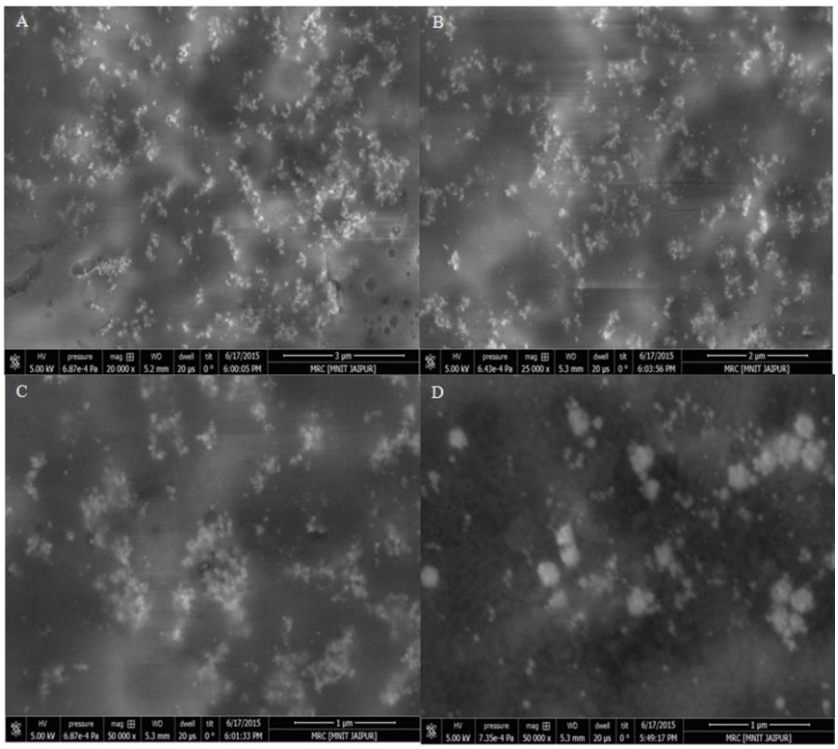

Figure 3.12: SEM image of synthesized silver nanoparticles at different initial $AgNO_3$ concentration (A) 5.0 x 10^{-4} M (B) 7.5 x 10^{-4} M (C) 1.0 x 10^{-3} M (D) 2.0 x 10^{-3} M.

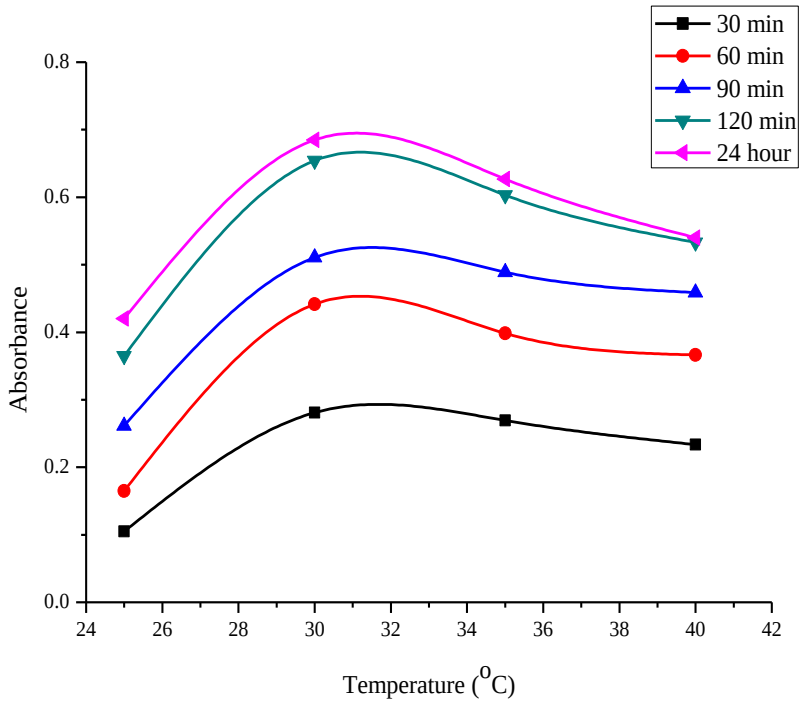

Figure 3.13: Time course of silver nanoparticles synthesis at different reaction temperature (25-40 °C), [$AgNO_3$] = 1.0 x 10^{-3} M and leaf broth =10 %.

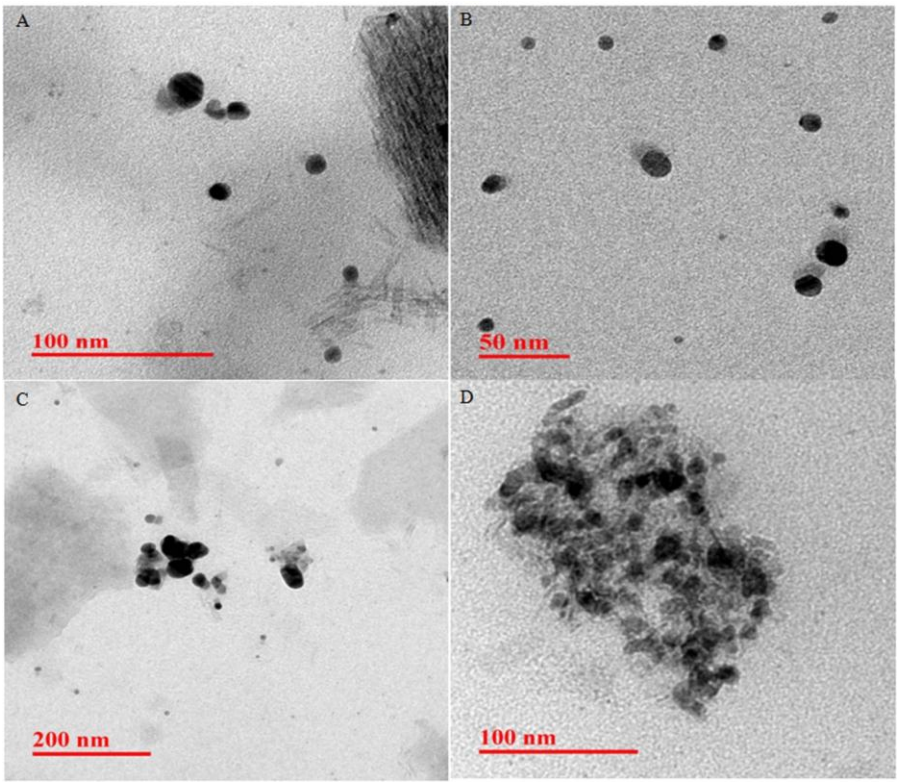

Figure 3.14: TEM images of synthesized silver nanoparticles at different reaction temperature (A) 25 ℃, (B) 30 ℃, (C) 35 ℃, (D) 40 ℃.

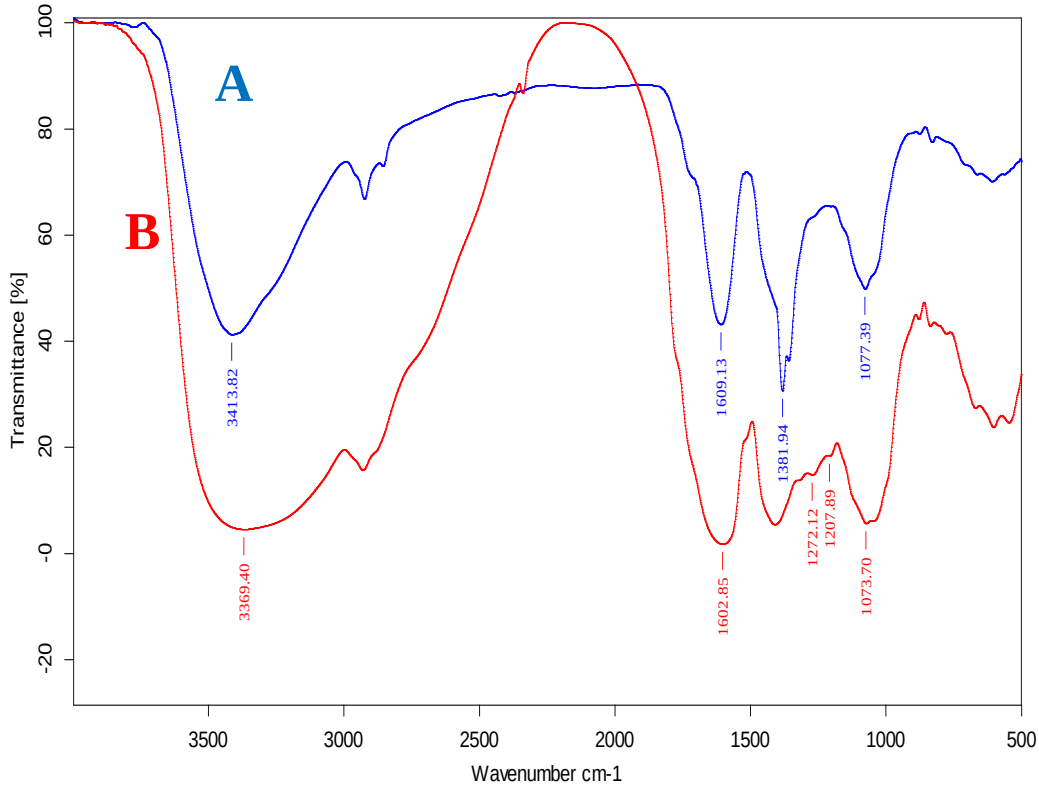

Figure 3.15: Comparative FTIR spectra of (A) Synthesized AgNPs and (B) Neem leaf broth.

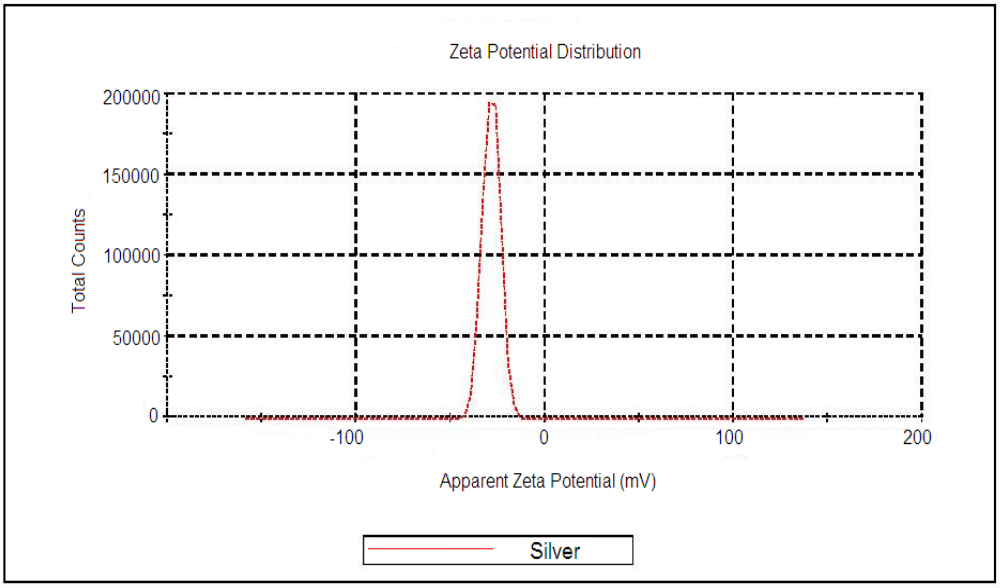

Figure 3.16: Zeta potential of synthesized silver nanoparticles.

3.5. Green Synthesis of Copper Nanoparticles

In a synthetic procedure, CuNPs were obtained via a green reduction route. The flask containing an aqueous solution of salt $CuCl_2 \cdot 2H_2O$ (7.5×10^{-3} M) was heated to 85 °C in oil bath with magnetic stirring then neem leaves broth (20 %) were added dropwise to this solution. At different time intervals, the color of dispersion was gradually changed from green, yellow, orange, radish brown, brown and finally dark brown with the number of intermediate stages. The resulting dark brown color solution was centrifuged for 15 minutes at 6000 rpm. The supernatant dispersion was placed at 4 °C temperature for two months.

3.5.1. Characterization

The synthesized nanoparticles were characterized by different spectrophotometric techniques for investigating the morphology, elemental composition, crystalline nature, functional group and stability of synthesized CuNPs. Details of these techniques are given in chapter 2 (Instrumentation and Materials).

3.5.2. Result and Discussion

The formation of CuNPs was confirmed primarily based on change in colour of reaction mixture and also by UV-visible spectroscopy. As the leaf broth was added to the $CuCl_2$ salt solution, the color of the solution changed from light blue to green and finally, dark brown indicates the formation of CuNPs (**Figure 3.17**). The color change in aqueous solution is due to surface Plasmon resonance (SPR) phenomenon. In this investigation, the obtained results are interesting because it can serve as a foundation in terms of identification of potential medicinal plants for synthesizing CuNPs.

The biomolecules such as Terpenoids, nimbaflavone and poly phenols are present in *A. indica* leaf broth, which can reduce metal ions to metal NPs as well as stablize them (**Figure 3.18**) [68-70].

Figure 3.17: Observation of color changes during synthesis of Copper nanoparticles at different time intervals: (A) 0 h, (B) 4 h, (C) 10 h, (D) 18 h, (E) 24 h, (F) 28 h.

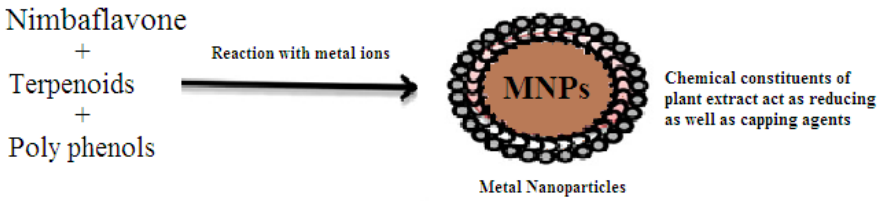

Figure 3.18: Possible constituents of plant extract responsible for the bioreduction of metal ions.

UV-visible absorbance spectroscopy has been proved to be a very useful technique for the detection of synthesized metallic NPs because of the peak position and shape of the spectra are sensitive to the particle size. The UV-visible spectra of dispersion were recorded at different time intervals from the initiation of reaction (**Figure 3.19**). The intensity of SPR peak increased as the passage of time, which indicated the continued reduction of copper ions into CuNPs. The adsorption peak maximum at 560 nm, which can be confidently ascribed to the SPR of CuNPs formed [71]. The adsorption band for CuNPs has been reported to be in the range of 500-600 nm [7]. The shape of synthesized CuNPs were cubical, confirmed by the TEM analysis [24] (**Figure 3.20 A**) and TEM results shows the synthesized NPs are surrounded by a thin layer of capping organic material of neem leaf broth. The Selected Area Electron Diffraction (SAED) pattern recorded of CuNPs, a ring like pattern shows synthesized CuNPs are highly crystalline (**Figure 3.20 B**) [36].

The EDS spectra of synthesized NPs give a clear indication regarding the elements of CuNPs. The strong signal of copper atom confirmed that CuNPs contain pure copper (**Figure 3.21**). The element of Carbon and oxygen are contaminated all around the peaks, which must be due to phytochemicals present in plant extract [72]. Thus these elements as the evidence for the organic substance attached to the CuNPs. No other impurities were observed in EDS profile.

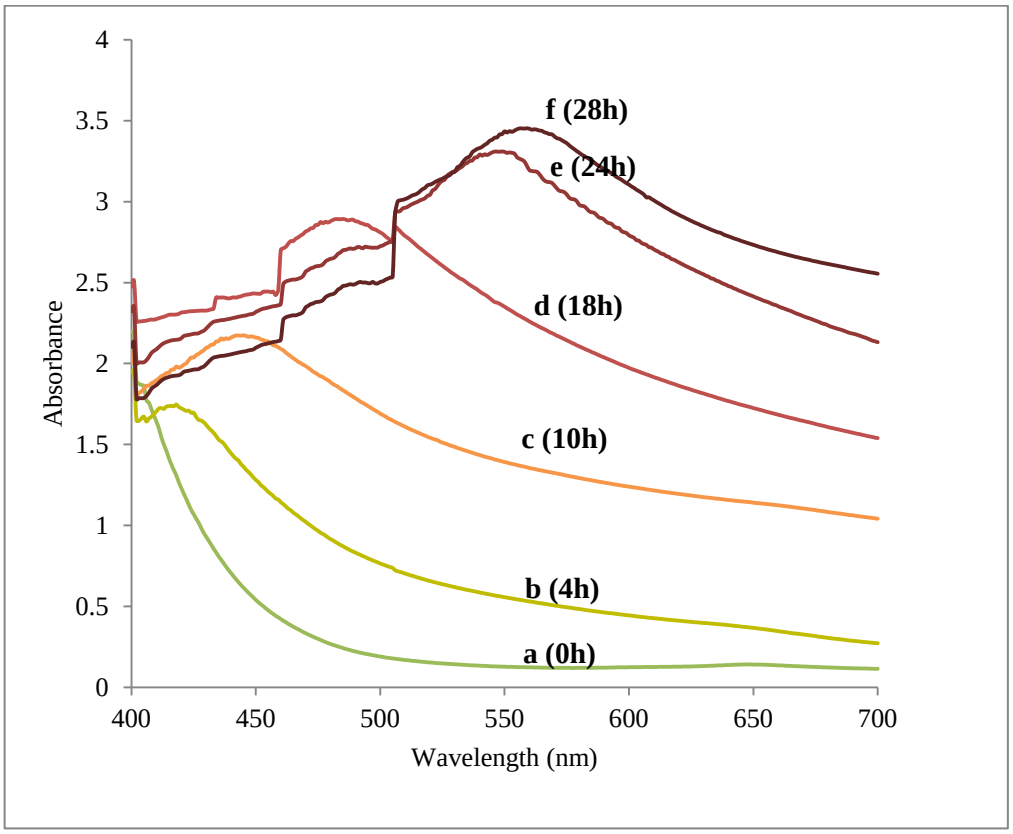

Figure 3.19: UV-visible absorption spectra of copper nanoparticles as a function of wavelength versus absorbance at a different time interval during the synthesis process.

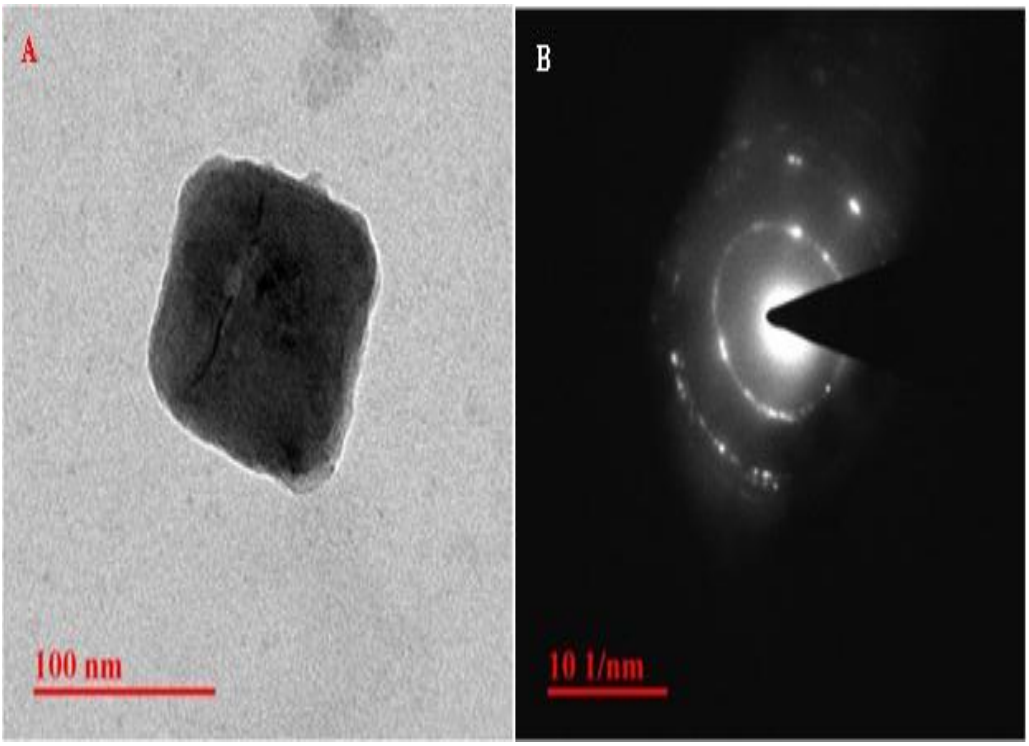

Figure 3.20: (A) TEM image of synthesized Copper Nanoparticle, (B) SAED pattern of Copper Nanoparticles.

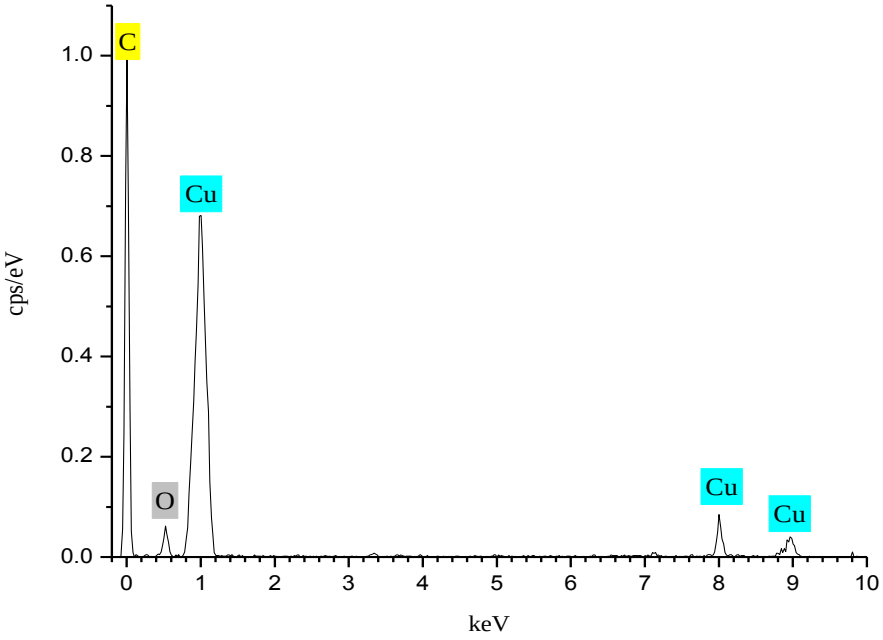

Figure 3.21: EDS spectra of synthesized CuNPs.

Figure 3.22 A presents the XRD pattern of synthesized CuNPs dried at room temperature, observation indicates the CuNPs capped by biomolecules but not give proper information about crystalline nature. Whereas the CuNPs dried in vacuum at 70 °C for 12 h, gives a sharp peak at 2θ = 43.5°, 49.9° and 74.01° corresponding to (111), (200) and (220) representing a face centered cubic (FCC) structure of copper (**Figure 3.22 B)**. Which are closely matched with the values of FCC phase copper reported by S. Yallappa et al. Above all, it is encouraging to note that the 2θ values of the synthesized CuNPs are also matched with joint committee for powder diffraction standard (JCPDS). The Synthesized CuNPs were found to be pure without any impurities like CuO, Cu_2O, $Cu(OH)_2$ [73]. Furthermore, the average particle size of NPs was 48 nm was calculated by well-known Scherer equation.

Dynamic light scattering result gives the information about the size distribution of NPs. **Figure 3.23** indicates the size of CuNPs situated in between 35 to102 nm range with an average particle size 48 nm of CuNPs.

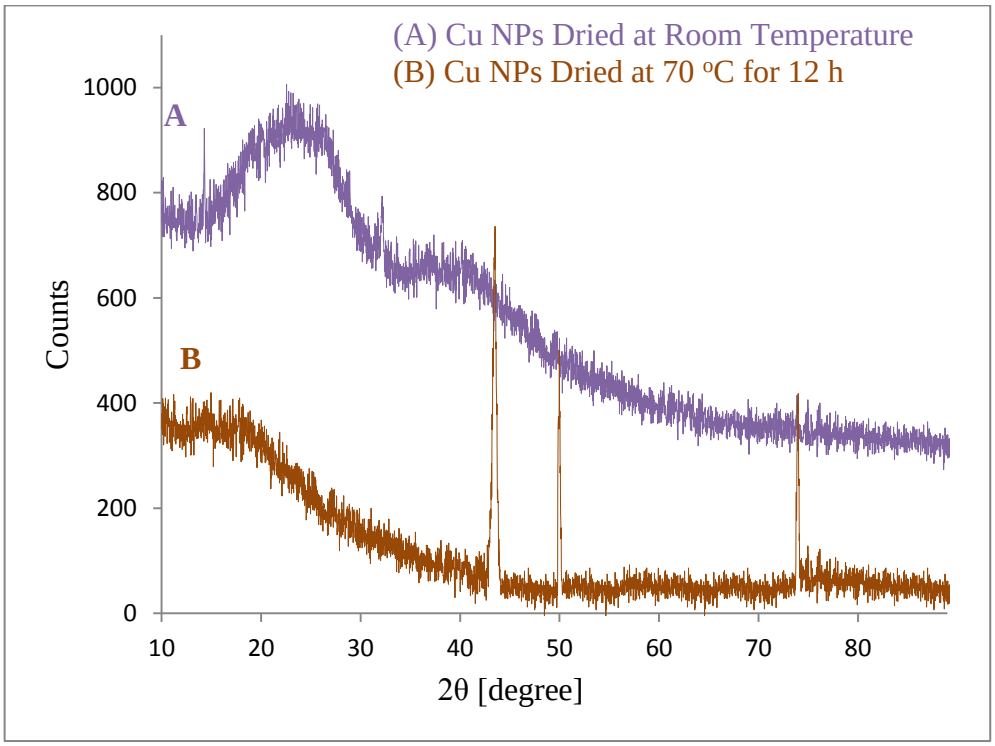

Figure 3.22: XRD of biosynthesized Copper Nanoparticles

(A) Dried at room temperature, (B) Vacuum dried at 70 °C for 12 h.

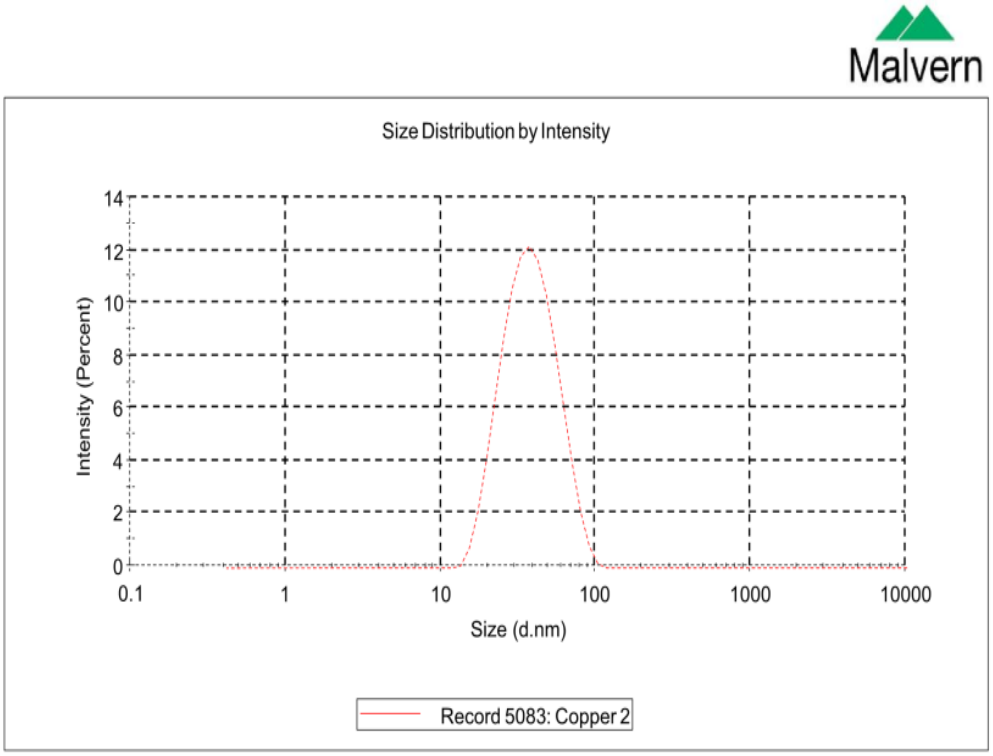

Figure 3.23: Particles size distribution of synthesized Copper Nanoparticles.

3.5.2.1. Effect of leaf Broth Percentage

The effect of various leaf broth percentage on the synthesis process has been studied by UV-visible absorbance spectroscopy as shown in **Figure 3.24**. The absorption peak is increasingly broadening with an increasing leaf broth percentage. At low percentage of leaf broth (5 %) a weak absorption peak was observed at wavelength 506 nm, may be an insufficient reduction of copper ion. As the percentage of leaf broth increases, the intensity of SPR peak increases. Such effect was also confirmed by a plot of the conversion rate of reaction versus different percentage of leaf broth (**Figure 3.25**). The results illustrated that conversion rate of reaction increases with increases in leaf broth percentage up to 20 % after that increasing trend not distinct, indicating the agglomeration of colloidal CuNPs at the higher percentage of leaf broth. It is due to the excess number of biomolecules present at the high percentage, secondary reduction process initiates on the surface of the perform nuclei, resultant growing the particle size. Therefore, the optimal leaf broth percentage is 20 for synthesis of CuNPs [60]. These results are consistent with observed UV-visible spectra at different leaf broth percentage.

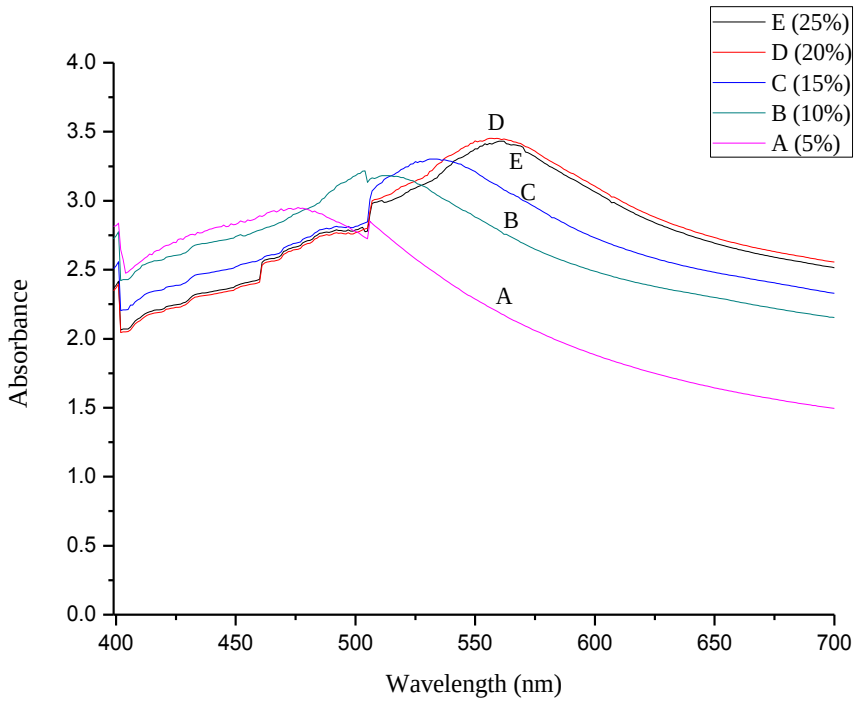

Figure 3.24: UV-visible absorption spectra of synthesized CuNPs recorded at various neem leaf broth percentages.

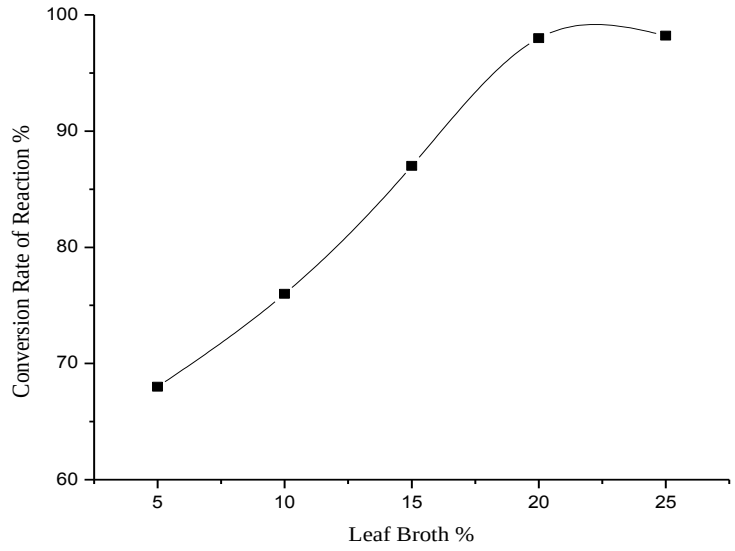

Figure 3.25: Effect of various leaf broth percentage on the conversion rate of reaction at constant [$CuCl_2 \cdot 2H_2O$] = 7.5 x 10^{-3} M, pH= 6.6 and Temperature 85 °C.

3.5.2.2. Effect of Initial Precurser Salt Concentration

The effect of initial concentration of precursor salt on the formation of CuNPs studied at the concentration of precursor salt between 6.0 x 10^{-3} to 10 x 10^{-3} M. It is important to optimize the initial concentration of procures salt to copper nuclei must generate faster and grows up slower [71]. The results of SEM images shows synthesized CuNPs particle size in the range of 48.01 to 78.51 nm at different concentration of precursor salt (**Figure 3.26**) [74]. The green synthesized CuNPs size is highly depending on the concentration of precursor salt. It was confirmed that, the concentration of $CuCl_2$ increased from 6.0 x 10^{-3} M to 7.5 x 10^{-3} M, decreases particle size of NPs after that increase in concentration of salt, particles size increases (**Figure 3.27**). It can be seen that as increases in the concentration of precursor salt, the copper nuclei rises and smaller particles size are obtained correspondingly. But an excess number of nuclei will be generated at high reactant concentration so results in the agglomeration of the nuclei and growth of particles size. Similarly, aggregation of Nanoparticles was earlier reported by G. Annadurai et al. by using the leaf extract of *Morinda tinctoria* in the reduction of silver ions [64]. So the optimal concentration of precursor salt is 7.5 x 10^{-3} M for the synthesis of CuNPs.

3.5.2.3. Effect of Temperature

The effect of temperature on the synthesis of CuNPs was studied by the conversion rate of process at an optimal concentration of reactants. The reduction of Cu^{2+} ions was not completed at 60 ^{0}C temperature due to insufficient for the reaction. It can be seen from **Figure 3.28** that conversion rate of Cu^{2+} ions considerable increases when temperature goes up (60 to 85 ^{0}C), but the synthesis rate is too high when increasing to a certain temperature. In the reaction system, the effect on the nucleation rate by temperature is greater than that the growth rate, therefore the nucleation rate is faster than growth rate when temperature increases. But the nuclei surface activity is enhanced when temperature is too high, which promotes the nuclei to colloid and agglomerated. Therefore the optimal reaction temperature is 85 ^{0}C.

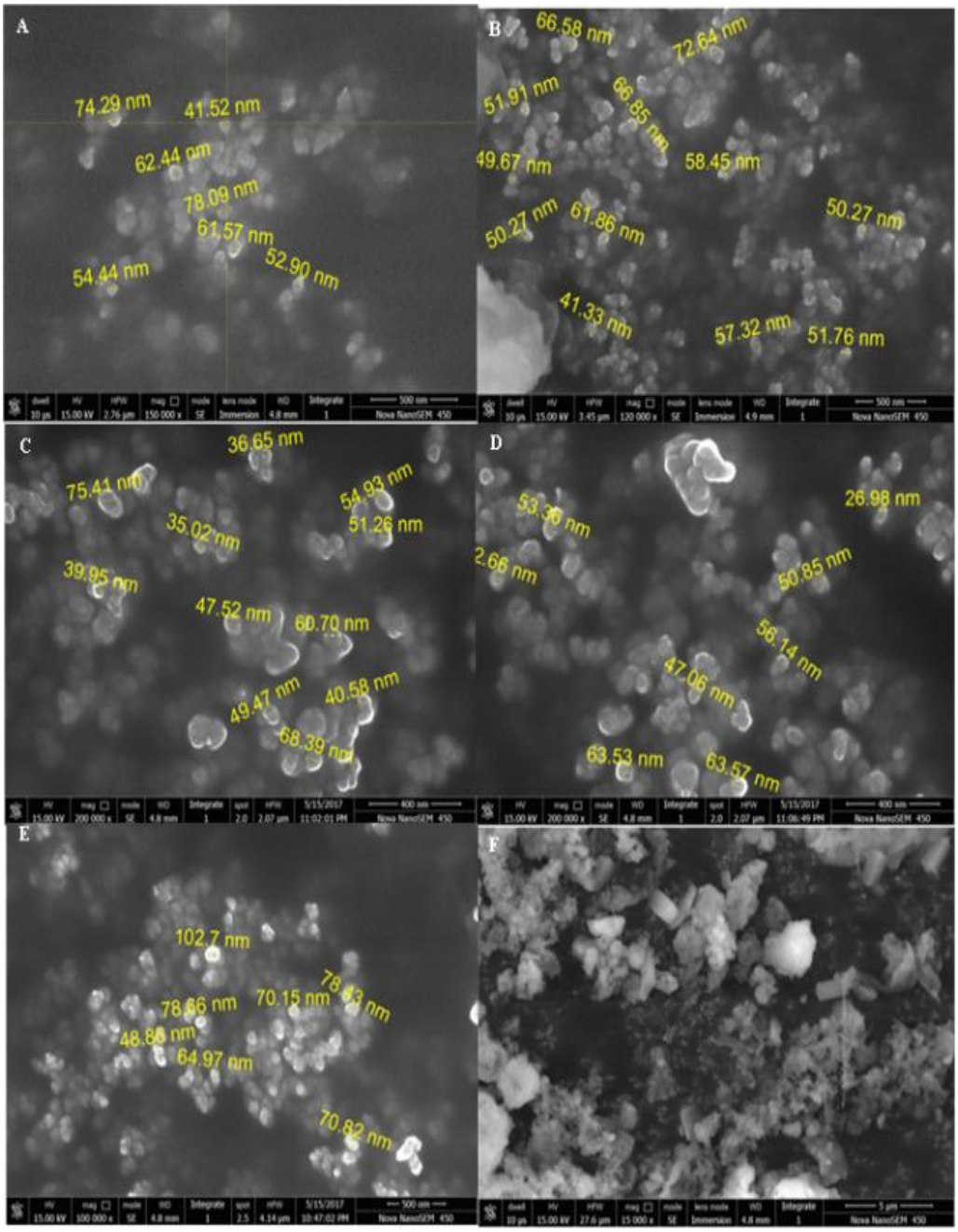

Figure 3.26: SEM images of synthesized Copper nanoparticles at different initial concentration of $CuCl_2$ (A) 6.0 x 10^{-3} M, (B) 6.5 x 10^{-3} M, (C) 7.0 x 10^{-3} M, (D) 7.5 x 10^{-3} M, (E) 8.0 x 10^{-3} M, (F) 10 x 10^{-3} M.

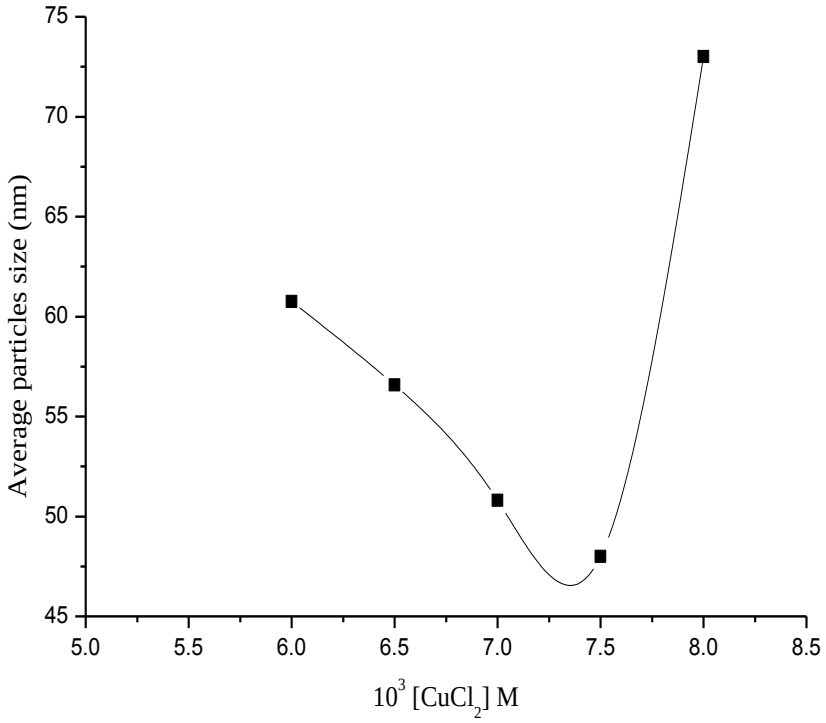

Figure 3.27: Effect of different concentration of [$CuCl_2.2H_2O$] on average particle size Copper nanoparticles at leaf broth= 20 %, pH= 6.6 and Temperature 85 °C.

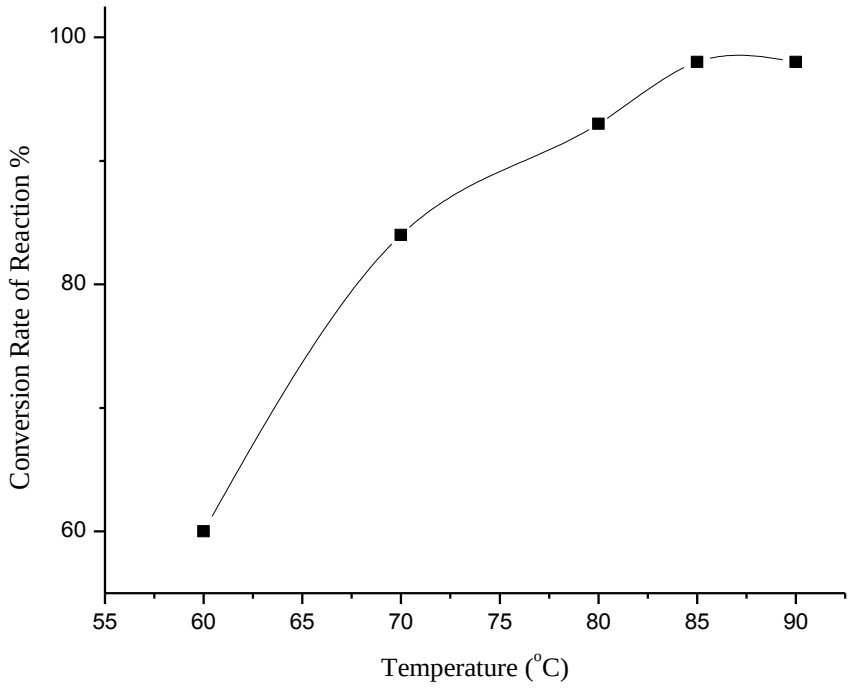

Figure 3.28: Effect of Temperature on conversion rate of Copper Nanoparticles synthesis at [$CuCl_2.2H_2O$] = 7.5 x 10^{-3} M, leaf broth= 20 % and pH= 6.6.

3.5.2.4. Effect of pH

pH of the reaction dispersion is another important parameter for the synthesis of NPs. Variation in pH affects the synthesis rate and morphology of NPs. Capping and stabilizing ability is dependent on the charge of biomolecules, which might affect by pH. It was observed that in acidic pH, NPs were not formed. It indicates acidic pH suppresses the NPs synthesis. Under the acidic condition such biomolecules are likely to be inactivated so that NPs synthesis could not occur at pH 4.7. At higher pH (6 to 6.6) however, more number of small sized NPs were synthesized due to availability of functional group for copper binding (**Table 3.1**). Interestingly, even high pH was also found to efficient in producing NPs, but they agglomerated and formed large size NPs. Therefore the pH 6.6 is favourable for the biosynthesis of CuNPs. It has been also observed that during synthesis process the pH of the medium decreases due to release of H^+ ions by the species of leaf broth at their oxidation in presence of Cu^{2+} ions [7].

3.5.2.5. The Stability of Synthesized Copper Nanoparticles

The stability of NPs is a very important key factor for their application [71]. The NPs are generally stabilized with capping agents such as polymers, surfactant etc [75, 76]. Here, we report the synthesized CuNPs are stable for 2 months at 4 °C by the bio capping of leaf broth, which was confirmed by the comparative FTIR spectra of pure neem and bio-reduced synthesized CuNPs (**Figure 3.29**). Synthesized CuNPs exhibits major peaks at 2922 cm^{-1} (O-H stretching of phenolic group), 2371 cm^{-1} (C-N stretching of aromatic amine), 1631 cm^{-1} (C=O stretching), 1456 cm^{-1} (C=C stretching), 1384 cm^{-1} (aldehydic C-H stretching) correspond to the neem leaf broth, suggests the presence of flavonoids, terpenoids and poly phenols, that may be responsible for reduction and stabilization process [45, 77]. Also, the band observed at around 1077 cm^{-1} was attributed to the C-O stretching, which is characteristic of ether functional moiety. S. S. Shankar et al. reported that these biomolecules bounded on the surface of *Azadirachta indica* leaf broth mediated synthesized AgNPs [47].

Further, the stability of synthesized CuNPs was determined by zeta potential value. The value of zeta potential gives the degree of electrostatic repulsion between adjacent, similarly charged particles in the dispersion. The high magnitude of zeta potential value shows the great stability of NPs [78, 79]. The result of the zeta potential of synthesized CuNPs has been found as a sharp peak at -17.5 mV (**Figure 3.30**) suggests that biosynthesized NPs are highly stable.

TABLE: 3.1

Effect of pH on average Copper nanoparticles size

$[CuCl_2.2H_2O] = 7.5 \times 10^{-3}$ M **leaf broth= 20 %**

Temperature = 85 °C.

S. No.	pH	Average Particle Size
1	4.7	CuNPs not formed
2	6.0	56 nm
3	6.6	48 nm
4	8.4	60 nm
5	9.3	73 nm

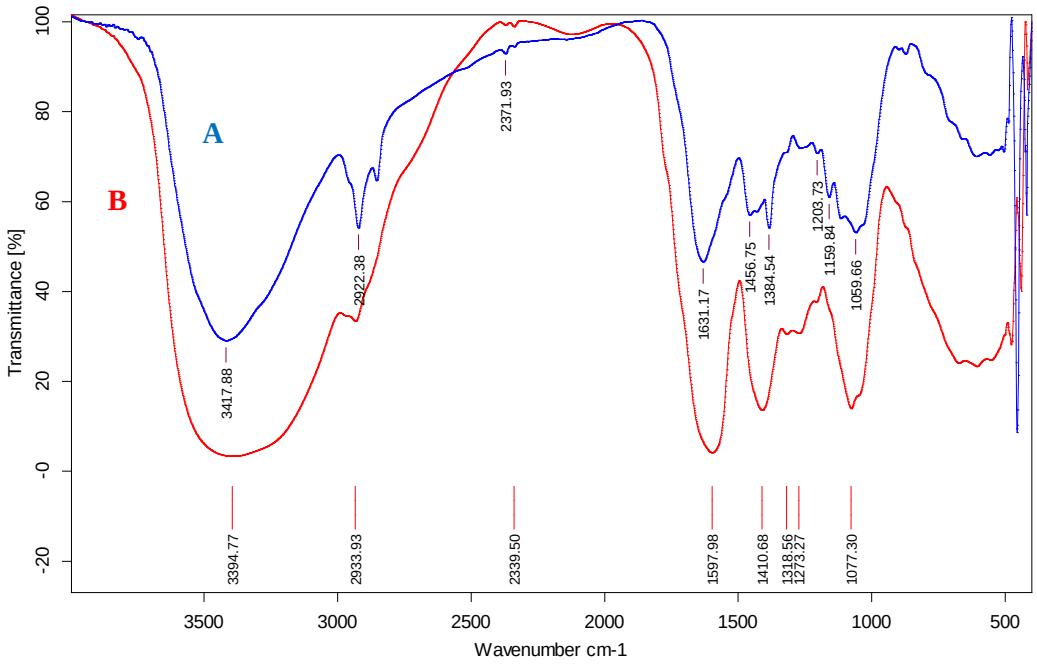

Figure 3.29: Comparative FTIR spectra of (A) synthesized CuNPs and (B) Neem leaf broth.

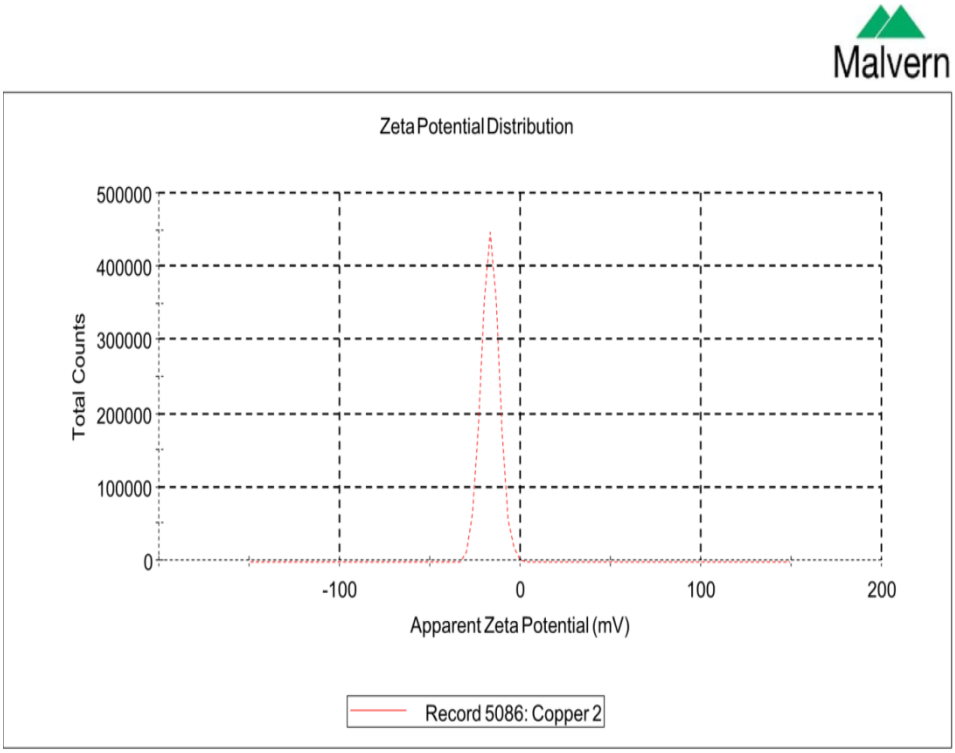

Figure 3.30: Zeta potential of synthesized CuNPs.

3.6. Conclusion

In conclusion, the presented green synthesis shows that environmentally benign and renewable source of *A. Indica* can be used as an efficient reducing agent as well as capping agent. This biological reduction of metal ions would be boon for the development of clean, non-toxic, environmentally suitable green approach to fabricate metal nanoparticles. The procedure designates that the initial concentration of reactants and reaction temperature has a remarkable effect on synthesis and marphology of synthesized metal nanoparticles. The result shows optimal condition for AgNPs is [$AgNO_3$] = 1.0 x 10^{-3} M, 10 % leaf broth at 30 °C temperature with 9 nm particle size, -22.4 mV zeta potential and for CuNPs is [$CuCl_2 \cdot 2H_2O$] = 7.5 x 10^{-3} M, 20 % leaf broth at 6.6 pH and 85 °C temperature with 48 nm particle size, -17.5 mV zeta potential. The synthesize nanoparticles have good stability thus has a potential to use in biomedical applications and will play an important role in the field of catalysis. The rate of reduction of metal ions by neem leaf broth is much faster than earlier reported studies using micro-organisms, highlighting that nanoparticle biological synthesis methodologies will achieve the rate of synthesis comparable to those of chemical methods.

3.7. References

[1] M. S. Niasari, Z. Fereshteh, F. Davar, ***Polyhedron***, 28 (2009) 126.

[2] M. S. Niasari, F. Davar, ***Mater. Lett.***, 63 (2009) 441.

[3] Q.-L. Zhang, Z.-M. Yang, B.-J. Ding, X.-Z. Lan, Y.-J. Guo, ***Trans. Nonferrous Met. Soc. China***, 20 (2010) 240.

[4] P. Pulkkinen, J. Shan, K. Leppanen, A. Kansakoshi, A. Laiho, M. Jarn, H. Tenhu, ***Appl. Mater. Interfaces.***, 1 (2009) 519.

[5] V. Sivanandam, M. Purushothaman, M. Karunanithi, ***Asian. Pac. J. Trop. Biomed.***, 1 (2012) 1.

[6] A. Verma, M. S. Mehata, ***J. Radiat. Res. Appl. Sci.***, 9 (2016) 109.

[7] S. Yallappa, J. Manjanna, M. A. Sindhe, N. D. Satyanarayan, S. N. Pramod, K. Nagaraja, ***Spectrochem. Acta A Mol. Biomol. Spectrosc.***, 110 (2013) 108.

[8] D. K. Sobha, K. Surendranath, V. Meena, K. T. Jwala, N. Swetha, K. S. M. Latha, ***J. Biotech. Mol. Bio. Rev.***, 5 (2010) 001.

[9] K. Sahayaraj, S. Rajesh, ***Bionanoparticles synthesis and antimicrobial applications***, A. Méndez-Vilas ed., ***Science against microbial pathogens: communicating current research and technological advances, 2011***.

[10] N. Krithiga, A. Jayachitra, A. Rajalakshmi, ***An Ind. J. Nano Sci.***, 1 (2013) 6.

[11] Y. Sun, Y. Yin, B. T. Mayers, T. Herricks, Y. Xia, ***Chem. Mater.***, 14 (2002) 4736.

[12] B. Yim, H. Ma, S. Wang, S. Chen, ***J. Phys. Chem. B.***, 107 (2003) 8898.

[13] N. M. Dimitrijevic, D. M. Bartels, C. D. Jonah, K. Takahashi, T. Rajh, ***J. Phys. Chem. B.***, 105 (2001) 954.

[14] A. Callegari, D. Tonti, M. Chergui, ***Nano Lett.***, 3 (2003) 1565.

[15] T. Klaus, R. Joerger, E. Olsson, C. G. Granqvist, ***Proc. Natl. Acad. Sci. U.S.A.***, 96 (1999) 13611.

[16] Y. Konishi, K. Ohno, N. Saitoh, T. Nomura, S. Nagamine, H. Hishida, Y. Takahashi, T. Uruga, ***J. Biotechnol.***, 128 (2007) 648.

[17] B. Nair, T. Pradeep, ***Cryst. Growth Des.***, 2 (2002) 293.

[18] I. Willner, R. Baron, B. Willner, ***Adv. Mater.***, 18 (2006) 1109.

[19] S. S. Shankar, A. Rai, A. Ahmad, M. Sastry, ***J. Colloid Interface Sci.***, 275 (2004) 496.

[20] N. Nagar, S. Jain, P. Kachhawah, V. Devra, ***Korean J. Chem. Eng.***, 33 (2016) 2990.

[21] P. Banerjee, M. Satapathy, A. Mukhopahayay, P. Das, ***Bioresourc. Bioprocess.***, 1 (2014) 1.

[22] D. Philip, C. Unni, S. A. Aromal, V. K. Vidhu, ***Acta A Mol. Biomol. Spectrosc.***, 78 (2011) 899.

[23] S. Iravani, ***Green Chem.***, 13 (2011) 2638.

[24] O.V. Kharissova, H.V. R. Dias, B. I. Kharisov, B. O. Pe´ rez, V. M. Jime´nez Pe´ rez, ***Trends in Biotechnol.***, 31 (2013) 240.

[25] A. K. Mittal, Y. Chisti, U. C. Banerjee, ***Biotechnol. Adv.***, 31 (2013) 346.

[26] I. Hussain, M. Brust, A. J. Papworth, A. I. Cooper, ***Langmuir***, 19 (2003) 4831.

[27] V. K. Sharma, R. A. Yngard, Y. Lin, ***Adv. Colloid Interface Sci.***, 145 (2009) 83.

[28] M. Okuda, Y. Kobayashi, K. Suzuki, K. Sonoda, T. Kondoh, A. Wagawa, A. Kondo, H. Yoshimura, ***Nano Lett.***, 5 (2005) 991.

[29] H. Jiang, S. Manolache, A. C. L. Wong, F. S. Denes, ***J. Appl. Polym. Sci.***, 93 (2004) 1411.

[30] R. Bhattacharya, P. Murkherjee, ***Adv. Drug Deliv. Rev.***, 60 (2008) 1289.

[31] D. R. Bhumkar, H. M. Joshi, M. Sastry, V. B. Pokharkar, ***Pharm. Res.***, 24 (2007) 1415.

[32] S. P. Chandran, M. Chaudhary, R. Pasricha, A. Ahmad, M. Sastry, ***Biotechnol. Prog.***, 22 (2006) 577.

[33] C. Krishnaraj, E. G. Jagan, S. Rajasekar, P. Selvakumar, P. T. Kalaichelvan, N. Mohan, ***Colloids Surf. B: Bio. Interfaces.***, 76 (2010) 50.

[34] R. Veerasamy, T. Z. Xin, S. Gunasagaran, T. F. W. Xiang, E. F. C. Yang, N. Jeyakumar, S. A. Dhanaraj, ***J. Saudi. Chem. Soc.***, 15 (2010) 113.

[35] A. Umer, S. Naveed, N. Ramzan, M.S. Rafiqui, ***Nano***, 7 (2012) 1230005-1.

[36] S. Jain, A. Jain, P. Kachhawah, V. Devra, ***Trans. Nonferrous Met. Soc. China***, 25 (2015) 3995.

[37] M. Tiwari, P. Jain, R. C. Hariharapura, K. Narayanan, B. K. Udaya, N. Udupa, J. V. Rao, ***Process Biochem.***, 51 (2016) 1348.

[38] V. Trisaksri, S. Wongwises, ***Renew. Sust. Energ. Rev.***, 11 (2007) 512.

[39] E. K. Athanassiou, R. N. Grass, W. J. Stark, ***Nanotechnology***, 17 (2006) 1668.

[40] Y. Abboud, T. Saffaj, A. Chagraoui, A. E. Bouari, K. Brouzi, O. Tanane, B. Ihssane, ***Appl. Nanosci.***, 4 (2013) 571.

[41] A. Nasirian, ***Int. J. Nano. Dimens.***, 2 (2012) 159.

[42] K. Saranyaadevi, V. Subha, R. S. E. Ravindran, S. Renganathan, ***Int. J. Chem. Tech. Res.***, 6 (2014) 4533.

[43] V. D. Kulkarni, P. S. Kulkarni, ***Int. J. Chem. Studies***, 1 (2013) 1.

[44] B. H. Patel, M. Z. Channiwala, S. B. Chaudhari, A. A. Mandot, ***Journal of Envionrmental Chemical Engineering (JECE)***, 4 (2016) 2163.

[45] I. Subhankari, P. L. Nayak, ***World J. Nano Sci. Technol.***, 2 (2013) 14.

[46] J. K. V. M. Angrasan, R. Subbaiya, ***Int. J. Curr. Microbiol. App. Sci.***, 3 (2014) 768.46

[47] K. Mukunthan, S. Balaji, ***Int. J. Green Nanotechnol.***, 4 (2012) 71.

[48] O. Koul, M. B. Isman, C. M. Ketkar, ***Can. J. Bot.***, 68 (1990) 1.

[49] H. Bar, D. K. Bhui, G. P. Sahoo, P. Sarkar, S. P. De, A. Misra, ***Colloids Surf. A: Physicochem. Eng. Asp.***, 339 (2009) 134.

[50] K. P. Kumar, W. Paul, C. P. Sharma, ***Process Biochem.***, 46 (2011) 2007.

[51] A. Ingle, M. Rai, A. Gade, M. Bawaskar, ***J. Nanopart. Res.***, 11 (2009) 2079.

[52] M. Rai, C. Posten, ***Green Biosynthesis of Nanoparticles Mechanisms and Applications,(CABI), 2013.*** doi: 10.1079/9781780642239.0000

[53] G. Ghodake, D. S. Lee, ***Journal of Nanoelectronics and Optoelectronics*** 6 (2011) 268.

[54] V. K. Shukla, S. Pandey, A. C. Pandey, Green synthesis of silver nanoparticles using neem leaf (*Azadirachta indica*) extract. (2010) In: Proceedings of International Conference on Advanced Nanomaterials and Nanotechnology, ICANN 2009, Guwahati, Assam (India). 9.11 December 2009.

[55] N. Namratha, P. V. Monica, ***Asian J. Pharm. Tech.***, 3 (2013) 170.

[56] A. Lalitha, R. Subbaiya, P. Ponmurugan, ***Int. J. Curr. Microbiol. App. Sci.***, 2 (2013) 228.

[57] T. Klaus, R. Joerger, E. Olsson, C. G. Granqvist, ***Trends Biotechnol.***, 19 (2001) 15.

[58] P. Mukherjee, A. Ahmad, D. Mandal, S. Senapati, S. R. Sainkar, M. I. Khan, R. Parischa, P. V. Ajayakumar, M. Alam, R. Kumar, M. Sastry, ***Nano Lett.***, 1 (2001) 515.

[59] K. D. Kim, D. N. Han, H. T. Kim, ***Chem. Eng. J.***, 104 (2004) 55.

[60] J. Y. Song, B. S. Kim, ***Bioprocess. Biosyst. Eng.***, 32 (2009) 79.

[61] K. Jyoti, A. Singh, ***journal of genetic engineering and biotechnology***, 14 (2016) 311.

[62] K. Anandalakshmi, J. Venugobal, V. Ramasamy, ***Appl. Nanosci.***, 6 (2016) 399.

[63] P. P. N. V. Kumar, S. V. N. Pammi, P. Kollu, K. V. V. Satyanarayana, U. Shameem, ***Ind. Crops Prod.***, 52 (2014) 562.

[64] M. Vanaja, K. Paulkumar, M. Baburaja, S. Rajeshkumar, G. Gnanajobitha, C. Malarkodi, M. Sivakavinesan, G. Annadurai, ***Bioinorg. Chem. Appl.***, 2014 (2014) 742346.

[65] J. I. Hussain, S. Kumar, A. A. Hashmi, Z. Khan, ***Adv. Mat. Lett.***, 2 (2011) 188.

[66] H. S. Garg, D. S. Bhakuni, ***Hand book of African medicinal plants, CRC Press, London, 1984***.

[67] B. S. Siddiqui, F. Afshan, Ghiasuddin, S. Faizi, S. N. H. Naqvi, R. M. Tariq, ***Phytochemistry***, 53 (2000) 371.

[68] H.S. Garg, D.S. Bhakuni, ***Phytochemistry***, 23 (1984) 2115.

[69] M. Dubey, S. Bhadauria, B. Kushwah, ***Dig. J. Nanomater Biostruct.***, 4 (2009) 537.

[70] J. L. Huang, Q. B. Li, D. H. Sun, Y. H. Lu, Y. B. Su, X. Yang, H. Wang, Y. Wang, W. Shao, N. He, J. Hong, C. Chen, ***Nanotechnology***, 18 (2007) 105104-1.

[71] S. Jain, A. Jain, V. Devra, ***Int. J. Sci. Eng. Res.***, 5 (2014) 973.

[72] M. Valodkar, R. N. Jadeja, M. C. Thounaojam, R. V. Devkar, S. Thakore, ***Mater. Chem. Phys.***, 128 (2011) 83.

[73] W. Yu, H. Xie, L. Chen, Y. Li, C. Zhang, ***Nanoscale Res. Lett.***, 4 (2009) 465.

[74] H. –J. Lee, G. Lee, N. R. Jang, J. H. Yun, J. Y. Song, B. S. Kim, ***NSTI-Nanotech.***, 1 (2011) 371.

[75] T. M. D. Dang, T. T. T. Le, E. F. Ourg-Blanc, M. C. Dang, ***Adv. Nat. Sci. Nanosci. Nanotechnol.***, 2 (2011) 025004.

[76] A. P. Reverberi, M. Salerno, S. Lauciello, B. Fabiano, ***Materials***, 9 (2016) 809.

[77] P. Velmurugan, K. Anbalagan, M. Manosathyadevan, K.-J. Lee, M. Cho, S.-M. Lee, J.-H. Park, S.-G. Oh, K.-S. Bang, B.-T. Oh, ***Bioprocess. Biosyst. Eng.***, 37 (2014) 1935.

[78] S. Raja, V. Ramesh, V. Thivaharan, ***J. Ind. Eng. Chem.***, 29 (2015) 257.

[79] T. Varadavenkatesan, R. Selvaraj, R. Vinayagam, ***J. Mol. Liq.***, 221 (2016) 1063.

Chapter – 4

Kinetic Study of Silver Nanoparticles Catalyzed Degradation of Methyl Orange by Peroxodisulphate

4.1. Introduction

Water pollution due to liberation of coloured effluents from textile dye engineering and textile coloring mills are one of the major ecological concerns, in the world today. Strong colour imparted by the dyes to the receiving aquatic ecosystem poses aesthetic problem and serious ecological problems. Therefore a numbers of techniques aimed at preferential removal dyes from wastewater have been developed [1-5]. However these techniques are non-destructive and merely transfer the dye from one form of waste to another, thus generally secondary pollutants requiring further treatment [6, 7]. Therefore treatment methods based on the biological methods are considered as an alternative option since they are cost effective and eco-friendly. However the textile dyes such as water soluble azo reactive dyes are resistant to aerobic biodegradation and hence traditional aerobic treatment methods cannot be employed.

In the past few decades the advance oxidation process (AOP) has attracted extensive attention as innovative wastewater treatment technologies for the degradation of organic pollutants in water [8, 9], some reactive oxidising species eg. $^{\bullet}OH$, $O_2^{\bullet-}/HO_2^{\bullet-}$ can be generated in AOP and are usually very efficient for dye bleaching and even mineralization. Recently sulphate radical ($SO_4^{\bullet-}$) based AOP has attracted great scientific and technological interest in environmental application [10-14]. Sulphate radicals (SRs), with reduction potential of +2.6 V vs NHE, can be produced by the activation of sulphate based oxidants (PMS, PDS) with heat, ultraviolet, microwave and ultrasound irradiation and/or transition metal ions. A series of experiments evidence has provide that silver nanoparticles (AgNPs) are the best catalyst for the activation of PDS to produce SRs for degradation of persistent organic pollutants in water [11, 15, 16].

In this chapter we evaluated catalytic activity of green synthesized AgNPs in the oxidative degradation of MO by PDS in aqueous medium. Though studies on the kinetics of oxidative degradation of dye with PDS have been widely carried out [17, 18], very few attempts have been made so far on the oxidative degradation of MO in presence of metal nanoparticles [19]. So we have attempt

the catalytic activities of the synthesized nanoparticles have been tested on the oxidative degradation of MO. The present research work also indicated the application of AgNPs as catalyst in dye containing wastewater remediation and these samples collected from drains of local industries situated in Kota city, Rajasthan (India). Wastewater samples have stable structure and chemical properties of organic substances so that necessary to degrade for safe environment. The present study reports first macro molecules of dye degrade into smaller fragments through AOP in presence of AgNPs and biodegradability index [20-22] were also measured by BOD and COD test of samples.

4.2. Experimental

4.2.1. Chemicals and Materials

The methods of preparation and standardization of the solution including peroxodisulphate are given in chapter 2 (Instrumentation and Materials). All the glassware pyrex or borosil were used in experiment. All reagents employed in this study were either of AnalaR or guaranteed reagent grade and were used as supplied without undertaking any further treatment. Always fresh solution of peroxodisulphate was used in experiment. Double distilled water was employed in all experiments. The wastewater samples were collected from the different local textile industries of Kota city (Rajasthan, India) situated at Shopping Centre, Ghantaghar, Vigyan Nagar.

4.2.2. Kinetic Measurements

The oxidative degradation of Methyl orange (MO) was carried out with desired concentration of reactants in stoppered flask at 30 ^{0}C. The reaction was initiated by adding known volume of PDS solution. The kinetics was monitored by the absorbance of MO measured spectrophotometrically at λ_{max} 465 nm in regular time interval. It was observed that the absorbance (A) of the dye solution decreases with increasing time showing the progress of dye degradation. Beer's law was obeyed at 465 nm over the concentration range (1.0×10^{-5} to 1.0×10^{-4} mol dm^{-3}); the molar absorptivity index of MO was found to be 24570 ± 50 mol^{-1} dm^3 cm^{-1}[23]. The degradation of dye containing wastewater samples was also

carried out in presence of AgNPs and degradation rate was monitered by decrease in absorbance at λ_{max} 438, 445, 480 nm in regular time interval. A plot of 2+ log (A) verses time was found linear which indicates pseudo first order kinetics. The pseudo first order rate constant (k_{obs}) were calculated from the slope of these plots. The values of rate constants, k_{obs} were reproducible within ±5 %. The course of reaction was followed for at least 80 % of the reaction.

4.3. Result and Discussion

4.3.1. Product Analysis

4.3.1.1. Determination of degradation products

The intermediates of MO formed during advanced oxidation process were inferred by analysing the samples with LC−MS analysis at different time interval with corresponding m/z values 304, 276, 292, 156, 80, 62 (**Figure 4.1)**. After 15 minutes of degradation, the new peak of successive demethylated product (m/z 276) of MO was obtained (**Figure 4.1B**). Furthermore, after 30 minutes, a new peak observed at m/z 292, which can attribute monohydroxylation of aromatic ring at ortho position of $–NH_2$ group (**Figure 4.1C**). After that the compound m/z 292 fragmented in to the compound at m/z 228 and 156 respectively then the compound at m/z 228 and 156 finally change into end products (CO_2, H_2O, NO_3^- and O_3S^-) (**Figure 4.1D**) [24].

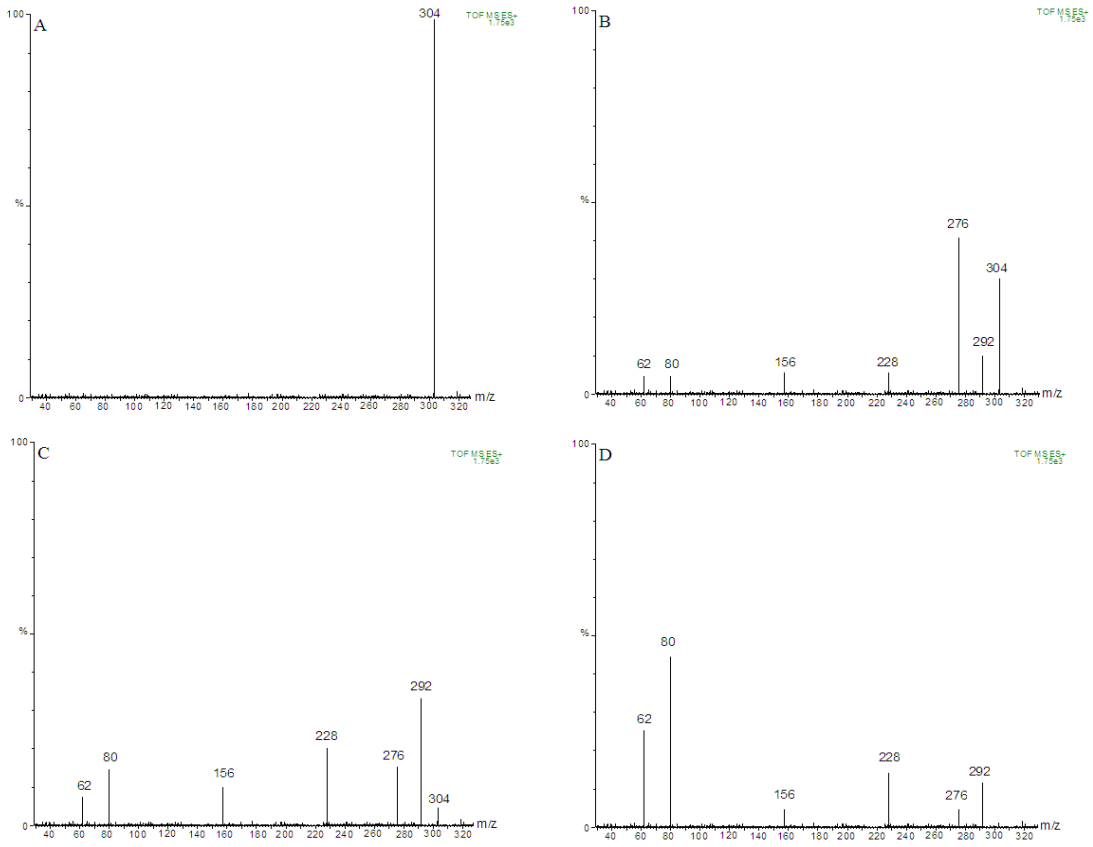

Figure 4.1: LC-MS of MO degraded in AgNPs/PDS system at (A) 0 minutes, (B) 15 minutes, (C) 30 minutes, (D) 45 minutes.

4.3.1.2. UV-visible spectra of intermediates and degradation pathway

The UV-visible spectra of MO degradation with m/z values 304, 276, 292 evaluate on the basis of $[M-H]^-$ ions of the MO (**Figure 4.2**). The UV-visible absorption spectra of reaction mixture before degradation, two main peaks obtained at 465 nm and 271 nm. The absorption of the extended aromatic ring and chromophore group of MO obtained at 465 nm and the additional band obtained at 271 nm are due to the presence of aromatic ring in MO molecule (m/z 304). As the degradation proceeded, the UV-visible spectrum of the compound due to the successive demethylation with m/z value 276 shows a blue shift (400 nm) may be attributed to the homolytic cleavage of the nitrogen-carbon bond, resulting in the substitution of the methyl group by the hydrogen atom. Afterward, hydroxyl radical inserted in benzene ring at ortho position of $–NH_2$ group (m/z 292) could lead to significant wavelength red shift (430 nm) [25]. Finally, polyaromatic ring present in MO convert into monosubstituted aromatic ring and end products, it is confirmed by the presence of two new peaks at 225 nm and 323 nm were obtained in UV-visible spectra (**Figure 4.2**). According to the LC-MS analysis and UV-visible spectral changes results during the degradation process of MO the following degradation pathway were proposed (**Scheme 4.1**).

4.3.2. Effect of Experimental Conditions

4.3.2.1. Dye Dependence

Reaction was carried out at constant [PDS] = 5.0 x 10^{-4} mol dm^{-3}, [AgNPs] = 1.0 x 10^{-8} mol dm^{-3}, pH = 6.5 and and by varying initial concentration of MO from 1.0 x 10^{-5} to 1.0 x 10^{-4} mol dm^{-3} at 30 ^{0}C temperature. The oxidation rate was found to increase with increasing concentration of dye. This may be explain on the basis of that on increasing the concentration of dye, more molecules of dyes were available for degradation. Dye concentration increases beyond certain limits, the reaction rates were decreased (**Table 4.1**), (**Figure 4.3**). It is unreacted PDS acting as scavenger of $SO_4^{\bullet -}$ radicals and producing a less potent HSO_4^- ions.

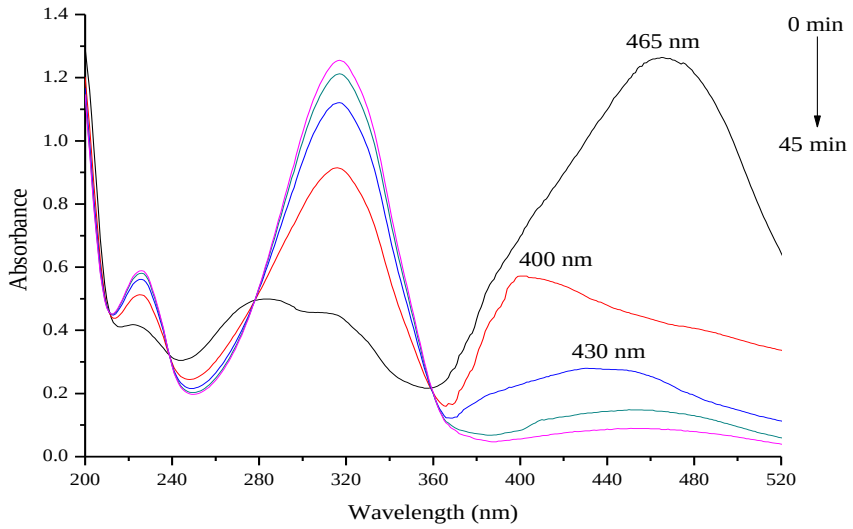

Figure 4.2: UV−Visible adsorption spectra of MO in AgNPs/PDS system with reaction time.

[Dye] = 5.0 x 10^{-5} mol dm^{-3} [PDS] = 5.0 x 10^{-4} mol dm^{-3}

[AgNPs] = 1.0 x 10^{-8} mol dm^{-3} pH = 6.5

Temperature 30 ^{0}C

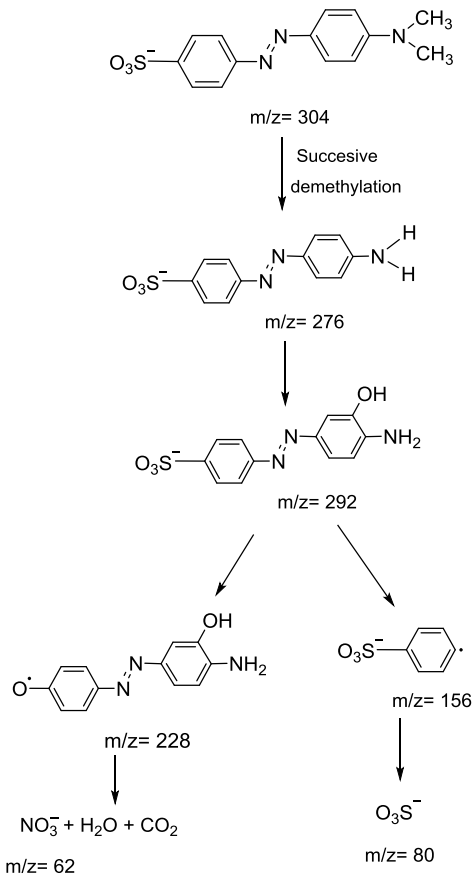

Scheme 4.1: Proposed oxidative degradation route of Methyl orange in AgNPs/PDS system.

TABLE: 4.1
VARIATION OF METHYL ORANGE

[PDS] = 5.0 x 10^{-4} mol dm^{-3} **Temp. = 30 °C**
[AgNPs] = 1.0 x 10^{-8} mol dm^{-3} **pH = 6.5**

10^5 [Dye], mol dm^{-3}	**1.0**	**2.5**	**5.0**	**7.5**	**10**
Time in minutes			**Absorbance**		
0	(0) 0.246	(0) 0.614	1.229	1.843	(0) 2.457
6	(15) 0.183	(8) 0.450	0.901	1.391	(8) 1.843
12	(30) 0.137	(16) 0.328	0.661	1.050	(16) 1.384
18	(45) 0.103	(24) 0.240	0.485	0.792	(24) 1.038
24	(60) 0.076	(32) 0.175	0.356	0.598	(32) 0.775
30	(75) 0.054	(40) 0.127	0.261	0.451	(40) 0.586
36	(90) 0.042	(48) 0.096	0.192	0.340	(48) 0.437
10^4 (k_{obs}), sec^{-1}	**3.2**	**6.5**	**8.6**	**7.81**	**5.99**

Figures in parentheses denote time in minutes.

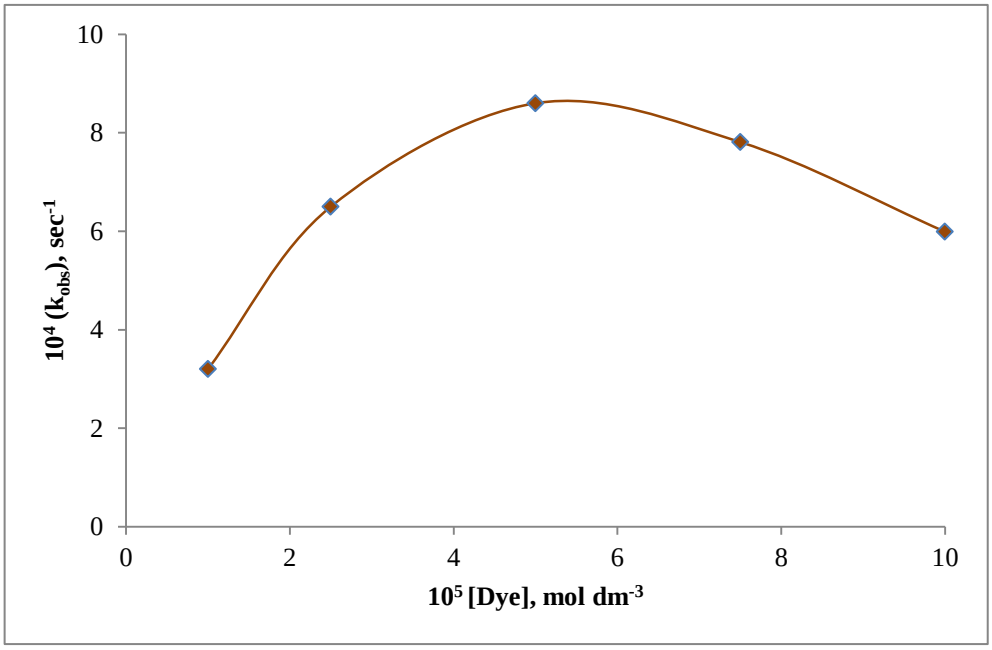

Figure 4.3: Variation of Methyl Orange.

[PDS] = 5.0 x 10^{-4} mol dm^{-3} Temp. = 30 °C

[AgNPs] = 1.0 x 10^{-8} mol dm^{-3} pH = 6.5

(Ref. Table: 4.1)

4.3.2.2. Peroxodisulphate Dependence

The AgNPs catalysed oxidative degradation of MO was studied at different concentration of PDS from 1.0 x 10^{-4} to 1.0 x 10^{-3} mol dm^{-3} at 30 ^{0}C temperature, fixed concentration of [Dye] = 5.0 x 10^{-5} mol dm^{-3}, [AgNPs] =1.0 x 10^{-8} mol dm^{-3} and pH = 6.5. The rate of dye degradation is increases with increases initial concentration of PDS. This is likely because $SO_4^{\bullet-}$ radical ions were generated simultaneously, which in turn increases the rate of oxidation of Ag° to Ag^+ ion, Ag^+ ion enhance the oxidative decolourization of MO. Furthermore the PDS concentration increases beyond 5.0 x 10^{-4} mol dm^{-3}, the degradation rate of MO slowed down slightly. At higher concentration of PDS the side reaction between persulphate anion ($S_2O_8^{2-}$) and $SO_4^{\bullet-}$ become more significant (Equation 1), which would consume more PDS, hence the remaining percentage of PDS decreases with the increases of PDS concentration [26] (**Table 4.2**), (**Figure 4.4**).

$$S_2O_8^{2-} + SO_4^{\bullet-} \rightarrow S_2O_8^{\bullet-} + SO_4^{2-} \quad (1)$$

4.3.2.3. Effect of Initial pH

The initial pH of the solution is a key factor which affects the degradation of dye, because pH influences the surface charge properties of the catalyst [27]. The degradation of dye from textile dye effluents was studied at different initial pH of solution values in the range 5-8. Hence the effect of initial pH on the rate of degradation of MO was investigated in the pH range 2.5 to 10 and other fixed reaction conditions [Dye] = 5.0 x 10^{-5} mol dm^{-3}, [PDS] = 5.0 x 10^{-4} mol dm^{-3}, [AgNPs] = 1.0 x 10^{-8} mol dm^{-3} at 30 °C temperature. The pH value of reaction was adjusted by H_2SO_4 and NaOH solution. The results illustrate that the degradation of MO was carried out effectively at 6.5 pH (**Table 4.3**) (**Figure 4.5**). At higher pH, AgNPs becomes negatively charged according to Equation 2.

$$AgOH + OH^- \rightarrow H_2O + Ag^- \quad (2)$$

At lower pH (pH = 5) then AgNPs is positively charged according to Equation 3.

$$AgOH + H^+ \rightarrow H_2O + Ag^+ \quad (3)$$

TABLE: 4.2
VARIATION OF PEROXODISULPHATE

[Dye] = 5.0 x 10^{-5} mol dm^{-3} **Temp. = 30 °C**
[AgNPs] = 1.0 x 10^{-8} mol dm^{-3} **pH = 6.5**

10^4 [PDS], mol dm^{-3}	**1.0**	**2.5**	**5.0**	**7.5**	**10**
Time in minutes			**Absorbance**		
0	(0) 1.228	(0) 1.225	1.229	1.230	1.226
6	(40) 0.944	(15) 0.865	0.901	0.921	0.935
12	(80) 0.725	(30) 0.609	0.661	0.691	0.711
18	(120) 0.557	(45) 0.429	0.485	0.518	0.541
24	(160) 0.427	(60) 0.302	0.356	0.388	0.411
30	(200) 0.328	(75) 0.212	0.261	0.291	0.313
36	(240) 0.244	-	0.192	0.218	0.238
10^4 (k_{obs}), sec^{-1}	**1.1**	**3.9**	**8.6**	**8.0**	**7.6**

Figures in parentheses denote time in minutes.

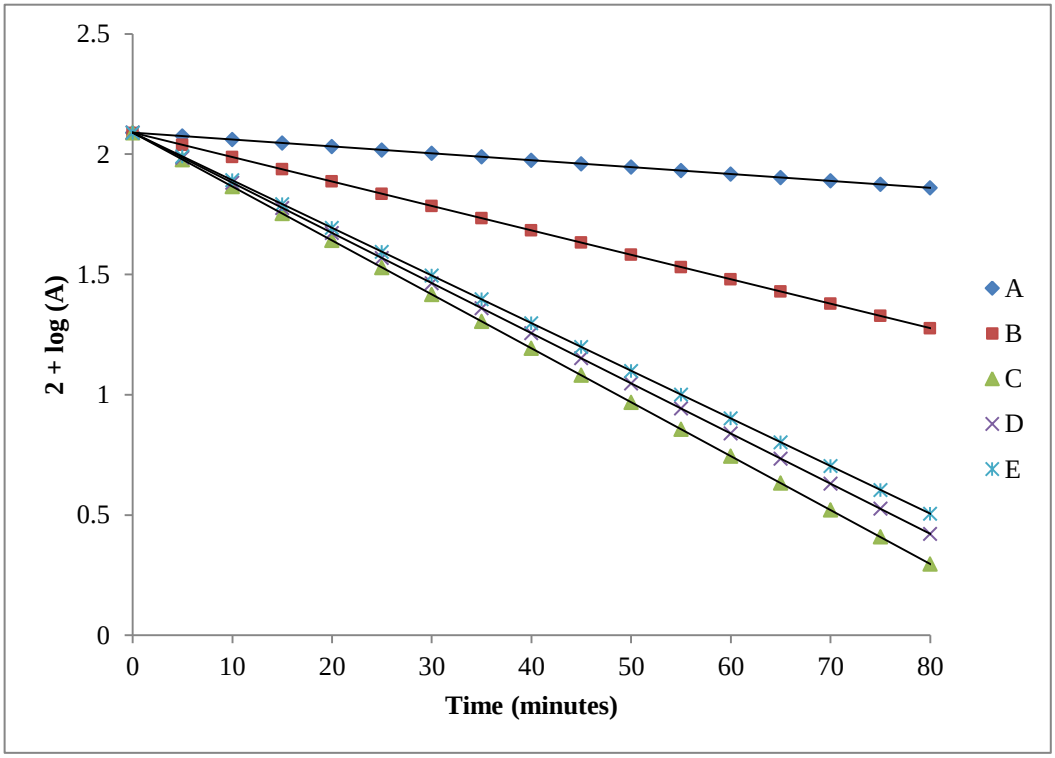

Figure 4.4: Variation of Peroxodisulphate.

[Dye] = 5.0 x 10^{-5} mol dm^{-3} Temp. = 30 °C

[AgNPs] = 1.0 x 10^{-8} mol dm^{-3} pH = 6.5

[PDS] = (A) 1.0 x 10^{-4} mol dm^{-3} (D) 7.5 x 10^{-4} mol dm^{-3}

(B) 2.5 x 10^{-4} mol dm^{-3} (E) 10.0 x 10^{-4} mol dm^{-3}

(C) 5.0 x 10^{-4} mol dm^{-3}

(**Ref. Table: 4.2**)

TABLE: 4.3
VARIATION OF pH

[Dye] = 5.0 x 10^{-5} mol dm^{-3} **[AgNPs] = 1.0 x 10^{-8} mol dm^{-3}**
[PDS] = 5.0 x 10^{-4} mol dm^{-3} **Temp. = 30 °C**

pH	**2.5**	**5**	**6.5**	**7**	**8**	**9**	**10**
Time in minutes				**Absorbance**			
0	(0) 1.227	1.225	1.229	1.226	1.228	1.229	1.230
8	(40) 0.921	0.857	0.813	0.845	0.865	0.882	0.908
16	(80) 0.691	0.598	0.539	0.581	0.610	0.634	0.671
24	(120) 0.518	0.417	0.354	0.401	0.429	0.455	0.496
32	(160) 0.388	0.291	0.236	0.274	0.303	0.327	0.367
40	(200) 0.291	0.203	0.156	0.190	0.213	0.235	0.271
48	(240) 0.218	0.142	-	-	0.151	0.169	0.201
10^4 (k_{obs}), sec^{-1}	**1.2**	**7.5**	**8.6**	**7.8**	**7.3**	**6.9**	**6.3**

Figures in parentheses denote time in minutes.

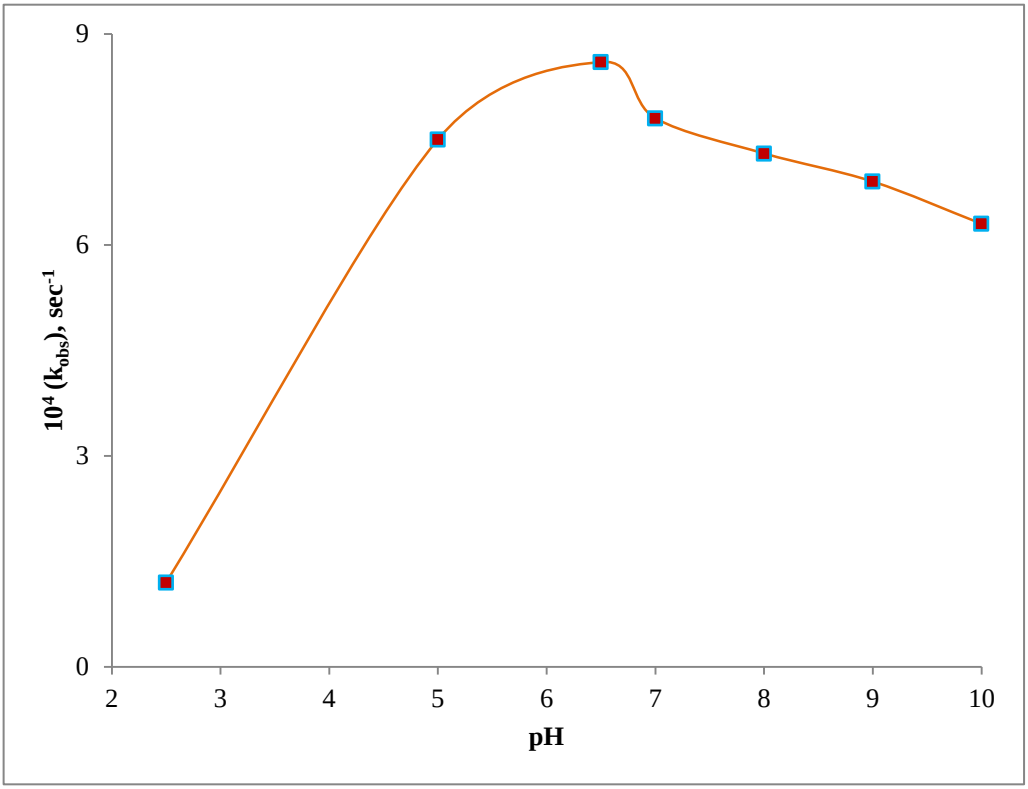

Figure 4.5: Variation of pH.

[Dye] = 5.0 x 10^{-5} mol dm^{-3} [PDS] = 5.0 x 10^{-4} mol dm^{-3}

[AgNPs] = 1.0 x 10^{-8} mol dm^{-3} Temp. = 30 °C

(**Ref. Table: 4.3**)

4.3.2.4. Silver Nanoparticles Dependence

The catalytic activity of synthesised AgNPs was evaluate in oxidative degradation of MO by PDS by varying concentration from 0.25 x 10^{-8} to 2.0 x 10^{-8} mol dm^{-3} at fixed [PDS] = 5.0 x 10^{-4} mol dm^{-3}, [Dye] = 5.0 x 10^{-5} mol dm^{-3}, pH = 6.5 and 30 ^{0}C temperature. The rate of reaction increases with increasing concentration of AgNPs (**Table 4.4**). Degradation reaction is 7 time faster in presence of small concentration of the AgNPs (**Figure 4.6**). The catalytic activity of AgNPs also tested on waste water samples, were collected from drains of three different local textile industries of Kota region. Catalytic oxidative degradation was performed with a similar method as mentioned above at different concentration of AgNPs (**Table 4.5, 4.6, 4.7**), (**Figure 4.6**). The difference between the rate constants of sample dye and waste water samples can be attributed to structural difference and concentrations of different dye molecules present in the waste water samples.

4.3.2.5. Mechanism

$K_2S_2O_8$ can be activated by Ag° to generate $SO_4^{\bullet-}$ at ambient temperature. The plausible mechanism is support of the observed kinetics as given below−

$$S_2O_8^{2-} + Ag^\circ \rightarrow SO_4^{\bullet-} + SO_4^{2-} + Ag(I)$$

$$SO_4^{\bullet-} + Ag(I) + Dye \rightarrow \text{Product} + Ag^\circ$$

$$S_2O_8^{2-} + Dye \xrightarrow{Ag^\circ} \text{Product} + SO_4^{2-}$$

Based on the results it may be concluded that the oxidative degradation of dye in presence of AgNPs by $K_2S_2O_8$ is radical ion based mechanism and the main radical ion species generated during the catalytic activation of $K_2S_2O_8$ was sulphate radical ions ($SO_4^{\bullet-}$) [19]. Finally sulphate radicals are attack on dye molecules resultant after demethylation and hydroxylation end products were obtained.

TABLE: 4.4
EFFECT OF SILVER NANOPARTICLES
(Pure Methyl Orange)

[Dye] = 5.0 x 10^{-5} mol dm^{-3} **Temp. = 30 °C**
[PDS] = 5.0 x 10^{-4} mol dm^{-3} **pH = 6.5**

10^8 [AgNPs], mol dm^{-3}	**0**	**0.25**	**0.5**	**0.75**	**1.0**	**1.5**	**2.0**
Time in minutes				**Absorbance**			
0	(0) 1.229	(0) 1.228	(0) 1.227	1.230	1.229	(0) 1.225	(0) 1.229
5	(40) 0.921	(15) 0.934	(10) 0.919	1.004	0.949	(4) 0.917	(4) 0.839
10	(80) 0.691	(30) 0.710	(20) 0.687	0.822	0.733	(8) 0.684	(8) 0.573
15	(120) 0.518	(45) 0.539	(30) 0.514	0.671	0.567	(12) 0.510	(12) 0.391
20	(160) 0.388	(60) 0.410	(40) 0.385	0.550	0.438	(16) 0.381	(16) 0.267
25	(200) 0.291	(75) 0.311	(50) 0.288	0.451	0.338	(20) 0.284	(20) 0.182
30	(240) 0.218	(90) 0.237	(60) 0.215	0.368	0.242	(24) 0.212	-
10^4 (k_{obs}), sec^{-1}	**1.2**	**3.05**	**4.84**	**6.7**	**8.6**	**12.2**	**15.9**

Figures in parentheses denote time in minutes.

TABLE: 4.5

EFFECT OF SILVER NANOPARTICLES

(Shopping Centre, Kota)

[PDS] = 5.0 x 10^{-4} mol dm^{-3} **Temp. = 30 °C**

pH = 7.2

10^8 [AgNPs], mol dm^{-3}	**0**	**0.25**	**0.5**	**0.75**	**1.0**	**1.5**	**2.0**
Time in minutes				**Absorbance**			
0	(0) 1.982	(0) 1.981	(0) 1.983	1.980	1.982	(0) 1.981	(0) 1.984
10	(50) 1.495	(20) 1.507	(15) 1.433	1.477	1.362	(8) 1.293	(5) 1.401
20	(100) 1.127	(40) 1.147	(30) 1.037	1.101	0.936	(16) 0.843	(10) 0.990
30	(150) 0.850	(60) 0.872	(45) 0.750	0.820	0.643	(24) 0.550	(15) 0.701
40	(200) 0.642	(80) 0.663	(60) 0.542	0.611	0.442	(32) 0.359	(20) 0.494
50	(250) 0.484	(100) 0.505	(75) 0.392	0.456	0.304	(40) 0.243	(25) 0.349
60	(300) 0.365	(120) 0.384	-	0.340	-	-	(30) 0.247
10^4 (k_{obs}), sec^{-1}	**0.94**	**2.28**	**3.6**	**4.9**	**6.25**	**8.9**	**11.57**

Figures in parentheses denote time in minutes.

TABLE: 4.6

EFFECT OF SILVER NANOPARTICLES

(Ghantaghar, Kota)

[PDS] = 5.0 x 10^{-4} mol dm^{-3} **Temp. = 30 °C**

pH = 6.8

10^8 [AgNPs], mol dm^{-3}	**0**	**0.25**	**0.5**	**0.75**	**1.0**	**1.5**	**2.0**
Time in minutes				**Absorbance**			
0	(0) 1.531	(0) 1.532	1.530	1.533	(0) 1.531	(0) 1.530	(0) 1.532
15	(50) 1.169	(25) 1.117	1.158	1.049	(10) 1.114	(6) 1.167	(5) 1.145
30	(100) 0.892	(50) 0.816	0.876	0.719	(20) 0.811	(12) 0.887	(10) 0.850
45	(150) 0.681	(75) 0.595	0.663	0.493	(30) 0.590	(18) 0.675	(15) 0.634
60	(200) 0.520	(100) 0.434	0.502	0.338	(40) 0.429	(24) 0.514	(20) 0.472
75	(250) 0.397	(125) 0.317	0.380	0.231	(50) 0.312	(30)0.390	(25) 0.352
90	(300) 0.303	(150) 0.231	0.287	-	(60) 0.227	(36) 0.285	(30) 0.261
10^4 (k_{obs}), sec^{-1}	**0.94**	**2.1**	**3.1**	**4.2**	**5.3**	**7.55**	**9.76**

Figures in parentheses denote time in minutes.

TABLE: 4.7
EFFECT OF SILVER NANOPARTICLES
(Vigyan Nagar, Kota)

[PDS] = 5.0 x 10^{-4} mol dm^{-3} **Temp. = 30 °C**
pH = 6.2

10^8 [AgNPs], mol dm^{-3}	**0**	**0.25**	**0.5**	**0.75**	**1.0**	**1.5**	**2.0**
Time in minutes				**Absorbance**			
0	(0) 1.791	(0) 1.793	(0) 1.792	(0) 1.790	1.791	1.790	(0) 1.792
10	(55) 1.339	(25) 1.369	(20) 1.303	(15) 1.307	1.373	1.234	(5) 1.409
20	(110) 1.002	(50) 1.047	(40) 0.948	(30) 0.954	1.052	0.851	(10) 1.109
30	(165) 0.749	(75) 0.800	(60) 0.690	(45) 0.696	0.807	0.587	(15) 0.876
40	(220) 0.560	(100) 0.612	(80) 0.502	(60) 0.508	0.619	0.404	(20) 0.687
50	(275) 0.419	(125) 0.468	(100) 0.365	(75) 0.371	0.474	0.279	(25) 0.541
60	(330) 0.314	(150) 0.358	(120) 0.266	(90) 0.271	0.318	-	(30) 0.426
10^4 (k_{obs}), sec^{-1}	**0.88**	**1.79**	**2.65**	**3.5**	**4.43**	**6.2**	**7.99**

Figures in parentheses denote time in minutes.

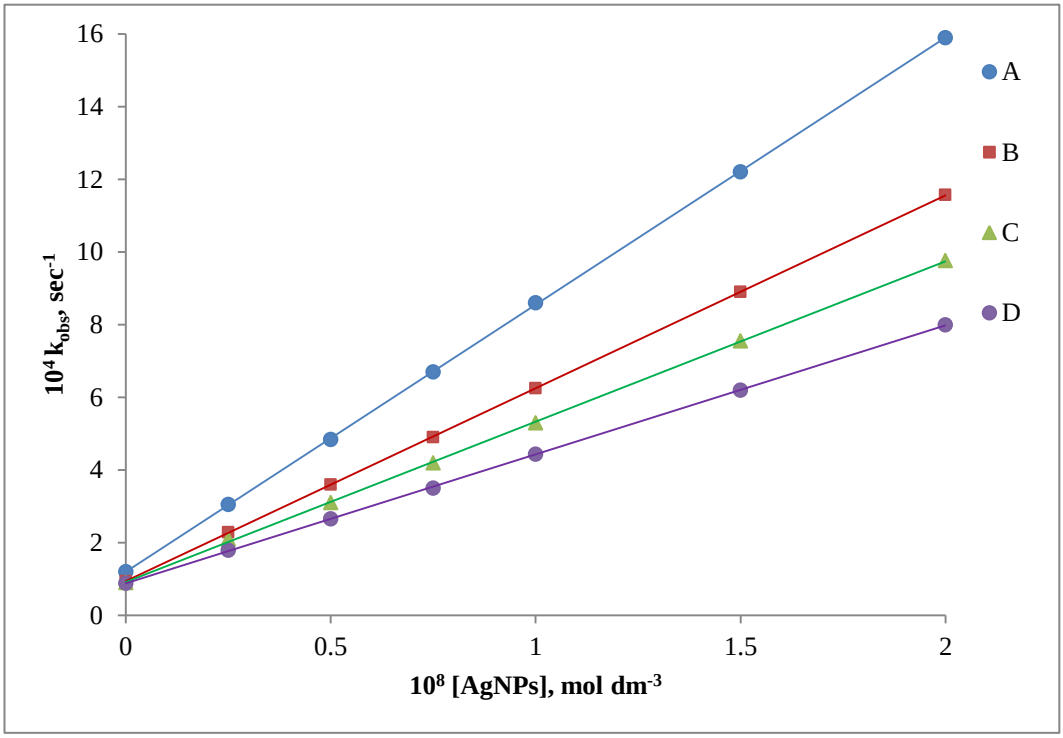

Figure 4.6: Effect of [AgNPs] on degradation rate of different water samples.

[PDS] = 1.0 x 10^{-4} mol dm^{-3} Temp. = 30 °C

[Dye] = 5.0 x 10^{-5} mol dm^{-3}

Water Samples (A) Pure Methyl Orange (pH = 6.5)

(B) Shopping Centre, Kota (pH = 7.2)

(C) Ghantaghar, Kota (pH = 6.8)

(D) Vigyan Nagar, Kota (pH = 6.2)

(Ref. Table: 4.4, 4.5, 4.6, 4.7)

4.3.2.6. Biodegradability

COD analysis simply indicate the total waste load in a textile waste effluent and the ratio of BOD and COD gives information about biodegradability of wastewater samples [28]. **Table 4.8** shows result of BOD and COD analysis of MO dye (5.0×10^{-5} mol dm^{-3}), wastewater samples; before and after AOP at [PDS] = 5.0×10^{-4} mol dm^{-3}, [AgNPs] = 1.0×10^{-8} mol dm^{-3}, Temperature 30 ^{0}C and pH = 6.5, 7.2, 6.8, 6.2. The results indicate that after apply AOP on MO dye, wastewater samples; COD decreases from 56-62 %, BOD increases 14-120 %. When biodegradability index is less than 0.3 (Before AOP), the wastewater is difficult to biodegraded. While biodegradability index is more than 0.3 (After AOP), the wastewater has better biodegradability [29].

TABLE: 4.8

Experimental Results of BOD and COD before and after Advanced Oxidation Process.

Samples	Before AOP				After AOP				% BOD increases	% COD reduction
	pH	BOD (mg/l)	COD (mg/l)	BOD/COD	pH	BOD (mg/l)	COD (mg/l)	BOD/COD		
MO	6.5	5	70	0.07	6.3	11	28	0.39	120 %	60.0 %
Sample 1	7.0	87	486	0.18	6.8	100	212	0.47	14.9 %	56.3 %
Sample 2	6.8	58	370	0.15	6.6	80	140	0.57	37.9 %	62.0 %
Sample 3	6.2	72	410	0.17	6.0	91	168	0.54	26.3 %	59.0 %

4.4. Conclusion

The green synthesised AgNPs were applied as a catalyst for oxidative degradation of a MO and wastewater samples in aqueous solution through SRs approach has been studied. The silver nanoparticles exhibited good efficiency for activation of PDS to provide sulphate radicals for degrading MO dye and wastewater samples. Increase in catalyst and PDS concentration the rate of MO degradation also increases. The results suggested that silver nanoparticles have a strong potential for fast dye degradation technologies. AgNPs as a catalyst was demonstrate also efficiently degrading dying wastewater samples, collected from drains of local industries situated in Kota city, Rajasthan (India). The results also reports AOP of wastewater samples, biodegradability index is an increase, so that organic matter can be decomposed easily.

4.5. Reference

[1] E. Forgacs, T. Cserhati, G. Oros, ***Environ. Internat.***, 30 (2004) 953.

[2] T. Robinson, G. McMullan, R. Marchant, P. Nigam, ***Biores. Technol.***, 77 (2001) 247.

[3] J. J. M. Orfao, A. I. M. Silva, J. C. V. Pereira, S. A. Barata, I. M. Fonseca, P. C. C. Faria, M. F. R. Pereira, ***J. Colloids Interf. Sci.***, 296 (2006) 480.

[4] C. L. Yang, J. McGarrahan, ***J. Hazard. Mater.***, B127 (2005) 40.

[5] M. Muruganandham, M. Swaminathan, ***Dyes Pigments.***, 68 (2006) 133.

[6] I. Arslan-Alaton, J. L. Ferry, ***Dyes Pigments.***, 54 (2002) 25.

[7] Y. M. Slokar, A. M. Le Marechal, ***Dyes Pigments.***, 37 (1998) 335.

[8] Z. H. Wang, W. H. Ma, C. C. Cheng, J. C. Zhao, ***J. Hazard Mater.***, 168 (2009) 1246.

[9] J. He, W. Ma, J. He, J. Zhao, J. C. Yu, ***Appl. Catal. B: Environ.***, 39 (2002) 211.

[10] X. Y. Chen, X. L. Qiao, D. G. Wang, J. Lin, J. W. Chen, ***Chemosphere.***, 67 (2007) 802.

[11] X- Y. Chen, J- W. Chen, X- L. Qiao, D- G. Wang, X- Y. Cai, ***Appl. Catal. B: Environ.***, 80 (2008) 116.

[12] S. K. Ling, S- B. Wang, Y- L. Peng, ***J. Hazard Mater.***, 178 (2010) 385.

[13] P. R. Shukla, S- B. Wang, H. M. Ang, M. O. Tadé, ***Sep. Purif. Technol.***, 30 (2010) 338.

[14] K. H. Chan, W. Chu, ***Water Res.***, 43 (2009) 2513.

[15] E. Psillakis, D. Mantzavinos, ***J. Chem. Technol. Biot.***, 79 (2004) 431.

[16] H. S. Devi, T. D. Singh, ***Advance in Electronic and Electric Engineering***, 4 (2014) 83.

[17] J. B. Zhong, J. Z. Li, Y. Lu, S. T. Huang, W. Hu, ***Iran J. Chem. Chem. Eng.***, 31 (2012) 21.

[18] M. H. Rasouliard, R. Marani, H. Majidzadeh, I. Baheri, ***Environ. Eng. Sci.***, 28 (2011) 229.

[19] L. Hou, H. Zhang, X. Xue, ***Sep. Purif. Technol.***, 84 (2012) 147.

[20] E. Chamarro, A. Marco, S. Esplugas., ***Water Res***., 35 (2001) 1047.

[21] J. P. Scott, D. F. Ollis, ***Environ. Prog,.*** 14 (1995) 88.

[22] F. Al-Momani, E. Touraud, J. R. Degorce-Dumas, J. Roussy, O. Thomas, ***Journal of Photochemistry and Photobiology A: Chemistry***, 153 (2002) 191.

[23] S. A. Daher, ***J. Edu. Sci.***, 25 (2001) 79.

[24] S. Hisaindee, M. A. Meetani, M. A. Rauf, ***Trends Anal. Chem.***, 49 (2013) 31.

[25] T. Chen, Y. Zheng, J. –M. Lin, G. Chen, Study on the Photocatalytic Degradation of Methyl Orange in Water Using Ag/ZnO as Catalyst by Liquid Chromatography Electrospray Ionization Ion-Trap Mass Spectrometry. ***J. Am. Soc. Mass Spectrom.*** 19 (2008) 997.

[26] J. Wu, H. Zhang, J. Qiu, ***J. Hazard. Mater.***, 215-216 (2012) 138.

[27] M. A. Behnajady, H. Eskandarloo, ***Res. Che. Intermed.***, 41 (2013) 2001.

[28] A. L. Bridie, C. J. M. Wolff, M. Winter, ***Water Res***.,13 (1979) 627.

[29] H. Chun, W. Yizhong, ***Chemosphere,*** 39 (1999), 2107.

Chapter – 5

Kinetic Study of Silver Nanoparticles Catalyzed Degradation of Orange G by Peroxomonosulphate

5.1. Introduction

Nanotechnology is presently one of the most dynamic disciplines of research in material science. The field of nanocatalysis has undergone an explosive growth during the past decades, both in homogeneous and heterogeneous catalysis [1,2]. Since nanoparticles have a large surface to volume ratio compared to bulk materials, they are attractive to use as catalyst [3-6] and sensor [7].

Water pollution due to the discharge of coloured effluents from textile dye manufacturing and textile coloring mills is one of the major environmental anxieties, in the world today. Hence a number of techniques directed at preferential removal dyes from wastewater have been developed [8-12]. The advanced oxidation processes (AOPs) shows great interest of scientiests due to it's extensive attention in wastewater treatment technologies [13, 14]. Sulphate radical ($SO_4^{\bullet-}$) based AOP has attracted extensive attention in environmental application [15-19]. Sulphate radicals (SRs) can be formed by the activation of sulphate based oxidants (peroxomonosulphate, peroxodisulphate) by different methods like heat, ultraviolet, microwave, ultrasound irradiation and transition metal ions and reduction potential of SRs is +2.6 V versus NHE. Application of nanomaterials in the AOP involving the greener method for the remediation of intensity coloured polluted water due to textile dyes from various industries are most prevalent in current research [20]. Orange G is an anionic mono-azo dye, which belongs to the hydrosoluble phenylazonaphthol dyes and chosen as a model compound because it is widely used in the dying of textiles, food, in weaving, tanning and paper industries [16].

The earlier study reports the metal nanoparticles are the best catalyst for the activation of oxone to produce SRs for complete degradation of persistent organic pollutants or compounds in water [21]. It has been studied that there is not enough information in the literature on the oxidative degradation of Orange G by peroxomonosulphate in presence of silver nanoparticles. The present investigation

is a part of a broad programme of green synthesis of Ag NPs and their catalytic effect on the oxidative degradation of OG by PMS in an aqueous medium.

5.2. Experimental

5.2.1. Chemicals and Materials

Peroxomonosulphate (PMS) is a triple salt with the composition of $2KHSO_5 \cdot KHSO_4 \cdot K_2SO_4$ and the commercial name "OXONE" (Sigma-Aldrich). A fresh solution of PMS was made before starting the experiment. All other reagents employed in this study were either of AnalaR grade or guaranteed reagent grade and were used as supplied without undertaking any further treatment and the methods of prepare solution are given in chapter 2 (Instrumentation and Materials). Doubly distilled water was used throughout the study. The second distillation was from alkaline permanganate solution in an all glass apparatus.

5.2.2. Kinetic Measurements

The oxidative degradation of Orange G was carried out with the required concentration of reactants in stoppered Erlenmeyer flask at 30 ± 0.1 °C. The reaction was initiated by adding the known volume of PMS solution. The kinetics was monitored by the absorbance of Orange G measured spectrophotometrically at λ_{max} 476 nm at regular time interval. It was observed that the absorbance (A) of the dye solution decreases with increasing time showing the progress of dye degradation. Beer's law was obeyed at 476 nm over the concentration range (1.0×10^{-5} to 1.0×10^{-4} mol dm^{-3}); the molar absorptivity index of OG was found to be 19650 ± 50 mol^{-1} dm^3 cm^{-1} [22, 23]. A plot of 2+ log (A) versus time was found linear which indicates pseudo-first-order kinetics and the value of rate constant were found from the slope of these plots. All the kinetics runs were followed up to 80 % completion of the reaction.

5.3. Result and Discussion

5.3.1. Product Analysis

AgNPs were used as a catalyst in oxidative degradation of the aqueous solution of OG as shown in UV-visible spectra at the different time interval (**Figure 5.1**). The spectrum obtained prior to the addition of nanocatalyst (Spectra A) is characterized by three main peaks at 248, 326 and 479 nm with a shoulder peak at 423 nm. The peaks at 248 and 326 nm are attributed to its aromatic rings which are arises due to the π–π* transition. The bands at 479 nm and the shoulder at 423 nm are attributed the conjugated system formed by azo bond and arises from the n–π* transition of –N=N– group [24, 25]. After addition of AgNPs, the absorbance decreases (Spectra B-J) reflects the decolouration of dye is a fast process under AgNPs/PMS system, it was detected that the two characteristic absorption peaks at 326 and 479 nm decreased and almost disappeared within 32 minutes initiation of the reaction. This specifies that the chromophore and conjugated system were being demolished, while the peak at 248 nm downfall gently, presenting that the aromatic rings were decay slowly [26]. No new absorption bands appear in either the visible or the UV-visible regions.

The identification of intermediates generates during degradation process and end products were carried out by LC-MS analysis of reaction products. The LC-MS analysis results shown in **figure 5.2** that Orange G were degraded in the presence of AgNPs, at the different time interval. The significant peaks present at the different time of degradation with corresponding m/z values 335, 222, and 194. The proposed degradation pathway shows that $SO_4^{\bullet-}$ radicals initially attacks on the azo bond, leading to the loss of characteristic fragments of 93 ($-C_6H_5NH_2$), 17 (-OH), 81 ($-SO_3H$) and 64 ($-SO_2$) groups. These products were produced by desulphonation and hydroxylation of the aromatic ring and oxidative cleavage of the azo bond (**Scheme 5.1**) [23, 26, 27].

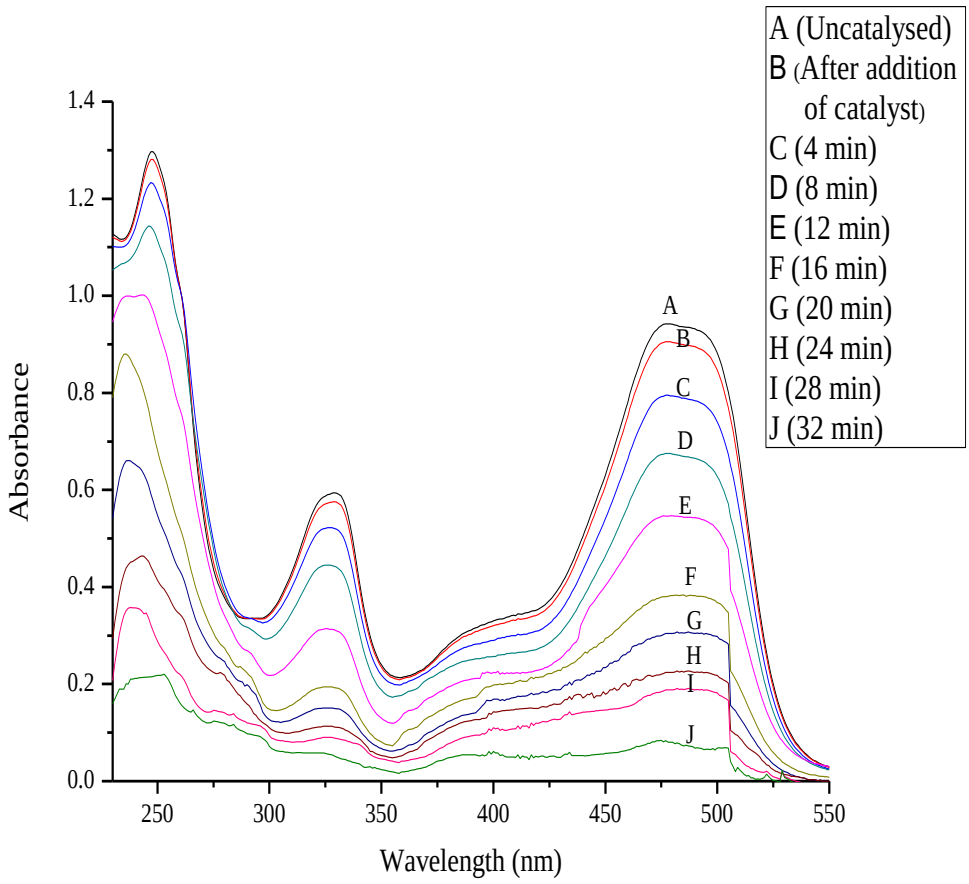

Figure 5.1: The change of UV-visible spectrum with reaction time in AgNPs/PMS system.

[Dye] = 5.0 x 10^{-5} mol dm^{-3} [PMS] = 5.0 x 10^{-4} mol dm^{-3}

[AgNPs] = 1.0 x 10^{-7} mol dm^{-3} pH = 9.2

Temperature 30 °C

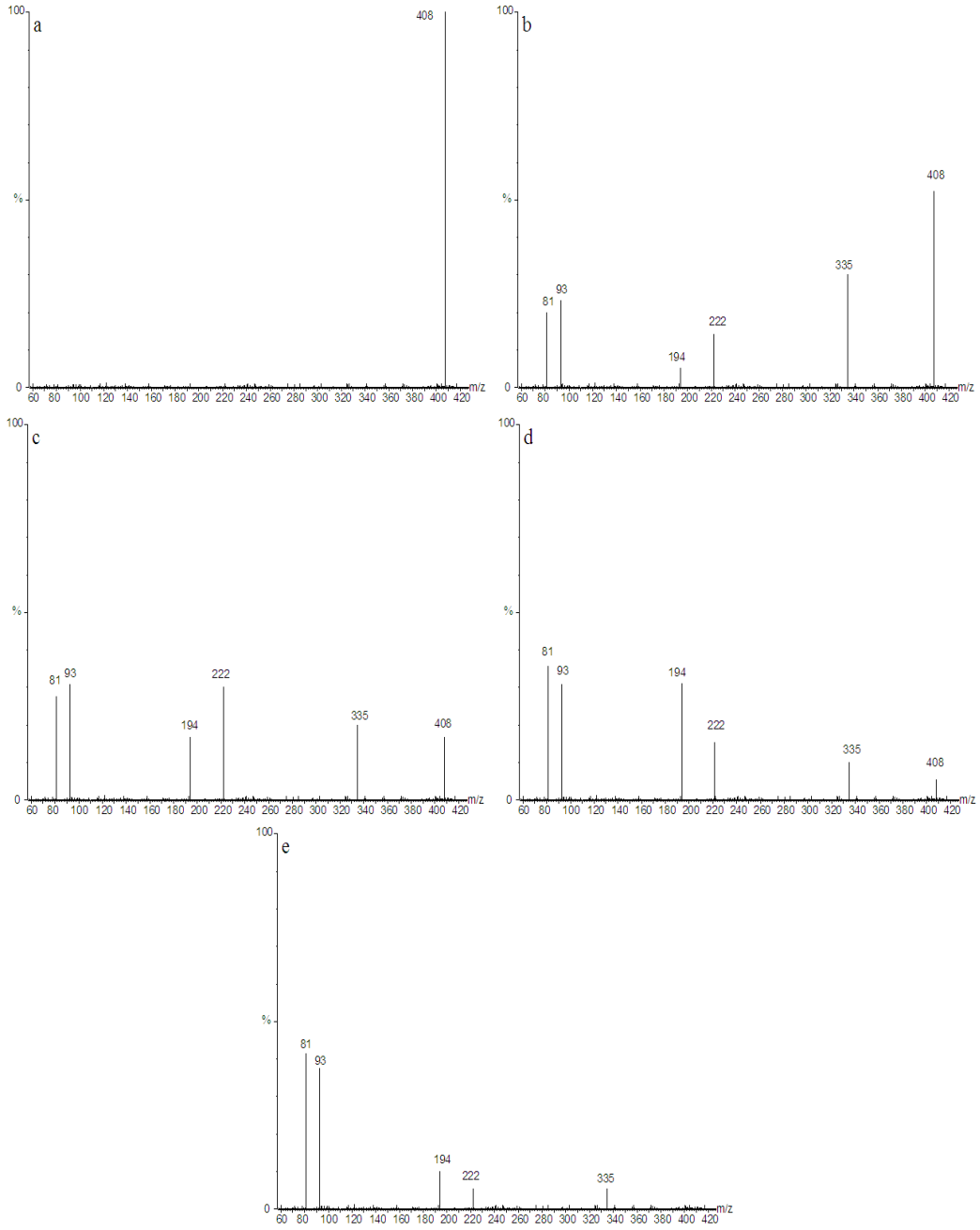

Figure 5.2: LC-MS of Orange G degraded at (a) 0 minutes, (b) 10 minutes, (c) 20 minutes, (d) 28 minutes, (e) 32 minutes; in AgNPs/PMS system.

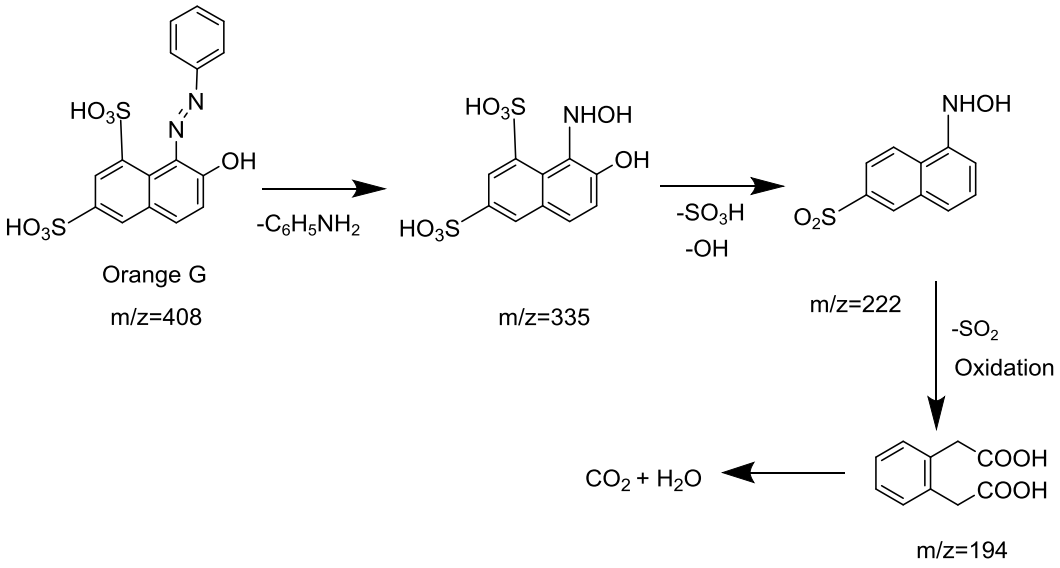

Scheme 5.1: Proposed oxidative degradation route of OG in AgNPs/PMS system.

5.3.2. Effect of Experimental Conditions

5.3.2.1. Dye Depedence

The reaction was carried out at the constant concentration of other reactants ([PMS] = 5.0 x 10^{-4} mol dm^{-3}, [AgNPs] = 1.0 x 10^{-7} mol dm^{-3} and pH = 9.2) and by varying the initial concentration of OG from 1.0 x 10^{-5} to 1.0 x 10^{-4} mol dm^{-3} at 30 °C temperature. The oxidation rate was found to increase with increasing concentration of dye. This may be explaining on the basis that on increasing the concentration of dye, the reaction rate was increased as more molecules of dyes were available for degradation. It also reports that increasing the concentration of dye beyond the certain limits, the oxidation rate was decreased (**Table 5.1**) (**Figure 5.3**). The decreasing degradation rate at higher dye concentration describes that at constant PMS concentration, the amount of PMS was smaller so degradation of dyes slowed down significantly.

5.3.2.2. Peroxomonosulphate Dependence

The AgNPs catalyzed oxidative degradation of OG was studied at the different concentration of PMS from 1.0 x 10^{-4} to 1.0 x 10^{-3} mol dm^{-3} at 30 °C temperature and the fixed concentration of other reactants were [Dye] = 5.0 x10^{-5} mol dm^{-3}, [AgNPs] = 1.0 x 10^{-7} mol dm^{-3} at pH = 9.2. The rate of oxidative degradation of OG was increased on increasing the PMS concentration (**Table 5.2**) (**Figure 5.4**). It may be due to the fact that as the concentration of PMS increases, the concentration of $SO_4^{\bullet-}$ sulphate radicals ions also increases, which in turn increases the rate of oxidation of Ag° to Ag^+ ion oxidizes dye molecule to its radical cation, resulting degraded into products by reacting with ions through a sequence of reactions.

TABLE: 5.1

VARIATION OF ORANGE G

[PMS] = 5.0 x 10^{-4} mol dm^{-3} **Temp. = 30 °C**

[AgNPs] = 1.0 x 10^{-7} mol dm^{-3} **pH = 9.2**

10^5 [Dye], mol dm^{-3}	**1.0**	**2.5**	**5.0**	**7.5**	**10.0**
Time in minutes			**Absorbance**		
0	(0) 0.197	(0) 0.491	0.983	1.474	(0) 1.965
5	(15) 0.140	(8) 0.338	0.730	1.121	(8) 1.404
10	(30) 0.100	(16) 0.232	0.543	0.853	(16) 1.004
15	(45) 0.071	(24) 0.160	0.403	0.649	(24) 0.716
20	(60) 0.050	(32) 0.112	0.302	0.493	(32)0.516
25	(75) 0.036	(40) 0.076	0.223	0.374	(40) 0.365
30	-	-	0.163	0.285	(48) 0.265
10^4 (k_{obs}), sec^{-1}	**3.78**	**7.81**	**9.9**	**9.12**	**7.01**

Figures in parentheses denote time in minutes.

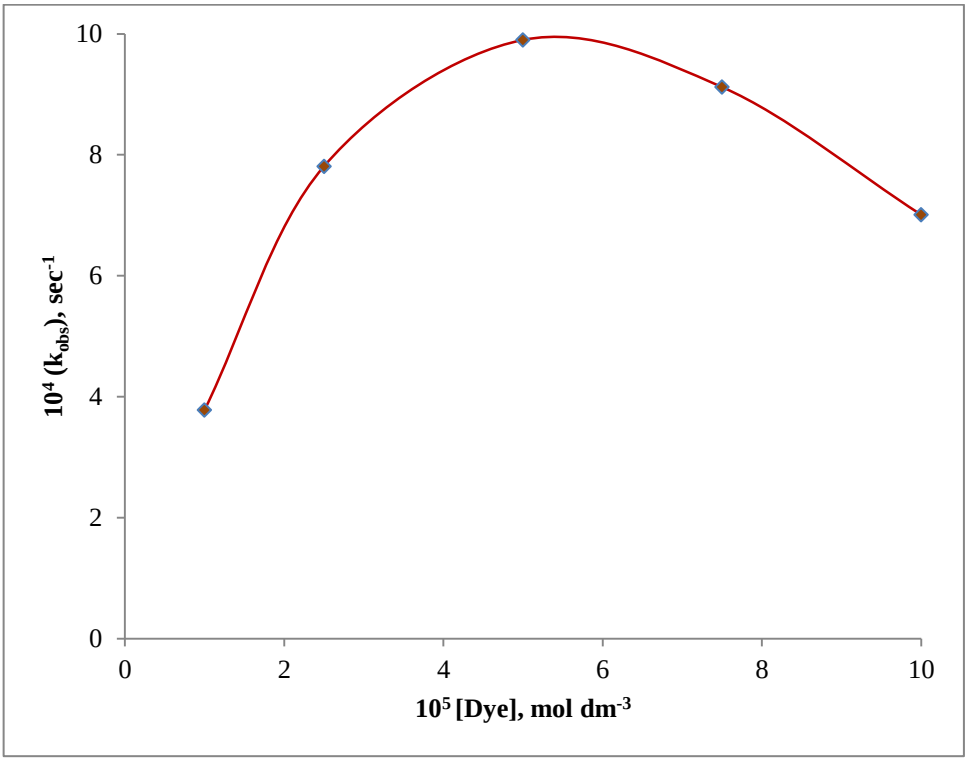

Figure 5.3: Variation of Orange G.

[PMS] = 5.0 x 10^{-4} mol dm^{-3} Temp. = 30 °C

[AgNPs] = 1.0 x 10^{-7} mol dm^{-3} pH = 9.2

(**Ref. Table: 5.1)**

TABLE: 5.2
VARIATION OF PEROXOMONOSULPHATE

[Dye] = 5.0 x 10^{-5} mol dm^{-3} **Temp. = 30 °C**
[AgNPs] = 1.0 x 10^{-7} mol dm^{-3} **pH = 9.2**

10^4 [PMS], mol dm^{-3}	**1.0**	**2.5**	**5.0**	**7.5**	**10.0**
Time in minutes			**Absorbance**		
0	0.982	(0) 0.981	(0) 0.983	(0) 0.980	(0) 0.984
30	0.750	(10) 0.741	(5) 0.730	(3) 0.750	(2) 0.773
60	0.573	(20) 0.559	(10) 0.543	(6) 0.571	(4) 0.602
90	0.437	(30) 0.422	(15) 0.403	(9) 0.437	(6) 0.471
120	0.334	(40) 0.318	(20) 0.300	(12) 0.331	(8) 0.372
150	0.255	(50) 0.240	(25) 0.223	(15) 0.252	(10) 0.290
180	0.194	(60) 0.181	(30) 0.165	(18) 0.192	(12) 0.226
10^4 (k_{obs}), sec^{-1}	**1.5**	**4.7**	**9.9**	**15.03**	**20.3**

Figures in parentheses denote time in minutes.

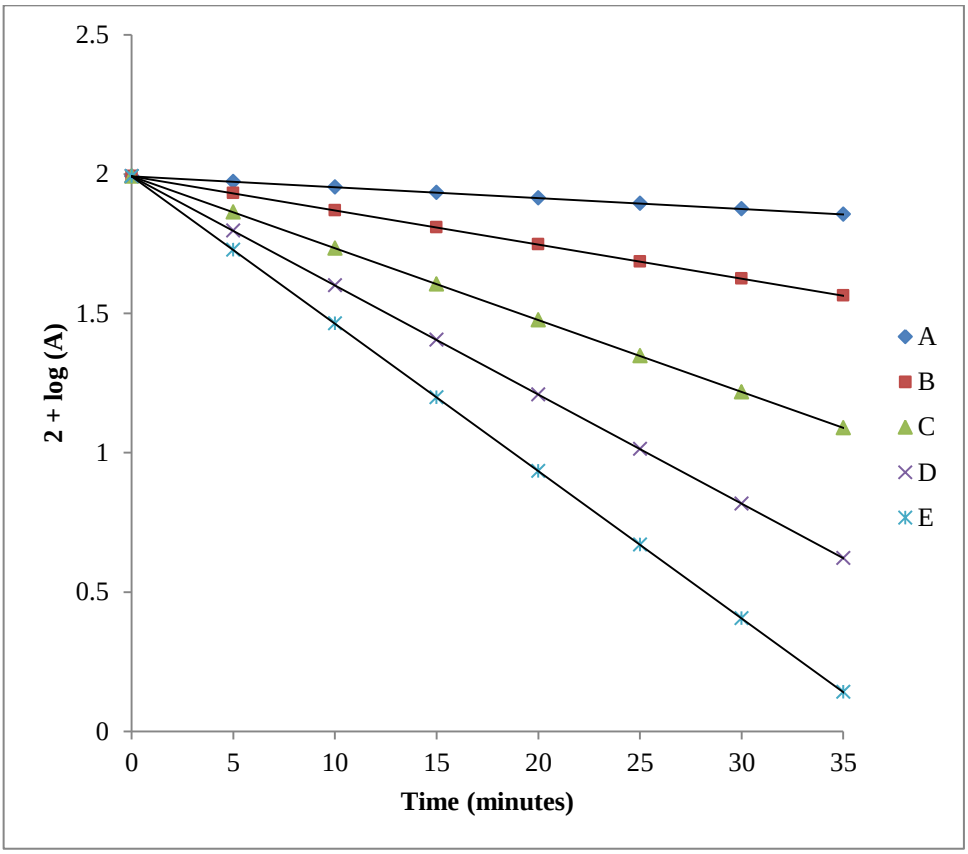

Figure 5.4: Variation of Peroxomonosulphate.

[Dye] = 5.0 x 10^{-5} mol dm^{-3}

[AgNPs] = 1.0 x 10^{-7} mol dm^{-3}

[PMS] = (A) 1.0 x 10^{-4} mol dm^{-3}

(B) 2.5 x 10^{-4} mol dm^{-3}

(C) 5.0 x 10^{-4} mol dm^{-3}

Temp. = 30 °C

pH = 9.2

(D) 7.5 x 10^{-4} mol dm^{-3}

(E) 10.0 x 10^{-4} mol dm^{-3}

(**Ref. Table: 5.2)**

5.3.2.3. Effect of Initial pH

In order to find the optimal pH of the reaction mixture for the degradation of OG, a series of experiments were conducted at different pH values 5 to 11at 30 °C temperature and other reaction conditions were [Dye] = 5.0 x 10^{-5} mol dm^{-3}, [PMS] = 5.0 x 10^{-4} mol dm^{-3},[AgNPs] = 1.0 x 10^{-7} mol dm^{-3} . Earlier studies revealed that the solution pH can dramatically influence the degradation of synthetic dyes in advanced oxidation process [28, 29]. The degradation rate of OG increases up to pH = 9.2 and then decreases at high pH (**Table 5.3**) (**Figure 5.5**). The increasing degradation efficiency up to pH = 9.2 is due to the result of the electrostatic attraction of the positively charged Ag^{+} with the ionized dye. A decrease in the reaction rate reflects the difficulty of anionic dye in approaching the negative charge Ag^{-} when increasing the solution pH.

5.3.2.4. Silver Nanoparticles Dependence

The concentration of AgNPs was varied from 0.25 x 10^{-7} to 2.0 x 10^{-7} mol dm^{-3} at three temperature viz. 25 °C, 30 °C and 35 °C respectively and other reactant concentrations were fixed ([Dye] = 5.0 x 10^{-5} mol dm^{-3}, [PMS] = 5.0 x 10^{-4} mol dm^{-3}) at 9.2 pH. The rate of oxidative degradation increases with increasing concentration of AgNPs (**Table 5.4, 5.5, 5.6**). In order to show the catalytic activity, a graph is plotted between the concentration of Ag NPs and rate constant obtained at the different temperature. The plot gives straight lines indicating the direct dependence of reaction rate on AgNPs concentration (**Figure 5.6**). This may be attributed to the fact that as the concentration of AgNPs is increased, the numbers of active radical species are also increases, which in turn increase the rate of oxidation. The intercept of the graph is evident that uncatalyzed oxidation of OG by PMS is also possible. The synthesized AgNPs exhibited good catalytic activity in small concentration (1.0 x 10^{-7} mol dm^{-3}) and rate of oxidation is five times faster than uncatalyzed reaction.

TABLE: 5.3
VARIATION OF pH

[Dye] = 5.0 x 10^{-5} mol dm^{-3} **[AgNPs] = 1.0 x 10^{-7} mol dm^{-3}**
[PMS] = 5.0 x 10^{-4} mol dm^{-3} **Temp. = 30 °C**

pH	**6**	**7**	**8**	**9.2**	**10**	**11**
Time in minutes			**Absorbance**			
0	(0) 0.981	(0) 0.982	(0) 0.984	0.983	0.985	(0) 0.980
5	(8) 0.757	(6) 0.764	(6) 0.734	0.732	0.760	(7) 0.742
10	(16) 0.583	(12) 0.592	(12) 0.551	0.543	0.591	(14) 0.560
15	(24) 0.449	(18) 0.461	(18) 0.412	0.401	0.456	(21) 0.421
20	(32) 0.346	(24) 0.358	(24) 0.311	0.300	0.353	(28) 0.317
25	(40) 0.267	(30) 0.276	(30) 0.231	0.221	0.275	(35) 0.241
30	(48) 0.206	(36) 0.217	(36) 0.173	0.165	0.214	(42) 0.182
10^4 (k_{obs}), sec^{-1}	**5.45**	**7.02**	**8.02**	**9.9**	**8.5**	**6.72**

Figures in parentheses denote time in minutes.

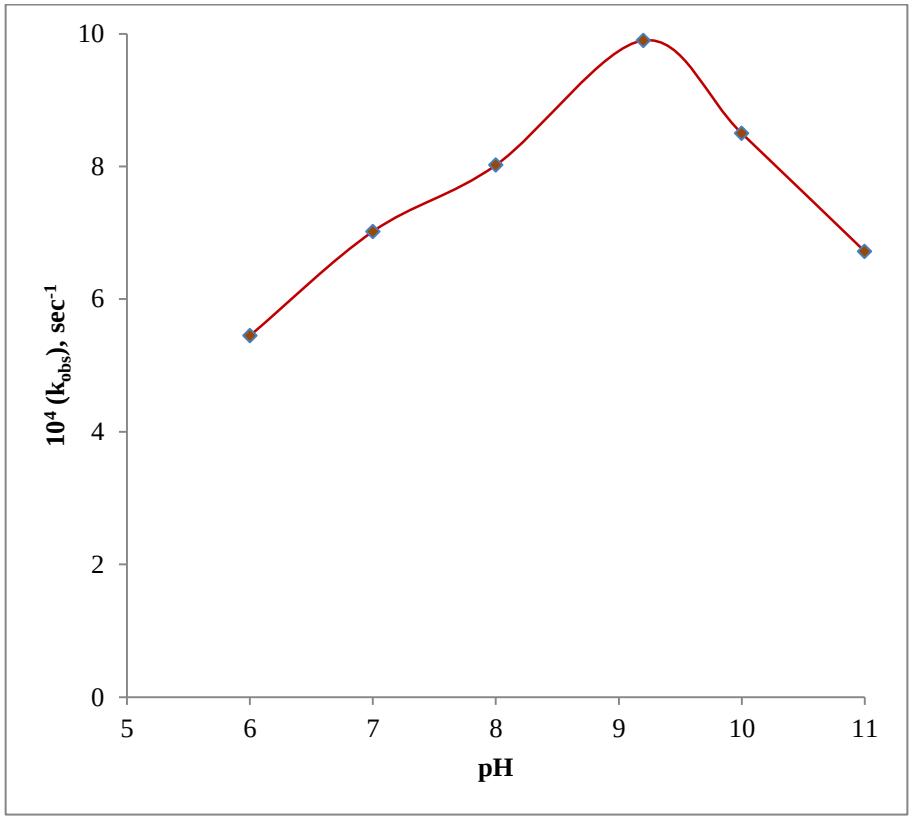

Figure 5.5: Variation of pH.

[Dye] = 5.0 x 10^{-5} mol dm^{-3} [PMS] = 5.0 x 10^{-4} mol dm^{-3}

[AgNPs] = 1.0 x 10^{-7} mol dm^{-3} Temp. = 30 °C

(**Ref. Table: 5.3**)

TABLE: 5.4
EFFECT OF SILVER NANOPARTICLES

[Dye] = 5.0 x 10^{-5} mol dm^{-3} **Temp. = 25 °C**
[PMS] = 5.0 x 10^{-4} mol dm^{-3} **pH = 9.2**

10^7 [AgNPs], mol dm^{-3}	**0**	**0.25**	**0.5**	**0.75**	**1.0**	**1.5**	**2.0**
Time in minutes				**Absorbance**			
0	0.980	(0) 0.982	(0) 0.981	(0) 0.984	(0) 0.983	(0) 0.985	(0) 0.981
50	0.728	(15) 0.751	(10) 0.734	(7) 0.738	(5) 0.762	(4) 0.729	(3) 0.734
100	0.539	(30) 0.574	(20) 0.549	(14) 0.554	(10) 0.591	(8) 0.541	(6) 0.551
150	0.400	(45) 0.438	(30) 0.410	(21) 0.418	(15) 0.456	(12) 0.402	(9) 0.412
200	0.296	(60) 0.335	(40) 0.307	(28) 0.316	(20) 0.352	(16) 0.302	(12) 0.309
250	0.219	(75) 0.256	(50) 0.229	(35) 0.234	(25) 0.276	(20) 0.223	(15) 0.231
300	0.162	(90) 0.196	(60) 0.171	(42) 0.176	(30) 0.214	(24) 0.165	(18) 0.174
10^4 (k_{obs}), sec^{-1}	**1.0**	**2.99**	**4.85**	**6.78**	**8.5**	**12.34**	**16.0**

Figures in parentheses denote time in minutes.

TABLE: 5.5
EFFECT OF SILVER NANOPARTICLES

[Dye] = 5.0 x 10^{-5} mol dm^{-3} **Temp. = 30 °C**
[PMS] = 5.0 x 10^{-4} mol dm^{-3} **pH = 9.2**

10^7 [AgNPs], mol dm^{-3}	**0**	**0.25**	**0.5**	**0.75**	**1.0**	**1.5**	**2.0**
Time in minutes				**Absorbance**			
0	(0) 0.986	(0) 0.984	(0) 0.985	(0) 0.981	(0) 0.982	0.983	0.983
3	(25) 0.728	(11) 0.753	(8) 0.735	(7) 0.702	(5) 0.730	0.762	0.711
6	(50) 0.539	(22) 0.581	(16) 0.552	(14) 0.501	(10) 0.543	0.593	0.514
9	(75) 0.399	(33) 0.446	(24) 0.414	(21) 0.358	(15) 0.403	0.461	0.373
12	(100) 0.296	(44) 0.343	(32) 0.312	(28) 0.254	(20) 0.300	0.358	0.272
15	(125) 0.219	(55) 0.261	(40) 0.234	(35) 0.181	(25) 0.223	0.275	0.194
18	(150) 0.162	(66) 0.201	(48) 0.176	(42) 0.130	(30) 0.165	0.211	0.141
10^4 (k_{obs}), sec^{-1}	**2.0**	**4.0**	**5.99**	**8.0**	**9.9**	**13.99**	**17.9**

Figures in parentheses denote time in minutes.

TABLE: 5.6
EFFECT OF SILVER NANOPARTICLES

[Dye] = 5.0 x 10^{-5} mol dm^{-3} **Temp. = 35 °C**
[PMS] = 5.0 x 10^{-4} mol dm^{-3} **pH = 9.2**

10^7 [AgNPs], mol dm^{-3}	**0**	**0.25**	**0.5**	**0.75**	**1.0**	**1.5**	**2.0**
Time in minutes				**Absorbance**			
0	(0) 0.984	(0) 0.985	0.984	0.983	(0) 0.981	(0) 0.982	(0) 0.980
5	(15) 0.750	(10) 0.719	0.788	0.740	(4) 0.743	(3) 0.732	(2) 0.772
10	(30) 0.573	(20) 0.526	0.634	0.558	(8) 0.567	(6) 0.554	(4) 0.605
15	(45) 0.437	(30) 0.385	0.508	0.421	(12) 0.428	(9) 0.415	(6) 0.476
20	(60) 0.334	(40) 0.282	0.409	0.317	(16) 0.327	(12) 0.318	(8) 0.375
25	(75) 0.255	(50) 0.207	0.327	0.239	(20) 0.246	(15) 0.237	(10) 0.297
30	(90) 0.194	(60) 0.151	0.264	0.180	(24) 0.187	(18) 0.175	(12) 0.232
10^4 (k_{obs}), sec^{-1}	**3.0**	**5.2**	**7.3**	**9.43**	**11.5**	**15.81**	**20.0**

Figures in parentheses denote time in minutes.

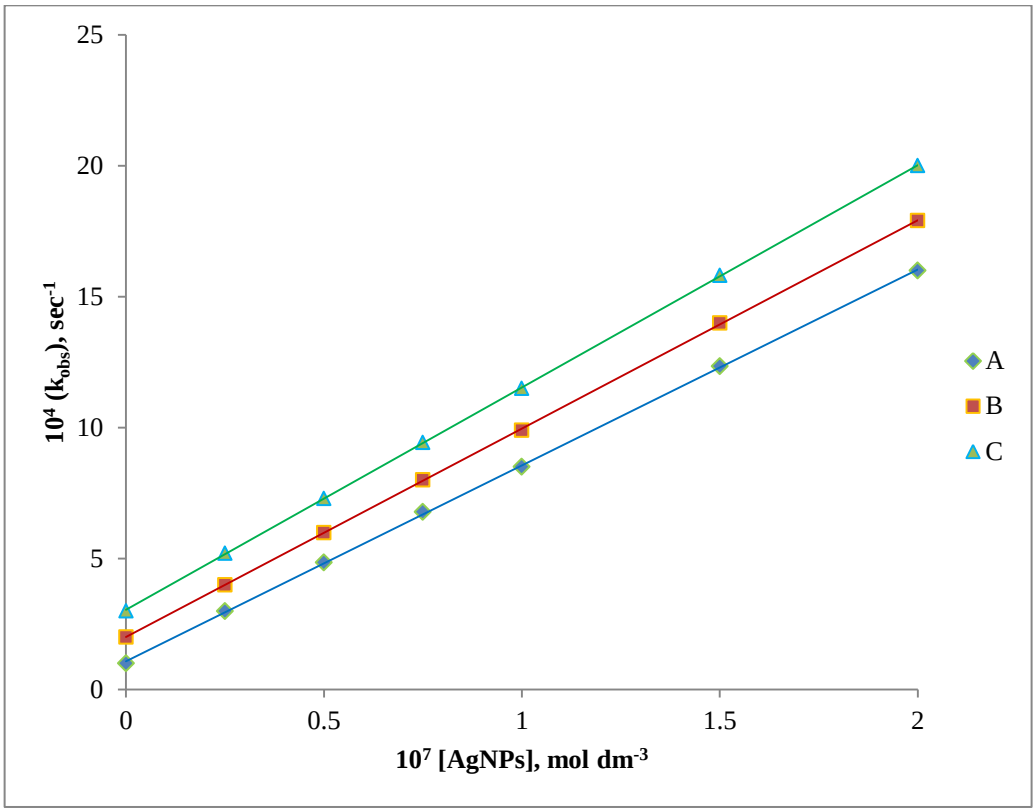

Figure 5.6: Variation of Silver Nanoparticles at different temperature (A) 25 °C, (B) 30 °C, (C) 35 °C.

[Dye] = 5.0 x 10^{-5} mol dm^{-3} [PMS] = 5.0 x 10^{-4} mol dm^{-3}

pH = 9.2

(**Ref. Table: 5.4, 5.5, 5.6**)

The rate of degradation of dye was accelerated by a rise in the temperature, because of at high temperature increases the rate of generation of oxidizing species such as $SO_4^{\bullet-}$ radical ions and higher valent Ag species. The energy of activation was determined by the plot of log k_{obs} versus 1/T (**Figure 5.7**). The activation parameters were also calculated from the observed constants at three temperatures (**Table 5.7**). The high positive value of free energy of activation ($\Delta G^{\#}$) and enthalpy of activation ($\Delta H^{\#}$) indicate that transition state was highly solvated while the negative value of entropy of activation ($\Delta S^{\#}$) was suggested the formation of more ordered transition state with reduction in the degree of freedom of the molecules [6].

5.3.2.5. Scavenger effect

It is well documented in the literature that PMS could generate sulphate $SO_4^{\bullet-}$/ or hydroxyl $^{\bullet}OH$ radicals by homogenous and heterogeneous activation [30]. Radical quenching tests using Ethanol (EtOH) and *t*-butyl alcohol (TBA) radical scavenger were performed to identify the dominant radical species formed from the AgNPs/PMS interaction and to evaluate their contribution to the process. Ethanol is capable of quenching both sulphate and hydroxyl radicals as it readily reacts with both radicals at high and comparable rates, whereas TBA is effective quenching agent for hydroxyl radicals [22]. The effect of both quenching reagents on the OG degradation efficiency over catalyst/oxone system illustrates in (**Table 5.8**) (**Figure 5.8**). The results indicate that sulphate radicals are active species in the oxidative degradation of dye in presence of AgNPs.

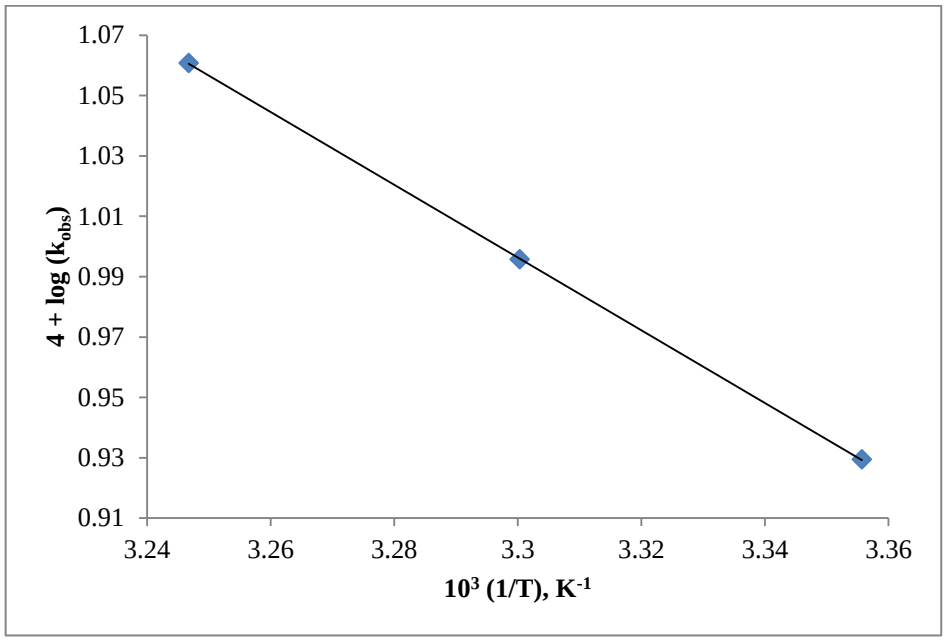

Figure 5.7: Plot of log k versus 1/T.

[Dye] = 5.0 x 10^{-5} mol dm^{-3} [PMS] = 5.0 x 10^{-4} mol dm^{-3}

[AgNPs] = 1.0 x 10^{-7} mol dm^{-3} pH = 9.2

(Ref. Table: 5.4, 5.5, 5.6)

TABLE: 5.7

Activation Parameters were Calculated from The Observed Rate Constants at Three Temperatures

Temperature (K)	**10^4 K_{obs} (sec^{-1})**	**$Ea^{\#}$ (kJ mol^{-1})**	**$\Delta H^{\#}$ (kJ mol^{-1})**	**$\Delta S^{\#}$ (J mol^{-1} K^{-1})**	**$\Delta G^{\#}$ (kJ mol^{-1})**
298	8.5	22.78	20.26	-206.40	82.80
303	9.9				
308	11.5				

TABLE: 5.8
SCAVENGER EFFECT

[Dye] = 5.0 x 10^{-5} mol dm^{-3} **Temp. = 30 °C**
[PMS] = 5.0 x 10^{-4} mol dm^{-3} **pH = 9.2**
[AgNPs] = 1.0 x 10^{-7} mol dm^{-3}

SCAVENGER	EtOH	TBA	No Scavenger
Time in minutes		**Absorbance**	
0	(0) 0.983	0.982	0.983
5	(10) 0.900	0.758	0.731
10	(20) 0.825	0.586	0.541
15	(30) 0.755	0.455	0.402
20	(40) 0.692	0.352	0.302
25	(50) 0.634	0.269	0.224
30	(60) 0.585	0.208	0.164
10^4 (k_{obs}), sec^{-1}	**1.46**	**8.61**	**9.9**

Figures in parentheses denote time in minutes.

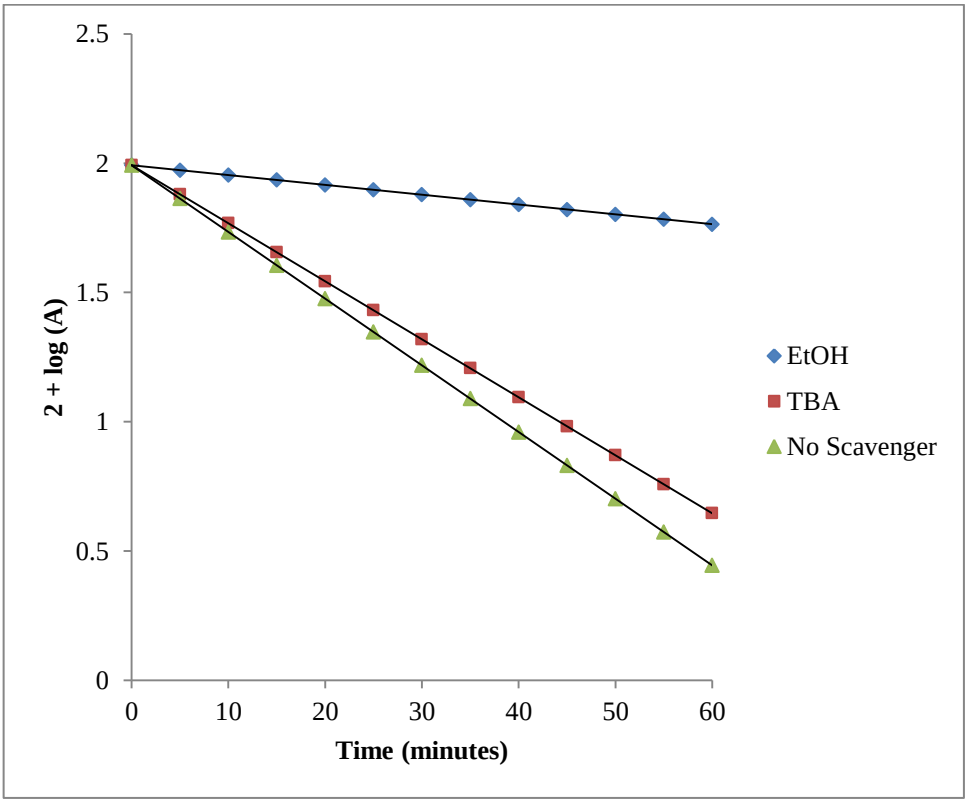

Figure 5.8: Scavenger effect of EtOH and TBA in AgNPs/PMS system.

[Dye] = 5.0 x 10^{-5} mol dm^{-3} [PMS] = 5.0 x 10^{-4} mol dm^{-3}

[AgNPs] = 1.0 x 10^{-7} mol dm^{-3} pH = 9.2

Temperature 30 ^{0}C

(**Ref. Table: 5.8**)

5.3.2.6. Mechanism

Based on above results it may be concluded that the oxidative degradation of dye in presence of AgNPs by oxone is dominated by radical-based mechanism and the main radical species generated during the catalytic activation of oxone were sulphate radicals. Firstly oxone can be activated by AgNPs to produce sulphate radicals. Once the sulphate radicals are formed it can produce a rapid attack on dye and convert it into end products. The plausible mechanism is given below-

$$HSO_5^- + Ag^\circ \rightarrow Ag(I) + SO_4^{\bullet -} + OH^-$$

$$\frac{SO_4^{\bullet -} + Ag(I) + Dye \rightarrow \text{Pr}oduct + Ag^\circ}{HSO_5^- + Dye \rightarrow \text{Pr}oduct}$$

5.4. Conclusion

The catalytic activity of Ag NPs was investigated through the oxidative degradation of OG by PMS in an aqueous medium. The reaction is five-time faster in presence of very small AgNPs concentration (1.0×10^{-7} mol dm^{-3}). LC-MS analysis of dye degradation indicates that oxidative depletion of azo bond to found aniline and hydroxylamine derivative. Scavenging effect of EtOH and *t*-butyl alcohol confirms the oxidative degradation of OG in nanocatalyst/oxone system is affected by the radical-based mechanism. This study will be helpful in wastewater treatment by the cost-effective method.

5.5 References

[1] J. S. Bradley, G. Scmided, ***Clusters and Colloids: From Theory to Application. VCH New York: Cluster Colloids, 1994***.

[2] J. M. Thomas, B. F. G. Johnson, R. Raja, G. Sankar, P. A. Midgley, ***Acc. Chem. Res.***, 36 (2003) 20.

[3] A. J. Bruss, M. A. Gelesky, G. Machado, J. Dupont, ***J. Mol. Catal. A: Chem.***, 252 (2006) 212.

[4] A. A. Firooz, A. R. Mahjoub, A. Khodadadi, ***WASET***, 5 (2011) 118.

[5] R. A. Soomro, S. T. H. Sherazi, Sirajuddin, N. Memon, M. R. Shah, N. H. Kalwar, K. R. Hallam, A. Shah, ***Advanced Materials Letters***, 5 (2014) 191.

[6] A. Goel, R. Bhatt, Neetu, ***IJRCE***, 2 (2012) 210.

[7] R. A. Soomro, A. Nafady, N. Memon, T. H. Sherazi, N. H. Kalwar, ***Talanta***, 130 (2014) 415.

[8] E. Forgacs, T. Cserhati, G. Oros, ***Enviro. Int.***, 30 (2004) 953.

[9] T. Robinson, G. Mcmullan, R. Marchant, P. Nigam, ***Bioresour. Technol.***,77 (2001) 247.

[10] J. J. M. Orfao, A. I. M. Silva, J. C. V. Pereira, S. A. Barata, I. M. Fonseca, P. C. C. Faria, M. R. F. Pereira, ***J. Colloid Interface Sci.***, 296 (2006) 480.

[11] C. L. Yang, J. Mcgarrahan, ***J. Hazard. Mater.***, B127I (2005) 40.

[12] M. Muruganandham, M. Swaminathan, ***Dyes Pigments***, 68 (2006) 133.

[13] Z. H. Wang, W. H. Ma, C. C. Cheng, J. C. Zhao, ***J. Hazard. Mater.***, 168 (2009) 1246.

[14] J. He, W. Ma, J. He, J. Zhao, J. C. Yu, ***Appl. Catal. B***, 39 (2002) 211.

[15] X. Y. Chen, X. L. Qiao, D. G. Wang, J. Lin, J. W. Chen, ***Chemosphere***, 67 (2007) 802.

[16] X. Y. Chen, J. W. Chen, X. L. Qiao, D. G. Wang, X. Y. Cai, ***Appl. Catal. B***, 80 (2008) 116.

[17] S. K. Ling, S. B. Wang, Y. L. Peng, ***J. Hazard. Mater.***, 178 (2010) 385.

[18] P. R. Shukla, S. B. Wang, H. M. Ang, M. O. Tadé, ***Sep. Purif. Technol.***, 70 (2010) 338.

[19] K. H. Chan, W. Chu, ***Water Res.***., 43 (2009) 2513.

[20] E. Psillakis, D. Mantzavinos, ***J. Chem. Technol. Biotechnol.***, 79 (2004) 431.

[21] I. A. Slavova, M. K. Stoyanova, S. G. Christoskova, V. V. Ivanova, ***Journal of International Scientific Publications: Ecology and Safety***, 8 (2008) 469.

[22] H. Lachheb, E. Puzenat, A. Houas, M. Ksibi, E. Elaloui, C. Guillard, J. M. Herrmann, ***Appl. Catal. B***, 39 (2002) 75.

[23] M. A. Meetani, M. A. Rauf, S. Hisaindee, A. Khaleel, A. Alzamly, A. Ahmad, ***RSC Adv.***, 1 (2011) 490.

[24] J. Zhang, M. Chen, L. Zhu, ***RSC Adv.,*** 6 (2016) 47562.

[25] X. –R. Xu, X. –Z. Li, ***Sep. Purif. Technol.,*** 72 (2010) 105.

[26] X. Wang, P. Wu, Y. Lu, Z. Huang, N. Zhu, C. Lin, Z. Dang, ***Sep. Purif. Technol.,*** 132 (2014) 195.

[27] M. –Q. Cai, Y. –Z. Zhu, Z. –S. Wei, J. –Q. Hu, S. –D. Pan, R. –Y. Xiao, C. –Y. Dong, M. –C. Jin, ***Sci. Total Environ.,*** 580 (2017) 966.

[28] Y. -H. Huang, Y. -F. Huang, C. -I. Huang, C. -Y. Chen, ***J. Hazard. Mater.***, 170 (2009) 1110.

[29] J. B. Zhong, J. Z. Li, Y. Lu, S. T. Huang, W. Hu, ***Iran J. Chem. Chem. Eng.***, 31 (2012) 21.

[30] G. P. Anipsitakis, D. D. Dionysiou, ***Appl. Catal. B***, 54 (2004) 155.

Chapter – 6

Comparative Kinetic Study of Copper Nanoparticles Catalyzed Degradation of Methyl Orange by Peroxodisulphate and Peroxomonosulphate

6.1. Introduction

Azo dyes, which contribute to about 70 % of all applied dyes, are difficult to degrade by conventional treatment methods, due to their complex structure and the stability. The common techniques available for dye effluents such as adsorption and flocculation are not efficient methods because they result in solid waste, thus creating other environmental problems requires further treatment [1]. The advanced oxidation technology is the most effective chemical oxidation method and currently gaining significant application in water treatment process [2]. Focused on the need and looking for a process, that introduces strong oxidants than Fenton based process, hydroxyl radicals ($OH^{\bullet}$), ozone [3], this works explain the generation of very strong oxidizing species (sulphate radicals) through the transition metal mediated activation of peroxosulphates [4]. The process is the modification of Fenton reagent since an oxidant is coupled with a transition metal in a similar manner. Although earlier study reports [5] that sulphate radicals are not universally more efficient than hydroxyl in degrading organic compounds. Either way, however, the fact that the sulphate contains compounds were proven the most effective oxidants to proves that sulphate radicals, generated by heat [6], ultrasound [7] and transition metal [8] are very powerful oxidizing species. Since transition metal coupled oxidative process show greater removal efficiency for the degradation of carcinogenic contaminants into lower toxicity and lower molecular weight. The generated reactive species sulphate radicals depend on the catalytic activity and oxidation state of transition metals. The copper catalyzed decomposition follows a sulphate radical based mechanism, the same was suggested when nickel, cobalt, iron, ruthenium and silver transition metals were used [8-11].

Nanosized metal nanoparticles are attracting the attention of present science field nanometer scale leads to particular intrinsic properties of the materials that render them very promising for application in catalysis. The application of transition metal NPs as a catalyst for hydrogenation [12], hydrosilation [13] along with redox [14] and additional electron transfer process [15] were described. Among the metal nanoparticles, copper nanoparticles are

very attractive due to their excellent physical and chemical properties and low cost of synthesis, have been of great interest. Copper nanoparticles have wide applications in heat transfer system [16], anti-microbial materials [17], super strong materials [18] and catalysis [19].

A textile azo dye, Methyl Orange (MO) was chosen as the target compound and many studies also report to employ MO as a model mainly because it is a widely used dye and resistant to degradation by conventional methods [20, 21]. As far as we are concerned, nano copper based catalyst/PDS and catalyst/PMS system for degradation of MO was still uncovered in the environmental field. Therefore the main objectives of this article are – (i) To determine the effect of the different concentration of CuNPs, PDS, PMS, and pH etc. on the degradation of MO. (ii) To propose the degradation pathway of MO in CuNPs/Peroxosulphates system. (iii) The performance discrepancy of CuNPs/PDS and CuNPs/PMS system was compared and discussed.

6.2. Experimental

6.2.1. Chemicals and Materials

The procedure of preparation and standardization of the reagents solution including peroxodisulphate, peroxomonosulphate are given in chapter 2 (Instrumentation and Methods). The solutions of PDS and PMS were prepared by direct weighing. A fresh solution of peroxodisulphate and peroxomonosulphate was prepared before starting the experiments every time. All other reagents used in this study were either of AnalaR grade or guaranteed reagent grade and were used as supplied without undertaking any further treatment. Doubly distilled water was used throughout the study.

6.2.2. Kinetic Measurements

The desired concentration of MO and other reactants placed in stoppered Erlenmeyer flask at 30 ± 0.1 °C temperature and degradation of MO was initiated by adding a known concentration of peroxosulphate solution. The rate of decolonization was obtained in terms of change in intensity at the characteristic

peak 465 nm wavelength in regular time interval studied by UV-Visible Spectrophotometer attached with Peltier accessory (Temperature- controlled). It was verified that other components of the reaction mixture do not absorb considerably at this wavelength. Application of Beer's law under the reaction condition was verified in MO concentration range 1.0 x 10^{-5} to 1.0 x 10^{-4} mol dm^{-3} at 465 nm. The molar absorptive index of MO was found to be 24570 ± 50 mol^{-1} dm^3 cm^{-1} employed [22]. All the kinetics runs were followed up to 80 % completion of the reaction. A plot of 2 + log (Absorbance) versus time was found liner which indicates pseudo first order kinetics. The pseudo first order rate constant (k_{obs}) were calculated from the slope of these plots. The values of rate constants, k_{obs} were reproducible within ±5 %.

6.3. Result and Discussion

6.3.1. Product Analysis

6.3.1.1. *Determination of Degradation Products*

In order to determine degradation products were carried out by LC-MS analysis of the dye solution in CuNPs/PMS system, at the different time interval of the degradation process. The results showed (**Figure 6.1**) the significant peaks present at the different time of degradation with corresponding m/z values 304, 320, 292, 228, 15, 80, 62. After ten minutes of degradation, the new peak of mono hydroxylated product (m/z 320) of MO was found (**Figure 6.1B**). The peak of m/z 292 can be attributed the successive demethylation of mono hydroxylated MO (**Figure 6.1C**) after 20 minutes. Further, LC-MS spectrum of the compound m/z 292, fragmented into the compound at m/z 228 and 156 respectively subsequently, these intermediate converted into the end products (**Figure 6.1D**).

6.3.1.2. UV-visible Absorption Spectra of Intermediates and Degradation Route

Figure 6.2 shows the UV-visible spectra of the compounds with m/z values 304, 320, 292 determined on the basis of $[M-H]^-$ ions of the MO. The spectrum of light absorption by reaction mixture before reaction consists of two main peaks at 465 nm and 270 nm. The peak at 465 nm is attributed to the absorption of the extended aromatic ring and chromophore group while the

additional band at 270 nm are assigned to its aromatic ring in MO molecule (m/z 304). As the reaction proceeded, the UV-visible spectrum of the compound with m/z value 320 shows a red-shift (480 nm) may be attributed to the hydroxyl radical inserted in the benzene ring linking with the dimethylamine group of MO. Subsequently, successive demethylation (m/z 292) could lead to significant wavelength blue shift (435 nm) can be suggested that homolytic cleavage of the nitrogen-carbon bond, resulting in the substitution of the methyl group by the hydrogen atom [23]. Finally, two new peaks at 220 nm and 320 nm were indicated polyaromatic ring in the MO degrade into monosubstituted aromatic ring and end products (**Figure 6.2**). According to observe results obtained from the spectral changes during degradation of MO the following route are proposed (**Scheme 6.1**) [24].

6.3.2. Effect of Experimental Conditions

6.3.2.1. Dye Dependence

The initial concentration of MO was varying from 1.0 x 10^{-5} to 1.0 x 10^{-4} mol dm^{-3} at 30 °C temperature and other reactant concentrations were [CuNPs] = 1.0 x 10^{-7} mol dm^{-3}, [PDS] = 5.0 x 10^{-4} mol dm^{-3} or [PMS] = 5.0 x 10^{-4} mol dm^{-3} and pH = 6.5. Oxidation rate was found to increase with increasing concentration of MO in both CuNPs/PDS and CuNPs/PMS system. This is may be due to the increase in the concentration of dye, the reaction rate was increased as more molecules of dye were present for degradation. But after the certain concentration of dye 5.0 x 10^{-5} mol dm^{-3}, the oxidation rate was decreased in both cases (**Table 6.1, 6.2**) (**Figure 6.3**). This can be described that at constant oxidant concentration the availability of $SO_4^{\bullet-}$ radicals is less, so degradation of MO slowed down significantly.

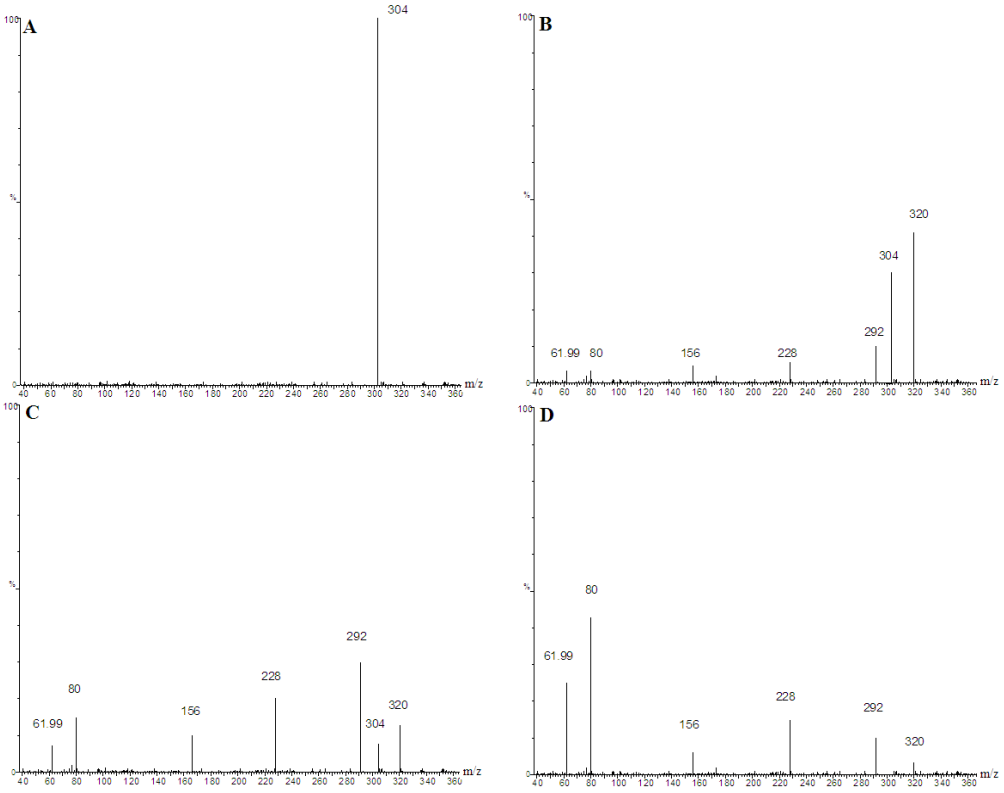

Figure 6.1: LC-MS of MO degraded at (A) 0 minutes, (B) 10 minutes, (C) 20 minutes, and (D) 30 minutes; in CuNPs/PMS system.

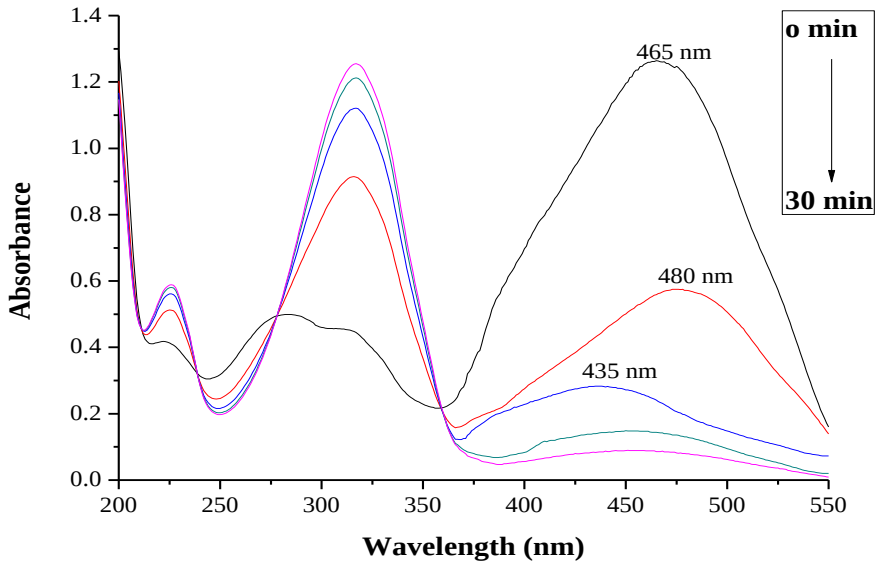

Figure 6.2: The change of UV-visible spectrum with reaction time in CuNPs/PMS system.

[Dye] = 5.0 x 10^{-5} mol dm^{-3} [PMS] = 5.0 x 10^{-4} mol dm^{-3}

[CuNPs] = 1.0 x 10^{-7} mol dm^{-3} pH = 6.5

Temperature 30 ^{0}C

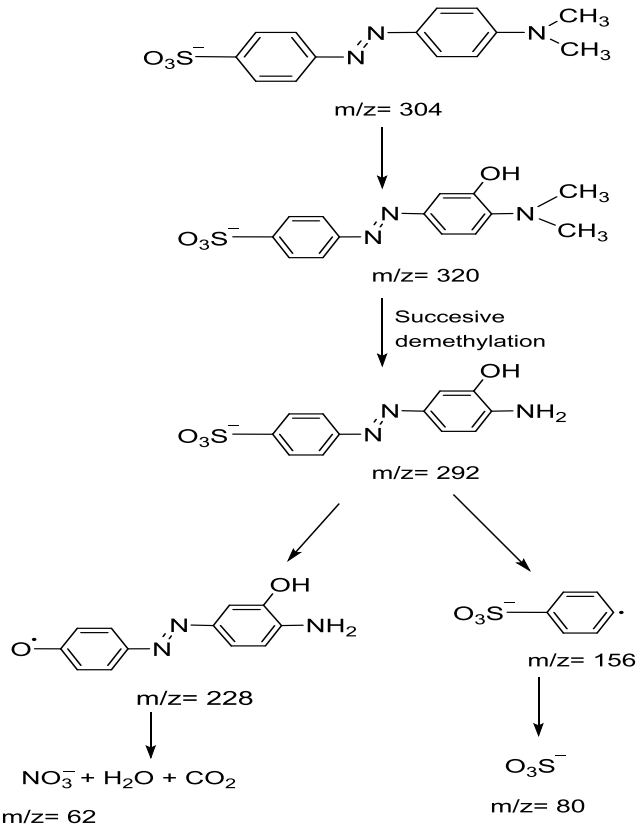

Scheme 6.1: Proposed oxidative degradation route of MO in CuNPs/PMS system.

TABLE: 6.1
VARIATION OF METHYL ORANGE

[PDS] = 5.0 x 10^{-4} mol dm^{-3} **Temp. = 30 °C**
[CuNPs] = 1.0 x 10^{-7} mol dm^{-3} **pH = 6.5**

10^5 [Dye], mol dm^{-3}	**1**	**2.5**	**5**	**7.5**	**10**
Time in minutes			**Absorbance**		
0	(0) 0.248	(0) 0.614	1.229	1.843	(0) 2.457
8	(14) 0.187	(8) 0.481	0.961	1.481	(7) 1.951
16	(28) 0.145	(16) 0.376	0.752	1.187	(14) 1.547
24	(42) 0.111	(24) 0.295	0.591	0.953	(21) 1.228
32	(56) 0.083	(32) 0.231	0.463	0.765	(28) 0.976
40	(70) 0.062	(40) 0.181	0.362	0.614	(35) 0.773
48	(84) 0.048	(48) 0.141	0.282	0.493	(42) 0.614
56	(98) 0.036	(56) 0.111	0.220	0.397	(49) 0.487
10^4 (k_{obs}), sec^{-1}	**3.2**	**5.1**	**6.8**	**6.1**	**5.5**

Figures in parentheses denote time in minutes.

TABLE: 6.2
VARIATION OF METHYL ORANGE

[PMS] = 5.0 x 10^{-4} mol dm^{-3} **Temp. = 30 °C**
[CuNPs] = 1.0 x 10^{-7} mol dm^{-3} **pH = 6.5**

10^5 [Dye], mol dm^{-3}	**1**	**2.5**	**5**	**7.5**	**10**
Time in minutes			**Absorbance**		
0	(0) 0.246	0.614	1.229	1.843	2.457
2	(3) 0.201	0.501	0.944	1.450	2.004
4	(6) 0.165	0.408	0.725	1.140	1.634
6	(9) 0.135	0.333	0.557	0.897	1.332
8	(12) 0.112	0.272	0.427	0.706	1.087
10	(15) 0.092	0.222	0.328	0.555	0.886
12	(18) 0.076	0.181	0.252	0.437	0.723
14	(21) 0.062	0.147	0.194	0.344	0.589
16	(24) 0.051	0.120	0.148	0.271	0.481
10^3 (k_{obs}), sec^{-1}	**1.1**	**1.7**	**2.2**	**2.0**	**1.7**

Figures in parentheses denote time in minutes.

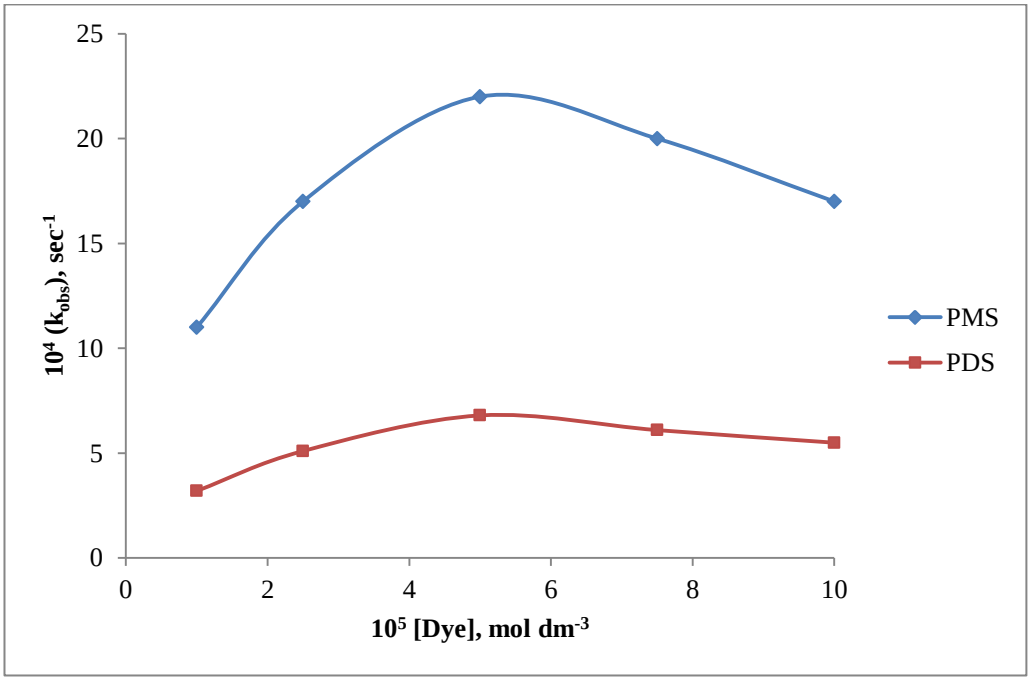

Figure 6.3: Variation of Methyl Orange.

[PDS] = 5.0 x 10^{-4} mol dm^{-3} [CuNPs] = 1.0 x 10^{-7} mol dm^{-3}

[PMS] = 5.0 x 10^{-4} mol dm^{-3} Temp. = 30 °C

pH = 6.5

(**Ref. Table: 6.1, 6.2**)

6.3.2.2. Peroxodisulphate and Peroxomonosulphate Dependence

The oxidants such as peroxodisulphate and peroxomonosulphate are generally used in the sulphate radical based advanced oxidation process and having the standard redox potential of E° = 2.1 V, 1.82 V respectively. The degradation experiment was performed at 30 °C temperature in the presence of [CuNPs] = 1.0 x 10^{-7} mol dm^{-3} at different concentration (1.0 x 10^{-4} to 1.0 x 10^{-3} mol dm^{-3}) of PDS as well as PMS respectively and other reaction conditions were [Dye] = 5.0 x 10^{-5} mol dm^{-3} and pH = 6.5. Both oxidants are dominated by $SO_4^{\bullet-}$ radicals (SRs) based mechanism and radicals were generated by the catalytic activation of PDS (Equation 1) and PMS (Equation 2).

$$2S_2O_8^{2-} + Cu^{\circ} \rightarrow 2SO_4^{\bullet-} + 2SO_4^{2-} + Cu(II) \quad (1)$$

$$2HSO_5^{-} + Cu^{\circ} \rightarrow Cu(II) + 2SO_4^{\bullet-} + 2OH^{-} \quad (2)$$

Once the SRs are formed it can produce a rapid attack on MO molecules and convert into end products. The rate of degradation initially increases with increase in the concentration of both oxidants (**Table 6.3, 6.4**) (**Figure 6.6**). The result suggests the increase in the concentration of oxidant the number of SRs increases, which in turn increases the rate of oxidation Cu° to Cu^{2+} ion, resultant enhance the oxidative decolonization of MO. Furthermore, the PDS concentration increases beyond certain limits (5.0 x 10^{-4} mol dm^{-3}); the degradation rate of dye is slowed down. This was due to the fact that excess generated SRs were involved in the side reactions and consumed more PDS, hence remaining percentage of PDS decreases for degradation with the increase in PDS concentration (**Table 6.3, 6.4**) (**Figure 6.4, 6.5, 6.6**) [25, 26].

$$S_2O_8^{2-} + SO_4^{\bullet-} \rightarrow S_2O_8^{\bullet-} + SO_4^{2-}$$

Whereas in case of PMS, the degradation rate increases up to the 5.0 x 10^{-4} mol dm^{-3} concentration of PMS after that rate was constant at higher concentration of PMS, indicating that the active sites of fixed concentration of catalyst gradually become the limiting factor (**Table 6.3, 6.4**) (**Figure 6.4, 6.5, 6.6**) [27].

TABLE: 6.3

VARIATION OF PEROXODISULPHATE

[Dye] = 5.0 x 10^{-5} mol dm^{-3} **Temp. = 30 °C**

[CuNPs] = 1.0 x 10^{-7} mol dm^{-3} **pH = 6.5**

10^4 [PDS], mol dm^{-3}	**1**	**2.5**	**5**	**7.5**	**10**
Time in minutes			**Absorbance**		
0	(0) 1.228	(0) 1.226	1.229	1.229	(0) 1.225
7	(50) 0.964	(15) 0.930	0.924	0.980	(10) 0.955
14	(100) 0.757	(30) 0.703	0.693	0.781	(20) 0.742
21	(150) 0.592	(45) 0.532	0.521	0.624	(30) 0.577
28	(200) 0.464	(60) 0.403	0.391	0.496	(40) 0.448
35	(250) 0.364	(75) 0.305	0.296	0.396	(50) 0.349
42	(300) 0.287	(90) 0.230	0.221	0.315	(60) 0.271
49	(350) 0.223	(105) 0.173	0.165	0.251	(70) 0.211
10^4 (k_{obs}), sec^{-1}	**0.81**	**3.10**	**6.80**	**5.39**	**4.20**

Figures in parentheses denote time in minutes.

TABLE: 6.4

VARIATION OF PEROXOMONOSULPHATE

[Dye] = 5.0 x 10^{-5} mol dm^{-3} **Temp. = 30 °C**

[CuNPs] = 1.0 x 10^{-7} mol dm^{-3} **pH = 6.5**

10^4 [PMS], mol dm^{-3}	**1**	**2.5**	**5**	**7.5**	**10**
Time in minutes			**Absorbance**		
0	(0) 1.229	(0) 1.230	1.230	1.224	1.227
2	(4) 0.965	(3) 0.934	0.944	0.935	0.930
4	(8) 0.761	(6) 0.711	0.725	0.711	0.704
6	(12) 0.597	(9) 0.540	0.557	0.541	0.533
8	(16) 0.470	(12) 0.413	0.427	0.411	0.404
10	(20) 0.371	(15) 0.315	0.328	0.313	0.305
12	(24) 0.292	(18) 0.241	0.252	0.238	0.231
14	(28) 0.228	(21) 0.185	0.194	0.182	0.174
10^3 (k_{obs}), sec^{-1}	**1.00**	**1.50**	**2.20**	**2.28**	**2.32**

Figures in parentheses denote time in minutes.

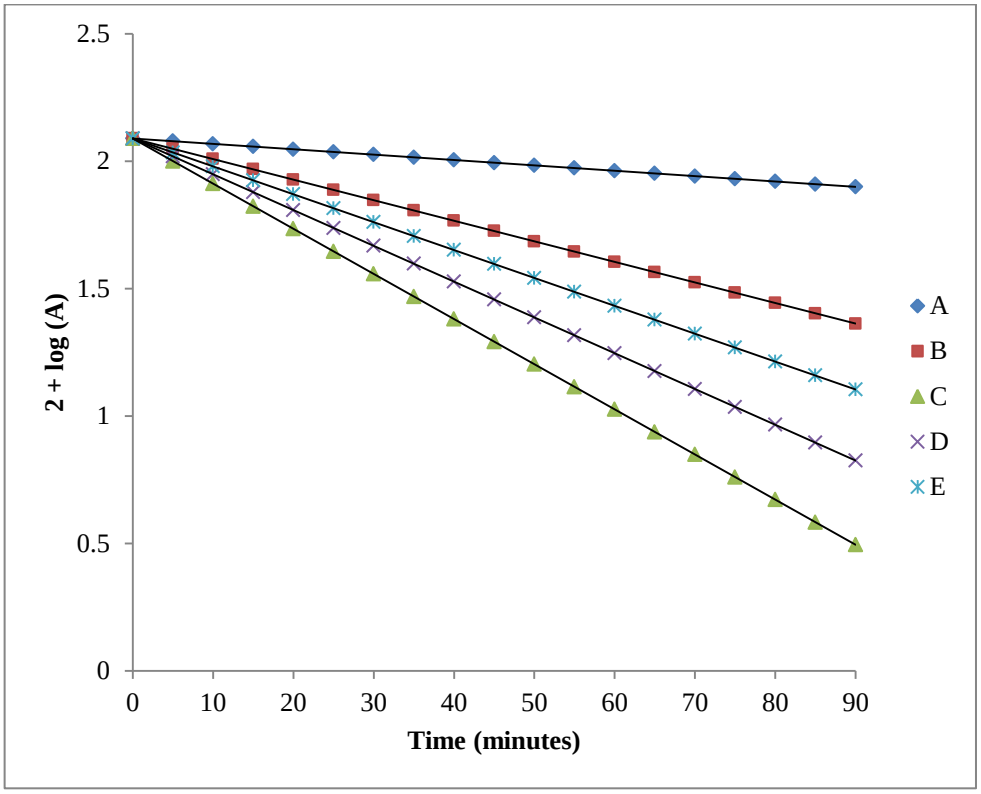

Figure 6.4: Variation of Peroxodisulphate.

[Dye] = 5.0 x 10^{-5} mol dm^{-3}

[CuNPs] = 1.0 x 10^{-7} mol dm^{-3}

[PDS] = (A) 1.0 x 10^{-4} mol dm^{-3}

(B) 2.5 x 10^{-4} mol dm^{-3}

(C) 5.0 x 10^{-4} mol dm^{-3}

Temp. = 30 °C

pH = 6.5

(D) 7.5 x 10^{-4} mol dm^{-3}

(E) 10.0 x 10^{-4} mol dm^{-3}

(**Ref. Table: 6.3**)

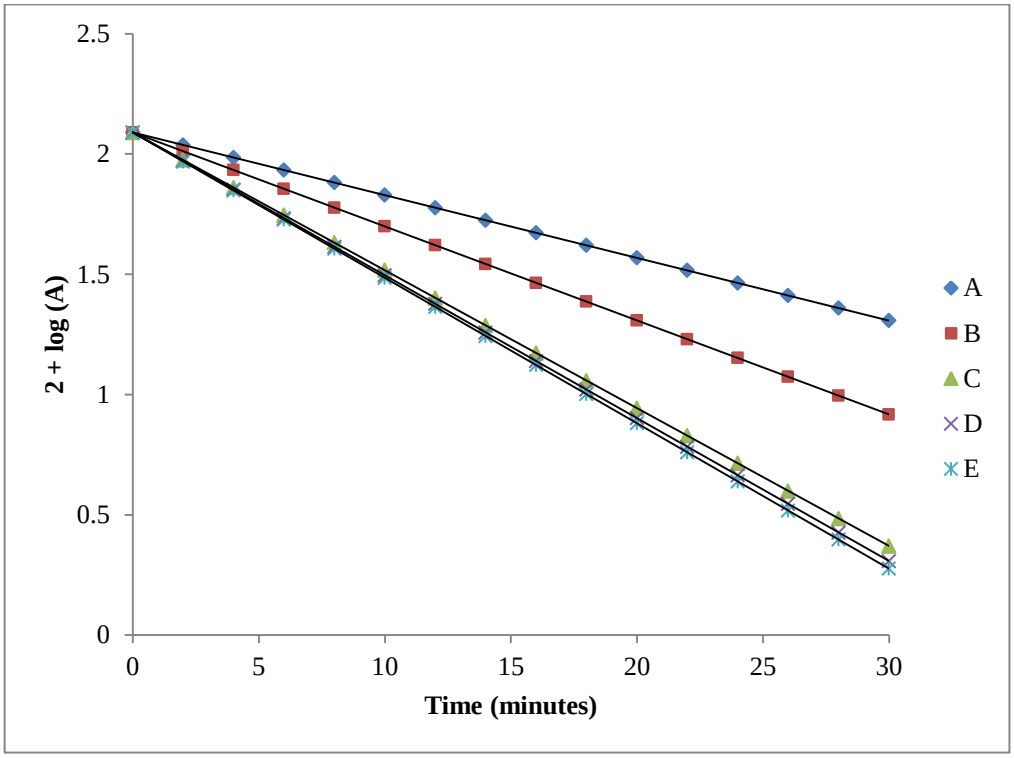

Figure 6.5: Variation of Peroxomonosulphate.

[Dye] = 5.0 x 10^{-5} mol dm^{-3} Temp. = 30 °C

[CuNPs] = 1.0 x 10^{-7} mol dm^{-3} pH = 6.5

[PMS] = (A) 1.0 x 10^{-4} mol dm^{-3} (D) 7.5 x 10^{-4} mol dm^{-3}

(B) 2.5 x 10^{-4} mol dm^{-3} (E) 10.0 x 10^{-4} mol dm^{-3}

(C) 5.0 x 10^{-4} mol dm^{-3}

(**Ref. Table: 6.4**)

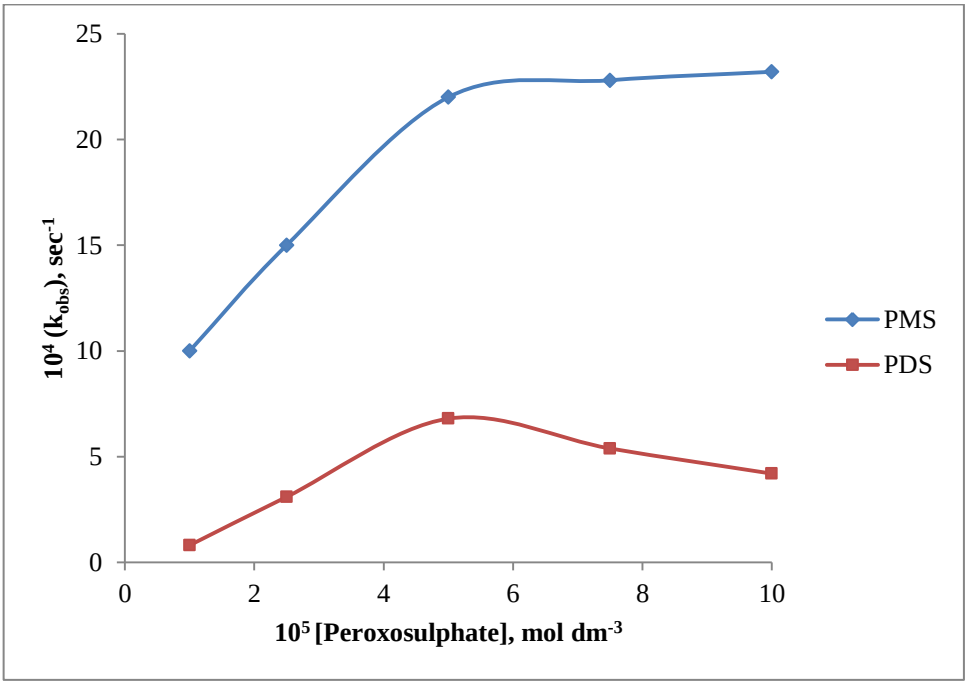

Figure 6.6: Variation of Peroxosulphate.

[Dye] = 5.0 x 10^{-5} mol dm^{-3} Temp. = 30 °C

[CuNPs] = 1.0 x 10^{-7} mol dm^{-3} pH = 6.5

(**Ref. Table: 6.3, 6.4**)

6.3.2.3. Effect of Initial pH

In order to find the optimal pH for dye degradation, a series of experiments were conducted at different pH (2.5 to 10) in CuNPs/PDS and CuNPs/PMS system respectively and other reaction conditions were [Dye] = 5.0 x 10^{-5} mol dm^{-3}, [CuNPs] = 1.0 x 10^{-7} mol dm^{-3}, [PMS] = 5.0 x 10^{-4} mol dm^{-3} concentration at pH = 6.5, 30 ^{0}C temperature. As pH increased from 2.5 to 6.5 the degradation rate dramatically increased further increase in pH shows the degradation rate dropped in both systems (**Table 6.5, 6.6**) (**Figure 6.7**). This may be attributed to the zeta potential and surface charges of the catalyst. When CuNPs was dispersed in water than the surface become cationic nature, which would more coverage of hydroxyl groups from water [28] so uncharged surface hydroxyl groups of CuNPs were the main active sites for generate sulphate radicals ($SO_4^{\bullet-}$). Thus as pH increases, the degradation rate is also increased and reached the maximum at the pH 6.5. After that, the catalyst surface become anionic and higher electronic force to repel the $SO_4^{\bullet-}$ anion so less $SO_4^{\bullet-}$ could reach the catalyst surface and rate of degradation decreased correspondingly at higher pH.

TABLE: 6.5

VARIATION OF pH

[Dye] = 5.0 x 10^{-5} mol dm^{-3} **Temp. = 30 °C**

[PDS] = 5.0 x 10^{-4} mol dm^{-3} **[CuNPs] = 1.0 x 10^{-7} mol dm^{-3}**

pH	**2.5**	**5.0**	**6.5**	**7.0**	**8.0**	**9.0**	**10.0**
Time in minutes				**Absorbance**			
0	(0) 1.230	(0) 1.227	(0) 1.229	1.228	1.229	(0) 1.226	(0) 1.225
8	(20) 0.954	(10) 0.921	(6) 0.962	0.902	0.947	(10) 0.938	(15) 0.921
16	(40) 0.743	(20) 0.691	(12) 0.752	0.664	0.731	(20) 0.716	(30) 0.691
24	(60) 0.578	(30) 0.518	(18) 0.591	0.488	0.564	(30) 0.547	(45) 0.518
32	(80) 0.447	(40) 0.388	(24) 0.463	0.361	0.435	(40) 0.417	(60) 0.388
40	(100) 0.348	(50) 0.291	(30) 0.362	0.264	0.335	(50) 0.319	(75) 0.291
48	(120) 0.272	(60) 0.218	(36) 0.282	0.194	0.257	(60) 0.243	(90) 0.218
10^4 (k_{obs}), sec^{-1}	**2.1**	**4.8**	**6.8**	**6.4**	**5.4**	**4.5**	**3.2**

Figures in parentheses denote time in minutes.

TABLE: 6.6

VARIATION OF pH

[Dye] = 5.0 x 10^{-5} mol dm^{-3} **Temp. = 30 °C**

[PMS] = 5.0 x 10^{-4} mol dm^{-3} **[CuNPs] = 1.0 x 10^{-7} mol dm^{-3}**

pH	**2.5**	**5.0**	**6.5**	**7.0**	**8.0**	**9.0**	**10.0**
Time in minutes			**Absorbance**				
0	(0) 1.230	1.225	1.230	1.229	(0) 1.224	(0) 1.227	(0) 1.226
2	(4) 0.921	0.965	0.945	0.954	(3) 0.889	(3) 0.937	(4) 0.968
4	(8) 0.691	0.761	0.724	0.741	(6) 0.639	(6) 0.715	(8) 0.758
6	(12) 0.518	0.597	0.556	0.576	(9) 0.460	(9) 0.546	(12) 0.501
8	(16) 0.388	0.472	0.426	0.447	(12) 0.332	(12) 0.416	(16) 0.472
10	(20) 0.291	0.375	0.327	0.348	(15) 0.242	(15) 0.317	(20) 0.368
12	(24) 0.218	0.292	0.251	0.270	(18) 0.179	(18) 0.242	(24) 0.293
10^3 (k_{obs}), sec^{-1}	**1.2**	**2.0**	**2.2**	**2.1**	**1.8**	**1.5**	**1.0**

Figures in parentheses denote time in minutes.

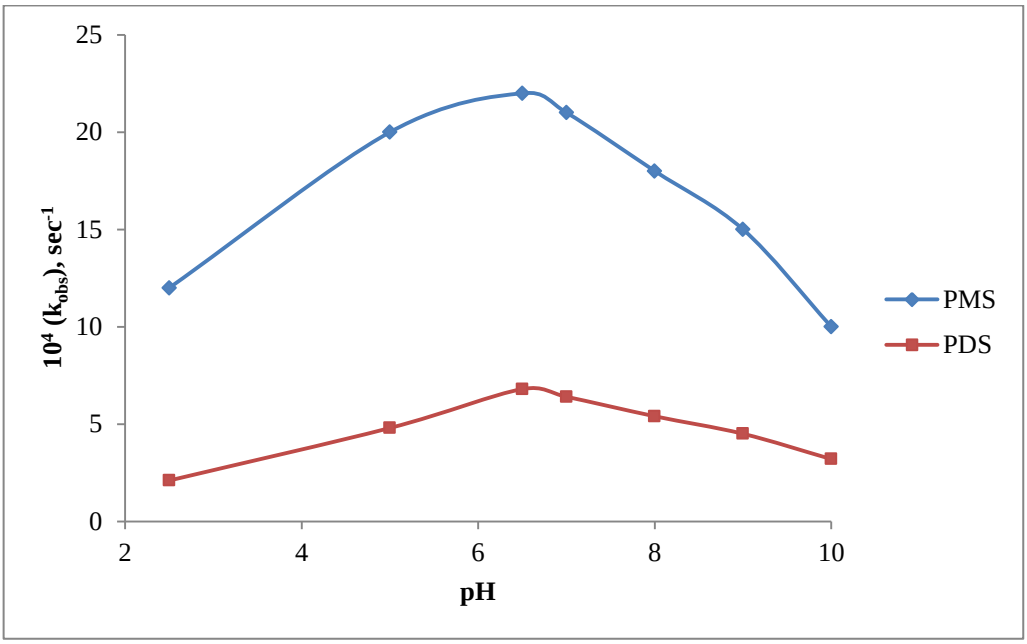

Figure 6.7: Variation of pH.

[Dye] = 5.0 x 10^{-5} mol dm^{-3} [PDS] = 5.0 x 10^{-4} mol dm^{-3}

[CuNPs] = 1.0 x 10^{-7} mol dm^{-3} [PMS] = 5.0 x 10^{-4} mol dm^{-3}

Temp. = 30 °C

(**Ref. Table: 6.5, 6.6**)

6.3.2.4. Copper Nanoparticles and Temperature Dependence

The catalytic activity of CuNPs was evaluated degradation of MO in both PDS and PMS system at various concentration 0.25 x 10^{-7} to 2.0 x 10^{-7} mol dm^{-3} at three temperature viz. 25 °C, 30 °C, and 35 °C respectively and pH = 6.5, other reactant concentration were [Dye] = 5.0 x 10^{-5} mol dm^{-3}, [PDS] = 5.0 x 10^{-4} mol dm^{-3}, [PMS] = 5.0 x 10^{-4} mol dm^{-3}. In order to show the catalytic activity (**Table 6.7, 6.8, 6.9, 6.10, 6.11, 6.12**), a graph is plotted between the concentration of CuNPs and rate constant obtained at different three temperatures (**Figure 6.8**). The plot gives straight lines indicating the direct dependence of reaction rate on CuNPs concentration. This may be attributed to the fact that as the concentration of CuNPs is increased; the number of active radical species is also increased, which in turn increases the rate of oxidation. The CuNPs exhibited good catalytic activity in presence of small concentration (1.0 x 10^{-7} mol dm^{-3}). As the temperature increases the rate of generation of oxidizing species such as $SO_4^{\bullet-}$ radicals and higher valent Copper species also increased, so the rate of degradation of MO was accelerated by the rise in temperature. The energy of activation was calculated from the plot of log (k_{obs}) versus 1/T in both systems (**Figure 6.9**). The value of activation energy (13.19 kJ mol^{-1}) in CuNPs/PMS system shows that the rate of degradation of MO is faster than CuNPs/PDS (21.64 kJ mol^{-1}) system. The values of thermodynamic parameters like the change in enthalpy (ΔH) and change in entropy activation (ΔS) and free energy (ΔG) were 19.12 kJ mol^{-1}, -242.68 J mol^{-1} K^{-1}, 92.65 kJ mol^{-1} for PDS and 11.39 kJ mol^{-1}, -258.48 J mol^{-1} K^{-1}, 89.69 kJ mol^{-1} for PMS respectively. In both systems positive ΔH and ΔG values shows that the process was endothermic and nonspontaneous while negative ΔS value represents endergonic reaction [9, 29, 30].

TABLE: 6.7
EFFECT OF COPPER NANOPARTICLES

[Dye] = 5.0 x 10^{-5} mol dm^{-3} **Temp. = 25 °C**
[PDS] = 5.0 x 10^{-4} mol dm^{-3} **pH = 6.5**

10^7 [CuNPs], mol dm^{-3}	**0.0**	**0.25**	**0.50**	**0.75**	**1.00**	**1.50**	**2.00**
Time in minutes				**Absorbance**			
0	(0) 1.227	(0) 1.228	(0) 1.225	1.226	1.225	(0) 1.227	(0) 1.230
6	(40) 1.019	(18) 1.012	(10) 1.008	1.046	0.996	(3) 1.057	(3) 1.011
12	(80) 0.845	(36) 0.834	(20) 0.827	0.887	0.805	(6) 0.912	(6) 0.831
18	(120) 0.701	(54) 0.685	(30) 0.678	0.757	0.654	(9) 0.786	(9) 0.684
24	(160) 0.581	(72) 0.563	(40) 0.557	0.642	0.532	(12) 0.675	(12) 0.563
30	(200) 0.482	(90) 0.462	(50) 0.457	0.546	0.431	(15) 0.581	(15) 0.463
36	(240) 0.400	(108) 0.381	(60) 0.375	0.464	0.350	(18) 0.502	(18) 0.385
42	(280) 0.331	(126) 0.314	(70) 0.307	0.394	0.286	(21) 0.431	(21) 0.314
48	(320) 0.275	(144) 0.258	(80) 0.252	0.335	0.230	(24) 0.373	(24) 0.255
54	(360) 0.228	(162) 0.212	(90) 0.207	0.287	0.188	(27) 0.321	(27) 0.213
10^4 (k_{obs}), sec^{-1}	**0.78**	**1.8**	**3.3**	**4.5**	**5.8**	**8.3**	**10.8**

Figures in parentheses denote time in minutes.

TABLE: 6.8

EFFECT OF COPPER NANOPARTICLES

[Dye] = 5.0 x 10^{-5} mol dm^{-3} **Temp. = 30 °C**

[PDS] = 5.0 x 10^{-4} mol dm^{-3} **pH = 6.5**

10^7 [CuNPs], mol dm^{-3}	**0.0**	**0.25**	**0.50**	**0.75**	**1.00**	**1.50**	**2.00**
Time in minutes				**Absorbance**			
0	(0) 1.225	(0) 1.226	(0) 1.225	(0) 1.228	(0) 1.229	1.230	1.226
4	(35) 0.955	(20) 0.932	(10) 0.966	(8) 0.943	(6) 0.961	0.973	0.907
8	(70) 0.742	(40) 0.707	(20) 0.760	(16) 0.727	(12) 0.751	0.771	0.672
12	(105) 0.577	(60) 0.537	(30) 0.598	(24) 0.561	(18) 0.587	0.612	0.501
16	(140) 0.448	(80) 0.407	(40) 0.471	(32) 0.431	(24) 0.455	0.485	0.371
20	(175) 0.349	(100) 0.309	(50) 0.370	(40) 0.334	(30) 0.359	0.384	0.275
24	(210) 0.271	(120) 0.235	(60) 0.291	(48) 0.258	(36) 0.282	0.305	0.204
28	(245) 0.211	(140) 0.176	(70) 0.229	(56) 0.201	(42) 0.220	0.244	0.152
10^4 (k_{obs}), sec^{-1}	**1.2**	**2.3**	**4.0**	**5.4**	**6.8**	**9.6**	**12.4**

Figures in parentheses denote time in minutes.

TABLE: 6.9

EFFECT OF COPPER NANOPARTICLES

[Dye] = 5.0 x 10^{-5} mol dm^{-3} **Temp. = 35 °C**

[PDS] = 5.0 x 10^{-4} mol dm^{-3} **pH = 6.5**

10^7 [CuNPs], mol dm^{-3}	**0.0**	**0.25**	**0.50**	**0.75**	**1.00**	**1.50**	**2.00**
Time in minutes				**Absorbance**			
0	(0) 1.229	(0) 1.227	(0) 1.228	1.225	1.225	(0) 1.226	(0) 1.230
6	(25) 0.938	(15) 0.938	(8) 0.975	0.976	0.932	(4) 0.947	(3) 0.961
12	(50) 0.716	(30) 0.716	(16) 0.774	0.777	0.705	(8) 0.731	(6) 0.752
18	(75) 0.547	(45) 0.547	(24) 0.615	0.621	0.534	(12) 0.565	(9) 0.592
24	(100) 0.416	(60) 0.417	(32) 0.487	0.494	0.404	(16) 0.437	(12) 0.461
30	(125) 0.319	(75) 0.319	(40) 0.386	0.392	0.306	(20) 0.339	(15) 0.362
36	(150) 0.243	(90) 0.243	(48) 0.307	0.315	0.234	(24) 0.263	(18) 0.281
42	(175) 0.186	(105) 0.185	(56) 0.244	0.250	0.178	(28) 0.203	(21) 0.222
10^4 (k_{obs}), sec^{-1}	**1.8**	**3.0**	**4.8**	**6.3**	**7.7**	**10.7**	**13.6**

Figures in parentheses denote time in minutes.

TABLE: 6.10
EFFECT OF COPPER NANOPARTICLES

[Dye] = 5.0 x 10^{-5} mol dm^{-3} **Temp. = 25 °C**
[PMS] = 5.0 x 10^{-4} mol dm^{-3} **pH = 6.5**

10^7 [CuNPs], mol dm^{-3}	**0.0**	**0.25**	**0.50**	**0.75**	**1.00**	**1.50**	**2.00**
Time in minutes				**Absorbance**			
0	(0) 1.225	(0) 1.228	(0) 1.225	(0) 1.226	1.229	1.229	(0) 1.227
2	(18) 0.978	(7) 0.965	(4) 0.944	(3) 0.931	0.961	0.872	(1) 0.972
4	(36) 0.782	(14) 0.761	(8) 0.725	(6) 0.701	0.752	0.613	(2) 0.775
6	(54) 0.623	(21) 0.598	(12) 0.557	(9) 0.531	0.595	0.431	(3) 0.619
8	(72) 0.496	(28) 0.473	(16) 0.427	(12) 0.403	0.465	0.302	(4) 0.492
10	(90) 0.397	(35) 0.372	(20) 0.328	(15) 0.303	0.367	0.215	(5) 0.394
12	(108) 0.316	(42) 0.293	(24) 0.252	(18) 0.231	0.289	0.152	(6) 0.315
14	(126) 0.252	(49) 0.231	(28) 0.194	(21) 0.173	0.228	0.108	(7) 0.250
10^3 (k_{obs}), sec^{-1}	**0.21**	**0.57**	**1.10**	**1.55**	**2.00**	**2.89**	**3.78**

Figures in parentheses denote time in minutes.

TABLE: 6.11

EFFECT OF COPPER NANOPARTICLES

[Dye] = 5.0 x 10^{-5} mol dm^{-3} **Temp. = 30 °C**

[PMS] = 5.0 x 10^{-4} mol dm^{-3} **pH = 6.5**

10^7 [CuNPs], mol dm^{-3}	**0.0**	**0.25**	**0.50**	**0.75**	**1.00**	**1.50**	**2.00**
Time in minutes	**Absorbance**						
0	(0) 1.227	(0) 1.229	(0) 1.228	(0) 1.225	1.230	1.229	(0) 1.227
2	(15) 0.921	(6) 0.954	(4) 0.907	(3) 0.899	0.943	0.851	(1) 0.958
4	(30) 0.691	(12) 0.741	(8) 0.672	(6) 0.655	0.724	0.575	(2) 0.749
6	(45) 0.518	(18) 0.576	(12) 0.497	(9) 0.478	0.556	0.392	(3) 0.587
8	(60)0.388	(24) 0.447	(16) 0.366	(12) 0.349	0.425	0.269	(4) 0.461
10	(75) 0.291	(30) 0.346	(20) 0.272	(15) 0.255	0.327	0.184	(5) 0.362
12	(90) 0.218	(36) 0.272	(24) 0.201	(18) 0.187	0.253	0.127	(6) 0.284
10^3 (k_{obs}), sec^{-1}	**0.32**	**0.70**	**1.26**	**1.74**	**2.20**	**3.15**	**4.07**

Figures in parentheses denote time in minutes.

TABLE: 6.12

EFFECT OF COPPER NANOPARTICLES

[Dye] = 5.0 x 10^{-5} mol dm^{-3} **Temp. = 35 °C**

[PMS] = 5.0 x 10^{-4} mol dm^{-3} **pH = 6.5**

10^7 [CuNPs], mol dm^{-3}	**0.0**	**0.25**	**0.50**	**0.75**	**1.00**	**1.50**	**2.00**
Time in minutes				**Absorbance**			
0	(0) 1.227	(0) 1.228	(0) 1.225	1.226	1.228	(0) 1.229	(0) 1.230
2	(8) 0.991	(5) 0.953	(3) 0.952	0.976	0.915	(1) 1.001	(1) 0.943
4	(16) 0.797	(10) 0.736	(6) 0.736	0.775	0.687	(2) 0.814	(2) 0.725
6	(24) 0.642	(15) 0.571	(9) 0.572	0.617	0.515	(3) 0.667	(3) 0.558
8	(32) 0.516	(20) 0.442	(12) 0.441	0.492	0.385	(4) 0.543	(4) 0.432
10	(40) 0.416	(25) 0.342	(15) 0.343	0.393	0.285	(5) 0.444	(5) 0.333
12	(48) 0.335	(30) 0.266	(18) 0.264	0.312	0.219	(6) 0.364	(6) 0.258
14	(56) 0.272	(35) 0.205	(21) 0.204	0.246	0.163	(7) 0.298	(7) 0.199
10^3 (k_{obs}), sec^{-1}	**0.45**	**0.85**	**1.42**	**1.91**	**2.40**	**3.38**	**4.34**

Figures in parentheses denote time in minutes.

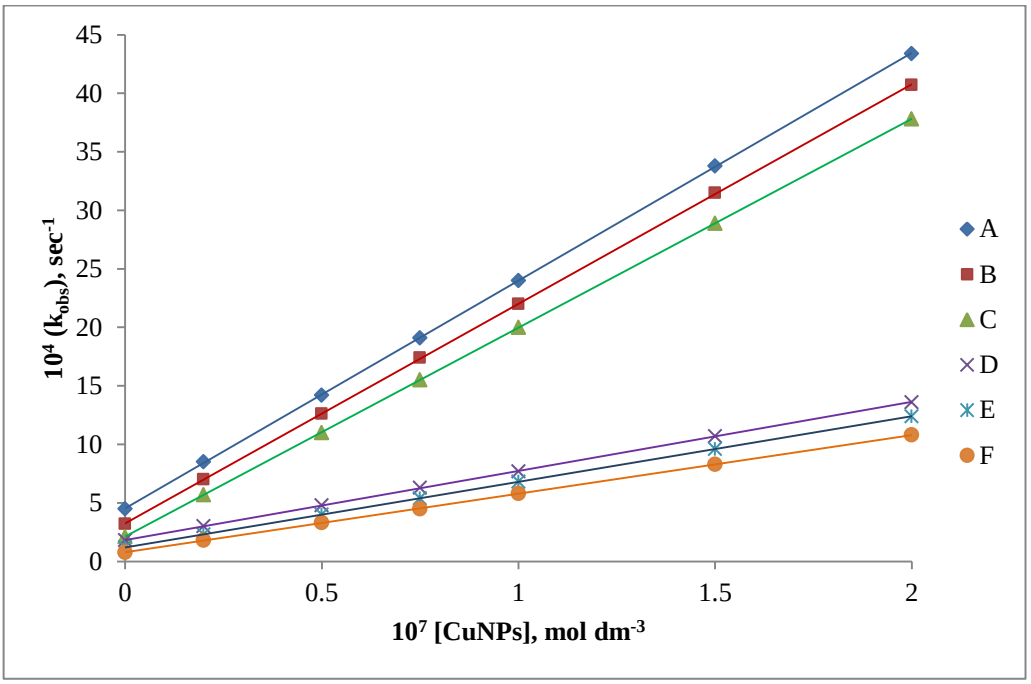

Figure 6.8: Effect of Copper nanoparticles.

[Dye] = 5.0 x 10^{-5} mol dm^{-3} pH = 6.5

[PMS] = 5.0 x 10^{-4} mol dm^{-3} (A) 35 °C, (B) 30 °C, (C) 25 °C

[PDS] = 5.0 x 10^{-4} mol dm^{-3} (D) 35 °C, (E) 30 °C, (F) 25 °C.

(Ref. Table: 6.7, 6.8, 6.9, 6.10, 6.11, 6.12)

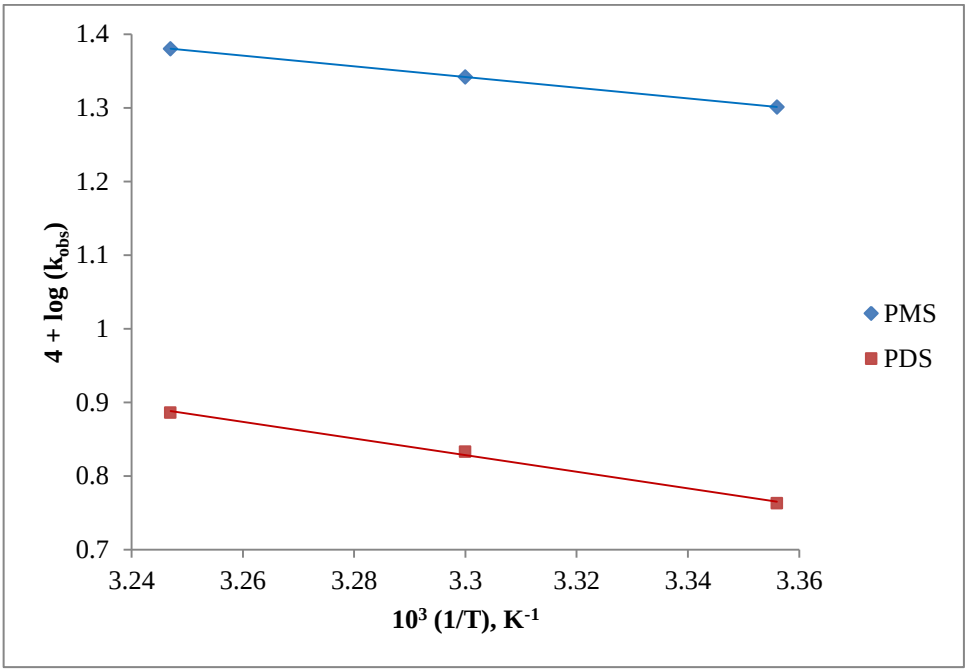

Figure 6.9: Plot of log k versus 1/T.

[Dye] = 5.0 x 10^{-5} mol dm^{-3}

[CuNPs] = 1.0 x 10^{-7} mol dm^{-3}

pH = 6.5

[PDS] = 5.0 x 10^{-4} mol dm^{-3}

[PMS] = 5.0 x 10^{-4} mol dm^{-3}

(Ref. Table: 6.7, 6.8, 6.9, 6.10, 6.11, 6.12)

6.3.2.5. Effect of Alcohol and t-Butyl alcohol (TBA)

For radical quenching tests using Ethanol (EtOH) and t-butyl alcohol (TBA) as a radical scavenger was performed to identify the dominant radical species generated from the CuNPs/PDS and CuNPs/PMS systems. Ethanol is capable of quenching both sulphate and hydroxyl radicals as it readily reacts with both radicals at high and comparable rates, whereas TBA is effective quenching agent for hydroxyl radicals [5, 9]. The results illustrate that quenching effect of EtOH is greater than TBA in both systems (**Table 6.13, 6.14**) (**Figure 6.10, 6.11**). Therefore, sulphate radicals are active species in the oxidative degradation of dye in presence of CuNPs.

6.3.2.6. Mechanism

In the present study, CuNPs was proved to the catalyst with good activity degradation of the azo compound with peroxosulphates as an oxidant. The zero valent copper serves as a mediator for the electron transfer to the peroxosulphates and generates higher active sulphate radicals. Then these radicals are the rapid attack on MO molecules and degrade into end products. The plausible mechanism PDS are given as-

$$2S_2O_8^{2-} + Cu^{\circ} \rightarrow 2SO_4^{\bullet -} + 2SO_4^{2-} + Cu(II)$$

$$2SO_4^{\bullet -} + Cu(II) + Dye \rightarrow \text{Product} + Cu^{\circ}$$

$$2S_2O_8^{2-} + Dye \xrightarrow{Cu^{\circ}} \text{Product} + 2SO_4^{2-}$$

And for PMS are given as-

$$2HSO_5^{-} + Cu^{\circ} \rightarrow Cu(II) + 2SO_4^{\bullet -} + 2OH^{-}$$

$$2SO_4^{\bullet -} + Cu(II) + Dye \rightarrow \text{Product} + Cu^{\circ}$$

$$HSO_5^{-} + Dye \xrightarrow{Cu^{\circ}} \text{Product} + 2OH^{-}$$

TABLE: 6.13

SCAVENGER EFFECT

[Dye] = 5.0 x 10^{-5} mol dm^{-3} **Temp. = 30 °C**

[PDS] = 5.0 x 10^{-4} mol dm^{-3} **pH = 6.5**

[CuNPs] = 1.0 x 10^{-7} mol dm^{-3}

SCAVENGER	**EtOH**	**TBA**	**No Scavenger**
Time in minutes		**Absorbance**	
0	1.229	1.230	1.229
10	1.225	0.851	0.817
20	1.221	0.592	0.543
30	1.218	0.411	0.362
40	1.214	0.283	0.241
50	1.210	0.196	0.162
60	1.207	0.134	0.105
10^4 (k_{obs}), sec^{-1}	**0.05**	**6.10**	**6.80**

TABLE: 6.14

SCAVENGER EFFECT

[Dye] = 5.0 x 10^{-5} mol dm^{-3} **Temp. = 30 °C**

[PMS] = 5.0 x 10^{-4} mol dm^{-3} **pH = 6.5**

[CuNPs] = 1.0 x 10^{-7} mol dm^{-3}

SCAVENGER	**EtOH**	**TBA**	**No Scavenger**
Time in minutes		**Absorbance**	
0	1.227	1.225	1.229
2	1.213	0.955	0.944
4	1.198	0.741	0.725
6	1.183	0.577	0.557
8	1.168	0.447	0.427
10	1.154	0.349	0.328
12	1.139	0.270	0.252
10^3 (k_{obs}), sec^{-1}	**0.10**	**2.10**	**2.20**

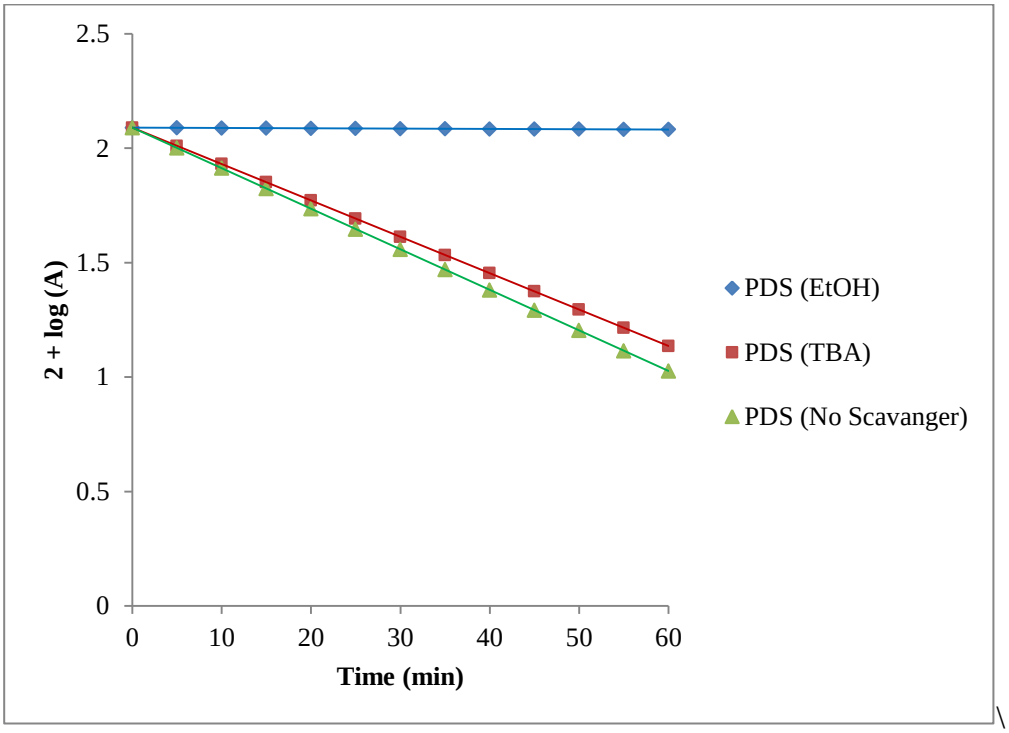

Figure 6.10: Scavenger effect of EtOH and TBA in CuNPs/PDS system.

[Dye] = 5.0 x 10^{-5} mol dm^{-3} [PDS] = 5.0 x 10^{-4} mol dm^{-3}

[CuNPs] = 1.0 x 10^{-7} mol dm^{-3} pH = 6.5

Temperature 30 °C

(**Ref. Table: 6.13**)

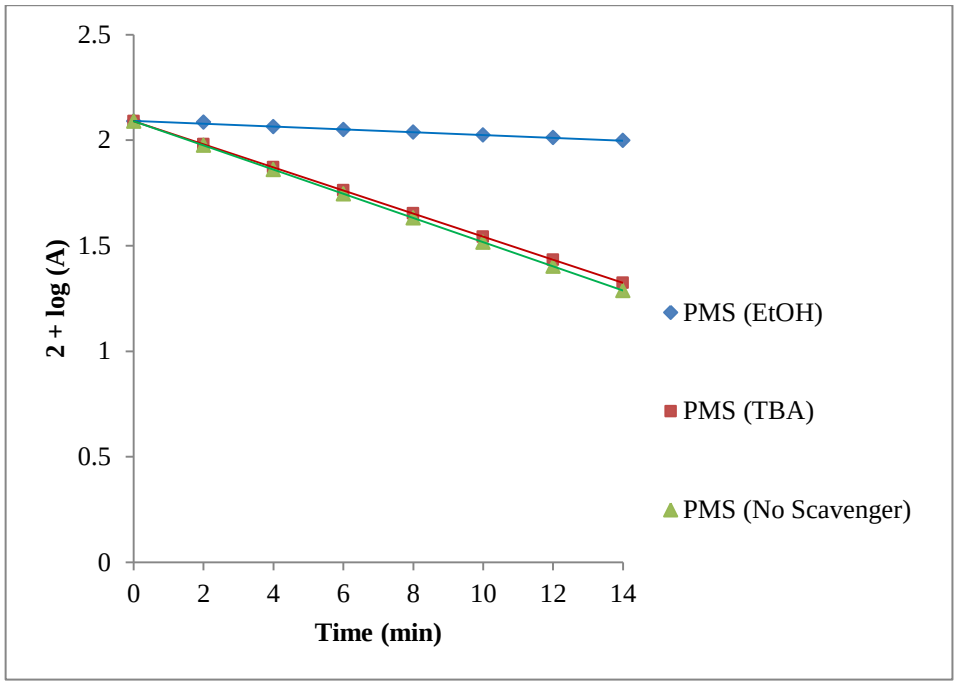

Figure 6.11: Scavenger effect of EtOH and TBA in CuNPs/PMS system.

[Dye] = 5.0 x 10^{-5} mol dm^{-3} [PMS] = 5.0 x 10^{-4} mol dm^{-3}

[CuNPs] = 1.0 x 10^{-7} mol dm^{-3} pH = 6.5

Temperature 30 ^{0}C

(**Ref. Table: 6.14**)

It was observed that CuNPs/Peroxosulphates system achieved the highest MO degradation rate at pH 6.5. The degradation rate decreased when the solution pH either acidic or alkaline. The earlier study also reports, at pH 7.0 PDS/CuO coupled system was must efficient for 2,4-DCP degradation, copper leaching was 50 times lower than drinking water standards [31] so in this chapter, the possibility of leaching of Cu^{2+} ions are very less at optimum reaction conditions. The application of homogenous (colloidal) catalysis is restricted due to the difficulty in reporting the soluble catalyst from the product and reaction solvent. Although recycling of colloidal catalysis could be achieved by using magnetic nanoparticles and solid-phase beads, NPs supported catalysis proceeded much faster than its counterpart on resins. These protocols should be tested to anchor CuNPs for peroxosulphates activation in future studies.

6.4. Conclusion

From the above experimental results, we conclude that CuNPs were used for activation of peroxosulphates for degradation of hazardous dye in a cost-effective manner. Cu° was the source of Cu^{2+}, which was verified to be the efficient activating agent for peroxosulphates to produce sulphate radicals. Kinetic results reveal that CuNPs/Peroxosulphates system could induce a 0.81×10^{-4} – 40.7×10^{-4} sec^{-1} folds increase in the degradation rate of MO at different concentration of CuNPs, peroxosulphate concentration, and initial pH. Moreover, the reactivity discrepancy of PDS and PMS followed the order of CuNPs/PMS > CuNPs/PDS in degradation of MO under similar conditions. Furthermore, the elucidation of degradation pathway is of special interest considering environmental priorities. More importantly, these nanoparticles showed a significantly longer lifespan with sustained reactivity, making them the potential application in dye degradation.

6.5. References

[1] A. Azam, A. Hamid, ***J. Hazard. Mater.***, 133 (2006) 167.

[2] C. P. Huang, C. Dong, Z. Tang, ***Waste Manag.***, 13 (1993) 361.

[3] Y. Deng, R. Zhao, ***Curr. Pollution Rep.***, 1 (2015) 167.

[4] X. Xiong, B. Sun, J. Zhang, N. Gao, J. Shen, J. Li, X. Guan, ***Water Res.***, 62 (2014) 53.

[5] G. P. Anipsitakis, D. D. Dionysiou, ***Environ. Sci. Technol.***, 37 (2003) 4790.

[6] S. Yanga, P. Wang, X. Yang, L. Shan, W. Zhang, X. Shao, R. Niu, ***J. Hazard. Mater.***, 179 (2010) 552.

[7] S. Su, W. Guo, C. Yi, Y. Leng, Z. Ma, ***Ultrason. Sonochem.***, 19 (2012) 469.

[8] M. Murugavelu, P. Andal, S. Shailaja, M.S. Ramachandran, ***J. Mol. Catal. A: Chem.***, 306 (2009) 1.

[9] J. Zhang, M. Chen, L. Zhu, ***RSC Adv.***, 6 (2016) 758.

[10] J. Zhang, M. Chen, L. Zhu, ***RSC Adv.***, 6 (2016) 47562.

[11] G. P. Anipsitakis, D. D. Dionysiou, ***Environ. Sci. Technol.***, 38 (2004) 3705.

[12] A. Nasirian, ***Int. J. Nano Dim.***, 2 (2012) 159.

[13] L. N. Lewis, J. F. Smith, ***J. Am. Chem. Soc.***, 108 (1986) 2728 .

[14] H. Hirai, H. Wakabayashi, M. Komiyama, ***Bull. Chem. Soc. Jpn.***, 59 (1986) 367.

[15] M. Spiro, ***Catal. Today***, 17 (1993) 517.

[16] J. A. Eastman, S. U. S. Choi, S. Li, W. Yu, L. J. Thompson, ***Appl. Phys. Lett.***, 78 (2001) 718.

[17] R. K. Guduru, K. L. Murty, K. M. Youssef, R. O. Scattergood, C. C. Koch, ***Mater. Sci. Eng. A***, 463 (2007) 14.

[18] M. L. Kantam, V. S. Jaya, M. J. Lakshmi, B. R. Reddy, B. M. Choudary, S. K. Bhargava, ***Catal. Commun.***, 8 (2007) 1963.

[19] S. Jain, N. Nagar, V. Devra, ***Pelagia Research Library***, 6 (2015) 171.

[20] A. E. -Ghenymy, F. Centellas, J. A. Garrido, R. M. Rodríguez, I. Sirés, P. L. Cabot, E. Brillas, ***Electrochim. Acta.***, 130 (2014) 568.

[21] A. B. D. Santos, F. J. Cervantes, J. B. V. Lier, ***Bioresour. Technol.***, 98 (2007) 2369.

[22] S. A. Daher, ***J. Edu. Sci.***, 25 (2001) 79.

[23] T. Chen, Y. Zheng, J. –M. Lin, G. Chen, ***J. Am. Soc. Mass Spectrom.***, 19 (2008) 997.

[24] C. Baiocchi, M. C. Brussino, E. Pramauro, A. B. Prevot, L. Palmisano, G. Marcì, ***Int. J. Mass Spectrom.***, 214 (2002) 247.

[25] J. Wu, H. Zhang, J. Qiu, ***J. Hazard. Mater.***, 215-216 (2012) 138.

[26] S. G. Kumar, L. G. Devi, ***J. Phys. Chem.***, 115 (2011) 13211.

[27] Y. -H. Huang, Y. -F. Huang, C. -I. Huang, C. -Y. Chen, ***J. Hazard. Mater.***, 170 (2009) 1110.

[28] M. -j. Pu, Y. -w. Ma, J. -q. Wan, Y. Wang, M. -z. Huang, Y. -m. Chen, ***J. Colloid Interface Sci.***, 418 (2014) 330.

[29] K. Lal, A. Garg, Utilization of Dissolved Iron as Catalyst During Fenton-Like Oxidation of Pretreated Pulping Effluent, ***Process Safety and Environment Protection (PSEP)***, 2017, doi.org/10.1016/j.psep.2017.09.005.

[30] R. J. Dougherty, J. Singh, V. V. Krishnan, ***J. Mol. Struct.***, 1131 (2017) 196.

[31] T. Zhang, Y. Chen, Y. Wang, J. L. Roux, Y. Yang, J. -P. Croue, ***Environ. Sci. Technol.***, 48 (2014) 5868.

Chapter – 7

Kinetic Study of Copper Nanoparticles Catalyzed Degradation of Orange G by Peroxomonosulphate

7.1. Introduction

The textile industry effluents contain large amounts of dye chemicals which may source of severe water pollution. There are numerous processes available for the removal of dyes by physical, biological and chemical processes [1-5]. These methods are frequently very expensive and not eco-friendly due to their low efficiency and a large amount of sludge generation. Advanced oxidation process (AOPs) has been broadly studied to reduce pollutants in water treatment. Peroxomonosulphate (PMS) is the latest oxidant used in chemical oxidation for water treatment [6]. Sulphate radicals (SRs) ($SO_4^{\bullet-}$) based AOPs have recently attracted due to their high efficiency and selectivity towards degradation of organic pollutants [7, 8]. SRs have higher redox potential (2.5-3.1 V) [9] than hydroxyl radicals ($HO^{\bullet}$) (1.8-2.7 V) [10]. The SRs can be generated by activating PMS by various catalysts i.e. UV [11-13], heat [14], transition metal [15-17] has been widely studied. Although UV and heat are efficient ways to activate PMS but requires high energy input limits their application. Among the transition metal ion, copper-mediated decomposition of PMS is an efficient catalytic system to generate $SO_4^{\bullet-}$ as the major oxidizing species [18]. The CuNPs/PMS system for the removal of organic pollutants has shown a lot of interest because of its benefits such as wide pH range small quantity of copper catalyst and high degradation efficiency at room temperature.

In order to promote the performance of catalysts, nano-scaled catalyst draws much attention in recent years due to their particular physical, chemical properties and excellent performance [19]. Most of the studies in the homogeneous colloidal nanocatalysis field involve using spherical NPs or undetermined shapes. There are very few studies in which catalysis is conducted with specific shape and size of NPs. NPs of different sizes have different surface area and active sites. Thus, one would expect the catalytic activity to be different in the same reaction. So that it is a key factor to reach controlled synthesis process of NPs for getting better results in catalysis [20]. The main objectives of this report are (1) Explore the catalytic activity of different size of NPs in CuNPs/PMS system for degradation of model organic contaminant Orange G. (2) To determine

the effect of different concentration of PMS, catalyst, pH and neutral salts on the degradation of Orange G. These issues are used to select and improve the performance of sulphate radical base AOPs for dye wastewater treatment.

7.2. Experimental

7.2.1. Chemicals and Materials

Peroxomonosulphate (PMS) (Sigma-Aldrich) is a triple salt and always fresh solution of PMS were prepare for experiment. Doubly distilled water was used throughout the study and for second distillation alkaline permanganate was used in an all glass assembly. All other reagents employed in this study were either of AnalaR grade or guaranteed reagent grade and were used as supplied without undertaking any further treatment. The methods of prepared solution of all reagents are given in chapter 2 (Instrumentation and Materials).

7.2.2. Kinetic Measurements

The oxidative degradation of Orange G in CuNPs/PMS system was carried out with the required concentration of reactants in stoppered Erlenmeyer flask at 30 ± 0.1 °C and reaction was initiated by adding the known volume of PMS solution. The kinetics was monitored by the absorbance of Orange G measured using UV-Visible Spectrophotometer attached with Peltier accessory (Temperature- controlled) at λ_{max} 476 nm at the regular time interval. It was observed that the absorbance (A) of the dye solution decreases with increasing time showing the progress of dye degradation. The kinetic plots for the rate constant were determined under pseudo-first order conditions which are generated by plotting log (absorbance) versus time and the molar absorptive index of OG was found to be 19650 ± 50 mol^{-1} dm^3 cm^{-1} [21, 22]. The best fit linear plots exhibit pseudo first-order kinetics of Orange G degradation in CuNPs/PMS system. The limiting region in these exponential plots indicates the completion of degradation.

7.3. Result and Discussion

7.3.1. Product Analysis

Figure 7.1 shows the UV-visible spectra of the reaction mixture of Orange G initially consist of three main peaks at 254, 329, and 476 nm. The band at 245 and 329 nm arises from the π–π* transition related to the aromatic ring attached to –N=N– group in the Orange G molecule, while 476 nm band could be assigned to the n–π* transition of –N=N– group [19, 22, 23]. As the degradation reaction proceeded, it was observed that the two characteristic absorption peaks at 329 and 476 nm decreased and almost disappeared within 60 minutes initiation of the reaction. This indicates that the chromophore and conjugated system were being destroyed, whereas the peak at 254 nm declined slowly, showing that the aromatic rings were still present.

In order to provide supportive evidence for the proposed degradation route, identification of degradation intermediates was carried out by LC-MS analysis of the dye solution in CuNPs/PMS system, at the different time interval of the degradation process. **Figure 7.2** showed the significant peaks present at the different time of degradation with corresponding m/z values 283, 239, and 175. The proposed degradation route revealed that $SO_4^{\bullet-}$ radicals (SRs) initially attacks on the aromatic ring, leading to the loss of characteristic fragments of 64 ($-SO_2$), 77 ($-C_6H_5$), and 30 (-NO) groups. Further, attacks by radicals, resultant the formation of the various hydroxyl substituted intermediates and finally into end products illustrated in **Scheme 7.1**.

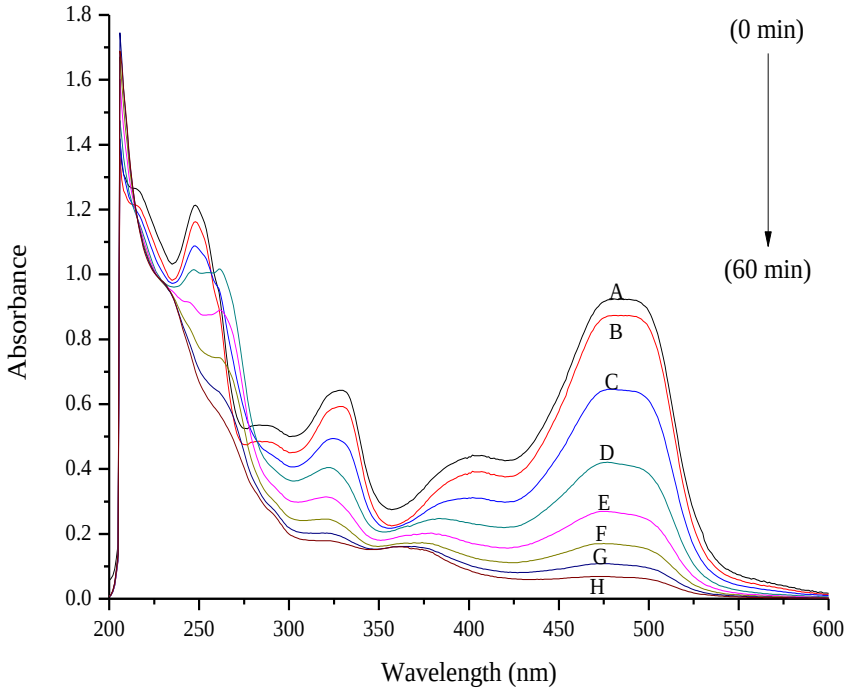

Figure 7.1: The change of UV-visible spectrum with reaction time in CuNPs/PMS system.

[Dye] = 5.0 x 10^{-5} mol dm^{-3} [PMS] = 5.0 x 10^{-4} mol dm^{-3}

[CuNPs] = 1.0 x 10^{-6} mol dm^{-3} pH = 9.2

Temperature 30 °C

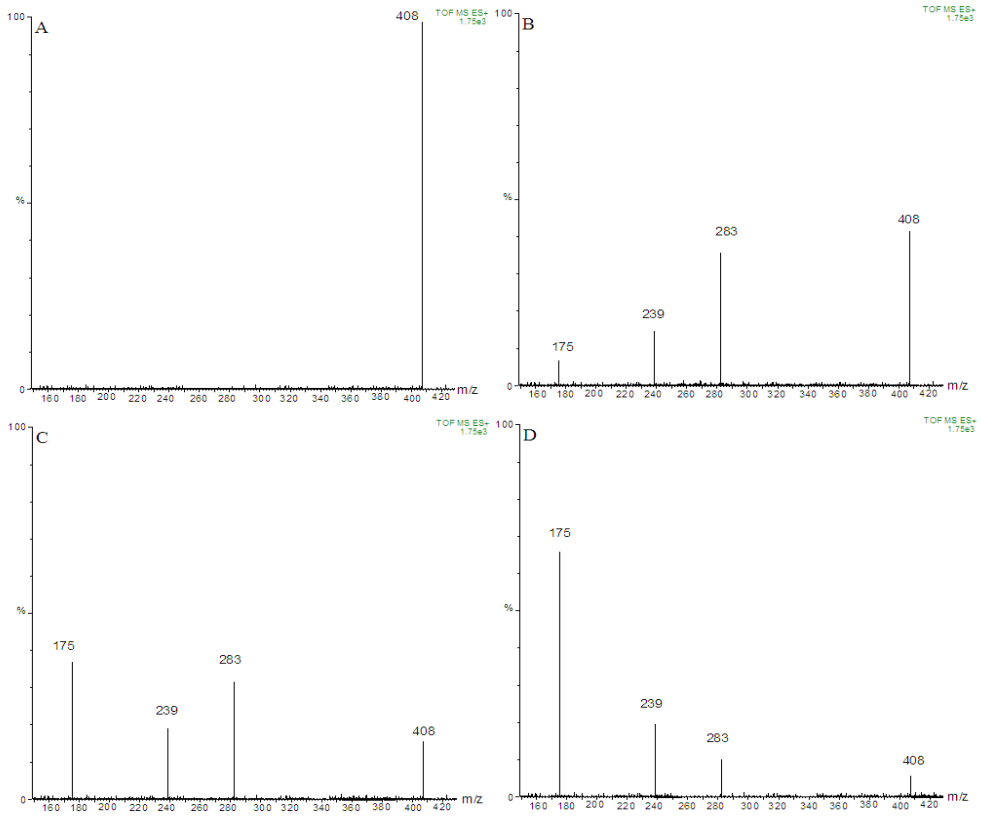

Figure 7.2: LC-MS of Orange G degraded at (A) 0 minutes, (B) 20 minutes, (C) 40 minutes, (D) 60 minutes; in CuNPs/PMS system.

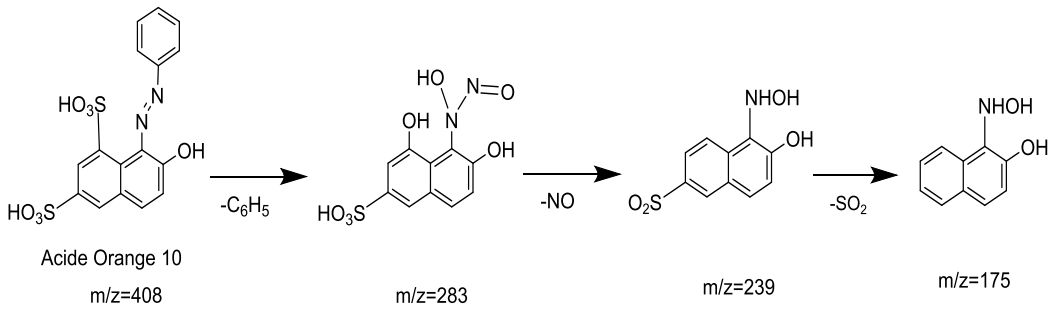

Scheme 7.1: Proposed oxidative degradation route of Orange G in CuNPs/PMS system.

7.3.2. Effect of Experimental Conditions

7.3.2.1. Dye Dependence

Seven different concentration of dye aqueous solution (1.0×10^{-5} to 7.0×10^{-5} mol dm^{-3}) were employed at the fixed concentration of PMS (5.0×10^{-4} mol dm^{-3}), CuNPs (1.0×10^{-6} mol dm^{-3}) and 9.2 pH at 30 °C temperature. **Figure 7.3** indicates that the degradation rate constant initially increases with increasing dye concentration then tends towards a limiting value at higher dye concentration (**Table 7.1**). The results describe that at high dye concentration and constant PMS concentration a number of sulphate radicals were constant consequently degradation rate was constant.

7.3.2.2. Peroxodisulphate Dependence

PMS is a powerful oxidizing agent with a standard potential of E° = 2.5 to 3.1 V and can be dominated by $SO_4^{\bullet-}$ radicals based mechanism and activated by transition metals [24]. **Table 7.2** and **Figure 7.4** illustrates the effect of different concentration of PMS on Orange G degradation of the fixed other reaction conditions ([Dye] = 5.0×10^{-5} mol dm^{-3}, [CuNPs] = 1.0×10^{-6} mol dm^{-3} and pH = 9.2 at 30 °C temperature). The increase in the concentration of PMS resulted in a significant degradation of Orange G. The degradation rate constant increased from 2.5×10^{-4} to 10.5×10^{-4} s^{-1} with the PMS concentration from 1.0×10^{-4} to 7.0×10^{-4} mol dm^{-3}. The positive correlation of PMS concentration with the degradation rate of dye implies that PMS itself and either its secondary decomposition species accounted for the attack of dye molecules. This effect of the degradation rate of organic pollutants on PMS concentration was consistent with the investigation on PMS activation by phosphate anion [6].

TABLE: 7.1
VARIATION OF ORANGE G

[PMS] = 5.0 x 10^{-4} mol dm^{-3} **Temp. = 30 °C**
[CuNPs] = 1.0 x 10^{-6} mol dm^{-3} **pH = 9.2**

10^5 [Dye], mol dm^{-3}	**1**	**2**	**3**	**4**	**5**	**6**	**7**
Time in minutes				**Absorbance**			
0	(0) 0.197	(0) 0.393	(0) 0.590	(0) 0.786	(0) 0.983	1.179	1.376
5	(15) 0.152	(10) 0.312	(8) 0.456	(6) 0.616	(5) 0.778	0.926	1.078
10	(30) 0.116	(20) 0.246	(16) 0.354	(12) 0.481	(10) 0.611	0.731	0.845
15	(45) 0.091	(30) 0.192	(24) 0.274	(18) 0.376	(15) 0.482	0.573	0.663
20	(60) 0.068	(40) 0.151	(32) 0.212	(24) 0.296	(20) 0.382	0.450	0.521
25	(75) 0.052	(50) 0.120	(40) 0.164	(30) 0.232	(25) 0.301	0.356	0.407
30	(90) 0.040	(60) 0.090	(48) 0.126	(36) 0.183	(30) 0.237	0.277	0.321
10^4 (k_{obs}), sec^{-1}	**2.9**	**3.9**	**5.3**	**6.8**	**7.8**	**8.0**	**8.1**

Figures in parentheses denote time in minutes.

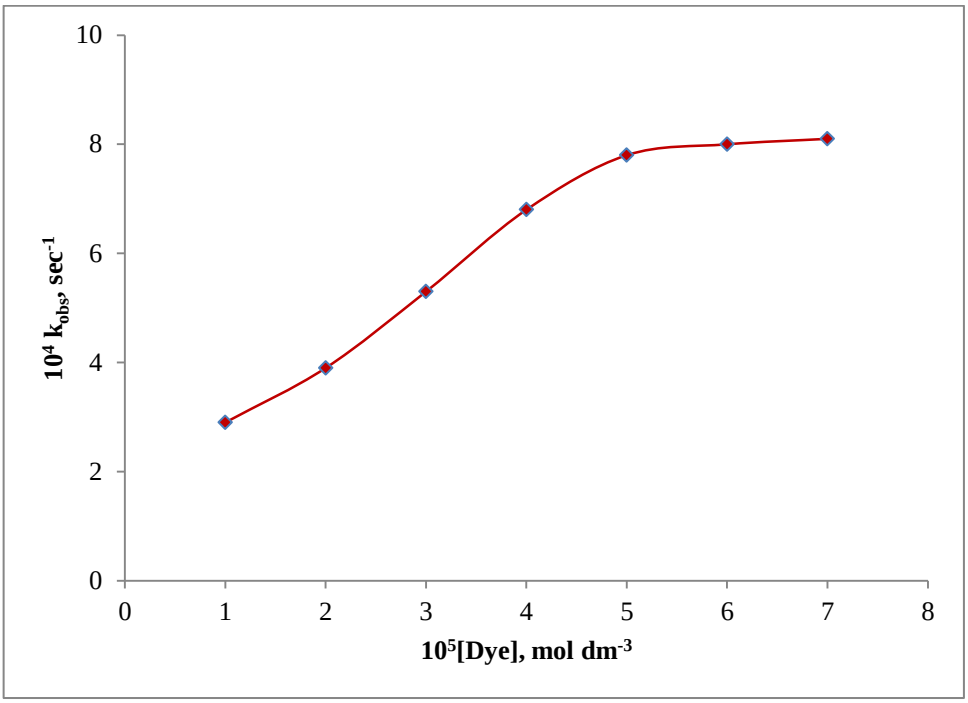

Figure 7.3: Variation of Orange G.

[PMS] = 5.0 x 10^{-4} mol dm^{-3} Temp. = 30 °C

[CuNPs] = 1.0 x 10^{-6} mol dm^{-3} pH = 9.2

(**Ref. Table: 7.1)**

TABLE: 7.2
VARIATION OF PEROXOMONOSULPHATE

[Dye] = 5.0 x 10^{-5} mol dm^{-3} **Temp. = 30 °C**

[CuNPs] = 1.0 x 10^{-6} mol dm^{-3} **pH = 9.2**

10^4 [PMS], mol dm^{-3}	**1**	**2**	**3**	**4**	**5**	**6**	**7**
Time in minutes				**Absorbance**			
0	(0) 0.983	(0) 0.981	(0) 0.984	(0) 0.980	0.983	0.985	(0) 0.983
5	(20) 0.728	(10) 0.773	(8) 0.779	(6) 0.791	0.778	0.748	(4) 0.765
10	(40) 0.539	(20) 0.608	(16) 0.612	(12) 0.639	0.615	0.569	(8) 0.592
15	(60) 0.400	(30) 0.478	(24) 0.485	(18) 0.512	0.487	0.433	(12) 0.458
20	(80) 0.296	(40) 0.376	(32) 0.382	(24) 0.415	0.385	0.330	(16) 0.355
25	(100) 0.219	(50) 0.296	(40) 0.301	(30) 0.332	0.305	0.251	(20) 0.276
30	(120) 0.162	(60) 0.233	(48) 0.238	(36) 0.268	0.241	0.191	(24) 0.214
35	-	(70) 0.183	(56) 0.186	(42) 0.215	0.191	0.145	(28) 0.163
10^4 (k_{obs}), sec^{-1}	**2.5**	**4.0**	**4.9**	**6.0**	**7.8**	**9.1**	**10.5**

Figures in parentheses denote time in minutes.

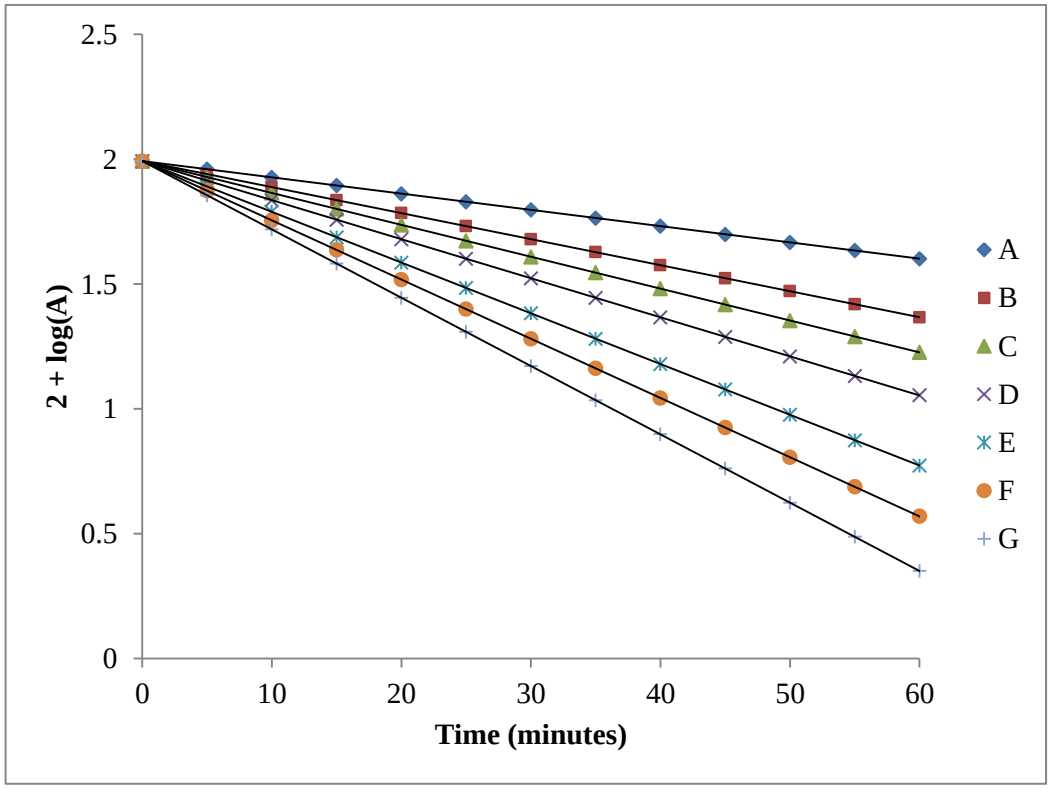

Figure 7.4: Variation of Peroxomonosulphate.

[Dye] = 5.0 x 10^{-5} mol dm^{-3}

[CuNPs] = 1.0 x 10^{-6} mol dm^{-3}

[PMS] = (A) 1.0 x 10^{-4} mol dm^{-3}

(B) 2.0 x 10^{-4} mol dm^{-3}

(C) 3.0 x 10^{-4} mol dm^{-3}

(D) 4.0 x 10^{-4} mol dm^{-3}

Temp. = 30 °C

pH = 9.2

(E) 5.0 x 10^{-4} mol dm^{-3}

(F) 6.0 x 10^{-4} mol dm^{-3}

(G) 7.0 x 10^{-4} mol dm^{-3}

(**Ref. Table: 7.2**)

7.3.2.3. Effect of Initial pH

In order to find the optimal initial pH of the reaction mixture for the degradation of Orange G a series of experiments were conducted in CuNPs/PMS system at different pH (5 to 11) values and other reactant concentration were ([Dye] = 5.0 x 10^{-5} mol dm^{-3}, [PMS] = 5.0 x 10^{-4} mol dm^{-3}, [CuNPs] = 1.0 x 10^{-6} mol dm^{-3}) fixed at 30 °C temperature. Earlier reports revealed that the pH of the solution can dramatically affect the degradation of synthetic dyes in AOPs [25, 26]. It can be seen in **Table 7.3** and **Figure 7.5** that the dye degradation rate is increased up to pH 9.2 and then decreases at higher pH. This effect reflects the result of the electrostatic attraction of the positively charged Cu^{2+} with the ionized dye at the pH (9.2) then decrease in the degradation rate describes the difficulty of anionic dye in approaching the negative charge Cu^{-} at higher solution pH.

7.3.2.4. Copper Nanoparticles Dependence

The catalytic activity of CuNPs on the degradation of Orange G has been studied at varying concentrations (0.20 x 10^{-6} to 2.0 x 10^{-6} mol dm^{-3}) at four different NPs, synthesized at four different temperatures (65, 75, 80 and 85 °C) with average sizes 73.59, 68.54, 50.57 and 48.01 nm respectively at fixed concentration of other reactants ([Dye] = 5.0 x 10^{-5} mol dm^{-3}, [PMS] = 5.0 x 10^{-4} mol dm^{-3}) at 9.2 pH and 30 °C temperature. The degradation rate increases with increase in the concentration of CuNPs (**Table 7.4, 7.5, 7.6, 7.7**) (**Figure 7.6**). The catalytic activity of CuNPs seems different at different temperature of the synthesis process. The difference in catalytic activity can be dependent on the size variation (73.59, 68.54, 50.57 and 48.01 nm) in synthesized CuNPs while keeping other reactant concentration and conditions are constant. The trend of the rate constant with the different size of NPs 48.01 > 50.57 > 68.54 > 73.59 nm is shown in **Table 7.4, 7.5, 7.6, 7.7** and **Figure 7.6**. This effect can be attributed to the nanosize of the particles that surface area and the active centre increases as particle size decreases [27, 28].

TABLE: 7.3
VARIATION OF pH

[Dye] = 5.0 x 10^{-5} mol dm^{-3} **[CuNPs] = 1.0 x 10^{-6} mol dm^{-3}**
[PMS] = 5.0 x 10^{-4} mol dm^{-3} **Temp. = 30 °C**

pH	**5**	**6**	**7**	**8**	**9.2**	**10**	**11**
Time in minutes				**Absorbance**			
0	(0) 0.980	(0) 0.981	(0) 0.982	0.982	0.983	0.983	(0) 0.984
6	(12) 0.746	(10) 0.732	(7) 0.761	0.760	0.742	0.768	(10) 0.715
12	(24) 0.568	(20) 0.546	(14) 0.587	0.588	0.561	0.603	(20) 0.520
18	(36) 0.431	(30) 0.407	(21) 0.453	0.455	0.422	0.472	(30) 0.379
24	(48) 0.328	(40) 0.303	(28) 0.352	0.352	0.321	0.368	(40) 0.275
30	(60) 0.251	(50) 0.226	(35) 0.274	0.273	0.243	0.287	(50) 0.200
36	(72) 0.192	(60) 0.168	(42) 0.210	0.211	0.181	0.225	(60) 0.146
10^4 (k_{obs}), sec^{-1}	**3.8**	**4.9**	**6.1**	**7.1**	**7.8**	**6.8**	**5.3**

Figures in parentheses denote time in minutes.

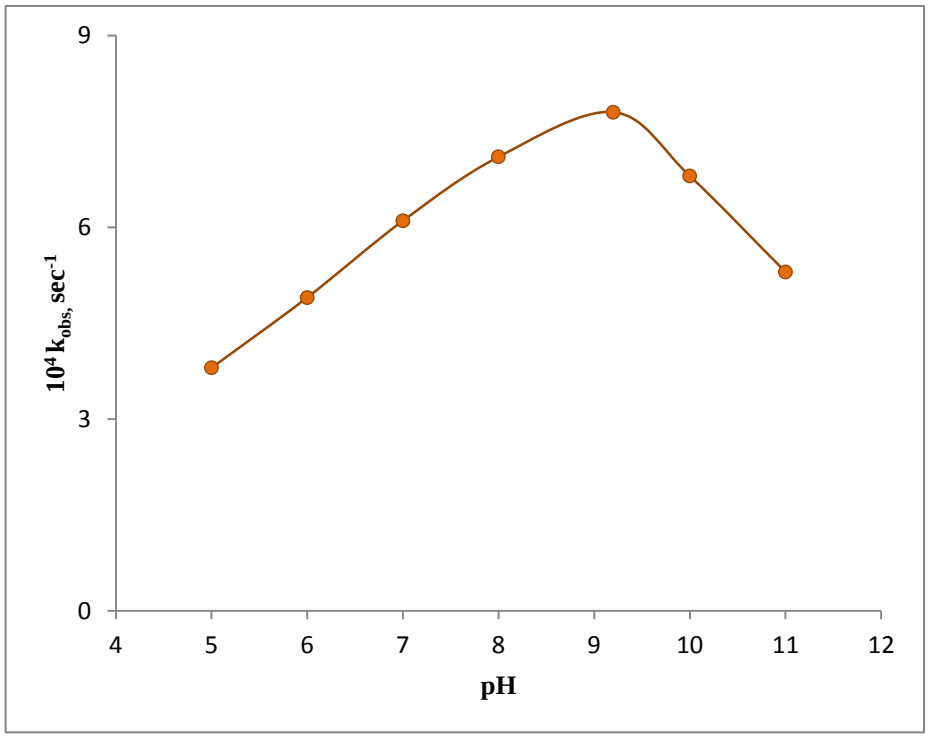

Figure 7.5: Variation of pH.

[Dye] = 5.0 x 10^{-5} mol dm^{-3} [PMS] = 5.0 x 10^{-4} mol dm^{-3}

[CuNPs] = 1.0 x 10^{-6} mol dm^{-3} Temp. = 30 °C

(**Ref. Table: 7.3**)

TABLE: 7.4
VARIATION OF COPPER NANOPARTICLES
(Size 48.01 nm)

[Dye] = 5.0 x 10^{-5} mol dm^{-3} **Temp. = 30 °C**
[PMS] = 5.0 x 10^{-4} mol dm^{-3} **pH = 9.2**

10^6 [CuNPs], mol dm^{-3}	**0**	**0.25**	**0.50**	**0.75**	**1.0**	**1.50**	**2.0**
Time in minutes				**Absorbance**			
0	(0) 0.984	(0) 0.984	(0) 0.983	(0) 0.982	(0) 0.983	0.980	0.981
4	(25) 0.728	(15) 0.742	(10) 0.731	(7) 0.753	(6) 0.743	0.760	0.709
8	(50) 0.539	(30) 0.561	(20) 0.547	(14) 0.576	(12) 0.561	0.588	0.512
12	(75) 0.399	(45) 0.425	(30) 0.406	(21) 0.443	(18) 0.421	0.455	0.369
16	(100) 0.296	(60) 0.321	(40) 0.304	(28) 0.342	(24) 0.323	0.352	0.266
20	(125) 0.219	(75) 0.243	(50) 0.225	(35) 0.261	(30) 0.240	0.272	0.192
24	(150) 0.162	(90) 0.185	(60) 0.169	(42) 0.202	(36) 0.180	0.211	0.138
10^4 (k_{obs}), sec^{-1}	**2.0**	**3.1**	**4.9**	**6.3**	**7.8**	**10.7**	**13.6**

Figures in parentheses denote time in minutes.

TABLE: 7.5
VARIATION OF COPPER NANOPARTICLES
(Size 50.57 nm)

[Dye] = 5.0 x 10^{-5} mol dm^{-3} **Temp. = 30 °C**
[PMS] = 5.0 x 10^{-4} mol dm^{-3} **pH = 9.2**

10^6 [CuNPs], mol dm^{-3}	**0**	**0.25**	**0.50**	**0.75**	**1.0**	**1.50**	**2.0**
Time in minutes				**Absorbance**			
0	(0) 0.984	(0) 0.982	(0) 0.984	0.983	0.983	(0) 0.981	(0) 0.982
8	(25) 0.728	(15) 0.755	(10) 0.760	0.755	0.717	(5) 0.752	(4) 0.755
16	(50) 0.539	(30) 0.582	(20) 0.586	0.581	0.522	(10) 0.576	(8) 0.572
24	(75) 0.399	(45) 0.447	(30) 0.452	0.446	0.381	(15) 0.441	(12) 0.439
32	(100) 0.296	(60) 0.345	(40) 0.348	0.343	0.276	(20) 0.338	(16) 0.336
40	(125) 0.219	(75) 0.265	(50) 0.267	0.261	0.201	(25) 0.259	(20) 0.254
48	(150) 0.162	(90) 0.206	(60) 0.205	0.200	0.148	(30) 0.198	(24) 0.192
10^4 (k_{obs}), sec^{-1}	**2.0**	**2.9**	**4.3**	**5.5**	**6.6**	**8.9**	**11.2**

Figures in parentheses denote time in minutes.

TABLE: 7.6
VARIATION OF COPPER NANOPARTICLES
(Size 68.45 nm)

[Dye] = 5.0 x 10^{-5} mol dm^{-3} **Temp. = 30 °C**
[PMS] = 5.0 x 10^{-4} mol dm^{-3} **pH = 9.2**

10^6 [CuNPs], mol dm^{-3}	**0**	**0.25**	**0.50**	**0.75**	**1.0**	**1.50**	**2.0**
Time in minutes				**Absorbance**			
0	(0) 0.984	(0) 0.982	(0) 0.980	0.983	0.983	(0) 0.981	(0) 0.982
10	(25) 0.728	(15) 0.772	(12) 0.752	0.746	0.711	(6) 0.761	(5) 0.754
20	(50) 0.539	(30) 0.603	(24) 0.575	0.566	0.514	(12) 0.589	(10) 0.581
30	(75) 0.399	(45) 0.475	(36) 0.440	0.429	0.372	(18) 0.456	(15) 0.446
40	(100) 0.296	(60) 0.370	(48) 0.337	0.326	0.269	(24) 0.353	(20) 0.341
50	(125) 0.219	(75) 0.290	(60) 0.258	0.247	0.194	(30) 0.274	(25) 0.262
60	(150) 0.162	(90) 0.225	(72) 0.198	0.188	0.140	(36) 0.212	(30) 0.201
10^4 (k_{obs}), sec^{-1}	**2.0**	**2.7**	**3.7**	**4.6**	**5.4**	**7.1**	**8.8**

Figures in parentheses denote time in minutes.

TABLE: 7.7
VARIATION OF COPPER NANOPARTICLES
(Size 73.59 nm)

[Dye] = 5.0 x 10^{-5} mol dm^{-3} **Temp. = 30 °C**
[PMS] = 5.0 x 10^{-4} mol dm^{-3} **pH = 9.2**

10^6 [CuNPs], mol dm^{-3}	**0**	**0.25**	**0.50**	**0.75**	**1.0**	**1.50**	**2.0**
Time in minutes				**Absorbance**			
0	(0) 0.984	(0) 0.983	0.982	0.981	0.980	0.984	(0) 0.980
10	(25) 0.728	(15) 0.793	0.818	0.789	0.758	0.706	(7) 0.744
20	(50) 0.539	(30) 0.635	0.675	0.627	0.586	0.508	(14) 0.563
30	(75) 0.399	(45) 0.512	0.560	0.501	0.454	0.365	(21) 0.427
40	(100) 0.296	(60) 0.411	0.466	0.403	0.351	0.263	(28) 0.325
50	(125) 0.219	(75) 0.331	0.383	0.321	0.272	0.189	(35) 0.244
60	(150) 0.162	(90) 0.265	0.320	0.253	0.208	0.138	(42) 0.185
10^4 (k_{obs}), sec^{-1}	**2.0**	**2.4**	**3.1**	**3.7**	**4.3**	**5.5**	**6.6**

Figures in parentheses denote time in minutes.

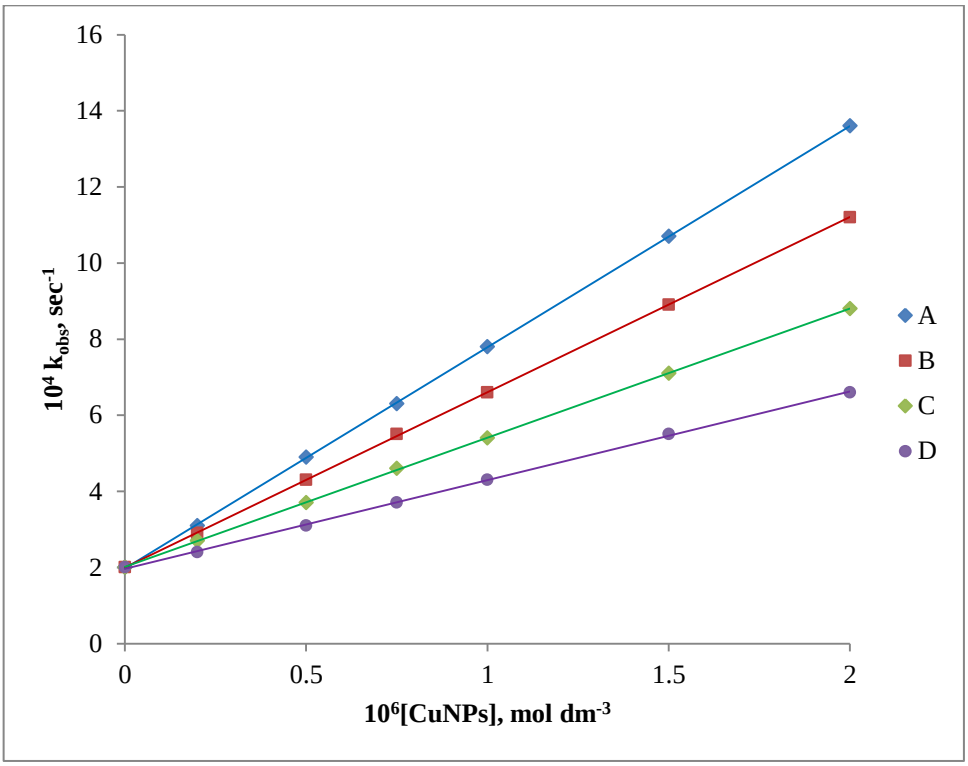

Figure 7.6: Effect of Copper Nanoparticles at different size in nm (A) 48.01, (B) 50.57, (C) 68.45, (D) 73.59.

[Dye] = 5.0 x 10^{-5} mol dm^{-3} [PMS] = 5.0 x 10^{-4} mol dm^{-3}

Temp. = 30 °C pH = 9.2

(**Ref. Table: 7.4, 7.5, 7.6, 7.7**)

7.3.2.5. Effect of temperature

The effect of temperature on Orange G degradation with CuNPs/PMS system was investigated at three temperatures and CuNPs concentration varied from 0.20 x 10^{-6} to 2.0 x 10^{-6} mol dm^{-3}. These experiments were done at constant concentration of [Dye] = 5.0 x 10^{-5} mol dm^{-3}, [PMS] = 5.0 x 10^{-4} mol dm^{-3} and pH was 9.2. As the temperature rises from 25 to 35 °C, the degradation rate constant increased from 6.6 x 10^{-4} to 8.8 x 10^{-4} s^{-1} (**Table 7.8**). This result could be ascribed to thermal activation of PMS and PMS decomposed faster at the higher temperature [29]. According to the first order kinetics, the activation energy for Orange G degradation by CuNPs/PMS process was calculated using the Arrhenius equation from plot of log k versus (1/T) (**Figure 7.7**). The activation energy was calculated to be 21.97 KJ mol^{-1}, indicating that the Orange G degradation in CuNPs/PMS process required moderate activation energy. Previous investigations reported that the value of activation energy on various catalysts could be different such as 88.45 KJ mol^{-1} on Carbon nanotubes/PMS – Orange G [30] 92.2 KJ mol^{-1} on Fe^{2+}/PMS – Orange G [24]. The low activation energy signified the CuNPs/PMS oxidation process was easy to occur and was very promising for the catalytic reaction. The value of thermodynamic parameters such as free energy of activation ($\Delta G^{\#}$), enthalpy of activation ($\Delta H^{\#}$) and entropy of activation ($\Delta S^{\#}$) are 92.17 kJ mol^{-1}, 19.45 kJ mol^{-1} and -240.43 J mol^{-1} K^{-1} respectively. The high positive values of $\Delta G^{\#}$ and $\Delta H^{\#}$ indicates that the process was endothermic and nonspontaneous while negative value of $\Delta S^{\#}$ represents endergonic reaction [19].

TABLE: 7.8
EFFECT OF TEMPERATURE

[Dye] = 5.0 x 10^{-5} mol dm^{-3} **[CuNPs] = 1.0 x 10^{-6} mol dm^{-3}**
[PMS] = 5.0 x 10^{-4} mol dm^{-3} **pH = 9.2**

Temperature (°C)	**25 °C**	**30 °C**	**35 °C**
Time in minutes		**Absorbance**	
0	(0) 0.980	(0) 0.983	0.980
5	(7) 0.742	(6) 0.742	0.755
10	(14) 0.563	(12) 0.560	0.580
15	(21) 0.427	(18) 0.423	0.445
20	(28) 0.323	(24) 0.319	0.342
25	(35) 0.245	(30) 0.242	0.263
30	(42) 0.184	(36) 0.185	0.202
10^4 (k_{obs}), sec^{-1}	**6.6**	**7.8**	**8.8**

Figures in parentheses denote time in minutes.

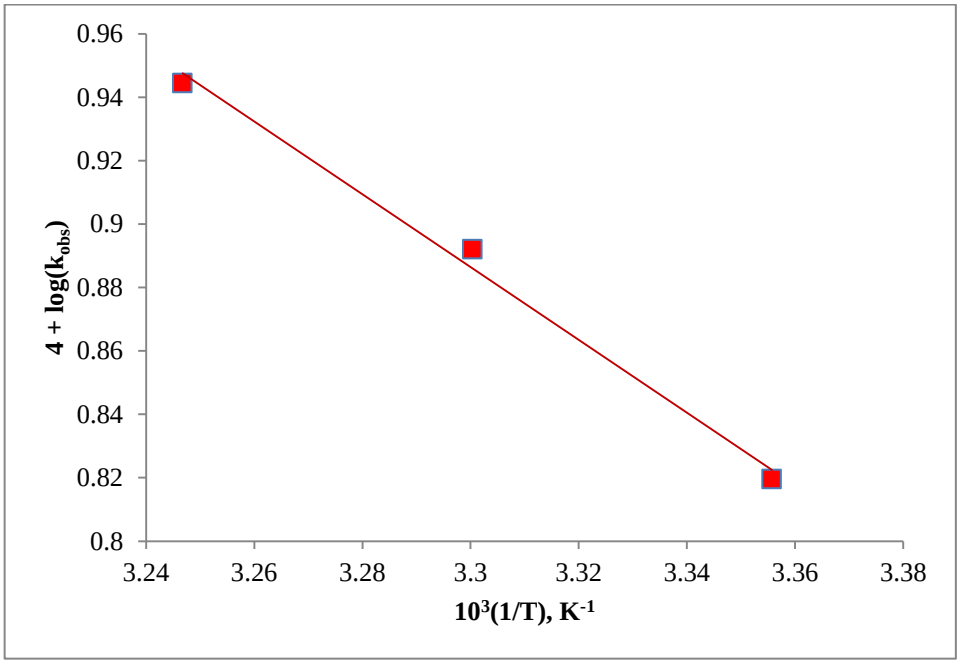

Figure 7.7: Plot of log k versus 1/T.

[Dye] = 5.0 x 10^{-5} mol dm^{-3} [PMS] = 5.0 x 10^{-4} mol dm^{-3}

[CuNPs] = 1.0 x 10^{-6} mol dm^{-3} pH = 9.2

(**Ref. Table: 7.8**)

7.3.2.6. Effect of Neutral salts

NaCl, $NaNO_3$, $NaHCO_3$ salt are generally added to dye solution for adjusting the ionic strength and improving the fixation of dye on fabrics. Thus the effect of Cl^-, NO_3^-, HCO_3^- ions on Orange G removal by CuNPs/PMS system was studied. The concentration of Cl^-, NO_3^-, and HCO_3^- was varied from 10 x 10^{-3} to 20 x 10^{-3} mol dm^{-3} at fix concentration of other reactants ([Dye] = 5.0 x 10^{-5} mol dm^{-3}, [PMS] = 5.0 x 10^{-4} mol dm^{-3}, [CuNPs] = 1.0 x 10^{-6} mol dm^{-3}) and constant conditions (pH = 9.2, 30 °C temperature). As the concentration of Cl^- ions increased, an inhibition was observed. It is feasible for $SO_4^{\bullet-}$ to oxidize chloride ions into less reactive chlorine species [19]. The oxidative degradation rate also decreases as an increase in the concentration of bicarbonate ions (HCO_3^-), contribute to active $SO_4^{\bullet-}$ radicals convert into sulphate ions (SO_4^{-2}) whereas NO_3^- ions have no obvious effect on the degradation of CuNPs/PMS system. The results illustrated in **Table 7.9, 7.10, 7.11** and **Figure 7.8**. Furthermore, it can be found that the anions could inhibit the degradation rate of Orange G and their inhibiting order is NO_3^- < Cl^-< HCO_3^- [23].

7.3.2.7. Mechanism

In the present research work CuNPs play a role of activator of oxidant (PMS) and generate higher active sulphate radicals. These sulphate radicals react with dye molecules and degrade into end product subsequently. The plausible mechanism is given as-

$$2HSO_5^- + Cu^\circ \rightarrow Cu(II) + 2SO_4^{\bullet-} + 2OH^-$$

$$2SO_4^{\bullet-} + Cu(II) + Dye \rightarrow \mathrm{Pr}oduct + Cu^\circ$$

$$HSO_5^- + Dye \xrightarrow{Cu^\circ} \mathrm{Pr}oduct + 2OH^-$$

TABLE: 7.9
EFFECT OF NETURAL SALT
($NaNO_3$)

[Dye] = 5.0 x 10^{-5} mol dm^{-3} **Temp. = 30 °C**
[PMS] = 5.0 x 10^{-4} mol dm^{-3} **pH = 9.2**
[CuNPs] = 1.0 x 10^{-6} mol dm^{-3}

10^3 [$NaNO_3$], mol dm^{-3}	**10**	**12**	**14**	**16**	**18**	**20**
Time in minutes			**Absorbance**			
0	0.982	0.985	0.986	0.981	0.983	0.984
6	0.742	0.742	0.743	0.743	0.743	0.743
12	0.561	0.560	0.561	0.562	0.562	0.562
18	0.424	0.423	0.424	0.425	0.425	0.425
24	0.320	0.320	0.321	0.321	0.321	0.321
30	0.242	0.241	0.242	0.243	0.243	0.243
36	0.183	0.182	0.183	0.183	0.184	0.183
10^4 (k_{obs}), sec^{-1}	**7.79**	**7.8**	**7.78**	**7.77**	**7.76**	**7.77**

TABLE: 7.10
EFFECT OF NETURAL SALT
(NaCl)

[Dye] = 5.0 x 10^{-5} mol dm^{-3} **Temp. = 30 °C**
[PMS] = 5.0 x 10^{-4} mol dm^{-3} **pH = 9.2**
[CuNPs] = 1.0 x 10^{-6} mol dm^{-3}

10^3 [NaCl], mol dm^{-3}	**10**	**12**	**14**	**16**	**18**	**20**
Time in minutes			**Absorbance**			
0	0.985	0.982	0.981	0.983	0.980	0.985
7	0.737	0.742	0.746	0.750	0.755	0.759
14	0.552	0.560	0.566	0.572	0.579	0.586
21	0.413	0.423	0.429	0.436	0.445	0.452
28	0.310	0.319	0.326	0.332	0.341	0.349
35	0.232	0.241	0.247	0.254	0.262	0.269
42	0.174	0.182	0.188	0.193	0.201	0.208
10^4 (k_{obs}), sec^{-1}	**6.89**	**6.71**	**6.59**	**6.47**	**6.31**	**6.18**

TABLE: 7.11
EFFECT OF NETURAL SALT
($NaHCO_3$)

[Dye] = 5.0 x 10^{-5} mol dm^{-3} **Temp. = 30 °C**
[PMS] = 5.0 x 10^{-4} mol dm^{-3} **pH = 9.2**
[CuNPs] = 1.0 x 10^{-6} mol dm^{-3}

10^3 [$NaHCO_3$], mol dm^{-3}	**10**	**12**	**14**	**16**	**18**	**20**
Time in minutes			**Absorbance**			
0	0.985	0.980	0.982	0.981	0.983	0.984
8	0.718	0.724	0.732	0.740	0.746	0.755
16	0.525	0.535	0.546	0.558	0.567	0.581
24	0.384	0.395	0.407	0.421	0.431	0.447
32	0.281	0.291	0.304	0.317	0.327	0.344
40	0.205	0.215	0.226	0.239	0.249	0.265
48	0.150	0.158	0.169	0.180	0.189	0.204
10^4 (k_{obs}), sec^{-1}	**6.51**	**6.32**	**6.1**	**5.87**	**5.71**	**5.45**

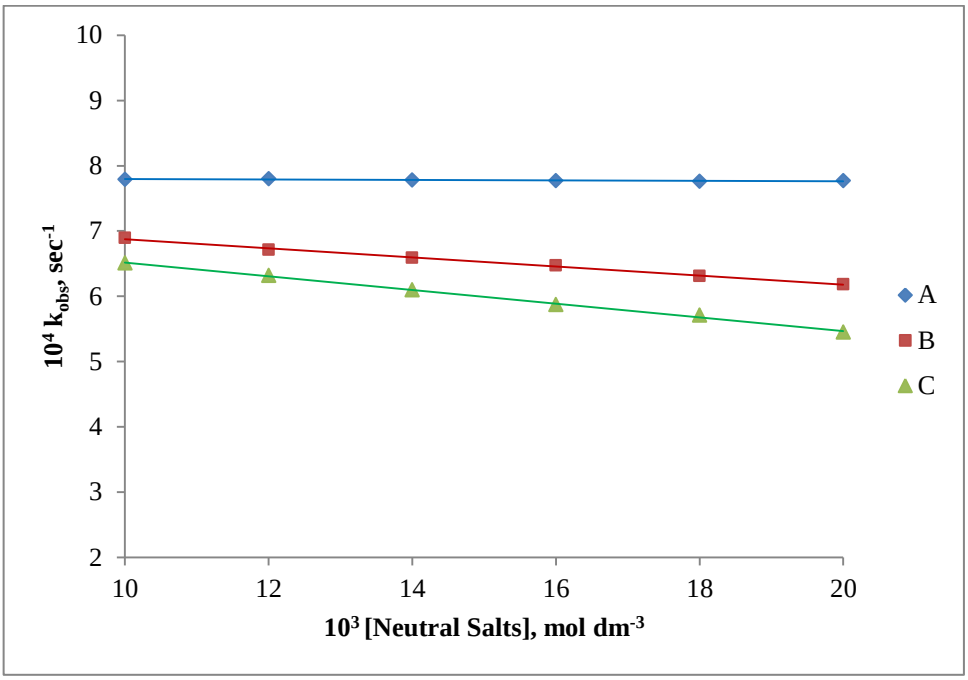

Figure 7.8: Neutral salt dependence (A) $NaNO_3$, (B) NaCl, (C) $NaHCO_3$.

[Dye] = 5.0 x 10^{-5} mol dm^{-3} Temp. = 30 °C

[PMS] = 5.0 x 10^{-4} mol dm^{-3} pH = 9.2

[CuNPs] = 1.0 x 10^{-6} mol dm^{-3}

(**Ref. Table: 7.9, 7.10, 7.11**)

7.4. Conclusion

The present study shows the degradation of OG by PMS in presence of CuNPs. CuNPs effectively catalysed the degradation of OG. During synthesis process, the effect of different temperature on the size of CuNPs (ranging from 48.01- 73.54 nm) as well as an effect of the catalytic activity of different size NPs on degradation rate was also investigated. The smaller particle size of CuNPs, higher concentration of PMS, catalyst and higher temperature promoted the degradation of Orange G in CuNPs/PMS system. The end products of Orange G degradation were identified by LC-MS and the degradation pathways were proposed. The NO_3^-, Cl^-, HCO_3^- have no or inhibited effect on the performance of CuNPs/PMS system because of their scavenging effect on the reactive radical species.

7.5. References

[1] T. Robinson, G. McMullan, R. Marchant, P. Nigam, ***Bioresour. Technol.***, 77 (2001) 247.

[2] A. A. Ahmad, A. Idris, B. H. Hameed, ***Desalin. Water Treat.***, 41 (2012) 224.

[3] F. Harrelkas, A. Azizi, A. Yaacoubi, A. Benhammou, M. N. Pons, ***Desalination.***, 235 (2009) 330.

[4] S. Hammami, M. A. Oturan, N. Oturan, N. Bellakhal, M. Dachraoul, ***Desalin. Water Treat.,*** 45 (2012) 297.

[5] I. Khouni, B. Marrot, R. B. Amar, ***Sep. Purif. Technol.***, 87 (2012) 110.

[6] X. Lou, L. Wu, Y. Guo, C. Chen, Z. Wang, D. Xiao, C. Fang, J. Liu, J. Zhao, S. Lu, ***Chemosphere.***, 117 (2014) 582.

[7] G. P. Anipsitakis, T. P. Tufano, D. D. Dionysiou, ***Water Res.***, 42 (2008) 2899.

[8] M. Ahmad, A. L. Teel, R. J. Watts, ***Environ. Sci. Technol.***, 47 (2013) 5864.

[9] P. Neta, R. E. Huie, A. B. Ross, ***J. Phys. Chem. Ref. Data.***, 17 (1988) 1027.

[10] J. Zhang, M. Chen, L. Zhu, ***RSC Adv.***, 6 (2016) 47562.

[11] Y. H. Guan, J. Ma, X. C. Li, J. Y. Fang, L. W. Chen, ***Environ. Sci. Technol.***, 45 (2011) 9308.

[12] M. M. Ahmed, S. Chiron, ***J. Hazard. Mater.***, 265 (2014) 41.

[13] J. A. Khan, X. He, H. M. Khan, N. S. Shah, D. D. Dionysiou, ***Chem. Eng. J.***, 218 (2013) 376.

[14] D. Deng, L. Peng, M. Guan, Y. Kang, ***J. Hazard. Mater.***, 264 (2014) 521.

[15] G. P. Anipsitakis, D. D. Dionysiou, ***Environ. Sci. Technol.***, 38 (2004) 3705.

[16] Y. R. Wang, W. Chu, ***Water Res.***, 45 (2011) 3883.

[17] J. Zou, J. Ma, L. Chen, X. Li, Y. Guan, P. Xie, C. Pan, ***Environ. Sci. Technol.***, 47 (2013) 11685.

[18] Y. Deng, R. Zhao, ***Curr. Pollution Rep.***, 1 (2015) 167.

[19] J. Zhang, M. Chen, L. Zhu, ***RSC Adv.***, 6 (2016) 758.

[20] A. A. El-Kheshen, S. F. G. El-Rab, ***Pharm. Chem.***, 4 (2012) 53.

[21] H. Lachheb, E. Puzenat, A. Houas, M. Ksibi, E. Elaloui, C. Guillard, J. M. Herrmann, ***Appl. Catal. B***, 39 (2002) 75.

[22] M. A. Meetani, M. A. Rauf, S. Hisaindee, A. Khaleel, A. Alzamly, A. Ahmad, ***RSC Adv.***, 1 (2011) 490.

[23] X. -R. Xu, X. -Z. Li, ***Sep. Purif. Technol.***, 72 (2010) 105.

[24] P. Nfodzo, H. Choi, ***Chem. Eng. J.***, 174 (2011) 629.

[25] Y. -H. Huang, Y. -F. Huang, C. -I. Huang, C. -Y. Chen, ***J. Hazard. Mater.***, 170 (2009) 1110.

[26] J. B. Zhong, J. Z. Li, Y. Lu, S. T. Huang, W. Hu, ***Iran J. Chem. Chem. Eng.***, 31 (2012) 21.

[27] M. Samim, N. K. Kaushik, A. Maitra, ***Bull. Mater. Sci.***, 30 (2007) 535.

[28] S. Jain, N. Nagar, V. Devra, V., ***Adv. Appl. Sci. Res.***, 6 (2015) 171.

[29] Q. Shi, A. Li, Z. Qing, Y. Li, ***J. Ind. Eng. Chem.***, 25 (2015) 308.

[30] Z. L. Ming, C. J. Bin, F. Cong, Z. Lu, H. J. Mei, H. S. Bin, L. W. Wei, W. Z. Ming, H. T. Yin, ***China Environ. Sci.***, 36 (2016) 3591.

CONCLUSION

The present research work light on environmentally benign, cost effective and green method for synthesis of NPs. In this method *Azadirachta Indica* (Neem) use as a renewable source for biological reduction of metal ions would be boon for the development of clean, nontoxic green approach to produce metal nanoparticles. The metal nanoparticles field is currently growing, and it is expected that these key challenges will be encountered in the close future and zone of nanoscience will be efficiently applied in tomorrow's laboratory and industry. The overall objective of research is to fabricate an eco-friendly catalyst to diminish the cost of production which can replace industrial scale conventional, costly catalysts such as noble metals and engineering a greener process via limiting the number of waste chemicals for disposal. Since nanoparticles show a significantly longer life span with sustained reactivity, making them the potential application in environmental remediation.

SUMMARY

Nanomaterials size is situated in nanometer range so that their surface area to volume ratio is high. Due to this nanomaterials have wide variety of applications, ranging from catalysis to antibacterial agents, to biosensors and so on [1–6]. Application of these nanomaterials was depend on their size, shape and synthesis process. Green synthesis of nanoparticles has continued to capture researcher's interest owing to their ecofriendly nature. Metallic nanoparticles synthesized using plant extract are of great interest in biotechnology due to their excellent chemical, physical and catalytic properties [7]. Among all the metallic nanoparticles available, silver and copper has always been one of the favorites because of silver nanoparticles in low concentration have no toxicity against human health [8] and copper nanoparticles have high abundance and low cost compared with other metal [9]. There is limited number of methods for the synthesis of nanoparticles. Development of green, simple, novel and high yielded methods for the preparation of nanoparticles is still a thrust area of research.

Synthetic dyes, especially azo dyes, were found to be toxic, carcinogenic and mutagenic. So that textile effluents are necessary to treat and degrade these dyes in to non-hazardous chemicals [10].

The present thesis describes the green synthesis and characterization of non-supported and highly active and stable nanoparticles of silver and copper nanoparticles to catalyze the degradation of azo dyes by peroxomonosulphate or peroxodisulphate in the aqueous/acidic/basic medium.

The whole work is divided into seven chapters.

The **first chapter** deals with overview of metal nanoparticles, nanocatalysts, peroxosulphate oxidants, dyes and classification of dyes. Nanoparticles have the capability to catalyze large scale dye degradation reactions and foster separation of degradation product from the remaining components and also used in wastewater treatment. The use of metal nanoparticles as catalysts has shown benefits in biotechnology, organic and inorganic reactions [11]. The benefits of metal nanoparticle catalysts are the ability of the particles to act

homogenously or heterogeneously [12]. The achievement of transition metal nanoparticle catalysts is, such as all nanoparticles, the high surface-to-volume ratio and a high surface energy [11]. Due to these properties, transition metal catalysts are being used in a variety of different reactions and mechanisms to further study their reactions and capabilities. Herein, we discusses about various metal nanoparticles viz. Ag [13], Au [14], Cu [15] etc. and their application in the diverse fields.

This chapter also sheds light on the physicochemical properties of nanoparticles [16-19]. The colloidal nanoparticles were found to be more active catalyst for degradation of dyes [20]. Peroxosulphate oxidants such as peroxomonosulphate (PMS), peroxydisulphate (PDS) etc. have gained paramount importance due to their utilization as auxiliary reagents in organic synthesis [21-23]. The present study aims at further exploring the degradation of azo dyes by peroxomonosulphate and peroxodisulphate in catalytic and non- catalytic pathways as well as possible degradation process in the presence of silver and copper nanoparticles.

The **second chapter** describe with the experimental part which divided into two sections. In the first section, we discuss the various analytical instruments and techniques were used during the research work. The instruments and techniques such as Transmission Electron Microscopy (TEM) and Scanning Electron Microscopy (SEM), X-Ray Diffrectometer (XRD), UV-visible spectrophotometer, FTIR spectrophotometer, Zetasizer, Liquid Chromatography-Mass Spectroscopy (LC-MS), Biochemical oxygen demand (BOD) and Chemical oxygen demand (COD), Ultrasonic Processor, centrifuge, electronic balance, pH meter, magnetic stirrer are used for the study. TEM and SEM are used for the characterization of synthesized nanoparticles. These instruments give the information about the morphology of synthesized metal nanoparticles. UV-visible spectrophotometer and FTIR spectrophotometer were used for preliminary investigation of nanoparticles. XRD analysis provides the information about the crystal structure and zetasizer give information of stability, average size of

synthesized nanoparticles. UV-visible spectrophotometer was frequently employed particularly in analyze the progress of reaction. LC-MS analysis provides information about intermediates and products formed during degradation process of dye. BOD and COD are used for measure the amount of organic matter in water. The second section of experimental describes preparation of various solutions like silver nitrate, copper chloride dihydrate, neem leaf broth, dyes, peroxomonosulphate, peroxodisulphate, sulphuric acid, sodium hydroxide, Ethanol etc.

The **third chapter** focuses on synthesis and characterization of nanoparticles, different methods adopted in literature for synthesize of various nanoparticles. Chapter describes the details of experimental work related to the fabrication of silver and copper nanoparticles. Among the various methods, the green method is adopted for synthesize of nanoparticles. In this method, metal salt is used as the precursor and *Azadirachta indica* (neem) leaf broth is used as the reducing agent as well as stabilizing agent for synthesis of nanoparticles which are stable for few months. Synthesized nanomaterials are characterized by different instrumental techniques such as UV-Visible, FT-IR, SEM, TEM, XRD, Zetasizer etc. and results are discussed in this chapter. The results inferred that synthesized nanoparticles are in nano range, silver nanoparticles have spherical shape, average particle size is 9 nm and copper nanoparticles have cubical shape with average particle size 48 nm. The chapter gives the details on the experimental investigation by varying the neem leaf broth percentage, concentration of precursor salts, pH and temperature on the synthesis process of nanoparticles. The application of synthesized metal nanoparticles as catalyst in the degradation of dyes was described in further chapters.

The **forth chapter** deals with the kinetic study of degradation of Methyl Orange (MO) with peroxodisulphate (PDS) in aqueous medium at 30 ^{o}C in the presence of synthesized silver nanoparticles (AgNPs). The degradation rate of dye increased with increase in concentration of PDS and MO concentration up to a certain limit after that rate decreases on further increases of PDS and MO

concentration. The rate of oxidative degradation of MO was increases up to pH=6.5 and then it decreases and the degradation of MO increases with increasing concentration of AgNPs. The catalytic activity of AgNPs tested on real waste water samples, were collected from drains of three different local textile industries of Kota region and BOD, COD also tested to know the organic component present in wastewater samples before and after teratement. The intermediate and products were identified by LC-MS analysis and plausible degradation pathway is proposed.

The **fifth chapter** illustrates the kinetics of degradation of Orange G (OG) by peroxomonosulphate (PMS) in the presence of silver nanocatalyst (AgNPs). The effects of various parameters are studied in this chapter and results shows that the rate of oxidative degradation of OG was increased on increasing the PMS and dye concentration but degradation rate was decreased if increase the dye concentration beyond the certain limits. The effects of concentration of silver nanocatalyst at three different temperatures (25, 30 and 35 ^{o}C) observed pseudo first order rate constant (k_{obs}) of degradation of dye. The activation parameters were also calculated and results illustrate that the high positive value of free energy of activation ($\Delta G^{\#}$) and enthalpy of activation ($\Delta H^{\#}$) indicate that transition state was highly solvated while the negative value of entropy of activation ($\Delta S^{\#}$) was suggested the formation of more ordered transition state. The degradation efficiency increases up to pH = 9.2, after that rate decreases with higher pH. LC-MS analysis of dye degradation indicates that oxidative depletion of azo bond to found aniline and hydroxylamine derivative. Radical quenching tests also done using Ethanol (EtOH) and t-butyl alcohol (TBA). Radical scavenger were performed to identify the dominant radical species during AgNPs/PMS assisted OG degradation.

The **sixth chapter** was focused on comparative study of the catalytic activity of copper nanoparticles (CuNPs) in CuNPs/Peroxodisulfate (PDS) and CuNPs/ Peroxomonosulfate (PMS) process for degradation of Methyl Orange (MO). The increasing concentration of nanocatalyst, peroxosulfates, Dye, initial

pH and high temperature rapidly promoted the degradation kinetics of MO. The degradation of MO in CuNPs/Peroxosulfates system is modeled as pseudo-first order kinetics and activation parameters were also determined. The maximum degradation efficiency of MO reached 92% in 60 min for CuNPs/PDS system and 98% in 30 min for CuNPs/PMS system. Sulfate radicals (SRs) ($SO_4^{\bullet -}$) were identified as oxidative species using specific alcohols. Furthermore, LC-MS analysis and results of UV-visible spectral changes were used to determine the structure of intermediates arising from MO by CuNPs/ Peroxosulfates degradation. The reactivity discrepancy of PDS and PMS followed the order of CuNPs/PMS > CuNPs/PDS in degradation of MO under similar conditions. More importantly, these nanoparticles showed a significantly longer lifespan with sustained reactivity, making them the potential application in dye degradation.

The **seventh chapter** deals with the degradation of Orange G (OG) by peroxomonosulphate (PMS) in basic medium in the presence of copper nanocatalyst. The effect of various parameters such as PMS concentration, OG concentration, nanocatalyst concentration, size of nanocatalyst, pH, temperature etc. is studied in this chapter. Four different size of nanoparticles (73.59, 68.54, 50.57 and 48.01 nm) were synthesized at four temperatures (65, 75, 80, 85 ^oC) and smaller particle show higher catalytic activity. The end products of OG degradation were identified by LC-MS and the degradation pathway was proposed. The effect of added neutral salt on the rate of degradation of OG has also been studied and results show NO_3^- ions have no effect whereas Cl^-, HCO_3^- ions show inhibited effect on the performance of CuNPs/PMS system due to their scavenging effect on the reactive radical species.

References

[1] Esteban-Cubillo, C. Pecharroman, E. Aguilar, J. Santaren, J. S. Moya, ***J. Mater. Sci.,*** 41 (2006) 5208.

[2] Y. Wang, W. Wei, J. Zeng, X. Liu, X. Zeng, ***Microchim. Acta***, 160, (2008) 253.

[3] P. Djinovic, J. Batista, A. Pintar, ***Appl. Catal. A,*** 347 (2008) 23.

[4] A. Saha, B. Ranu, ***J. Org. Chem.,*** 73 (2008) 6867.

[5] G. Schmidt, ***Nanoparticles: From Theory to Application, Wiley-VCH, Weinheim, Germany, 2010.***

[6] V. M. Rotello, ***Nanoparticles: Building Blocks for Nanotechnology, Springer, New York, USA, 2004.***

[7] T. M. D. Dang, T. T. T. Le, E. F. Blanc, M. C. Dang, ***Adv. Nat. Sci. Nanosci. Nanotechnol.,*** 2 (2011) 015009.

[8] M. G. –Moghaddam, R. H. –Dabanlou, M. Khajeb, M. Rakhshanipour, K. Shameli, ***Korean J. Chem. Eng.***, 31 (2014) 548.

[9] G. Shobha, V. Moses, S. Ananda, ***Int. J. Pharm. Sci. Invent.***, 3 (2014) 28.

[10] F. O. Kehinde, H. A. Aziz, ***International Journal of Innovative Research in Science, Engineering and Technology***, 3 (2014) 15310.

[11] J. Magano, J. R. Dunetz, ***Chemical Reviews,*** 111 (2011) 2177.

[12] R. Narayanan, M. A. El-Sayed, ***Journal of Physical Chemistry B,*** 109, (2005) 12663.

[13] (a) Y. Shiraishi, N. Toshima***, J. Mol. Catal. A***, 141 (1999) 187.
(b) Y. Shiraishi, N. Toshima, ***Colloid Surf. A,*** 169 (2000) 59.

[14] P.G.N. Mertens, M. Bulut, L.E.M. Gevers, I.F.J. Vankelecom, P.A. Jacobs, D.E. De Vos, ***Catal. Lett.,*** 102 (2005) 57.

[15] L. He, H. Liu, C. Xiao, Y. Kou, ***Green Chem.***, 10 (2008) 619.

[16] S. Eustis, M. A. El-Sayed, ***Chem. Soc. Rev.***, 35 (2006) 209.

[17] D. Guo, G. Xie, J. Luo, ***J. Phys. D. Appl. Phys.***, 47 (2014) 13001.

[18] S. Lee, S. U. -S. Choi, S. Li, J. A. Eastman, ***J. Heat Transfer***, 121 (1999) 280.

[19] Y. C. Cao, ***Science***, 297 (2002) 1536.

[20] A. Goel, R. Bhatt, Neetu, ***International Journal of Research in Chemistry and Environment***, 2 (2012) 210.

[21] Swern, D. ***"Organic peroxides", Interscience, Newyork,*** 2 (1971) 355.

[22] Sosnovsky, G. and Rawlison, D. J. ***"Organic peroxide", (ed. By Swern, D.), Interscience, Newyork***, 2 (1971) 269.

[23] M. G. Ram Reddy, B. Sethuram, and T. Navaneeth Rao, ***Ind. J. Chem.,*** 16A, (1978) 591.

Research Scholar Supervisor

Niharika Nagar

Dr. (Mrs.) Vijay Devra

(Associate Professor)

J.D.B. Govt. Girls College, Kota

BIBLIOGRAPHY

LIST OF PAPERS PUBLISHED and COMMUNICATED: 12

1. "Degradation and Biodegradability of Silver Nanoparticles Catalyzed Methyl Orange and Textile effluents – A Kinetic Study" **Niharika Nagar**, Vijay Devra, **Heliyon (Elsevier), (Communicated)**.

2. "Silver Nanoparticles: Green Synthesis and Their Catalytic Application in Kinetic Oxidation Study of Acid Orange 10" **Niharika Nagar**, Vijay Devra, **International Journal of Environmental Research (Springer), (Communicated)**.

3. "Experimental investigation on synthesis of copper nanoparticles via green route", **Niharika Nagar**, Vijay Devra, **Materials Chemistry and Physics (Elsevier),** 213 (2018), 44-51.

4. "Oxidative degradation of orange G by peroxomonosulfate in presence of biosynthesized copper nanoparticles- A kinetic study", **Niharika Nagar,** Vijay Devra, **Environmental Technology & Innovation,** 10 (2018), 281-289.

5. "Synthesis of copper nanoparticles and their catalytic activity in oxidation of threonine", **Niharika Nagar**, Vijay Devra, **Research Journal of Recent Sciences**, 7 (2018) 14-21.

6. "Application of copper nanoparticles in the degradation of Methyl Orange in aqueous medium", **Niharika Nagar**, Vijay Devra, **International Journal of Advance Reesearch in Science and Engineering**, 7 (Special Issu No. 2) (2018) 443-436.

7. "Activation of peroxodisulfate and peroxomonosulfate by green synthesized copper nanoparticles for methyl orange degradation: A kinetic study", **Niharika Nagar**, Vijay Devra, **Journal of Environmental Chemical Engineering (Elsevier),** 5 (2017) 5793-5800.

8. "Synthesis, characterization of copper nanoparticles and their catalytic application", **Niharika Nagar**, Shikha Jain, Vijay Devra, **International Conference on Innovative Research in Science, Technology and Management**, (2017) 540-548.

9. "Synthesis and charecterization of silver nanoparticles via green route", **Niharika Nagar,** Shikha Jain, Pranav Kachhawah, Vijay Devra, **Korean Journal of Chemical Engineering (Springer),** 33 (2016) 2990-2997.

10. "Synthesis and characterization of highly efficient copper nanoparticles and their catalytic application in oxidative kinetic study", Shikha Jain**,** **Niharika Nagar,** Vijay Devra, **Advances in Applied Science Research,** 6 (2015) 171-180.

11. "Synthesis, characterization and catalytic application of copper nanoparticles on oxidation of alanine in acid aqueous medium", Shikha Jain, **Niharika Nagar,** Vijay Devra, **International Journal of Current Engineering and Technology**, 5 (2015) 966-973.

12. "Correlation Analysis of Physico-Chemical Parameters and Water Quality of Chambal River: A case study of Kota City", Ankita Jain**,** Shikha Jain, **Niharika Nagar**, Pankaj Kachhawah, Vijay Devra, **International Journal of Engineering, Research and Technology,** (ETWQQM -2014 Conference Proceedings), (2014) 52-55.

Papers Presented and Participate In International and National Conferences/ Seminars/ Workshops.

1. **Niharika Nagar** participate in "Workshop on intellectual property right (IPR) and Indian patent system" organised by Rajasthan Technical University Kota and Department of Science & Technology (DST), Rajasthan Council of Science & Technology (RAJCOST) at Rajasthan Technical University Kota, during 28-29 September 2018.

2. "Environmental pollution" Vijay Devra, Gajala Tazwar, **Niharika Nagar**, Pranav Kachhawah, participate in "Rajasthan Hackathon 4.0" organised by Rajasthan State Pollution Control Board at Jaipur, during 19th-21th March 2018.
3. "Application of copper nanoparticles in the degradation of methyl orange in aqueous medium", **Niharika Nagar**, Vijay Devra. Paper Presentation in **"13th International Conference on Recent trends in engineering Science and Management"** at Vedant College of Engineering & Technology, Bundi (Rajasthan), during 21th to 22nd January, 2018.
4. **Niharika Nagar** participate in "Author Workshop jointly organized by Springer Nature and University of Kota" at University of Kota, Kota, during 2nd March 2017.
5. "Experimental investigation on green synthesis of metal nanoparticles and then catalytic application", **Niharika Nagar**, Gajala Tazwar, Vijay Devra, research Project participation in "**Anveshan Students' Research Convention (West Zone)**" at Nims University Rajasthan (Jaipur), during 7th-8th March 2017.
6. "Experimental investigation on green synthesis of metal nanoparticles and then catalytic application", **Niharika Nagar**, Gajala Tazwar, Vijay Devra, research Project presentation in "**University Student Research Convention**" at University of Kota, Kota, during 27th to 28th Feburary, 2017.
7. "Synthesis, characterization of copper Nanoparticles and their catalytic application", **Niharika Nagar**, Shikha Jain**,** Vijay Devra. Paper Presentation in **"International Conference on Innovative Research in Science, Technology and Management"** at Modi Institute of Management and Technology, Dadabari, Kota, Rajasthan during 22nd to 23rd January, 2017.
8. **Niharika Nagar** participate in "Workshop on patents, trade marks & copyrights" at Department of Science & Technology, Vigyan Kendra, Kota, during 19th March 2016.

9. "Experimental investigation on the synthesis of copper nanoparticles", **Niharika Nagar**, Shikha Jain, Vijay Devra, oral paper presentation in Indian Chemical Society "**52nd Annual Convention of Chemists 2015**" at JECRC University, Jaiur (Rajasthan), during 28th – 30th December 2015.

10. "Synthesis of Copper Nanoparticles and their catalytic application in oxidation reaction", Shikha Jain, Gajala Tazwar, **Niharika Nagar,** Vijay Devra. Paper Presentation in 5th International Conference on **"Advance Trends in Engineering, Technology and Research" (ICATETR-2015),** at Bal Krishna Institute of Technology, Ranpur, Kota (Rajasthan), during 23rd to 24th December, 2015.

11. **Niharika Nagar,** Vijay Devra. Oral Presentation of Research Work of Thesis in **Annual Research Seminar Organised by Centre For Excellence (Model College)** at J. D.B. Govt. Girls College, Kota on 30th January, 2015.

12. "Synthesis of Dispersed Copper Nanoparticles by Chemical Reduction Method", Shikha Jain, Ankita Jain, **Niharika Nagar,** Shanu Mathur, Vijay Devra. Paper Presentation in 3rd International Conference on **"Advance Trends in Engineering, Technology and Research" (ICATETR-2014),** at Bal Krishna Institute of Technology, Ranpur, Kota, Rajasthan during 22nd to 24th December, 2014.

13. "Correlation Analysis of Physico-Chemical Parameters and Water Quality of Chambal River: A case study of Kota City", Ankita Jain**,** Shikha Jain, **Niharika Nagar**, Pankaj Kachhawah, Vijay Devra. Participated in National Conference on **"Emerging Trends in water Quantity and Quality Management"** organised by Department of Chemistry and Department of Civil Engineering, Poornima University, Jaipur during 19th to 20th December, 2014.

Korean J. Chem. Eng., 33(10), 2990-2997 (2016)
DOI: 10.1007/s11814-016-0156-9

pISSN: 0256-1115
eISSN: 1975-7220

Synthesis and characterization of silver nanoparticles via green route

Niharika Nagar*, Shikha Jain*, Pranav Kachhawah, and Vijay Devra*,†**

*Department of Chemistry, J. D. B. Govt. P. G. Girls College, Kota, Rajasthan 324001, India
**Institute of Chemical Technology, Matunga, Mumbai, Maharashtra 400019, India
(*Received 18 February 2016 • accepted 8 June 2016*)

Abstract−The development of competent green chemistry methods for synthesis of metal nanoparticles has become a main focus of researchers. In this study we report the green synthesis of silver nanoparticles (AgNps) by reduction of silver nitrate, using leaf broth of *Azadirakta indica* (Neem). The plant leaf broth simultaneously acts as reducing agent as well as capping agent at 30 °C. The effect of different concentration of silver ions, percentage of leaf broth and temperature on morphology of dispersed silver nanoparticles was studied. The formation of silver nanoparticles in dispersion was monitored through the analysis of absorbance spectra by UV-Visible spectrophotometer at different stages during the process of synthesis. Scanning electron microscopy (SEM) and transmission electron microscopy (TEM) analysis revealed that silver nanoparticles were pure and monodispersed and size was ranging from 9-56 nm. Fourier transform infrared (FTIR) analysis indicates prominent bands of absorbance, which are responsible for reducing of Ag^+ ions and stabilization of obtained silver nanoparticles. Results confirmed this protocol as simple, rapid, cost effective, eco-friendly and alternative conventional physical/chemical methods.

Keywords: Silver Nitrate, *Azadirakta indica* (Neem), Silver Nanoparticles, Green Synthesis, Characterization

INTRODUCTION

Indian greeneries are the chief and cheap source of medicinal plants and plant products. Generally, medicinal plants have been extensively utilized in Ayurveda. Recently, such plants have been gaining importance due to their unique properties and their versatile applicability in various developing fields of research and development. Nanotechnology is presently one of the most dynamic disciplines of research in material science whereby plants and plant products are finding an imperative use in the synthesis of nanoparticles. Nanoscale materials and structures usually range from 1-100 nm and are an emerging area of nano-science and nanotechnology. Nobel metal nanoparticles such as gold, silver and platinum are well recognized to have significant applications in electronics, catalysis, environmental and biotechnology [1-3]. One such important number of noble metal nanoparticles is silver nanoparticles. Silver has long been recognized as having an inhibitory effect towards many bacterial strain and microorganism commonly present in medical and industrial processes [4]. The most widely used and known applications of silver and silver nanoparticles are in medical and pharmaceutical products and are hence directly encountered by the human system [5,6]. Earlier, the antifungal properties of silver were well incorporated in the field of medical science. Although the medicinal importance of innumerable plants was known, the plant-mediated silver nano-product is a relatively newer concept. These nano-products are unique not only in their treatment methodology but also due to their uniqueness in particle size, physical, chemical, biochemical properties and broad range of application as well. The current emerging field of nanotechnology is at the primary stage of development due to lack of implementation on large industrial scale. Hence, there is a need to design an economic, nontoxic and eco-friendly route of synthesis of silver nanoparticles in order to meet its growing demand in diverse fields.

Silver nanoparticles can be synthesized through different methods, such as chemical [7], electrochemical [8], radiation [9] and photochemical [10]. The chemical approach is the most popular method for the synthesis of nanoparticles. However, some chemical methods cannot avoid the use of toxic chemicals in the synthesis protocol. Since silver nanoparticles are widely applied to human contact areas, there is growing need to develop an environmentally friendly process of nanoparticle synthesis that does not use toxic chemicals. Biosynthesis of nanoparticles using microorganism [11-13], enzyme [14] and plant extract [15] has been suggested as a possible eco-friendly alternative to chemical and physical methods. Existing study also reports successful synthesis of silver nanoparticles through a green route where the reducing and capping agent selected was the leaf extract of Aloe Vera [16], *Acalypha indica* [17], *Garcinia mangostana* [18].

We have developed a rapid, eco-friendly and convenient green method for the synthesis of silver nanoparticles from silver nitrate using leaf extract of Indian medicinal plant, namely *Azadiracta indica*. *Azadiracta indica*, commonly known as neem, belongs to the meliaceae family and has been well known in India and its neighboring countries for more than 200 years as one of the most versatile medicinal plants having a wide spectrum of biological activity [19]. In the present study, the effects of reaction conditions such as reaction temperature, leaf broth percentage and silver nitrate concentration on the dispersion of aqueous silver nanoparticles

†To whom correspondence should be addressed.
E-mail: v_devra1@rediffmail.com

were investigated, and synthesized silver nanoparticles were characterized by different instrumental techniques.

EXPERIMENTAL

1. Materials

Materials used for the synthesis of silver nanoparticles are silver nitrate (E. Merck) and neem (*Azadirachta indica*) leaf broth. Deionized water is used for preparation of solutions.

2. Preparation of Leaf Broth

The plant *Azadirakta indica* (neem) was selected from Kota (Rajasthan) India, on the basis of cost effectiveness, ease of availability and medicinal property. Fresh and healthy leaves were collected and rinsed thoroughly first with tap water followed by deionized water to remove all the dust and unwanted particles, cut into small pieces and dried at room temperature. Ten gm of these finely incised leaves was transferred into 250 ml beaker containing 100 ml deionized water and stirred on magnetic stirrer at 80 °C for 20 minutes. The extract was then filtered twice through Whatman filter paper, then refrigerated (4 °C) in Erlenmeyer flasks for further experiments. In each and every step of the experiment, sterile conditions were maintained for the effectiveness and accuracy in results.

3. Synthesis of Silver Nanoparticles

Aqueous solution 1mM of silver nitrate ($AgNO_3$) was prepared in 250 ml Erlenmeyer flask and 10% leaf broth was added for reduction of Ag^+ ions. The complete mixture was kept on magnetic stirring at 30 °C. Time and color change were recorded along with periodic sampling and scanning by UV-Visible (UV-Vis) spectrophotometer. Suitable controls were maintained all through the conditions of experiments. Complete reduction of Ag^+ ions was confirmed by the change in color from light or faint to yellowish colloidal brown. The colloidal solution was kept aside for 24 hour for complete bio-reduction and saturation denoted by UV-Vis spectrophotometric scanning. The solution was sealed and stored properly for further use. The formation of silver nanoparticles was further confirmed by different spectrophotometric analysis. The effects of different concentration of $AgNO_3$ solution, percentage of leaf

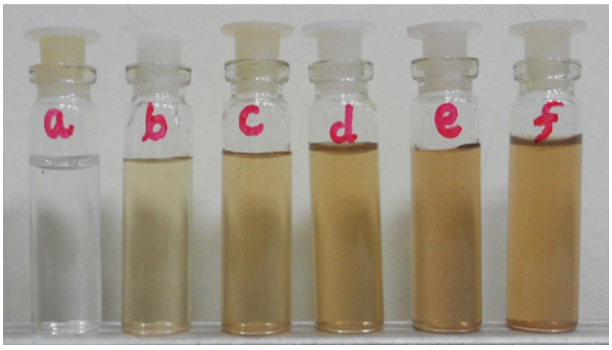

Fig. 1. Observation of color change during synthesis of silver nanoparticles at different time intervals: (a) 0 min (b) 30 min (c) 60 min (d) 90 min (e) 120 min (f) 24 hour.

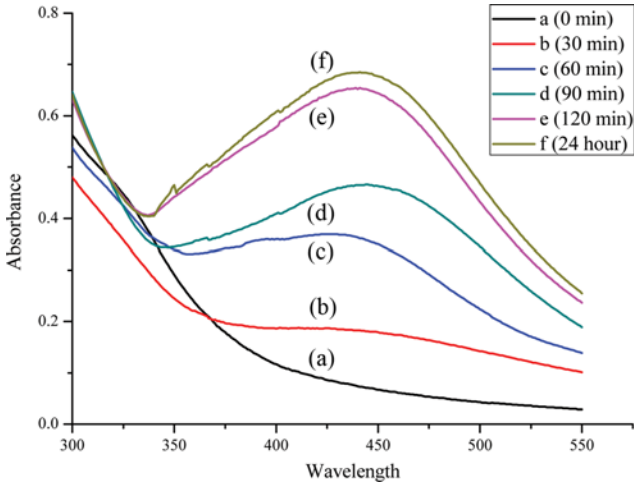

Fig. 2. U.V. spectra recorded as a function of reaction at different wavelength versus absorbance during synthesis of silver nanoparticles at different time intervals.

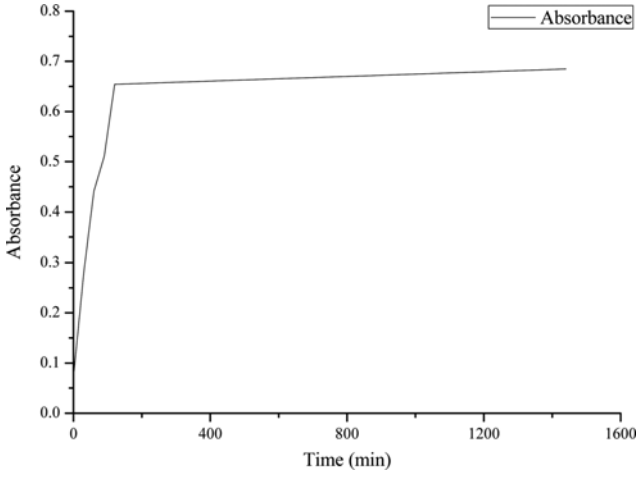

Fig. 3. Respective plot of absorbance at λ_{max}=433 nm versus time.

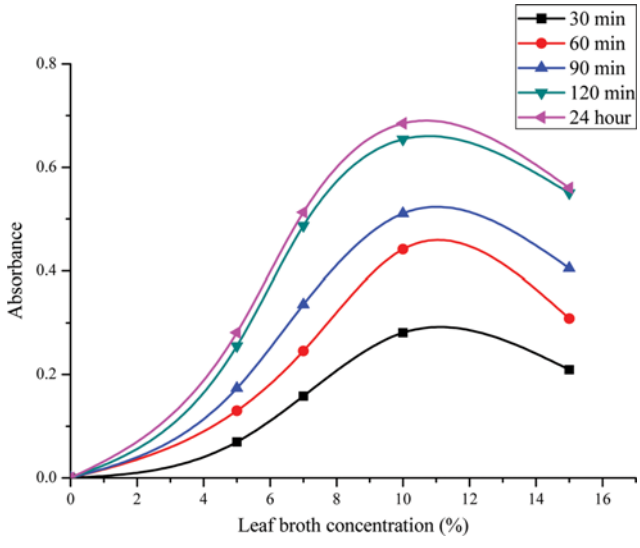

Fig. 4. Time course of silver nanoparticles synthesis with different leaf broth concentration (5% to 15%), $AgNO_3$=1 mM, temperature=30 °C.

broth and temperature on the synthesis rate and morphology of the synthesised nanoparticles were also investigated.

4. U.V. Visible Spectra Analysis

Samples of the suspension were collected periodically to monitor the completion of bio-reduction of $AgNO_3$ in aqueous solution, followed by UV-Vis spectra recorded as function of time of reaction on a spectrophotometer (UV 3000$^+$ LABINDIA) having resolution of 1 nm.

5. FTIR Analysis

For Fourier transform infrared (FTIR) spectroscopy measurements, dry powder of the nanoparticles was obtained in the following manner: After 24 hour of the reaction, synthesized dispersion of aqueous silver nanoparticles was centrifuged at 3,500 rpm (Remi C-854/6 Laboratory Centrifuge with 6×15 swings out Head) for 15 minutes, following then the pellets were re-dispersed in deionized water. The process of centrifugation and re-dispersion by deionized water was repeated three times to ensure better separation of free entities from the metal nanoparticles. The purified pellets were then dried and powder subjected with potassium bromide (KBr) to FTIR spectroscopy measurement. The spectrum was recorded using FTIR model (ALPHA-T Bruker, Germany) transmittance mode operating at a resolution of 4 cm^{-1}.

6. SEM Analysis

Scanning electron microscopy (SEM) analysis of the neem leaf broth reduced silver nanoparticles was carried out on films of the solution drop-coated onto glass substrates on SEM (Model-Nova Nano FE-SEM 450 (FEI)) instrument. The details regarding applied voltage, magnification used and size of the contents of the images

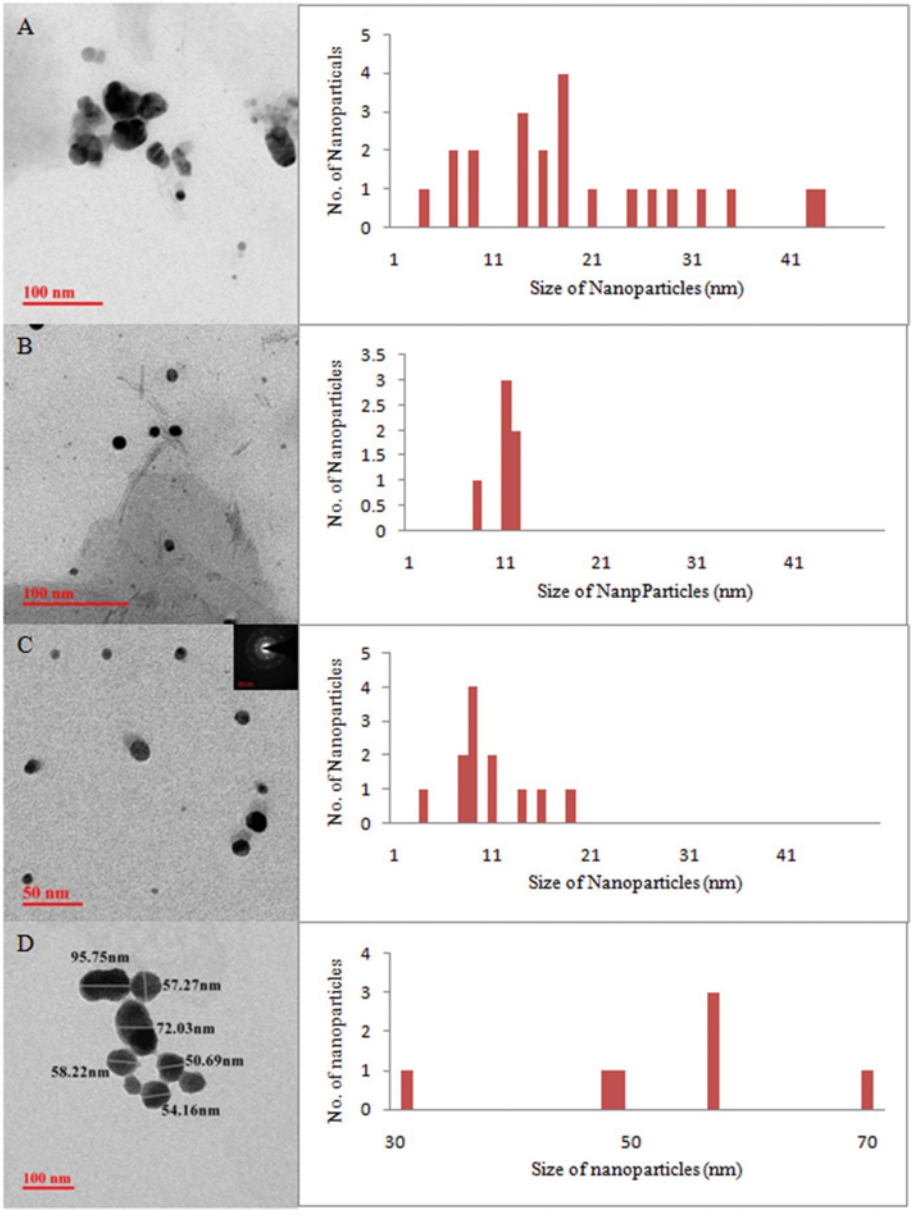

Fig. 5. TEM images with histogram of synthesized silver nanoparticles at different percentage of leaf broth (A) 5%, d=20 nm, (B) 7%, d=11 nm, (C) 10%, d=9 nm, (D) 15%, d=56 nm.

were implanted on the images itself.

7. TEM Analysis

Transmission electron microscopy (TEM) was used to study the morphology of the silver nanoparticles. Samples for TEM analysis were prepared by drop-coating silver nanoparticles solution onto carbon coated copper grid. The film on the TEM grid was allowed to stand for 2 minutes, following then the extra solution was removed using a blotting paper and the grid allowed to dry prior to measurement on TEM (Model-Tecnai G^2 20 (FEI) S-Twin) instrument. Additionally, the presence of metal in the sample was analyzed by energy dispersive spectroscopy (EDS) technique.

RESULTS AND DISCUSSION

1. Effect of Leaf Broth as Reducing Agent

Synthesis of metal nanoparticles by reduction of the aqueous metal ions during reaction to the broth of *Azadirakta indica* leaves was studied by UV-Vis spectroscopy. Silver nanoparticles appear yellowish brown in aqueous medium as a result of surface plasma resonance [17]. As the leaf broth was added to silver nitrate solution, the color of the solution changed from light or faint to yellowish colloidal brown, indicating silver nanoparticles formation (Fig. 1). Similar color changes have also been observed in previous studies [15,20-23]. The UV-Vis spectra were recorded after different time intervals from the initiation of reaction as shown in Fig. 2.

It is observed that absorption spectra of synthesized silver nanoparticles show the maxima at wavelength 433 nm. The reduction of the metal ions occurs fairly rapidly within 30 min addition of neem leaf broth to metal ion solution and steadily increases in intensity as a function of time of reaction without any shift in the peak wavelength. After 24 hours there are no increases in the absorbance due to the depletion of the silver ions (Fig. 3). In earlier studies, the synthesis of silver nanoparticles using bacteria [24], fungi [25] required time for completion of reaction as 24 to 120 hours and was thus rather slow.

The effect of different concentration of leaf broth on synthesis rate and particle size of synthesized nanoparticles was also investigated. Fig. 4 shows the time course of silver nanoparticle formation with different neem leaf broth percentage (5% to 15%) and 1 mM $AgNO_3$ at 30 °C. When low percentage (5%) of leaf broth was used, a weak absorption peak at 433 nm was observed, indicating that due to insufficient reduction relatively low concentration of silver nanoparticles were produced. It is well known that UV-Vis absorption peak gives information on the degree of dispersion of silver nanoparticles [26]. As the the percentage of leaf broth increases up to 10%, the intensity of absorption peak at 433 nm increases after that absorption peak becomes lower, indicating the aggregation of silver nanoparticles at high percentage of leaf broth. However, the maximum absorption peak was obtained at 10% neem leaf broth, suggesting the optimum percentage of leaf broth for synthesis of silver nanoparticles.

It has been reported that biosynthesized silver nanoparticles are surrounded by a thin layer of some capping organic material of plant leaf broth, and are thus stable in solution up to four weeks after synthesis [15,26]. In this study TEM images (Fig. 5) also indicate that synthesized silver nanoparticles are surrounded by a thin layer of some capping material and are stable in solution during four weeks. The histogram of synthesized silver nanoparticles with size distribution is also presented in Fig. 5 at the different percentage of leaf broth. The histogram reveals an increase in leaf broth percentage up to 10%; the particle size decreases from 20 to 9 nm after that size of nanoparticles increases (56 nm) with increases in percentage of leaf broth (15%), suggesting that too many reducing agents cause aggregation of the synthesized silver particles. It is

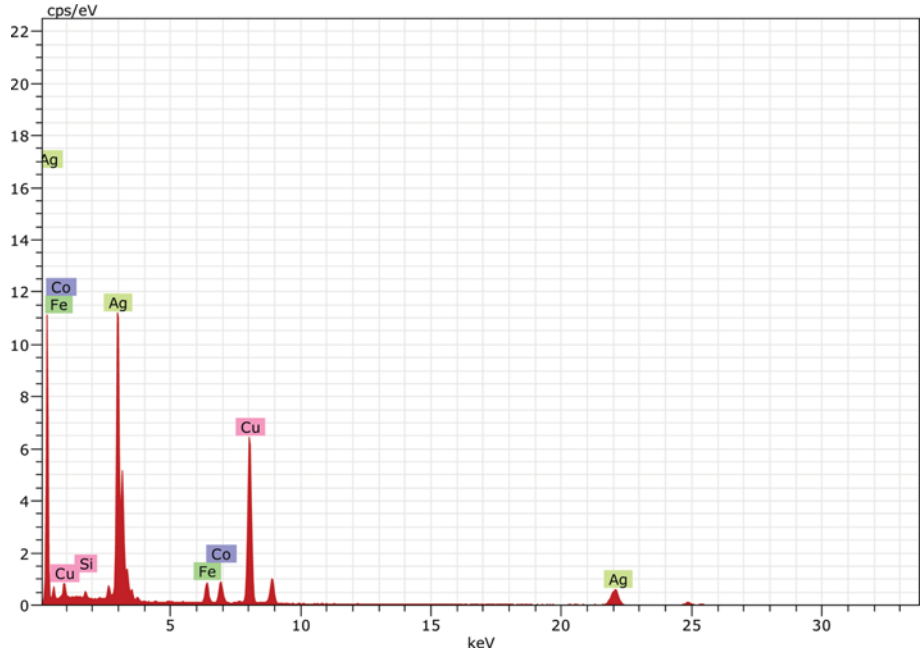

Fig. 6. Spot profile EDS spectra of synthesized silver nanoparticles.

possible due to the interaction between capping molecules bound to the surface of particles and secondary reduction process on the surface of the performed nuclei. Similar aggregation of nanoparticles was earlier reported by Vanaja et al. [27] using the extract of *Morindat inctoria* in the reduction of Ag^+ ions. The results are well consistent with UV-Vis spectra in Fig. 4. The inset of (Fig. 5) shows the selected area electron diffraction (SAED) pattern recorded of the silver nanoparticles; the ring-like diffraction indicates that the particles are crystalline. Similar SAED pattern was obtained with silver nanoparticles synthesis using *Diopyras kaki* leaf broth by Song [28]. Elemental analysis of silver was measured by energy-dispersive X-ray spectroscopy (EDS). EDS spectra reveal strong signals in the silver region 3 Kev and confirm the formation of nano silver in its elemental nature (Fig. 6). This signal appears due to the excitation of surface plasma resonance (SPR) of silver nanoparticles.

2. Effect of Initial Concentration of $AgNO_3$

The effect of initial concentration of $AgNO_3$ on the formation of silver nanoparticles was studied between 0.5 to 2 mM concentrations of silver nitrate. There are two stages when silver nanoparticles formed in the solution: the first stage to generate silver nuclei and second stage is the growth of silver nuclei [29], so it is important to control the synthesis process that silver nuclei must generate faster and grow slower, which requires optimum concentration of $AgNO_3$. Fig. 7 shows the UV-Vis. spectra recorded as a function of reaction at different concentration of $AgNO_3$ versus absor-

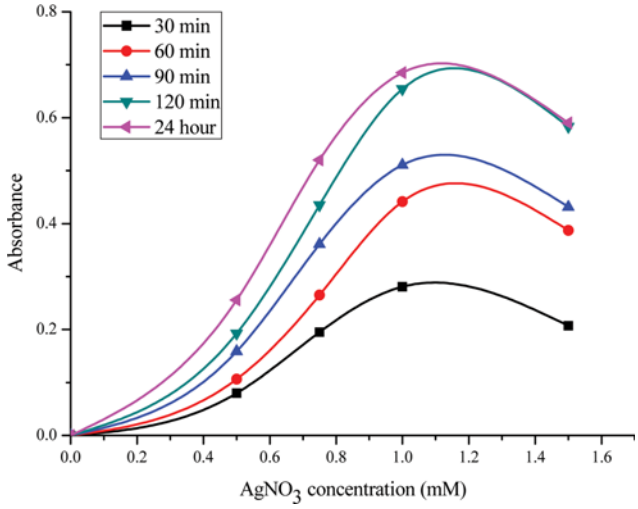

Fig. 7. Time course of silver nanoparticles synthesis with different initial concentration of $AgNO_3$ (0.5 to 2 mM), leaf broth=10%, temperature=30 °C.

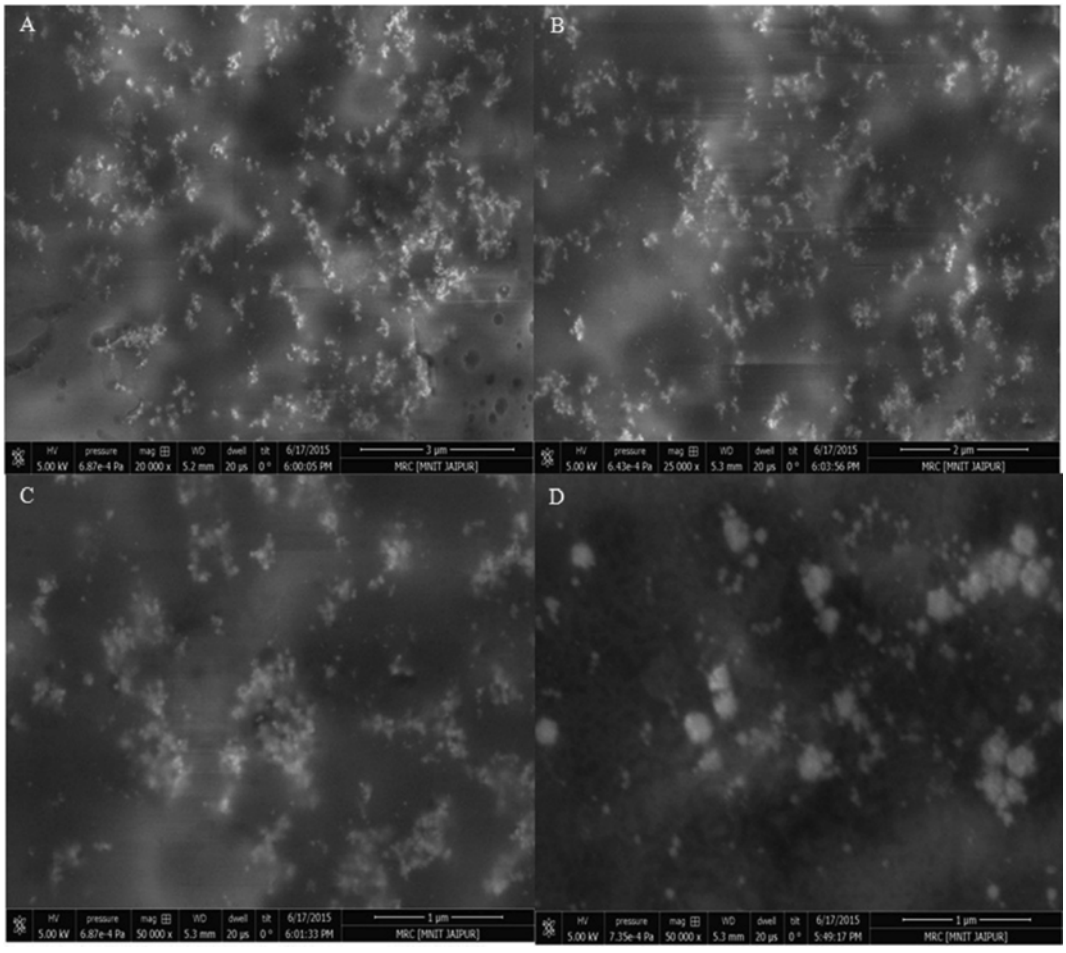

Fig. 8. SEM image of synthesized silver nanoparticles at different initial $AgNO_3$ concentration (A) 0.5 mM (B) 0.75 mM (C) 1 mM (D) 2 mM.

bance during synthesis of silver nanoparticles at different time interval. It was observed that the highest absorbance was obtained when the concentration of $AgNO_3$ was 1 mM. This confirmed that the synthesis process can be affected by initial concentration of $AgNO_3$ and suggests that the reaction rate increases with the increasing amount of silver nuclei rises and smaller particle size are obtained, correspondingly. The SEM images of synthesized silver nanoparticles at different initial concentration of $AgNO_3$ are shown in Fig. 8. The results indicate that an excess number of nuclei will be generated when the Ag^+ ions concentration is too high, i.e., 2 mM, thus resulting in the agglomeration of the nuclei and growing particle size. So the optimal reaction condition for synthesis of monodispersed and average size 9 nm silver nanoparticles is 1 mM $AgNO_3$ concentration, 10% leaf broth and 30 °C temperature.

3. Effect of Temperature

Fig. 9 shows the time course of silver nanoparticle formation with different reaction temperature (25 °C to 40 °C) at concentration of 1 mM $AgNO_3$ and 10% neem leaf broth. As the reaction temperature increases, the synthesis rate of silver nanoparticles also increases. Song [28] reported the increase of reduction rate with increasing the reaction temperature of silver nanoparticles synthesis with *Diopyros kaki* leaf broth. The TEM images of synthesized nanoparticles at different temperature are shown in Fig. 10. When reaction temperature increased from 25 °C to 30 °C, the particle size decreased from 20 to 9 nm, but the gained size grows with increase after a certain temperature, which is because at high temperature (40 °C) the nanoparticles were agglomerated, while at 30 °C were well dis-

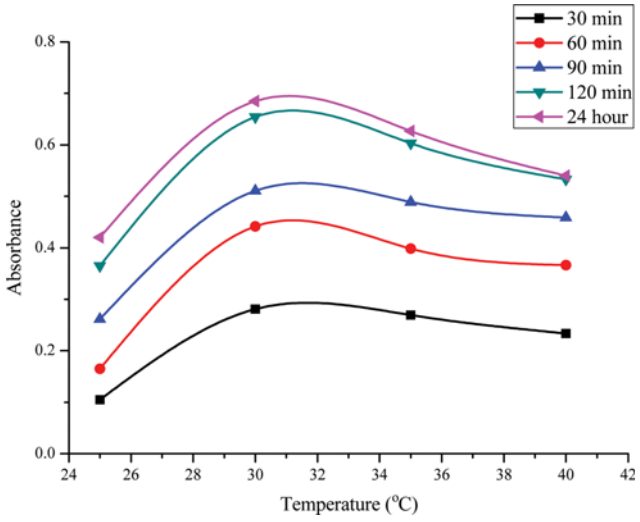

Fig. 9. Time course of silver nanoparticles synthesis with different reaction temperature (25-40 °C), $AgNO_3$ (1 mM), leaf broth= 10%.

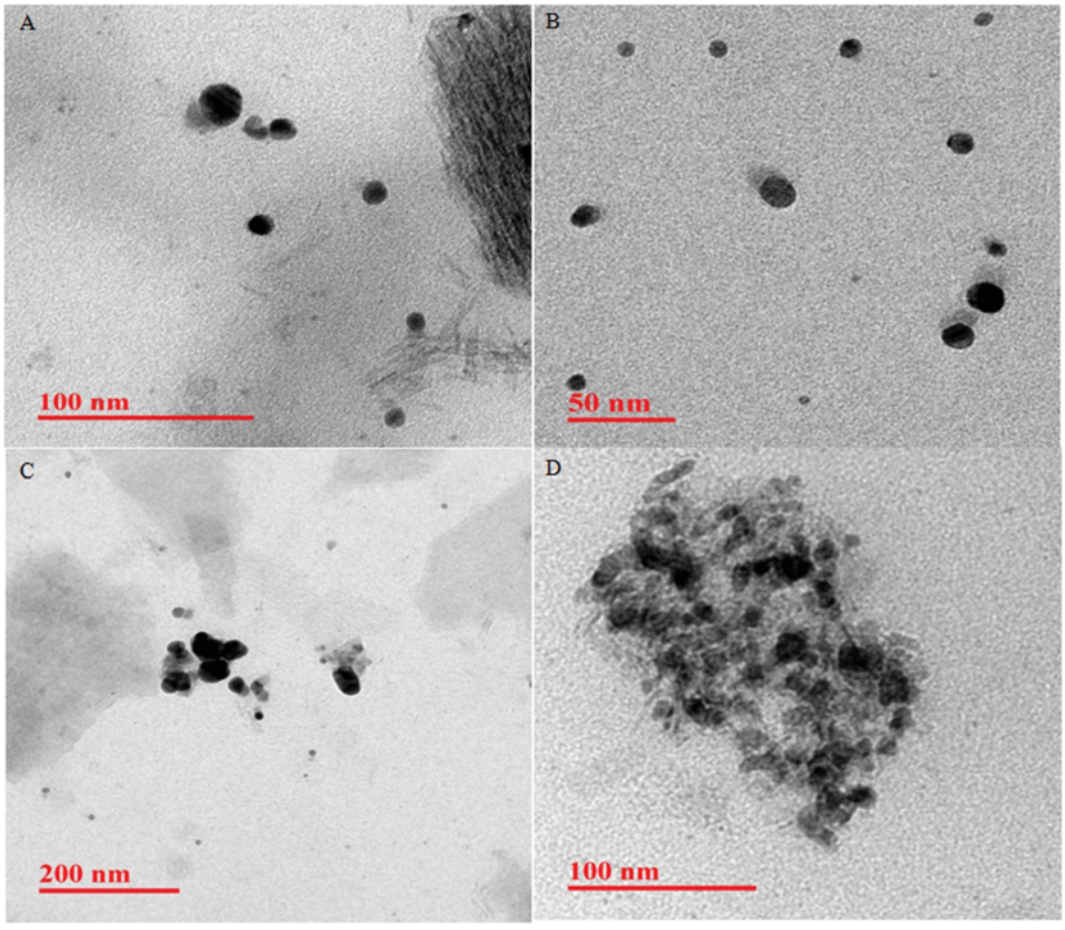

Fig. 10. TEM images of synthesized silver nanoparticles at different reaction temperature (A) 25 °C, (B) 30 °C, (C) 35 °C, (D) 40 °C.

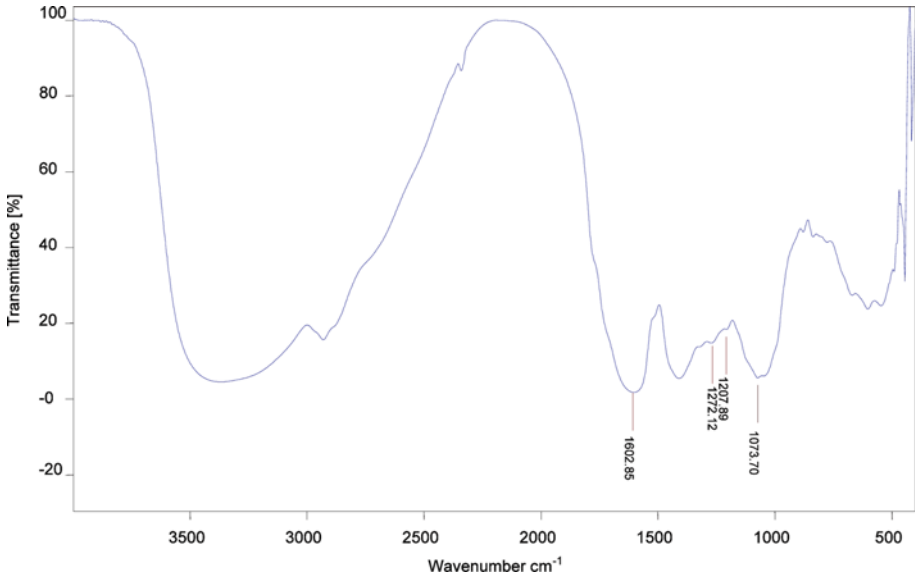

Fig. 11. FTIR Spectra of pure leaf extract of *Azadiracta indica*.

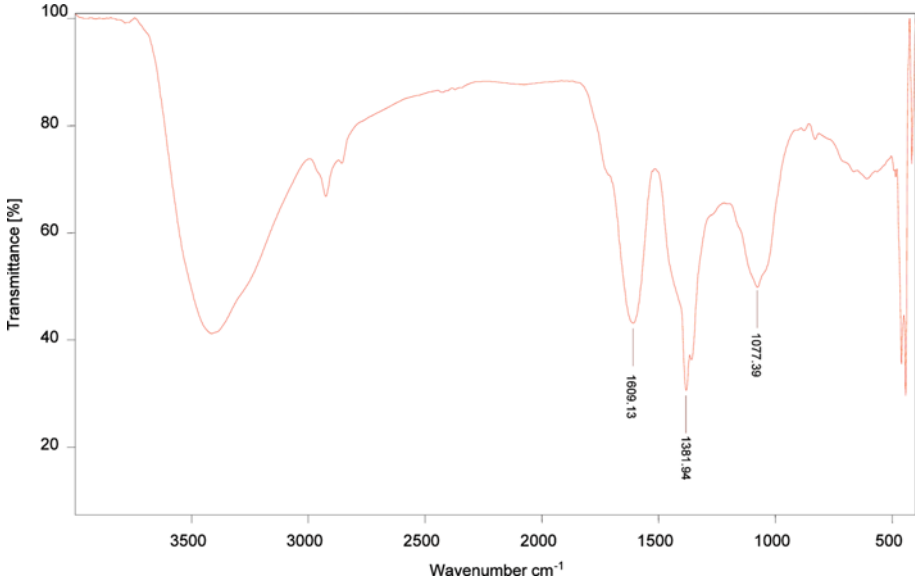

Fig. 12. FTIR Spectra of green synthesized silver nanoparticles.

persed which average size about 9 nm. Basically, the reduction of Ag^+ ions was increased by increasing the reaction temperature. Therefore, the synthesis rate was too high to control particle size at high temperature. When reducing agent (Neem extract) was added in silver nitrate solution at 40 °C, the rate of growth and agglomeration as well as nucleation of silver nanoparticles accelerated almost coincidently, and the resultant higher averaged size of silver nanoparticles were agglomerated. Therefore, a moderate temperature of 30 °C should be selected for synthesis of silver nanoparticles with appropriate controlling on size.

FTIR measurements were carried out to identify the potential functional groups of the bio-molecules in the leaf extract of *Azadirakta indica* (neem), which are responsible for the reduction of silver ions into silver nanoparticles. From comparison with FTIR of leaf extract of pure neem (Fig. 11) and green synthesized silver nanoparticles (Fig. 12), the observed peaks at 1,609 cm^{-1}, 1,381 cm^{-1}, 1,077 cm^{-1} in Fig. 12 are more characteristic of flavanones and terpenoids that are abundant in neem plant broth [30,31]. The peak observed at 1,609 cm^{-1} indicating C=C groups, 1,381 cm^{-1} occurring to the germinal methyls and 1,077 cm^{-1} shows ether linkages, suggesting the presence of flavanones or terpenoids adsorbed on the surface of silver nanoparticles. These reducing sugars could be responsible for the reduction of silver ions into silver nanoparticles.

Currently, the mechanism of biological nanoparticle synthesis is not fully understood. Terpenoids are believed to be the surface active molecules stabilizing the nanoparticles, and reduction of the

metal ions is possible facilitated by reducing sugars or terpenoids present in neem leaf extract as reported in [15].

CONCLUSION

The presented green synthesis shows that environmentally benign and renewable source of *Azadirakta indica* can be used as an efficient reducing agent as well as capping agent. This biological reduction of silver ions would be a boon for the development of clean, non-toxic, environmentally acceptable green approach to produce silver nanoparticles. The process indicates that the initial concentration of reactants and reaction temperature has a remarkable effect on synthesis and particle size of synthesized silver nanoparticles. The synthesized nanoparticles have good stability, thus have a potential for use in biomedical applications and will play an important role in the field of catalysis.

ACKNOWLEDGEMENT

This work was supported in part by Department of Science and Technology sponsored FIST laboratory of our institution for experimental work and University Grants Commission for financial support as JRF.

REFERENCES

1. I. Hussain, M. Brust, A. J. Papworth and A. I. Cooper, *Langmuir*, **19**, 4831 (2003).
2. V. K. Sharma, R. A.Yngard and Y. Lin, *Adv. Colloid Interface Sci.*, **145**, 83 (2009).
3. M. Okuda, Y. Kobayashi, K. Suzuki, K. Sonoda, T. Kondoh, A. Wagawa, A. Kondo and H. Yoshimura, *Nano Lett.*, **5**, 991 (2005).
4. H. Jiang, S. Manolache, A. C. L. Wong and F. S. Denes, *J. Appl. Polym. Sci.*, **93**, 1411 (2004).
5. R. Bhattacharya and P. Murkherjee, *Adv. Drug Deliv. Rev.*, **60**, 1289 (2008).
6. D. R. Bhumkar, H. M. Joshi, M. Sastry and V. B. Pokharkar, *Pharm. Res.*, **24**, 1415 (2007).
7. Y. Sun, Y. Yin, B. T. Mayers, T. Herricks and Y. Xia, *Chem. Mater.*, **14**, 4736 (2002).
8. B. Yim, H. Ma, S. Wang and S. Chen, *J. Phys. Chem. B.*, **107**, 8898 (2003).
9. N. M. Dimitrijevic, D. M. Bartels, C. D. Jonah, K. Takahashi and T. Rajh, *J. Phys. Chem. B.*, **105**, 954 (2001).
10. A. Callegari, D. Tonti and M. Chergui, *Nano Lett.*, **3**, 1565 (2003).
11. T. Klaus, R. Joerger, E. Olsson and C. G. Granqvist, *Proc. Natl. Acad. Sci. U.S.A.*, **96**, 13611 (1999).
12. Y. Konishi, K. Ohno, N. Saitoh, T. Nomura, S. Nagamine, H. Hishida, Y. Takahashi and T. Uruga, *J. Biotechnol.*, **128**, 648 (2007).
13. B. Nair and T. Pradeep, *Cryst. Growth Des.*, **2**, 293 (2002).
14. I. Willner, R. Baron and B. Willner, *Adv. Mater.*, **18**, 1109 (2006).
15. S. S. Shankar, A. Rai, A. Ahmad and M. Sastry, *J. Colloid Interface Sci.*, **275**, 496 (2004).
16. S. P. Chandran, M. Chaudhary, R. Pasricha, A. Ahmad and M. Sastry, *Biotechnol. Prog.*, **22**, 577 (2006).
17. C. Krishnaraj, E. G. Jagan, S. Rajasekar, P. Selvakumar, P. T. Kalaichelvan and N. Mohan, *Colloids Surf., B: Bio. Interfaces*, **76**, 50 (2010).
18. R. Veerasamy, T. Z. Xin, S. Gunasagaran, T. F. W. Xiang, E. F. C. Yang, N. Jeyakumar and S. A. Dhanaraj, *J. Saudi. Chem. Soc.*, **15**, 113 (2010).
19. O. Koul, M. B. Isman and C. M. Ketkar, *Can. J. Bot.*, **68**, 1 (1990).
20. V. K. Shukla, S. Pandey and A. C. Pandey, Green synthesis of silver nanoparticles using neem leaf (*Azadirachta indica*) extract. (2010) In: Proceedings of International Conference on Advanced Nanomaterials and Nanotechnology, ICANN 2009, Guwahati, Assam (India). 9.11 December 2009.
21. N. Namratha and P. V. Monica, *Asian J. Pharm. Tech.*, **3**, 170 (2013).
22. A. Lalitha, R. Subbaiya and P. Ponmurugan, *Int. J. Curr. Microbiol. Appl. Sci.*, **2**, 228 (2013).
23. P. Banerjee, M. Satapathy, A. Mukhopahayay and P. Das, *Bioresour. Bioprocessing*, **1**, 1 (2014).
24. T. Klaus, R. Joerger, E. Olsson and C. G. Granqvist, *Trends Biotechnol.*, **19**, 15 (2001).
25. P. Mukherjee, A. Ahmad, D. Mandal, S. Senapati, S. R. Sainkar, M. I. Khan, R. Parischa, P. V. Ajayakumar, M. Alam, R. Kumar and M. Sastry, *Nano Lett.*, **1**, 515 (2001).
26. K. D. Kim, D. N. Han and H. T. Kim, *Chem. Eng. J.*, **104**, 55 (2004).
27. M. Vanaja, K. Paulkumar, M. Baburaja, S. Rajeshkumar, G. Gnanajobitha, C. Malarkodi, M. Sivakavinesan and G. Annadurai, *Bioinorg. Chem. Appl.*, **8**, Article ID 742346 (2014).
28. J. Y. Song and B. S. Kim, *Bioprocess. Biosyst. Eng.*, **32**, 79 (2009).
29. J. I. Hussain, S. Kumar, A. A. Hashmi and Z. Khan, *Adv. Mat. Lett.*, **2**, 188 (2011).
30. H. S. Garg and D. S. Bhakuni, *Hand book of African medicinal plants*, CRC Press, London (1984).
31. B. S. Siddiqui, F. Afshan, G. S. Faizi, S. N. H. Naqvi and R. M. Tariq, *Phytochemistry*, **53**, 371 (2000).

Journal of Environmental Chemical Engineering 5 (2017) 5793–5800

Contents lists available at ScienceDirect

Journal of Environmental Chemical Engineering

journal homepage: www.elsevier.com/locate/jece

Activation of peroxodisulfate and peroxomonosulfate by green synthesized copper nanoparticles for Methyl Orange degradation: A kinetic study

Niharika Nagar, Vijay Devra*

Department Of Chemistry, J.D.B. Government Girls College, Kota, Rajasthan, 324001, India

ARTICLE INFO

Keywords:
Copper nanoparticle
Neem (*Azadirachta Indica*) leaves broth
Methyl Orange degradation
Sulfate radicals
Reaction parameters

ABSTRACT

The study was primarily focused on novel, simple and environmentally benign technique for the synthesis of copper nanoparticles (CuNPs) and comparing the catalytic activity in CuNPs/Peroxodisulfate (PDS) and CuNPs/Peroxomonosulfate (PMS) process for degradation of Methyl Orange (MO). Green synthesized CuNPs were characterized by different instrumental techniques and results indicate synthesized NPs are in crystalline nature and cubical shape with 48 nm size. The increasing concentration of nanocatalyst, peroxosulfates, Dye, initial pH and high temperature rapidly promoted the degradation kinetics of MO. The degradation of MO in CuNPs/Peroxosulfates system is modeled as pseudo-first order kinetics and activation parameters were also determined. The maximum degradation efficiency of MO reached 92% in 60 min for CuNPs/PDS system and 98% in 30 min for CuNPs/PMS system at optimum reaction condition. Sulfate radicals (SRs) ($SO_4\cdot^-$) were identified as oxidative species using specific alcohols. Furthermore, LC–MS analysis and results of UV–vis spectral changes were used to determine the structure of intermediates arising from MO by CuNPs/Peroxosulfates degradation. The degradation products revealed that the degradation mechanism proceeds through an oxidative cleavage of the azo linkage in the formation of SO_3^- and NO_3^- as end products. Employing CuNPs to enhance oxidation capacity of peroxosulfates for degradation of MO is a novel, efficient, promising and environmental-friendly method since it does not require costly reagents.

1. Introduction

Azo dyes, which contribute to about 70% of all applied dyes, are difficult degraded by conventional treatment methods, due to their complex structure and the stability. The common techniques available for dye effluents such as adsorption and flocculation are not efficient methods because they result in solid waste, thus creating other environmental problems requires further treatment [1]. The advanced oxidation technology is the most effective chemical oxidation method and currently gaining significant application in water treatment process [2]. Driven by the need and seeking for a process, that introduces strong oxidants than hydroxyl radicles (OH·), ozone, Fenton based process [3], this works explores the generation of very strong oxidizing species (sulfate radicals) through the transition metal mediated activation of peroxosulfates [4]. The process is the modification of Fenton reagent since an oxidant is coupled with a transition metal in a similar manner. Although earlier study reports [5] that sulfate radicals are not universally more efficient than hydroxyl in degrading organic compounds. Either way, however, the fact that the sulfate contains compounds were proven the most effective oxidants to proves that sulfate radicals, generated by heat [6], ultrasound [7] and transition metal [8] are very powerful oxidizing species. Since transition metal coupled oxidative process show greater removal efficiency for the degradation of carcinogenic contaminants into lower molecular weight and lower toxicity. The formed reactive species sulfate radicals depend on the catalytic activity and oxidation state of transition metals. The copper catalyzed decomposition follows a sulfate radical based mechanism, the same was suggested when nickel, cobalt, iron, ruthenium and silver transition metals were used [8–11].

Nanosized metal nanoparticles are attracting the attention of present science field nanometer scale leads to particular intrinsic properties for the materials that render them very promising for application in catalysis. The application of transition metal NPs as a catalyst for hydrogenation [12], hydrosilation [13] as well as redox [14] and other electron transfer process [15] were reported. Among the metal nanoparticles, copper nanoparticles are very attractive due to their excellent physical and chemical properties and low cost of synthesis, have been of great interest. Copper nanoparticles have wide applications in heat transfer system [16], anti-microbial materials [17], super strong materials [18] and catalysis [19].

* Corresponding author.
E-mail addresses: nnniharikanagar@gmail.com (N. Nagar), v_devra1@rediffmail.com (V. Devra).

http://dx.doi.org/10.1016/j.jece.2017.11.014
Received 30 August 2017; Received in revised form 1 November 2017; Accepted 3 November 2017
Available online 04 November 2017

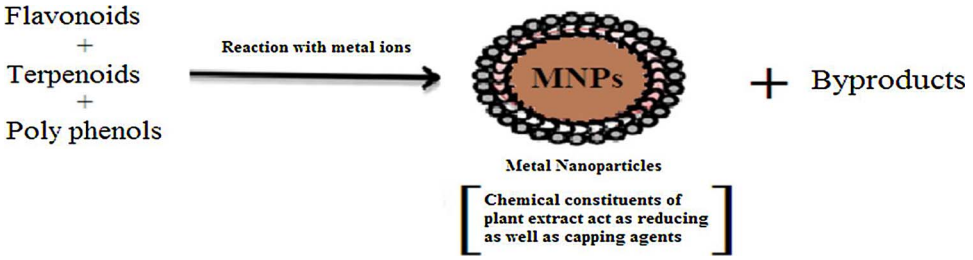

Fig. 1. Possible constituents of plant extract responsible for the bioreduction of metal ions.

The need of biosynthesis of nanoparticles gained importance than physical and chemical methods [20–23] because they are costly and hazardous. Therefore, in the search for the cheaper method for nanoparticle bio-synthesis, researchers used plant extract and microorganism for synthesis [24–27]. Existing literature reports successful synthesis of CuNPs through a green route which includes the *T. arjuna* bark extract [28], *Capparious zeylanica* leaf broth [29], *Ocimum sanctum* leaf broth [30,31], *Syzygium aromaticum* (cloves) aqueous extract [32] and *vitis vinifera* leaf broth [33] as well as various other plant extract used as reducing and capping agent. Fig. 1 shows the possible constituents of plant extract responsible for the bioreduction of metal ions, their growth, and stabilization [34,35].

Characteristics of nanoparticles influenced by the source of the plant extract [36] because of each plant extract contain unique concentration and combinations of organic reducing agents [37]. Pure metallic CuNPs in an aqueous phase still challenge for the researcher. Furthermore, it is of interest to obtain monodispersed CuNPs by a simple and green route, very less known about the size dependent performance of CuNPs as a suitable catalyst. Here, we have developed a rapid, eco-friendly and convenient green route for the synthesis of CuNPs from copper chloride using leaf broth of Indian medicinal plant namely *A. indica* (Neem). It belongs to Meliaceae family and found abundantly in India and in nearby subcontinents. The study also highlights the synthesis of CuNPs with various experimental parameters and corresponding morphology changes of CuNPs. A textile azo dye, Methyl Orange (MO) was chosen as the target compound and many studies also report to employ MO as a model mainly because it is a widely used dye and resistant to degradation by conventional methods [38,39]. As far as we are concerned, nano copper based catalyst/PDS and catalyst/PMS system for degradation of MO was still uncovered in the environmental field. Therefore the main objectives of this article are – (i) To synthesize the stable CuNPs by simple green route and low cost of this technology will be of great attraction for countering waterborne disease and public health. ii) To determine the effect of the different concentration of CuNPs, PDS, PMS, and pH etc. on the degradation of MO. iii) To propose the degradation pathway of MO in CuNPs/Peroxosulfates system. iv) The performance discrepancy of CuNPs/PDS and CuNPs/PMS system was compared and discussed.

2. Experimental

2.1. Chemicals and materials

Copper chloride dihydrate ($CuCl_2{\cdot}2H_2O$) (E. Merck), Potassium Peroxodisulfate ($K_2S_2O_8$) (Sigma-Aldrich), Peroxomonosulfate ($2KHSO_5{\cdot}KHSO_4{\cdot}K_2SO_4$ 95%) (Sigma-Aldrich), Methyl Orange (MO) and other reagents were of analytical grade. Neem (*Azadirachta Indica*) leaves were collected from Kota (Rajasthan) India, fresh and healthy 20 g leaves with 100 mL H_2O stirred on a magnetic stirrer at 80 °C for 20 min. The prepared extract was filtered twice through Whatman paper and stored at 4 °C temperature further experiments. Deionized water was employed throughout the study.

2.2. Instrumentation

Characteristic optic properties of the CuNPs were recorded periodically to confirm completion of bioreduction of the $CuCl_2$ solution, followed by UV–vis spectra on a double beam spectrophotometer (3000^+ LABINDIA) having resolution 1 nm. The morphology of the CuNPs was determined using Scanning Electron Microscopy (SEM, Nova Nano FE-SEM 450 (FEI), US) and Transmission Electron Microscopy (TEM, Tecnai G^2 20 (FEI) S-Twin, US) operating at 200 kV. The preparation of the sample for SEM analysis dispersed NPs were centrifuged and ultra-sonicated for 40 min then 30 μL aliquots were extracted and deposited on the stub and for TEM analysis ultra-sonicated dispersed suspension mounted on standard carbon-coated Cu grid then drying under IR lamp. The crystalline structure of nanoparticles was characterized by X-ray Diffractometer (XRD, X'PERT PRO Panalytical, Netherlands) with Cu K_α radiation (λ = 0.1540 nm) in the 2θ scanning range from 10° to 89° and a scanning rate of 2°/min. Fourier Transformation Infra-Red (FTIR, ALPHA-T Bruker, Germany) was used to detect of functional groups of biomolecules in neem leaf broth was identified by spectrometer using KBr pellet technique and transmittance mode operating at a resolution of ± 4 cm^{-1}. Analysis of oxidative degradative products of MO was detected by Liquid Chromatography-Mass Spectrometry (LC–MS, XEVO G2-XS QTOF, Waters India Ltd.) and the mass spectrometer was operated with a quaternary pump, Quadropole detector.

2.3. Synthesis of copper nanoparticles

The aqueous solution of 7.5×10^{-3} mol dm^{-3} copper chloride ($CuCl_2{\cdot}2H_2O$) was prepared in round bottom flask, heated at 85 °C in the oil bath with magnetic stirring and dropwise 20% leaf broth added in this solution. With the passage of time the color of the reaction mixture was gradually changed from green, yellow, orange, radish brown, brown and finally dark brown with the number of intermediate stages. The resulting dispersion was centrifuged for 15 min and obtained supernatant was placed at 4 °C temperature. The reduction of copper salt into CuNPs by *Azadirachta indica* leaf broth at 85 °C is given by (Eq. (1)).

$$Cu^{+2}_{(aq)} + \textit{Neem}\ \text{leaf broth} \xrightarrow[85\,^\circ C]{\textit{stirring}} [Cu/\textit{Neem}\ \text{leaf broth}]^{+2} \xrightarrow[85\,^\circ C]{\textit{stirring for 28 h}} [Cu/\textit{Neem}\ \text{leaf broth}] \quad (1)$$

2.4. Kinetic measurements

The desired concentration of MO and other reactants placed in stoppered Erlenmeyer flask at 30 °C temperature and degradation of MO was initiated by adding a known concentration of PDS or PMS solution. The rate of decolonization was obtained in terms of change in intensity at the characteristic peak 465 nm wavelength in regular time interval studied by UV–vis Spectrophotometer attached with Peltier accessory (Temperature- controlled). All the kinetics runs were followed up to 80% completion of the reaction. A plot of log(C/C0) versus time was found liner which indicates pseudo first order kinetics. The

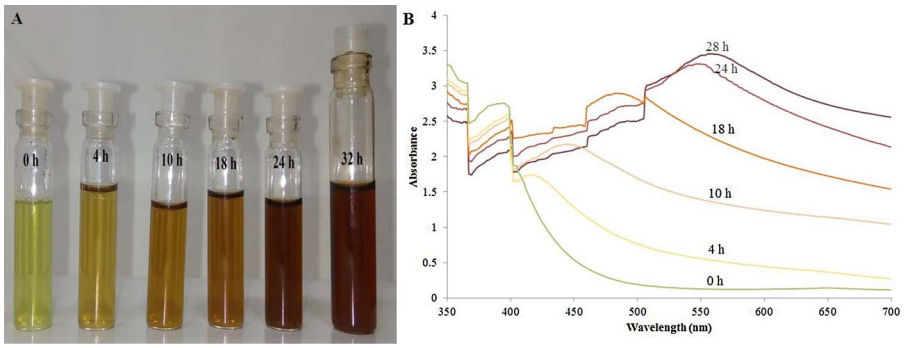

Fig. 2. (A) The time evolution of the dispersion photographs and (B) UV–vis spectra during the synthesis process.

pseudo first order rate constant (k_{obs}) were calculated from the slope of these plots. The values of rate constants, k_{obs} were reproducible within ± 5%.

3. Results and discussion

3.1. Characterization of copper nanoparticles

The one step synthesis scheme for the formation of CuNPs was confirmed by the color of dispersion turned from green to dark brown and UV–vis spectroscopy (Fig. 2). The UV–vis spectra of dispersion were recorded after different time intervals from the initiation of reaction and the intensity of SPR peak increased as the passage of time. Owing to the continued reduction of copper ions into CuNPs and finally, SPR band characteristic of CuNPs was detected around 560 nm (Fig. 2B). The morphology of synthesized CuNPs was confirmed by TEM analysis and results indicate that particle shape is cubical with the average size in 48 nm (Fig. 3). XRD spectrum showed a sharp peak at 2θ = 43.5°, 49.9° and 74.01° corresponding to (111), (200) and (220) representing the face-centered cubic structure of copper (Fig. 4). The result indicates synthesized CuNPs was pure without any impurities like CuO, Cu_2O, $Cu(OH)_2$ [40].

The effects of leaf broth percentage on the morphology of nanoparticles were also investigated by SEM analysis (Fig. 5). The results illustrate that particles size decreases from 73.51 nm to 48 nm with increase in the leaf broth percentage from 5% to 20% further increases in percentage then the dispersion was agglomerated. Results suggesting that biomolecules bound to the surface of particles, at the high percentage of leaf broth excess number of nuclei generated and interacts with each other so secondary reduction process occurs on the surface of the performed nuclei then particles were agglomerated. The effect of temperature on the reduction of copper ion is another important parameter for the synthesis of nanoparticles. It was observed that below 65 °C of reaction temperature the reduction of copper salt was not completed. The reduction rate considerably increases by increasing reaction temperature from 65 to 85 °C but at the higher temperature (90 °C) the synthesis rate is too high to control particle size so NPs formed with higher average size were agglomerated. The effect of initial concentration of $CuCl_2$ illustrates in Text S1 and Fig. S1. Thus the optimal conditions are 7.5×10^{-3} mol dm^{-3} concentration of copper chloride ($CuCl_2 \cdot 2H_2O$), 20% of leaf broth and 85 °C temperature for synthesis of NPs. Furthermore, the stability of NPs is the key factor for their application [41]. The FTIR spectra of bio reduced synthesized CuNPs exhibits peaks at 2922.46 cm^{-1} (O—H stretching of phenolic group), 2372.07 cm^{-1} (C—N stretching of aromatic amine), 1631.99 cm^{-1} (C=O stretching), 1457.26 cm^{-1} (C=C stretching), 1384.50 cm^{-1} (aldehydic C—H stretching) suggests the presence of flavonoids and terpenoids, that may be responsible for reduction as well as stabilization process [29,42] (Fig. S2). The stability of synthesized CuNPs was also determined by zeta potential value −16 mV suggests that synthesized CuNPs are highly stable.

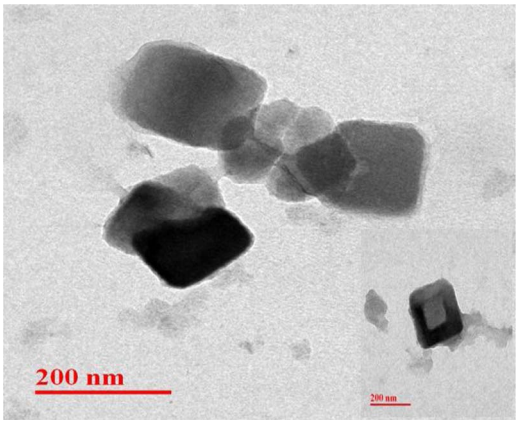

Fig. 3. TEM image of synthesized Copper Nanoparticles.

3.2. Effect of experimental conditions

3.2.1. Dye dependence

The initial concentration of MO was varying from 1.0×10^{-5} to 1.0×10^{-4} mol dm^{-3} at 30 °C temperature and other reactant concentrations were constant. Oxidation rate was found to increase with increasing concentration of MO in both CuNPs/PDS and CuNPs/PMS system. This is may be due to the increase in the concentration of dye, the reaction rate was increased as more molecules of dye was present for degradation. But after the certain concentration of dye 5×10^{-5} mol dm^{-3}, the oxidation rate was decreased (Table 1). This can be described that at constant oxidant concentration the availability of $SO_4^{\cdot -}$ radicals is less, so degradation of MO slowed down significantly.

3.2.2. Peroxodisulfate and peroxomonosulfate dependence

The oxidants such as persulfate and peroxomonosulfate are generally used in the sulfate radical based advanced oxidation process and having the standard redox potential of E° = 2.1 V, 1.82 V respectively. The degradation experiment was performed in the presence of CuNPs at different concentration (1.0×10^{-4}–1.0×10^{-3} mol dm^{-3}) of PDS and PMS respectively. Both oxidants are dominated by $SO_4^{\cdot -}$ radicals (SRs) based mechanism and radicals were generated by the catalytic activation of PDS (Eq. (2)) and PMS (Eq. (3)).

$$2S_2O_8^{2-} + Cu^{\circ} \rightarrow 2SO_4^{\bullet -} + 2SO_4^{2-} + Cu(II) \quad (2)$$

$$2HSO_5^{-} + Cu^{\circ} \rightarrow Cu(II) + 2SO_4^{\bullet -} + 2OH^{-} \quad (3)$$

Once the SRs are formed it can produce a rapid attack on MO molecules and convert into end products. The rate of degradation initially increases with increase in the concentration of both oxidants (Table 1). The result suggests the increase in the concentration of oxidant the number of SRs increases, which in turn increases the rate of oxidation Cu° to Cu^{2+} ion, resultant enhance the oxidative decolonization of MO.

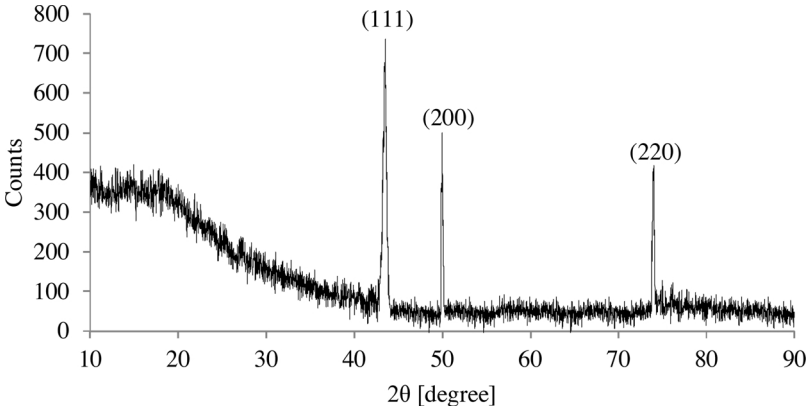

Fig. 4. XRD of bio-synthesized Copper Nanoparticles.

Furthermore, the PDS concentration increases beyond certain limits (5.0×10^{-4} mol dm^{-3}); the degradation rate of dye is slowed down. This was due to the fact that excess generated SRs were involved in the side reactions and consumed more PDS, hence remaining percentage of PDS decreases for degradation with the increase in PDS concentration (Table 1) [43,44].

$$S_2O_8^{2-} + SO_4^{\bullet -} \rightarrow S_2O_8^{\bullet -} + SO_4^{2-}$$

Whereas in case of PMS, the degradation rate increases up to the 5.0×10^{-4} mol dm^{-3} concentration of PMS after that rate was constant at higher concentration of PMS, indicating that the active sites of fixed concentration of catalyst gradually become the limiting factor (Table 1) [45].

3.2.3. Effect of initial pH

In order to find the optimal pH for dye degradation, a series of experiments were conducted at different pH (2.5–10) in CuNPs/PDS and CuNPs/PMS system respectively. As pH increased from 2.5 to 6.5 the degradation rate dramatically increased further increase in pH shows the degradation rate dropped in both systems (Fig. 6) (Table 1). This may be attributed to the zeta potential and surface charges of the catalyst. When CuNPs was dispersed in water than the surface become cationic nature, which would more coverage of hydroxyl groups from water [46] so uncharged surface hydroxyl groups of CuNPs were the main active sites for generate sulfate radicals ($SO_4^{\bullet -}$). Thus as pH increases, the degradation rate is also increased and reached the maximum at the pH 6.5. After that, the catalyst surface become anionic and higher electronic force to repel the $SO_4^{\bullet -}$ anion so less $SO_4^{\bullet -}$ could reach the catalyst surface and rate of degradation decreased correspondingly at higher pH.

3.2.4. Copper nanoparticles and temperature dependence

The catalytic activity of CuNPs was evaluated degradation of MO in both PDS and PMS system at various concentration 0.25×10^{-7}–2.0×10^{-7} mol dm^{-3} at three temperature viz. 25 °C, 30 °C, and 35 °C respectively. In order to show the catalytic activity, a graph is plotted between the concentration of CuNPs and rate constant obtained at different three temperatures (Fig. S3). The plot gives straight lines indicating the direct dependence of reaction rate on CuNPs concentration. This may be attributed to the fact that as the concentration of CuNPs is increased; the number of active radical species is also increased, which in turn increases the rate of oxidation. The synthesized CuNPs exhibited good catalytic activity in presence of small concentration (1.0×10^{-7} mol dm^{-3}). As the temperature increases the rate of generation of oxidizing species such as $SO_4^{\bullet -}$ radicals and higher valent Copper species also increased, so the rate of degradation of MO was accelerated by the rise in temperature. The energy of activation was calculated from the plot of log (k_{obs}) versus 1/T in both systems. The value of activation energy (13.19 kJ mol^{-1}) in CuNPs/PMS system shows that the rate of degradation of MO is faster than

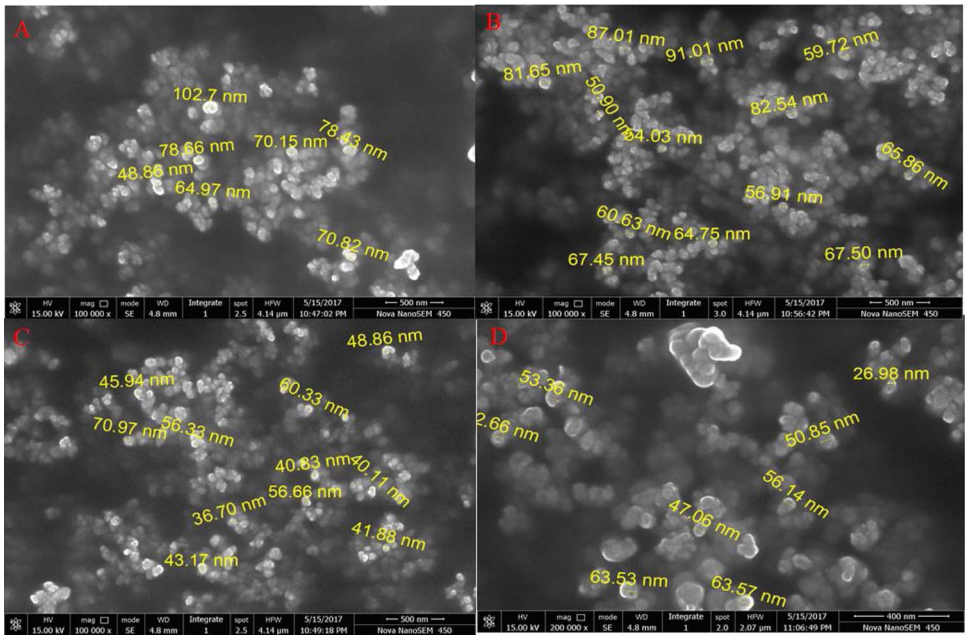

Fig. 5. SEM images of synthesized Copper nanoparticles at different leaf broth percentage with average particle size are (A) 5%, d = 73.51 nm (B) 10%, d = 68.45 nm (C) 15%, d = 50.1 nm (D) 20%, d = 48 nm.

Table 1
Effect of variation of [PDS], [PMS], [Dye], [CuNPs] and pH on oxidative degradation of MO in aqueous solution at 30 °C.

S. No.	10^4 [PDS] mol dm^{-3}	10^4 [PMS] mol dm^{-3}	10^5 [Dye] mol dm^{-3}	10^7 [CuNPs] mol dm^{-3} (9 nm)	pH	10^4 K_{obs} for [PDS] (s^{-1})	10^3 K_{obs} for [PMS] (s^{-1})
1	1.0	1.0	5.0	1.00	6.5	0.81	1.00
2	2.5	2.5	5.0	1.00	6.5	3.10	1.50
3	5.0	5.0	5.0	1.00	6.5	6.80	2.20
4	7.5	7.5	5.0	1.00	6.5	5.39	2.28
5	10	10	5.0	1.00	6.5	4.20	2.32
6	5.0	5.0	1.0	1.00	6.5	3.20	1.10
7	5.0	5.0	2.5	1.00	6.5	5.10	1.70
8	5.0	5.0	5.0	1.00	6.5	6.80	2.20
9	5.0	5.0	7.5	1.00	6.5	6.10	2.00
10	5.0	5.0	10	1.00	6.5	5.50	1.70
11	5.0	5.0	5.0	0.00	6.5	1.20	0.32
12	5.0	5.0	5.0	0.25	6.5	2.30	0.70
13	5.0	5.0	5.0	0.50	6.5	4.00	1.26
14	5.0	5.0	5.0	0.75	6.5	5.40	1.74
15	5.0	5.0	5.0	1.00	6.5	6.80	2.20
16	5.0	5.0	5.0	1.50	6.5	9.60	3.15
17	5.0	5.0	5.0	2.00	6.5	12.40	4.07
18	5.0	5.0	5.0	1.00	2.5	2.10	1.20
19	5.0	5.0	5.0	1.00	5.0	4.80	2.00
20	5.0	5.0	5.0	1.00	6.5	6.80	2.20
21	5.0	5.0	5.0	1.00	7.0	6.40	2.10
22	5.0	5.0	5.0	1.00	8.0	5.40	1.80
23	5.0	5.0	5.0	1.00	9.0	4.50	1.50
24	5.0	5.0	5.0	1.00	10.0	3.20	1.00

CuNPs/PDS (21.64 kJ mol^{-1}) system. The values of thermodynamic parameters like the change in enthalpy (ΔH) and change in entropy activation (ΔS) and free energy (ΔG) were 19.12 kJ mol^{-1}, −242.68 J mol^{-1} K^{-1}, 92.65 kJ mol^{-1} for PDS and 11.39 kJ mol^{-1}, −258.48 J mol^{-1} K^{-1}, 89.69 kJ mol^{-1} for PMS respectively. In both systems positive ΔH and ΔG values shows that the process was endothermic and nonspontaneous while negative ΔS value represents endergonic reaction [9,47,48].

3.2.5. Effect of alcohol and t-butyl alcohol (TBA)

For radical quenching tests using Ethanol (EtOH) and t-butyl alcohol (TBA) as a radical scavenger was performed to identify the dominant radical species generated from the CuNPs/PDS and CuNPs/PMS systems. Ethanol is capable of quenching both sulfate and hydroxyl radicals as it readily react with both radicals at high and comparable rates, whereas TBA is effective quenching agent for hydroxyl radicals [5,9]. The results illustrate that quenching effect of EtOH is greater than TBA in both systems (Fig. 7). Therefore, sulfate radicals are active species in the oxidative degradation of dye in presence of CuNPs.

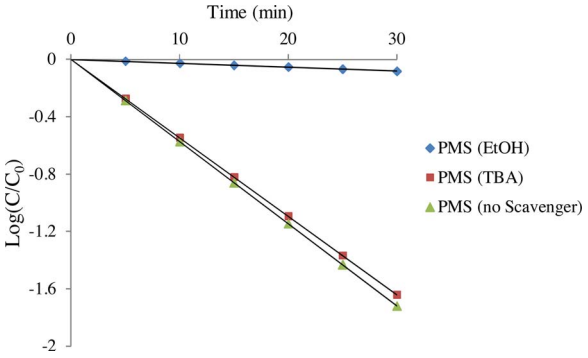

Fig. 7. Scavenger effect of Ethanol and TBA in CuNPs/Peroxosulfates system. ([PMS] = 5×10^{-4} mol dm^{-3}, [Dye] = 5×10^{-5} mol dm^{-3}, [CuNPs] = 1×10^{-7} mol dm^{-3}, pH = 6.5 and Temperature 30 °C).

3.2.6. Mechanism

In the present study, CuNPs was proved to the catalyst with good activity degradation of the azo compound with peroxosulfates as an oxidant. The zero valent copper serves as a mediator for the electron transfer to the peroxosulfates and generates higher active sulfate radicals. Then these radicals are the rapid attack on MO molecules and degrade into end products. The plausible mechanism PDS and PMS are given below -

$$2S_2O_8^{2-} + Cu^{\circ} \rightarrow 2SO_4^{\bullet -} + 2SO_4^{2-} + Cu(II)$$
$$2SO_4^{\bullet -} + Cu(II) + Dye \rightarrow Product + Cu^{\circ}$$
$$2S_2O_8^{2-} + Dye \xrightarrow{Cu^{\circ}} Product + 2SO_4^{2-}$$

$$2HSO_5^{-} + Cu^{\circ} \rightarrow Cu(II) + 2SO_4^{\bullet -} + 2OH^{-}$$
$$2SO_4^{\bullet -} + Cu(II) + Dye \rightarrow Product + Cu^{\circ}$$
$$HSO_5^{-} + Dye \xrightarrow{Cu^{\circ}} Product + 2OH^{-}$$

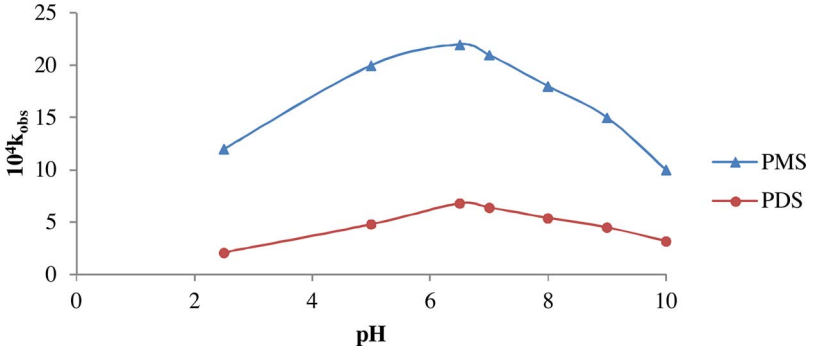

Fig. 6. Effect of variation of pH at fixed [Dye] = 5×10^{-5} mol dm^{-3}, [PDS] and [PMS] = 5×10^{-4} mol dm^{-3}, [CuNPs] = 1×10^{-7} mol dm^{-3} and Temperature 30 °C.

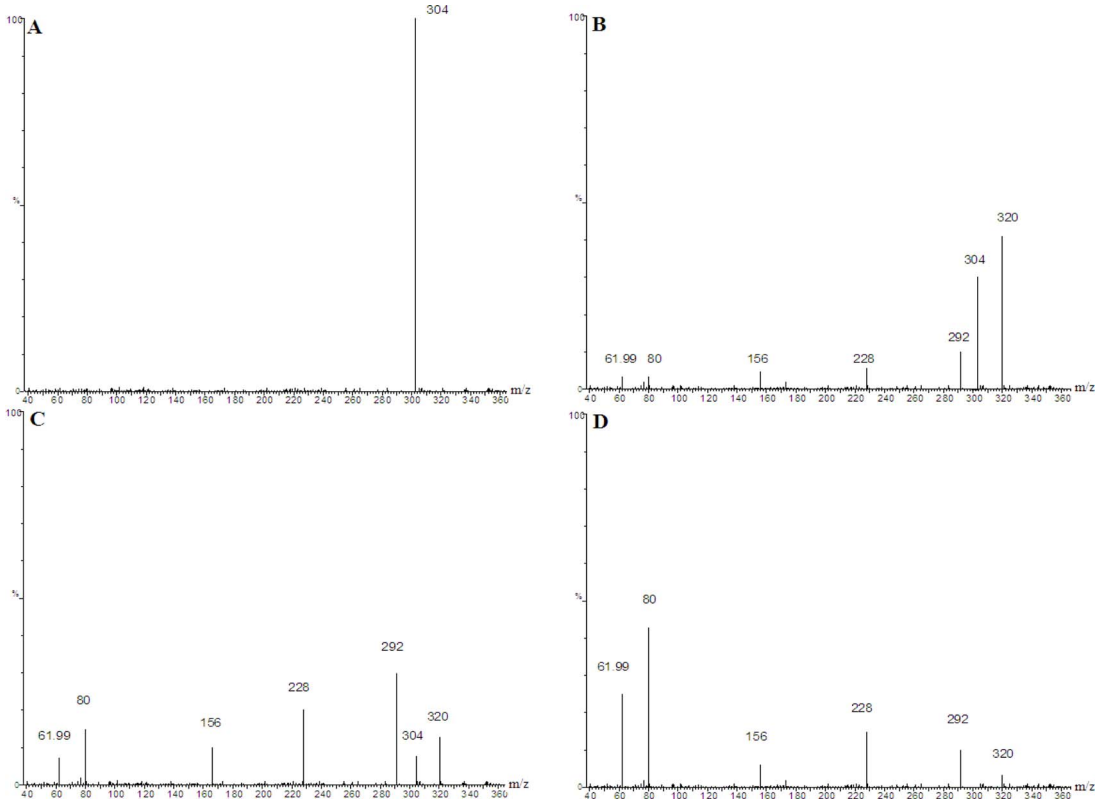

Fig. 8. LC–MS of MO degraded at (A) 0 min, (B) 10 min, (C) 20 min, (D) 30 min; in CuNPs/PMS system.

3.3. Product analysis

3.3.1. Determination of degradation products

In order to determine degradation products were carried out by LC–MS analysis of the dye solution in CuNPs/PMS system, at the different time interval of the degradation process. The results showed (Fig. 8) the significant peaks present at the different time of degradation with corresponding *m/z* values 304, 320, 292, 228, 15, 80, 62. After ten min of degradation, the new peak of mono hydroxylated product (*m/z* 320) of MO was found (Fig. 8B). The peak of *m/z* 292 can be attributed the successive demethylation of mono hydroxylated MO (Fig. 8C) after 20 min. Further, LC–MS spectrum of the compound *m/z* 292, fragmented into the compound at *m/z* 228 and 156 respectively subsequently, these intermediate converted into the end products (Fig. 8D).

3.3.2. UV–vis absorption spectra of intermediates and degradation route

Fig. 9 shows the UV–vis spectra of the compounds with *m/z* values 304, 320, 292 determined on the basis of $[M-H]^-$ ions of the MO. The spectrum of light absorption by reaction mixture before reaction consists of two main peaks at 465 nm and 270 nm. The peak at 465 nm is attributed to the absorption of the extended aromatic ring and chromophore group while the additional band at 270 nm are assigned to its aromatic ring in MO molecule (*m/z* 304). As the reaction proceeded, the UV–vis spectrum of the compound with *m/z* value 320 shows a red-shift (480 nm) may be attributed to the hydroxyl radical inserted in the benzene ring linking with the dimethylamine group of MO. Subsequently, successive demethylation (*m/z* 292) could lead to significant wavelength blue shift (435 nm) can be suggested that homolytic cleavage of the nitrogen-carbon bond, resulting in the substitution of the methyl group by the hydrogen atom [49]. Finally, two new peaks at 220 nm and 320 nm were indicated polyaromatic ring in the MO

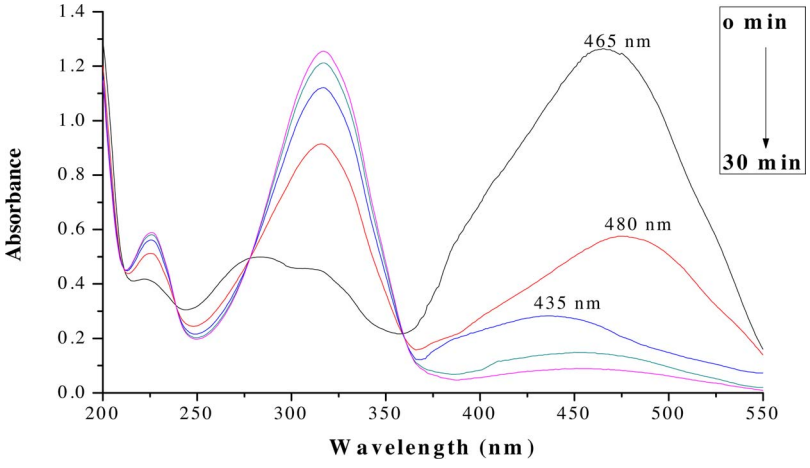

Fig. 9. The change of UV–vis spectrum with reaction time in CuNPs/PMS system. ([PMS] = 5×10^{-4} mol dm^{-3}, [Dye] = 5×10^{-5} mol dm^{-3}, [CuNPs] = 1×10^{-7} mol dm^{-3}, pH = 6.5 and Temperature 30 °C).

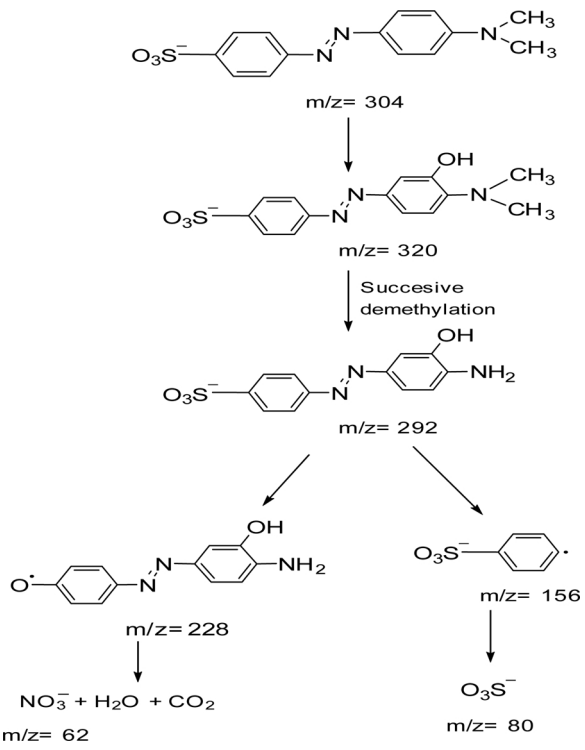

Fig. 10. Proposed oxidative degradation route of MO in CuNPs/PMS system.

degrade into monosubstituted aromatic ring and end products (Fig. 9). According to observe results obtained from the spectral changes during degradation of MO the following route are proposed (Fig. 10) [50].

It was observed that CuNPs/Peroxosulfates system achieved the highest MO degradation rate at pH 6.5. The degradation rate decreased when the solution pH either acidic or alkaline. Earlier study also reports, at pH 7.0 PDS/CuO coupled system was must efficient for 2,4-DCP degradation, copper leaching was 50 times lower than drinking water standards [51] so in this report the possibility of leaching of Cu^{2+} ions are very less at optimum reaction conditions. The application of homogenous (colloidal) catalysis is restricted due to the difficulty in reporting the soluble catalyst from the product and reaction solvent. Although recycling of colloidal catalysis could be achived by using magnetic nanoparticles and solid-phase beads, but NPs supported catalysis proceded much faster than its counter part on resins. These protocols should be tested to anchor CuNPs for peroxosulfates activation in future studies.

4. Conclusion

From the above experimental results, we conclude that different size of CuNPs produced through bio-reduction of copper salt was strongly dependent on the process parameters like neem leaf broth concentration, the concentration of copper salt and synthesis temperature. It was confirmed by the different instrumental techniques that there was a full conversion of copper chloride to CuNPs and bioorganic components from neem leaf broth act as a stabilizer for the CuNPs. These synthesized CuNPs were used for activation of peroxosulfates for degradation of hazardous dye in a cost-effective manner. Cu° was the source of Cu^{+2}, which was verified to be the efficient activating agent for peroxosulfates to produce sulfate radicals. Kinetic results reveal that CuNPs/Peroxosulfates system could induce a 0.81×10^{-4}–$40.7 \times 10^{-4}\,s^{-1}$ folds increase in the degradation rate of MO at different concentration of CuNPs, peroxosulfate concentration, and initial pH. Moreover, the reactivity discrepancy of PDS and PMS followed the order of CuNPs/PMS > CuNPs/PDS in degradation of MO under similar conditions. Furthermore, the elucidation of degradation pathway is of special interest considering environmental priorities. More importantly, these nanoparticles showed a significantly longer lifespan with sustained reactivity, making them the potential application in dye degradation.

Acknowledgements

This work was supported in part by Department of Science and Technology, India sponsored FIST Laboratory of our institution for experimental work, MNIT Jaipur for SEM and TEM analysis of synthesis of CuNPs, SAIF (Punjab University, Chandigarh) for XRD measurement, and IIT Ropar for LC–MS measurement and University Grants Commission, India for financial support as JRF (Ref. No: 22/12/2013(ii) EU-V).

Appendix A. Supplementary data

Supplementary data associated with this article can be found, in the online version, at https://doi.org/10.1016/j.jece.2017.11.014.

References

[1] A. Azam, A. Hamid, Effects of gap size and UV dosage on decolorization of C.I. Acid Orange 7 by UV/H_2O_2 process, J. Hazard. Mater. 133 (2006) 167–171.
[2] C.P. Huang, C. Dong, Z. Tang, Advanced chemical oxidation: its present role and potential future in hazardous waste treatment, Waste Manag. 13 (1993) 361–377.
[3] Y. Deng, R. Zhao, Advanced oxidation process (AOPs) in wastwater treatment, Curr. Pollut. Rep. 1 (2015) 167–176.
[4] X. Xiong, B. Sun, J. Zhang, N. Gao, J. Shen, J. Li, X. Guan, Activating persulfate by Fe0 coupling with weak magnetic field: performance and mechanism, Water Res. 62 (2014) 53–62.
[5] G.P. Anipsitakis, D.D. Dionysiou, Degradation of organic contaminants in water with sulfate radicals generated by the conjunction of peroxymonosulfate with cobalt, Environ. Sci. Technol. 37 (2003) 4790–4797.
[6] S. Yanga, P. Wang, X. Yang, L. Shan, W. Zhang, X. Shao, R. Niu, Degradation efficiencies of azo dye Acid Orange 7 by the interaction of heat, UV and anions with common oxidants: persulfate, peroxymonosulfate and hydrogen peroxide, J. Hazard. Mater. 179 (2010) 552–558.
[7] S. Su, W. Guo, C. Yi, Y. Leng, Z. Ma, Degradation of amoxicillin in aqueous solution using sulphate radicals under ultrasound irradiation, Ultrason. Sonochem. 19 (2012) 469–474.
[8] M. Murugavelu, P. Andal, S. Shailaja, M.S. Ramachandran, Kinetic studies on the reaction between nickel(II) lactate and peroxomonosulphate ion—the effect of formaldehyde, J. Mol. Catal. A: Chem. 306 (2009) 1–5.
[9] J. Zhang, M. Chen, L. Zhu, Activation of persulfate by Co_3O_4 nanoparticles for orange G degradation, RSC Adv. 6 (2016) 758–768.
[10] J. Zhang, M. Chen, L. Zhu, Activation of peroxymonosulfate by iron-based catalysts for orange G degradation: role of hydroxylamine, RSC Adv. 6 (2016) 47562–47569.
[11] G.P. Anipsitakis, D.D. Dionysiou, Radical generation by the interaction of transition metals with common oxidants, Environ. Sci. Technol. 38 (2004) 3705–3712.
[12] A. Nasirian, Synthesis and characterization of Cu nanoparticles and studying of their catalytic properties, Int. J. Nano Dim. 2 (2012) 159–164.
[13] L.N. Lewis, J.F. Smith, Catalytic carbon-carbon bond formation via ortho-metalated complexes, J. Am. Chem. Soc. 108 (1986) 2728–2735.
[14] H. Hirai, H. Wakabayashi, M. Komiyama, Preparation of polymer-protected colloidal dispersion of copper, Bull. Chem. Soc. Jpn. 59 (1986) 367–372.
[15] M. Spiro, Catalysis by noble metals of redox reaction in solution, Catal. Today 17 (1993) 517–525.
[16] J.A. Eastman, S.U.S. Choi, S. Li, W. Yu, L.J. Thompson, Anomalously increased effective thermal conductivities of ethylene glycol-based nanofluids containing copper nanoparticles, Appl. Phys. Lett. 78 (2001) 718–720.
[17] R.K. Guduru, K.L. Murty, K.M. Youssef, R.O. Scattergood, C.C. Koch, Mechanical behavior of nanocrystalline copper, Mater. Sci. Eng. A 463 (2007) 14–21.
[18] M.L. Kantam, V.S. Jaya, M.J. Lakshmi, B.R. Reddy, B.M. Choudary, S.K. Bhargava, Alumina supported copper nanoparticles for aziridination and cyclopropanation reactions, Catal. Commun. 8 (2007) 1963–1968.
[19] S. Jain, N. Nagar, V. Devra, Synthesis and characterization of highly efficient copper nanoparticles and their catalytic application in oxidative kinetic study, Pelagia Res. Libr. 6 (2015) 171–180.
[20] M.S. Niasari, Z. Fereshteh, F. Davar, Synthesis of oleylamine capped copper nanocrystal via thermal reduction of a new precursor, Polyhedron 28 (2009) 126–130.
[21] M.S. Niasari, F. Davar, Synthesis of copper and copper (I) oxide nanoparticles by thermal decomposition of a new precursor, Mater. Lett. 63 (2009) 441–443.
[22] Q.-L. Zhang, Z.-M. Yang, B.-J. Ding, X.-Z. Lan, Y.-J. Guo, Preparation of copper nanoparticles by chemical reduction method using potassium borohydride, Trans. Nonferrous Met. Soc. China 20 (2010) 240–244.
[23] P. Pulkkinen, J. Shan, K. Leppanen, A. Kansakoshi, A. Laiho, M. Jarn, H. Tenhu, Poly (ethylene imine) and tetraethylenepentamines as protecting agents for metallic copper nanoparticles, Appl. Mater. Interfaces 1 (2009) 519–525.

[24] M. Tiwari, P. Jain, R.C. Hariharapura, K. Narayanan, B.K. Udaya, N. Udupa, J.V. Rao, Biosynthesis of copper nanoparticles using copper-resistant Bacilluscereus, a soil isolate, Process Biochem. 51 (2016) 1348–1356.
[25] S. Iravani, Green synthesis of metal nanoparticles using plants, Green Chem. 13 (2011) 2638–2650.
[26] O.V. Kharissova, H.V.R. Dias, B.I. Kharisov, B.O. Pé rez, V.M. Jiménez Pé rez, The greener synthesis of nanoparticles, Trends Biotechnol. 31 (2013) 240–248.
[27] A.K. Mittal, Y. Chisti, U.C. Banerjee, Synthesis of metallic nanoparticles using plant extracts, Biotechnol. Adv. 31 (2013) 346–356.
[28] S. Yallappa, J. Manjanna, M.A. Sindhe, N.D. Satyanarayan, S.N. Pramod, K. Nagaraja, Microwave assisted rapid synthesis and biological evaluation of stable copper nanoparticles using T. arjuna bark extract, Spectrochim. Acta A Mol. Biomol. Spectrosc. 110 (2013) 108–115.
[29] K. Saranyaadevi, V. Subha, R.S.E. Ravindran, S. Renganathan, Synthesis and characterization of copper nanoparticle using *Capparis zeylanica* leaf extract, Int. J. ChemTech Res. 6 (2014) 4533–4541.
[30] V.D. Kulkarni, P.S. Kulkarni, Green synthesis of copper nanoparticles using *Ocimum sanctum* leaf extract, Int. J. Chem. Stud. 1 (2013) 1–4.
[31] B.H. Patel, M.Z. Channiwala, S.B. Chaudhari, A.A. Mandot, Biosynthesis of copper nanoparticles; its characterization and efficacy against human pathogenic bacterium, J. Environ. Chem. Eng. (JECE) 4 (2016) 2163–2169.
[32] I. Subhankari, P.L. Nayak, Synthesis of copper nanoparticles using *Syzygium aromaticum* (cloves) aqueous extract by using green chemistry, World J. Nano Sci. Technol. 2 (2013) 14–17.
[33] J.K.V.M. Angrasan, R. Subbaiya, Biosynthesis of copper nanoparticles by *Vitis vinifera* leaf aqueous extract and its antibacterial activity, Int. J. Curr. Microbiol. Appl. Sci. 3 (2014) 768–774.
[34] M. Dubey, S. Bhadauria, B. Kushwah, Green synthesis of nanosilver particles from extract of *Eucalyptus hybrida* (safeda) leaf, Dig. J. Nanomater. Biostruct. 4 (2009) 537–543.
[35] J.L. Huang, Q.B. Li, D.H. Sun, Y.H. Lu, Y.B. Su, X. Yang, H. Wang, Y. Wang, W. Shao, N. He, J. Hong, C. Chen, Biosynthesis of silver and gold nanoparticles by novel sundried Cinnamomum camphora leaf, Nanotechnology 18 (2007) 105104 (11pp).
[36] S.S. Shankar, A. Rai, A. Ahmad, M. Sastry, Rapid synthesis of Au, Ag, and bimetallic Au core–Ag shell nanoparticles using Neem (*Azadirachta indica*) leaf broth, J. Colloid Interface Sci. 275 (2004) 496–502.
[37] K.S. Mukunthan, S. Balaji, Cashew apple juice (Anacardium Occidentale L.) speeds up synthesis of silver nanaoparticles, Int. J. Green Nanotechnol. 4 (2012) 71–79.
[38] A. El-Ghenymy, F. Centellas, J.A. Garrido, R.M. Rodríguez, I. Sirés, P.L. Cabot, E. Brillas, Decolorization and mineralization of Orange G azo dye solutions by anodic oxidation with a boron-doped diamond anode in divided and undivided tank reactors, Electrochim. Acta 130 (2014) 568–576.
[39] A.B.D. Santos, F.J. Cervantes, J.B.V. Lier, Review paper on current technologies for decolourisation of textile wastewaters: perspectives for anaerobic biotechnology, Bioresour. Technol. 98 (2007) 2369–2385.
[40] W. Yu, H. Xie, L. Chen, Y. Li, C. Zhan, Synthesis and characterization of monodispersed copper colloids in polar solvents, Nanoscale Res. Lett. 4 (2009) 465–470.
[41] S. Jain, A. Jain, V. Devra, Experimental investigation on the synthesis of copper nanoparticles by chemical reduction method, Int. J. Sci. Eng. Res. 5 (2014) 973–978.
[42] P. Velmurugan, K. Anbalagan, M. Manosathyadevan, K.-J. Lee, M. Cho, S.-M. Lee, J.-H. Park, S.-G. Oh, K.-S. Bang, B.-T. Oh, Green synthesis of silver and gold nanoparticles using Zingiber officinale root extract and antibacterial activity of silver nanoparticles against food pathogens, Bioprocess. Biosyst. Eng. 37 (2014) 1935–1943.
[43] J. Wu, H. Zhang, J. Qiu, Degradation of Acid Orange 7 in aqueous solution by a novel electro/Fe^{2+}/peroxydisulfate process, J. Hazard. Mater. 215–216 (2012) 138–145.
[44] S.G. Kumar, L.G. Devi, Review on modified TiO2 photocatalysis under UV/visible light: selected results and related mechanisms on interfacial charge carrier transfer dynamics, J. Phys. Chem. 115 (2011) 13211–13241.
[45] Y.-H. Huang, Y.-F. Huang, C.-i. Huang, C.-Y. Chen, Efficient decolorization of azo dye Reactive Black B involving aromatic fragment degradation in buffered Co^{2+}/PMS oxidative processes with a ppb level dosage of Co^{2+}-catalyst, J. Hazard. Mater. 170 (2009) 1110–1118.
[46] M.-j. Pu, Y.-w. Ma, J.-q. Wan, Y. Wang, M.-z. Huang, Y.-m. Chen, Fe/S doped granular activated carbon as a highly active heterogeneous persulfate catalyst toward the degradation of Orange G and diethyl phthalate, J. Colloid Interface Sci. 418 (2014) 330–337.
[47] K. Lal, A. Garg, Utilization of dissolved iron as catalyst during fenton-like oxidation of pretreated pulping effluent, Process Saf. Environ. Prot. (PSEP) 111 (2017) 766–774, http://dx.doi.org/10.1016/j.psep.2017.09.005.
[48] R.J. Dougherty, J. Singh, V.V. Krishnan, Kinetics and thermodynamics of oxidation mediated reaction in Lcysteine and its methyl and ethyl esters in dimethyl sulfoxide-d6 by NMR spectroscopy, J. Mol. Struct. 1131 (2017) 196–200.
[49] T. Chen, Y. Zheng, J.-M. Lin, G. Chen, Study on the photocatalytic degradation of methyl orange in water using Ag/ZnO as catalyst by liquid chromatography electrospray ionization ion-trap mass spectrometry, J. Am. Soc. Mass Spectrom. 19 (2008) 997–1003.
[50] C. Baiocchi, M.C. Brussino, E. Pramauro, A.B. Prevot, L. Palmisano, G. Marcì, Characterization of methyl orange and its photocatalytic degradation products by HPLC/UV–VIS diode array and atmospheric pressure ionization quadrupole ion trap mass spectrometry, Int. J. Mass Spectrom. 214 (2002) 247–256.
[51] T. Zhang, Y. Chen, Y. Wang, J.L. Roux, Y. Yang, J.-P. Croue, Efficient peroxydisulfate activation process not relying on sulfate radical generation for water pollutant degradation, Environ. Sci. Technol. 48 (2014) 5868–5875.

Environmental Technology & Innovation 10 (2018) 281–289

Contents lists available at ScienceDirect

Environmental Technology & Innovation

journal homepage: www.elsevier.com/locate/eti

Oxidative degradation of Orange G by peroxomonosulfate in presence of biosynthesized copper nanoparticles—A kinetic study

Niharika Nagar, Vijay Devra *

Department Of Chemistry, Janki Devi Bajaj Government Girls College, Kota, Rajasthan, 324001, India

ARTICLE INFO

Article history:
Received 28 September 2017
Received in revised form 8 March 2018
Accepted 15 March 2018
Available online 23 March 2018

Keywords:
Copper nanoparticles
Azadirachta indica (Neem)
Orange G
Catalysis
Oxidative degradation
Peroxomonosulfate

ABSTRACT

The present study reports the highly stable dispersed nanosized copper particles (CuNPs) was prepared by the biosynthesis process. The reduction of copper salts by *Azadirachta indica* (neem) leaf broth is a new and green approach, in which biomolecules present in leaf broth is act as reducing and stabilizing agent in aqueous medium. The effect of reaction temperature on the size of dispersed CuNPs was studied. The morphology of CuNPs was investigated by Transmission Electron Microscopy (TEM) and Scanning Electron Microscopy (SEM) analysis. Fourier Transform Infrared Spectroscopy (FTIR) studies reveal the presence of bioactive functional groups such as phenolic, amines and an aromatic ring are responsible for capping and stabilizing of nanoparticles (NPs). Further, the catalytic activity of synthesized NPs was measured on the degradation of Orange G (OG) in presence of peroxomonosulfate (PMS) spectrophotometrically. The results indicates that biosynthesized CuNPs at different temperature have different degradation efficiency at different average size 48.01 >50.57 >68.54 >73.54 nm respectively. The effect of different experimental condition as well as addition of neutral salts on the rate of degradation was also studied.

1. Introduction

The textile industry effluents contain large amounts of dye chemicals which may cause severe water pollution. There are many processes available for the removal of dyes by biological, physical and chemical processes (Robinson et al., 2001; Ahmad et al., 2012; Harrelkas et al., 2009; Hammami et al., 2012; Khouni et al., 2012). These methods are often very costly and not eco-friendly due to their low efficiency and a large amount of sludge generation. Advanced oxidation process (AOPs) has been widely studied to degrade pollutants in water treatment. Peroxomonosulphate (PMS) is the newest oxidant used in chemical oxidation for water treatment (Lou et al., 2014). The degradation of organic pollutants by sulfate radicals (SRs) ($SO_4^{\bullet-}$) based AOPs have draw attention due to their high efficiency and selectivity towards pollutants (Anipsitakis et al., 2008; Ahmad et al., 2013). SRs have higher redox potential (2.5–3.1 V) (Lou et al., 2014) than hydroxyl radicals ($HO^{\bullet}$) (1.8–2.7 V) (Zhang et al., 2016a, b). The SRs can be generated from activating PMS by various transition metal such as Fe(II), Co(II), Ru(III), Ce(III), Mn(II), and Ag(I) (Anipsitakis and Dionysiou, 2004; Wang and Chu, 2011; Zou et al., 2013) has been widely studied. Among these transition metal ion, copper-mediated decomposition of PMS is an efficient catalytic system to generate $SO_4^{\bullet-}$ as the major oxidizing species (Deng and Zhao, 2015). The CuNPs/PMS system for the degradation of organic

* Corresponding author.
E-mail addresses: nnniharikanagar@gmail.com (N. Nagar), v_devra1@rediffmail.com (V. Devra).

https://doi.org/10.1016/j.eti.2018.03.005
2352-1864/

pollutants has shown a lot of interest due to its advantages such as wide pH range small quantity of copper catalyst and high degradation efficiency at room temperature.

In order to promote the performance of catalysts, nano-size catalyst draws attention in recent years due to their unique properties and the broad range of applications such as photocatalysis, sonocatalysis etc. (Behnajady and Eskandarloo 2015; Eskandarloo et al. 2015; Adhikari et al. 2014a,b; Adhikari et al. 2015; Eskandarloo et al. 2016). Most of the studies in the homogeneous colloidal nanocatalysis field involve using spherical NPs or undetermined shapes. There are very few studies in which catalysis is conducted with specific shape and size of NPs. NPs of different sizes have different surface area and active sites. Thus, one would expect the catalytic activity to be different in the same reaction. So that it is a key factor to reach controlled synthesis process of NPs for getting better results in catalysis (El-Kheshen and El-Rab, 2012). This report includes the eco-friendly, cost-effective biosynthesis of CuNPs from copper chloride using leaf extract by Indian medicinal plant namely *A. Indica* (Neem). The existing biomolecules in plant extracts act as reducing agents for metal ions and capping agents to reduce the agglomeration of NPs. Studies have shown that the size of CuNPs are influenced strongly by the temperature of synthesis process and synthesized CuNPs were characterized by different instrumental techniques. The main objectives of this report are (1) To biosynthesis of CuNPs by simple and green route without any special experimental conditions. (2) The effect of synthesis temperature on the size of nanoparticles. (3) Explore the catalytic activity of different size of NPs in CuNPs/PMS system for degradation of model organic contaminant Orange G. (4) To determine the effect of different concentration of PMS, catalyst, pH and neutral salts on the degradation of Orange G. These issues are used to select and improve the performance of sulfate radical base AOPs for dye wastewater treatment.

2. Experimental

2.1. Chemicals and materials

Peroxomonosulfate ($2KHSO_5{\cdot}KHSO_4{\cdot}K_2SO_4$ 95%) (Sigma-Aldrich), Copper chloride dihydrate ($CuCl_2{\cdot}2H_2O$) (E. Merck), Orange G (OG) and other reagents were of analytical grade. Neem (*Azadirachta Indica*) leaves were collected from Kota (Rajasthan) India, fresh, clean and healthy 10 g leaves with 50 ml water stirred on a magnetic stirrer at 80 °C for 20 min. The neem extract was filtered through Whatman filter paper, then refrigerated (4 °C) in black stoppered bottle for further experiments. Deionized water was used throughout the study.

2.2. Characterization techniques

Characterization of nanoparticles is significant to understand the control synthesis of nanoparticles and their applications. The preliminary confirmation of the formation of CuNPs by sampling the reaction mixture at regular intervals and the maximum absorption was obtained by UV–Visible spectra, in a range of wavelength between 400 and 700 nm using (UV 3000^+ LABINDIA) double beam spectrophotometer. The presence of functional groups of biomolecules in neem leaf broth was identified by ALPHA-T Bruker, Germany FTIR (Fourier Transformation Infra-Red) spectrometer using KBr pellet technique. The morphology of synthesized CuNPs was confirmed by Scanning Electron Microscopy (SEM) analysis was done on Nova Nano FE-SEM 450 (FEI) coupled with Energy Dispersive Spectroscopy (EDS) machine. A thin film of the sample was prepared on a glass slide by dropping a small amount of the sample and then allowed to dry by putting it under a mercury lamp for 5 min. The morphology and shape of the nanoparticles were estimated using a Transmission Electron Microscopy (TEM) (Tecnai G^2 20 (FEI) S-Twin) operated at an accelerating voltage of 200 kV samples were loaded on the carbon coated grid before being introduced into the vacuum chamber. Further confirmation of purely synthesized CuNPs were checked by XRD characterization on XPERT-PRO X-Ray Diffractometer of Cu Kα radiation ($\lambda = 0.1540$ nm) with a scanning rate of 2°/min and 2θ ranging from 10° to 80°. The oxidative degradation route of Orange G in CuNPs/PMS system was detected by Liquid Chromatography-Mass Spectrometry (LC-MS) (XEVO G2-XS QTOF). In this detection, the mass spectrometer was operated with a quaternary pump, Quadrupole detector and 1 μL of the sample solution was injected with flow rate 0.3 mL min^{-1}.

2.3. Synthesis of copper nanoparticles

7.5×10^{-3} mol L^{-1} solution of aqueous copper chloride ($CuCl_2{\cdot}2H_2O$) containing round bottom flask heated at 85 °C on magnetic stirrer, after that 20% neem leaf broth was dropwise added. The color of the reaction mixture was initially green, gradually changed into yellow, orange, radish brown, brown and finally dark brown with the passage of time. The resulting dark brown solution was centrifuged for 15 min and obtained supernatant was placed at 4 °C temperature. The studies were conducted at the different temperature to investigate the effect of synthesis temperature on morphology and size of CuNPs.

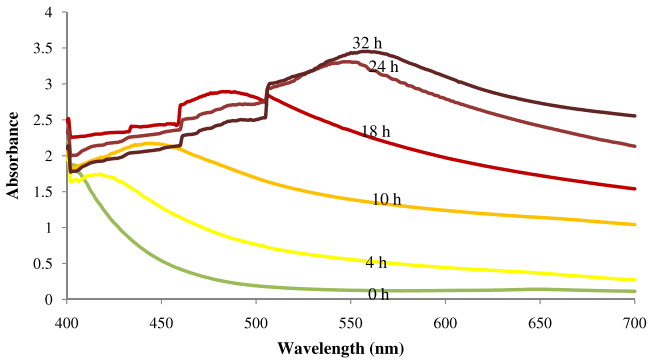

Fig. 1. UV–Visible spectra during the synthesis process.

2.4. Kinetic measurements

The oxidative degradation of Orange G in CuNPs/PMS system was carried out with the required concentration of reactants in stoppered Erlenmeyer flask at 30 °C and reaction was initiated by adding the known volume of PMS solution. The kinetics was monitored by the absorbance of Orange G measured spectrophotometrically at λ_{max} 476 nm with regular time interval. It was observed that the absorbance (A) of the dye solution decreases with increasing time showing the progress of dye degradation. The kinetic plots for the rate constant were determined under pseudo-first order conditions which are generated by plotting log (absorbance) versus time. The best fit linear plots exhibit pseudo first-order kinetics of Orange G degradation in CuNPs/PMS system. The limiting region in these exponential plots indicates the completion of degradation.

3. Results and discussion

3.1. Characterization of copper nanoparticles

The biosynthesis of CuNPs has confirmed the color of dispersion changed from green to dark brown shown in Fig. S1, indicates the reduction of Cu^{2+} into Cu° because Cu° particles can impart such a color. The presence of active components in neem leaf broth such as terpenoids, nimbaflavone and poly phenols are responsible for reduction of copper ions as well as stabilization of CuNPs as shown in Fig. S0. Which is further confirmed by XRD (X-Ray Diffractometer) analysis (Text S1 and Fig. S3) (Yu et al. 2009; Dubey et al. 2009; Garg and Bhakuni 1984; Huang et al. 2007). The absorption spectra of the reaction mixture at the different time are shown in Fig. 1. The absorption peak obtained maximum at 560 nm, which can be confidently ascribed to SPR of Cu° particles or CuNPs formation (Jain et al., 2015a, b). As expected the absorbance increased with increase in reaction time. The morphology of synthesized CuNPs was confirmed by TEM analysis and results indicate that particle shape is cubical with the average size in 48.01 nm given in Fig. 2(A) (Saranyaadevi et al., 2014). The SAED pattern recorded of CuNPs was rings like pattern shows synthesized CuNPs are highly crystalline in nature illustrated in Fig. 2(B). EDS spectrum gives a clear indication regarding the elements present in CuNPs dispersion. The strong signal of copper atom obtained at 1 keV confirmed that CuNPs contain pure copper depicted in Fig. S2. EDS spectra also show Carbon and Oxygen signals, which must be due to phytochemicals present in neem leaf broth (Valodkar et al., 2011). Thus these elements as the evidence for the organic substance attached to the surface of CuNPs. No other impurities were observed in EDS profile. Which is further confirmed by XRD (X-Ray Diffractometer) analysis (Text S1 and Fig. S3) (Yu et al. 2009). These synthesized CuNPs are stable for 2 months at 4 °C by the bio capping of neem leaf broth, which was confirmed by the FTIR spectra of synthesized CuNPs given in Fig. 3. Synthesized CuNPs exhibits major peaks at 2922 cm^{-1} (O–H stretching of phenolic group), 2371 cm^{-1} (C–N stretching of aromatic amine), 1631 cm^{-1} (C=O stretching), 1456 cm^{-1} (C=C stretching), 1384 cm^{-1} (aldehydic C–H stretching) suggests the presence of flavonoids and terpenoids, that may be responsible for reduction and stabilization process (Saranyaadevi et al., 2014; Velmurugan et al., 2014).

For instance, the synthesis process is also carried out at different temperature for investigating the effect of temperature on the morphology of synthesized NPs by SEM analysis shown in Fig. 4. The results illustrate that particles size decreases from 73.51 nm to 48.01 nm with increase in the temperature 65 °C–85 °C further increases in temperature resultant dispersion were agglomerated. The conversion rate of Cu^{2+} ions considerably increases by increasing reaction temperature (65 to 85 °C). But at high temperature, the synthesis rate is too high to control particle size. The resulting rate of growth and agglomeration, as well as nucleation of CuNPs, accelerated almost coincidently. So NPs formed with higher average size was precipitated.

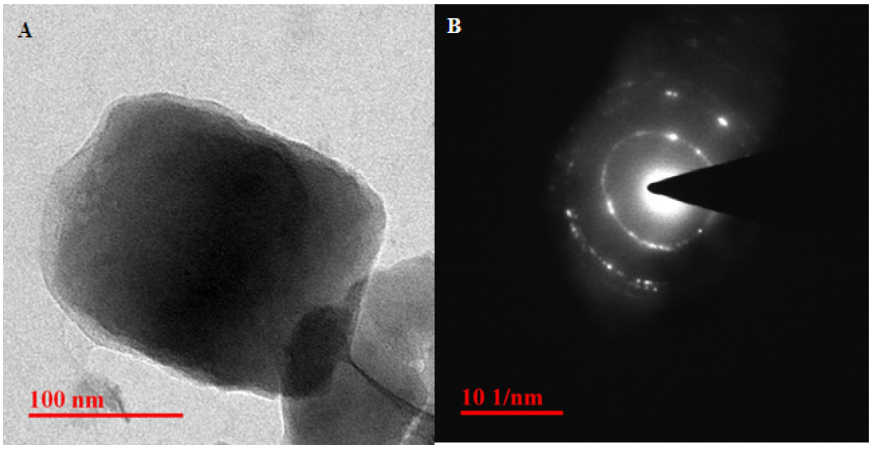

Fig. 2. (A) TEM image of synthesized copper nanoparticles, (B) SAED pattern of copper nanoparticles.

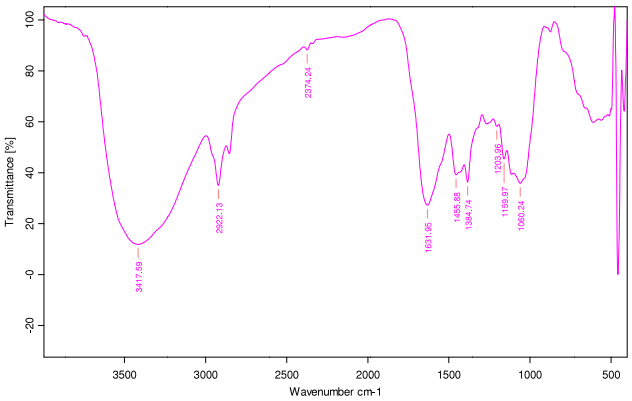

Fig. 3. FTIR spectra of synthesized CuNPs.

3.2. Spectra changes and identification of degradation route and products

Fig. 5 shows the UV–Vis spectra of the reaction mixture of Orange G initially consist of three main peaks at 254, 329, and 476 nm. The band at 245 and 329 nm arises from the π–π^* transition related to the aromatic ring attached to –N=N–group in the Orange G molecule, while 476 nm band could be assigned to the n–π^* transition of –N=N–group (Zhang et al., 2016a, b; Xu and Li, 2010; Meetani et al., 2011). As the degradation reaction proceeded, it was observed that the two characteristic absorption peaks at 329 and 476 nm decreased and almost disappeared within 60 min initiation of the reaction. This indicates that the chromophore and conjugated system were being destroyed, whereas the peak at 254 nm declined slowly, showing that the aromatic rings were still present.

In order to provide supportive evidence for the proposed degradation route, identification of degradation intermediates was carried out by LC-MS analysis of the dye solution in CuNPs/PMS system, at the different time interval of the degradation process. Fig. 6 showed the significant peaks present at the different time of degradation with corresponding m/z values 283, 239, and 175. The proposed degradation route revealed that $SO_4^{\bullet-}$ radicals (SRs) initially attacks on the aromatic ring, leading to the loss of characteristic fragments of 64 (–SO_2), 77 (–C_6H_5), and 30 (–NO) groups. Further, attacks by radicals, resultant the formation of the various hydroxyl substituted intermediates and finally into end products illustrated in Fig. 7.

3.3. Effect of experimental conditions

3.3.1. Dye dependence

Seven different concentration of dye aqueous solution (1.0×10^{-5} to 7.0×10^{-5} mol L^{-1}) were employed at the fixed concentration of PMS (5.0×10^{-4} mol L^{-1}) and other reactants. Fig. S3 indicates that the degradation rate constant initially increases with increasing dye concentration then tends towards a limiting value at higher dye concentration. The

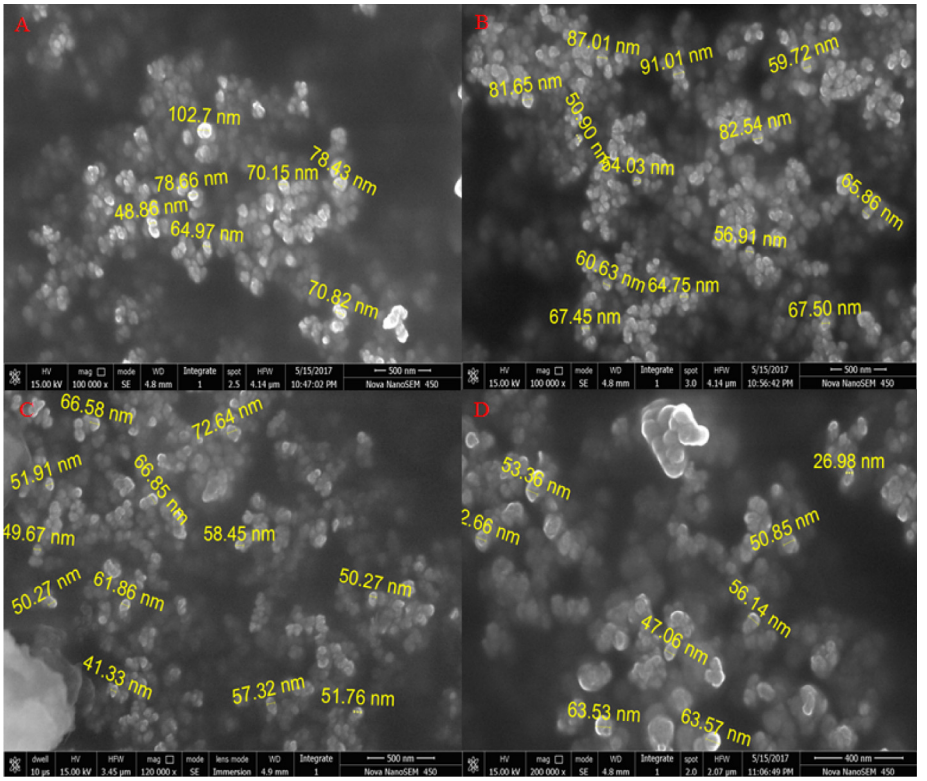

Fig. 4. SEM images of synthesized copper nanoparticles at the different temperature. The average particle size are (A) 65 °C, $d = 73.59$ nm (B) 75 °C, $d = 68.45$ nm (C) 80 °C, $d = 50.57$ nm (D) 85 °C, $d = 48.01$ nm.

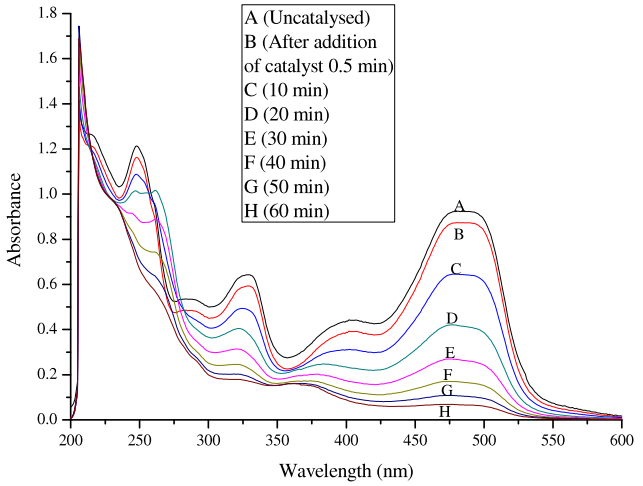

Fig. 5. UV–Vis adsorption spectra of oxidative degradation of Orange G at different time interval at fix [PMS] $= 5.0 \times 10^{-4}$ M, [Dye] $= 5.0 \times 10^{-5}$ M, [CuNPs] $= 1.0 \times 10^{-6}$ mol L^{-1}, pH 9.2 and temperature 30 °C.

results describe that at high dye concentration and constant PMS concentration a number of sulfate radicals were constant consequently degradation rate was constant.

3.3.2. Peroxomonosulfate dependence

PMS is a powerful oxidizing agent with a standard potential of $E^\circ = 2.5$ to 3.1 V and can be dominated by $SO_4^{\bullet-}$ radicals based mechanism and activated by transition metals (Nfodzo and Choi, 2011). Fig. S4 illustrates the effect of different concentration of PMS on Orange G degradation of the fixed concentration of other reactants. Increase in the concentration

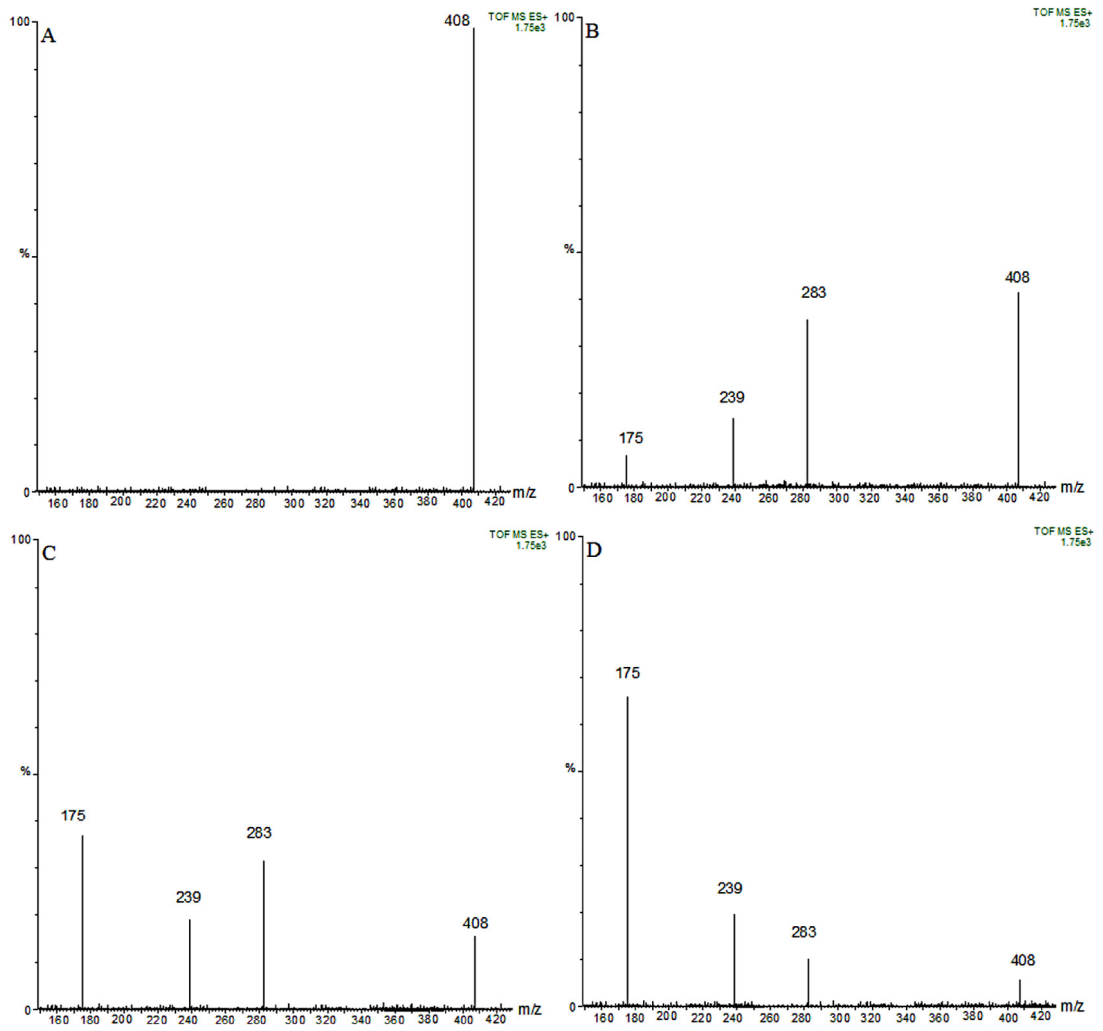

Fig. 6. LC-MS of Orange G degraded at (A) 0 min, (B) 20 min, (C) 40 min, (D) 60 min; in CuNPs/PMS system.

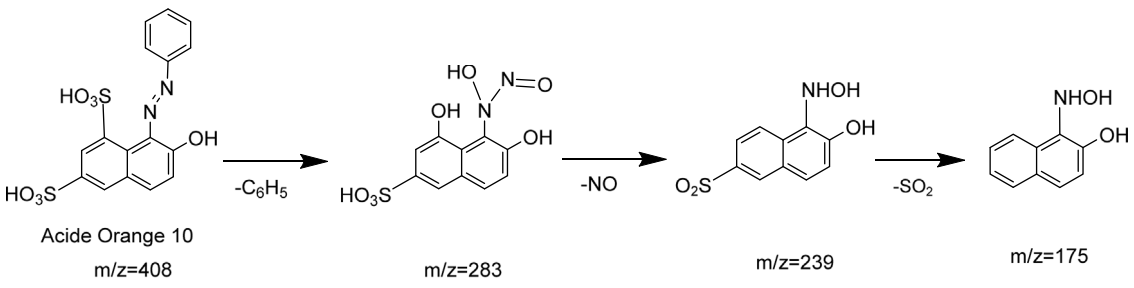

Fig. 7. Proposed oxidative degradation route of Orange G in CuNPs/PMS system.

of PMS contributes for significant degradation of Orange G. The degradation rate constant increased from 2.5×10^{-4} to 10.5×10^{-4} s^{-1} with the PMS concentration from 1.0×10^{-4} to 7.0×10^{-4} mol L^{-1}. The positive correlation of PMS concentration with the degradation rate of dye implies that PMS itself and either its secondary decomposition species accounted for the attack of dye molecules. The results are also consistent with the previous study on PMS activation by phosphate anion (Lou et al., 2014).

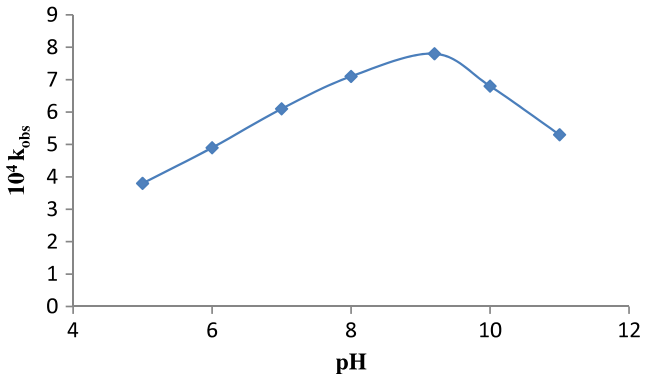

Fig. 8. Effect of variation of pH at fixed [Dye] = 5.0×10^{-5} mol L^{-1}, [PMS] = 5.0×10^{-4} mol L^{-1}, [CuNPs] = 1.0×10^{-6} mol L^{-1} and temperature 30 °C.

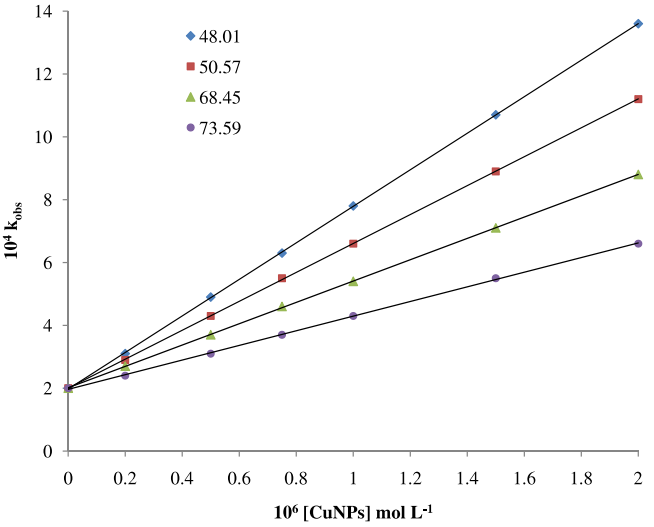

Fig. 9. Effect of [CuNPs] at different size in nm (A) 48.01, (B) 50.57, (C) 68.45, (D) 73.59 at fix [PMS] = 5.0×10^{-4} mol L^{-1} , [Dye] = 5.0×10^{-5} mol L^{-1}, pH 9.2 and temperature 30 °C.

3.3.3. *Effect of initial pH*

In order to find the optimal initial pH of the reaction mixture for the degradation of Orange G a series of experiments were conducted in CuNPs/PMS system at different pH (5 to 11) values. Earlier reports revealed that the pH of the solution can dramatically affect the degradation of synthetic dyes in AOPs (Huang et al., 2009; Zhong et al., 2012). It can be seen in Fig. 8 that the dye degradation rate is increased up to pH 9.2 and then decreases at higher pH. This effect reflects the result of the electrostatic attraction of the positively charged Cu^{2+} with the ionized dye upto the pH (9.2) then decrease in the degradation rate describes the difficulty of anionic dye in approaching the negative charge Cu^{-}at higher solution pH.

3.3.4. *Catalytic activity of copper nanoparticles*

The catalytic activity of CuNPs on the degradation of Orange G has been studied at varying concentrations (0.20×10^{-6} to 2.0×10^{-6} mol L^{-1}) of NPs and four different NPs, synthesized at four different temperatures (65, 75, 80 and 85 °C) with average sizes 73.59, 68.54, 50.57, and 48.01 nm respectively at fixed concentration of other reactants. The degradation rate increases with increase in the concentration of CuNPs (Fig. 9). The catalytic activity of CuNPs seems different at different temperature of the synthesis process. The difference in catalytic activity can be dependent on the size variation (73.59, 68.54, 50.57 and 48.01 nm) in synthesized CuNPs while keeping other reactant concentration and conditions are constant. The trend of the rate constant with the different size of NPs 48.01 > 50.57 > 68.54 > 73.59 nm is shown in Fig. 9. This effect reflects that smallest size gives a larger surface area: volume ratio and make its high surface reactivity. Thus it has a greater chance for contact with dye molecules, hence more degrade them (Samim et al., 2007; Jain et al., 2015a, b).

Table 1
Effect of neutral salts at 30 °C temperature, fix [Dye] = 5.0×10^{-5} mol L^{-1}, [PMS] = 5.0×10^{-4} mol L^{-1}, [CuNPs] = 1.0×10^{-6} mol L^{-1} and pH 9.2.

10^3 [Neutral salts] (mol L^{-1})	10^4 k_{obs} (s^{-1})		
	$NaNO_3$	NaCl	$NaHCO_3$
10.0	7.79	6.89	6.51
12.0	7.80	6.71	6.32
14.0	7.78	6.59	6.10
16.0	7.77	6.47	5.87
18.0	7.76	6.31	5.71
20.0	7.77	6.18	5.45

3.3.5. Effect of temperature

The effect of temperature on Orange G degradation with CuNPs/PMS system was investigated at three temperatures. As the temperature rises from 25 to 35 °C, the degradation rate constant increased from 6.6×10^{-4} to 8.8×10^{-4} s^{-1}. This result could be ascribed to thermal activation of PMS, subsequently decomposed faster at the higher temperature (Shi et al., 2015). According to the first order kinetics, the activation energy for Orange G degradation by CuNPs/PMS process was calculated by the Arrhenius equation. The value of activation energy (21.97 KJ mol^{-1}) indicates that the Orange G degradation in CuNPs/PMS process required moderate activation energy. Previous investigations reported that the value of activation energy on various catalysts could be different such as 88.45 kJ mol^{-1}on Carbon nanotubes/PMS–Orange G (Ming et al., 2016) 92.2 kJ mol^{-1}on Fe^{2+}/PMS–Orange G (Xu and Li, 2010). The low activation energy signified the CuNPs/PMS oxidation process was easy to occur and was very promising for the catalytic reaction.

3.3.6. Effect of neutral salts

NaCl, $NaNO_3$, $NaHCO_3$ salt are generally added to dye solution for adjusting the ionic strength and improving the fixation of dye on fabrics. Thus the effect of Cl^-, $NO_3{}^-$, $HCO_3{}^-$ ions on Orange G removal by CuNPs/PMS system was studied. The concentration of Cl^-, $NO_3{}^-$, and $HCO_3{}^-$ was varied from 10×10^{-3} to 20×10^{-3} mol L^{-1} at fix concentration of other reactants and constant conditions. As the concentration of Cl^- ions increased, an inhibition was observed. It may be chloride ions oxidize into less reactive chlorine species with sulfate radicals (Zhang et al., 2016a, b). The oxidative degradation rate also decreases as an increase in the concentration of bicarbonate ions ($HCO_3{}^-$), contribute to active $SO_4{}^{\bullet-}$ radicals convert into sulfate ions ($SO_4{}^{-2}$) whereas $NO_3{}^-$ ions have no obvious effect on the degradation of CuNPs/PMS system. The results illustrated in Table 1. Furthermore, it can be found that the anions could inhibit the degradation rate of Orange G and their inhibiting order is $NO_3{}^- < Cl^- < HCO_3{}^-$ (Xu and Li, 2010).

4. Conclusion

The use of neem leaf extract for preparation of CuNPs is inexpensive, easily scaled up and environmentally benign. The plant extract based synthesis can provide NPs of a controlled size and morphology. The present biomolecules in plant extract act as reducing and stabilizing agent. So in this report biosynthesized CuNPs have stability for two months at 4 °C temperature without any protecting gas. During synthesis process, the effect of different temperature on the size of CuNPs as well as an effect of the catalytic activity of different size NPs on degradation rate was also investigated. The smaller particle size of CuNPs, higher concentration of PMS, catalyst and higher temperature promoted the degradation of Orange G in CuNPs/PMS system. The end products of Orange G degradation were identified by LC-MS and the degradation pathways were proposed. The $NO_3{}^-$ ions have no effect whereas Cl^-, $HCO_3{}^-$ ions show inhibited effect on the performance of CuNPs/PMS system due to their scavenging effect on the reactive radical species.

Acknowledgments

This work was supported in part by Department of Science and Technology (SR/FST/CSI-172/2008 Dated on 10/11/2009) sponsored FIST Laboratory of our institution for experimental work, MNIT Jaipur for SEM and TEM analysis of synthesis of CuNPs, IIT Ropar for LC-MS measurement and University Grants Commission for financial support as JRF (Ref. No: 22/12/2013(ii) EU-V).

Conflict of interest

The authors have no conflicts of interest to declare.

Appendix A. Supplementary data

Supplementary material related to this article can be found online at https://doi.org/10.1016/j.eti.2018.03.005.

References

Adhikari, R., Gyawali, G., Cho, S.H., García, R.N., Sekino, T., Lee, S.W., 2014a. Er3+ /Yb3+ co-doped bismuth molybdate nanosheets upconversion photocatalyst with enhanced photocatalytic activity. J. Solid State Chem. 209, 74–81.

Adhikari, R., Gyawali, G., Kim, T.H., Sekino, T., Lee, S.W., 2014b. EDTA mediated microwave hydrothermal synthesis of WO3 hierarchical structure and its photoactivity under simulated solar light. JECE 2, 1365–1370.

Adhikari, R., Trital, H., Rajbhandari, A., Won, J., Lee, S.W., 2015. Microwave induced morphology evolution of bismuth tungstate photocatalyst: evaulation of phocatalytic activity under visible light. J. Nanosci. Nanotechnol. 15, 7249–7253.

Ahmad, A.A., Idris, A., Hameed, B.H., 2012. Color and COD reduction from cotton textile processing wastewater by activated carbon derived from solid waste in column mode. Desalin. Water Treat. 41, 224–231.

Ahmad, M., Teel, A.L., Watts, R.J., 2013. Mechanism of persulfate activation by phenols. Environ. Sci. Technol. 47, 5864–5871.

Anipsitakis, G.P., Dionysiou, D.D., 2004. Radical generation by the interaction of transition metals with common oxidants. Environ. Sci. Technol. 38, 3705–3712.

Anipsitakis, G.P., Tufano, T.P., Dionysiou, D.D., 2008. Chemical and microbial decontamination of pool water using activated potassium peroxymonosulfate. Water Res. 42, 2899–2910.

Behnajady, M.A., Eskandarloo, H., 2015. Preparation of TiO2 nanoparticles by the sol-gel method under different pH conditions and modeling of photocatalytic activity by artificial neural network. Res. Chem. Intermed. 41, 2001–2017.

Deng, Y., Zhao, R., 2015. Advanced oxidation process (AOPs) in wastwater treatment. Curr. Pollut. Rep. 1, 167–176.

El-Kheshen, A.A., El-Rab, S.F.G., 2012. Effect of reducing and protecting agents on size of silver nanoparticles and their anti-bacterial activity. Pharm. Chem. 4, 53–65.

Eskandarloo, H., Badiei, A., Behnajady, M.A., Ziarani, G.M., 2015. Photo and chemical reduction of copper onto anatase-type TiO2 nanoparticles with enhanced surface hydroxyl groups as efficient visible light photocatalysts. Photochem. Photobiol. 91, 797–806.

Eskandarloo, H., Badiei, A., Behnajady, M.A., Tavakoli, A., Ziarani, G.M., 2016. Ultrasonic-assisted synthesis of Ce doped cubic-hexagonal ZnTiO3 with highly efficient sonocatalytic activity. Ultrason. Sonochem. 29, 258–269.

Garg, H.S., Bhakuni, D.S., 1984. An isoprenylated flavanone from leaves of Azadirachta Indica. Phytochemistry 23, 2115–2118.

Hammami, S., Oturan, M.A., Oturan, N., Bellakhal, N., Dachraoul, M., 2012. Comparative mineralization of textile dye indigo by photo-Fenton process and anodic oxidation using boron-doped diamond anode. Desalin. Water Treat. 45, 297–304.

Harrelkas, F., Azizi, A., Yaacoubi, A., Benhammou, A., Pons, M.N., 2009. Treatment of textile dye effluents using coagulation–flocculation coupled with membrane processes or adsorption on powdered activated carbon. Desalination 235, 330–339.

Huang, J.L., Li, Q.B., Sun, D.H., Lu, Y.H., Su, Y.B., Yang, X., Wang, H., Wang, Y., Shao, W., He, N., Hong, J., Chen, C., 2007. Biosynthesis of silver and gold nanoparticles by novel sundried Cinnamomum camphora leaf. Nanotechnology. 18, 105104-1–105104-11.

Huang, Y.-H., Huang, Y.-F., Huang, C.-P., Chen, C.-Y., 2009. Efficient decolorization of azo dye Reactive Black B involving aromatic fragment degradation in buffered Co^{2+}/PMS oxidative processes with a ppb level dosage of Co^{2+}- catalyst. J. Hazard. Mater. 170, 1110–1118.

Jain, S., Jain, A., Kachhawah, P., Devra, V., 2015a. Synthesis and size control of copper nanoparticles and their catalytic application. Trans. Nonferrous Met. Soc. China 25, 3995–4000.

Jain, S., Nagar, N., Devra, V., 2015b. Synthesis and characterization of highly efficient copper nanoparticles and their catalytic application in oxidative kinetic study. Adv. Appl. Sci. Res. 6, 171–180.

Khouni, I., Marrot, B., Amar, R.B., 2012. Treatment of reconstituted textile wastewater containing a reactive dye in an aerobic sequencing batch reactor using a novel bacterial consortium. Sep. Purif. Technol. 87, 110–119.

Lou, X., Wu, L., Guo, Y., Chen, C., Wang, Z., Xiao, D., Fang, C., Liu, J., Zhao, J., Lu, S., 2014. Peroxymonosulfate activation by phosphate anion for organics degradation in water. Chemosphere 117, 582–585.

Meetani, M.A., Rauf, M.A., Hisaindee, S., Khaleel, A., Alzamly, A., Ahmad, A., 2011. Mechanistic studies of photoinduced degradation of Orange G using LC/MS. RSC Adv. 1, 490–497.

Ming, Z.L., Bin, C.J., Cong, F., Lu, Z., Mei, H.J., Bin, H.S., Wei, L.W., Ming, W.Z., Yin, H.T., 2016. Effect of chloride ions on degradation of Orange G with peroxymonosulfate activated by carbon nanotubes. China Environ. Sci. 36, 3591–3600.

Nfodzo, P., Choi, H., 2011. Triclosan decomposition by sulfate radicals: Effects of oxidant and metal doses. Chem. Eng. J. 174, 629–634.

Robinson, T., McMullan, G., Marchant, R., Nigam, P., 2001. Remediation of dyes in textile effluent: a critical review on current treatment technologies with a proposed Alternative. Bioresour. Technol. 77, 247–255.

Samim, M., Kaushik, N.K., Maitra, A., 2007. Effect of size of copper nanoparticles on its catalytic behaviour in Ullman reaction. Bull. Mater. Sci. 30, 535–540.

Saranyaadevi, K., Subha, V., Ravindran, R.S.E., Renganathan, S., 2014. Synthesis and Characterization of Copper Nanoparticle using *Capparis Zeylanica* leaf. Extract Int. J. Chem. Tech. Res. 6, 4533–4541.

Shi, Q., Li, A., Qing, Z., Li, Y., 2015. Oxidative degradation of Orange G by persulfate activated with iron-immobilized resin chars. J. Ind. Eng. Chem. 25, 308–313.

Valodkar, M., Jadeja, R.N., Thounaojam, M.C., Devkar, R.V., Thakore, S., 2011. Biocompatible synthesis of peptide capped copper nanoparticles and their biological effect on tumor cells. Mater. Chem. Phys. 128, 83–89.

Velmurugan, P., Anbalagan, K., Manosathyadevan, M., Lee, K.-J., Cho, M., Lee, S.-M., Park, J.-H., Oh, S.-G., Bang, K.-S., Oh, B.-T., 2014. Green synthesis of silver and gold nanoparticles using *Zingiber officinale* root extract and antibacterial activity of silver nanoparticles against food pathogens. Bioprocess Biosyst. Eng. 37, 1935–1943.

Wang, Y.R., Chu, W., 2011. Degradation of 2,4,5-trichlorophenoxyacetic acid by a novel Electro-Fe(II)/Oxone process using iron sheet as the sacrificial anode. Water Res. 45, 3883–3889.

Xu, X.-R., Li, X.-Z., 2010. Degradation of azo dye Orange G in aqueous solutions by persulfate with ferrous ion. Sep. Purif. Technol. 72, 105–111.

Yu, W., Xie, H., Chen, L., Li, Y., Zhang, C., 2009. Synthesis and characterization of monodispersed copper colloids in polar solvents. Nanoscale Res. Lett. 4, 465–470.

Zhang, J., Chen, M., Zhu, L., 2016a. Activation of peroxymonosulfate by iron-based catalysts for orange G degradation: role of hydroxylamine. RSC Adv. 6, 47562–47569.

Zhang, J., Chen, M., Zhu, L., 2016b. Activation of persulfate by Co_3O_4 nanoparticles for orange G degradation. RSC Adv. 6, 758–768.

Zhong, J.B., Li, J.Z., Lu, Y., Huang, S.T., Hu, W., 2012. Oxidation of methyl orange solutionwith potassium peroxydisulfate. Iran. J. Chem. Chem. Eng. 31, 21–24.

Zou, J., Ma, J., Chen, L., Li, X., Guan, Y., Xie, P., Pan, C., 2013. Rapid Acceleration of ferrous iron/peroxymonosulfate oxidation of organic pollutants by promoting Fe(III)/Fe(II) cycle with hydroxylamine. Environ. Sci. Technol. 47, 11685–11691.

Materials Chemistry and Physics 213 (2018) 44–51

Contents lists available at ScienceDirect

Materials Chemistry and Physics

journal homepage: www.elsevier.com/locate/matchemphys

Green synthesis and characterization of copper nanoparticles using *Azadirachta indica* leaves

Niharika Nagar, Vijay Devra*

Department of Chemistry, Janki Devi Bajaj Government Girls College, Kota, Rajasthan, 324001, India

HIGHLIGHTS

- Develop a novel, simple and greaner method for CuNPs synthesis by *A. indica* leaves.
- Effects of different reaction parameters on the formation of CuNPs were analyzed.
- Synthesized CuNPs are cubical and 48 nm size with high zeta potential (−17.5 mV).
- Biomolecules present in Neem leaves reduce Cu^{2+} ions and also stabilize NPs.

ARTICLE INFO

Article history:
Received 14 June 2017
Received in revised form
29 March 2018
Accepted 3 April 2018
Available online 9 April 2018

Keywords:
Green synthesis
Azadirachta indica
Copper nanoparticles
Experimental conditions
Characterization

ABSTRACT

Development of an eco-friendly process for the synthesis of copper nanoparticles (CuNPs) is an important aspect in the field of nanotechnology. In recent years the utilization of secondary metabolites from plant leaf broth has emerged as a novel technology for the synthesis of various nanoparticles. In this report, copper nanoparticles were synthesized by the leaf broth of *Azadirachta indica* and effect of different reaction parameters such as precursor salt concentration, leaf broth percentage, temperature and pH of the medium on the conversion rate and morphology of the CuNPs were analyzed. The plant biomolecules induce the reduction of Cu^{2+} ions to CuNPs and also act as a capping and stabilizing agent. The formation of CuNPs was monitored by absorbance spectra of UV-visible spectrophotometer at different stages during the synthesis process. The biosynthesized CuNPs were characterized by different instrumental techniques and results described the particles are crystalline, cubical shape with the average size 48 nm and highly stable. The optimum conditions for synthesis are as follows: percentage of leaf broth 20%, $[CuCl_2] = 7.5 \times 10^{-3}$ M, pH 6.6 and temperature 85 °C. The present study could prove to have an enormous impact in the immediate future to synthesize metallic nanoparticles on an industrial scale.

1. Introduction

Nanoparticles (NPs) are being considered to be the fundamental building blocks of nanotechnology. Nanotechnology branch is interdisciplinary which includes physics, biology, chemistry, medicines and material science. Presently, synthesis of metal NPs has been reported by many physical and chemical means [1–4]. All reported chemical methods and energy-intensive routes, which make these choices eco-hazardous and preclude their applications in biology, medicine, and clinical field. Therefore developing environmental friendly protocols are the need of the hour in nanomaterial synthesis [5–7]. A focused integration of bio and nano-techniques for biosynthesis of NPs, known as biotechnology has emerged from nanotechnology [8–10]. The recent emerging field of nano-biotechnology is at the primary stage of development due to lack of implementation of innovative methods in industrial scale and yet has been improved with the modern methods. There is a need to design an economic, commercially feasible as well as eco-friendly sustainable route for the synthesis of metal NPs in order to meet its growing demand in various sectors. The biosynthesis of NPs has been mainly focused on noble metal NPs like silver, gold, platinum [11–16] and their alloys. Amongst them, CuNPs are of great interest because of low cost, easy availability and properties possessed are similar o that of other metallic NPs [17–19]. CuNPs finds applications in heat transfer fluids, sensors,

* Corresponding author.
E-mail addresses: nnniharikanagar@gmail.com (N. Nagar), v_devra1@rediffmail.com (V. Devra).

https://doi.org/10.1016/j.matchemphys.2018.04.007
0254-0584/

antimicrobial and catalysis [20–23]. Existing literature also reports successful synthesis of CuNPs through a green route where *T. arjuna* bark extract [7], *Capparious zeylanica* leaf broth [24], *Ocimum sanctum* leaf broth [25,26], *Syzygium aromaticum* (cloves) aqueous extract [27] and *vitis vinifera* leaf broth [28], as well as various other plant extract, were used as reducing and capping agent. Characteristics of nanoparticles influenced by the source of the plant extract [29] because each plant extract contains unique concentration and the combination of organic reducing agents [30]. The invention of these new biological sources for the synthesis of CuNPs is more beneficial than physical and chemical methods as these sources are abundantly available, cost-effective and conveniently applicable. In fact, pure metallic CuNPs in an aqueous phase still challenge for the researcher. Furthermore, it is of interest to obtain monodispersed CuNPs by a simple and green route. The plant extracts often contain flavonoids, proteins, terpenoids, polyphenols etc., these biomolecules act as reducing agent for metal ion and capping agents to minimize the agglomeration of NPs, thus improves the biological potential. Here, we have developed a rapid, eco-friendly and convenient green route for the synthesis of CuNPs from salt cupric chloride using leaf broth of Indian medicinal plant namely *A. indica* (Neem). It belongs to Meliaceae family and found abundantly in India and in nearby subcontinents. Although leaf broth of neem is used for the synthesis of various metal NPs like silver, gold, silver-gold alloys [11,29] in our best knowledge, there are no reports on the synthesis of CuNPs using the leaf broth of *A. indica*.

Therefore, the aim of present reports is to synthesize CuNPs using leaf broth of *A. indica* as a reducing and capping agent. The synthesized CuNPs are stable for a long time in colloidal condition at 4 °C temperature. The influence of different parameters on the course of reaction such as reactant concentration, temperature, and pH was examined. The plant-mediated synthesized CuNPs were characterized by different instrumental techniques and studied in details with all of their properties significant to prevailing technologies.

2. Experimental

2.1. Material and preparation of leaf broth

Cupric chloride dihydrate (E. Merck) was used as a precursor salt and neem (*Azadirachta indica*) leaves were collected from Kota, Rajasthan, India. Deionized water was used throughout the study. Fresh and healthy leaves of neem rinsed thoroughly 2–3 times with deionized water to remove dust and unwanted particles. Leaves were dried in an oven for 15 min at 50 °C temperature. The 250 mL Erlenmeyer flask containing 20 g of small pieces of leaves with 100 mL deionized water was heated at 60 °C temperature for 20 min. Obtained leaf broth was filtered twice through Whatman paper and stored at 4 °C temperature for further experiments.

2.2. Green synthesis of copper nanoparticles

In a synthetic procedure, CuNPs were obtained via a green reduction route. The flask containing an aqueous solution of salt $CuCl_2 \cdot 2H_2O$ (7.5×10^{-3} M) was heated to 85 °C in oil bath with magnetic stirring then neem leaves broth (20%) were added dropwise to this solution. At different time intervals, the color of dispersion was gradually changed from green, yellow, orange, radish brown, brown and finally dark brown with the number of intermediate stages. The resulting dark brown color solution was centrifuged for 15 min at 6000 rpm. The supernatant dispersion was placed at 4 °C temperature for two months. Different spectrophotometric techniques like SEM, TEM, XRD, FTIR, and Zetasizer analysis were used for investigating the morphology, crystalline nature, functional group and stability of synthesized CuNPs.

2.3. Characterization

Characteristic optic properties of the colloidal NPs were recorded using UV 3000$^+$ LABINDIA double beam spectrophotometer (Path length 1.0 cm spectral range from 200 nm to 800 nm). FTIR Spectra of neem leaf broth and synthesized CuNPs were recorded as KBr pellets on ALPHA-T –Bruker model in the range of 4000–400 cm^{-1}. Morphological study of the CuNPs was carried out by SEM images analysis on a Nova Nano FE-SEM 450 (FEI), for analysis dispersed NPs were centrifuged (Laboratory Centrifuges Remi, model R-8C) and ultrasonicated (Ultramet 2005 (Buehler), USA) for 40 min 30 μL aliquots were then extracted deposited on the stub for SEM analysis. TEM (Tecnai G_2 20 (FEI) S-Twin model operating at 200 kV) images were recorded to confirm the shape of newly synthesized CuNPs. For TEM analysis, the sample prepared by mounting one drop of ultrasonicated dispersed suspension on standard carbon-coated copper grids and then dried under an IR Lamp for 50 min. XRD characterization was done by using XPERT-PRO X-Ray Diffractometer of Cu K_α radiation ($\lambda = 0.1540$ nm) with a scanning rate of 2°/min and 2θ ranging from 10° to 89°. The stability of synthesized CuNPs was determined by Zetasizer ver. 7.11 Malvern and pH measured by MAC (MSW-552) digital pH meter.

3. Result and discussion

Biological synthesis of nanoparticles using the plant as bio reductants can have advantages over other biological processes because it eliminates the process of maintaining cell culture and can be suitable scale up for large-scale synthesis. In this pursuit, here an aqueous extract of leaf of *Azadirachta indica* was used as a reactant to nucleate nanoparticles in solution. The formation of CuNPs was confirmed primarily basis on the change in colour of reaction mixture and also by UV-visible spectroscopy. As the leaf broth was added to the $CuCl_2$ solution, the color of the solution changed from light blue to green and finally, dark brown indicates the formation of CuNPs (Fig. 1). The color change in aqueous solution is due to surface Plasmon resonance (SPR) phenomenon. In this investigation, the obtained results are interesting because it can serve as a foundation in terms of identification of potential medicinal plants for synthesizing CuNPs.

The biomolecules such as Terpenoids, nimbaflavone, and

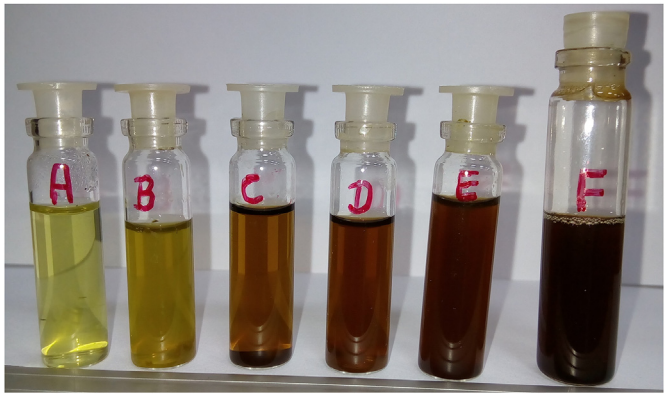

Fig. 1. Observation of color changes during synthesis of Copper nanoparticles at different time intervals: (A) 0 h, (B) 4 h, (C) 10 h, (D) 18 h, (E) 24 h, (F) 28 h. (For interpretation of the references to color in this figure legend, the reader is referred to the Web version of this article.)

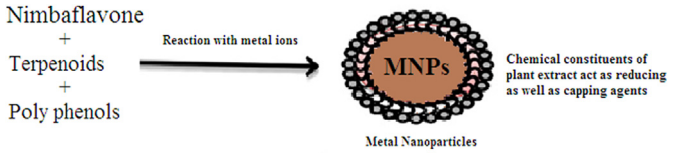

Fig. 2. Possible constituents of plant extract responsible for the bioreduction of metal ions.

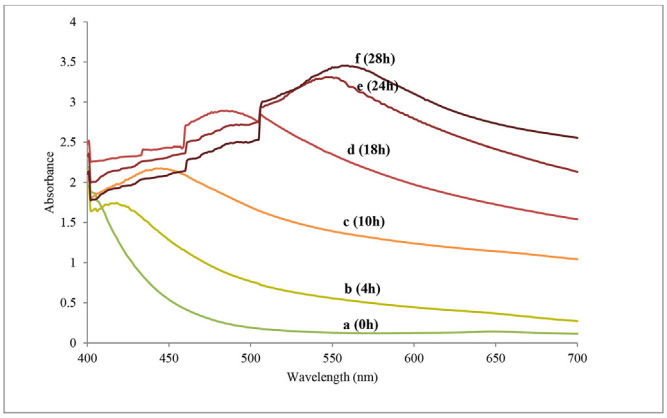

Fig. 3. UV-Visible absorption spectra of copper nanoparticles as a function of wavelength versus absorbance at a different time interval during the synthesis process.

polyphenols are present in *A. indica* leaf broth, which can reduce metal ions to metal NPs (Fig. 2) [31–33].

The possible equation for the synthesis of CuNPs are —

$$Cu^{+2}_{(aq)} + A.indica \text{ leaf broth} \xrightarrow[85\ ^{\circ}C]{stirring} [Cu/A.indica \text{ leaf broth}]^{+2} \quad (1)$$

$$[Cu/A.indica \text{ leaf broth}]^{+2} \xrightarrow[85\ ^{\circ}C]{stirring \text{ for } 28h} [Cu/A.indica \text{ leaf broth}] \quad (2)$$

After the dispersion of copper ions in the *A. indica* leaf broth matrix (Equation (1)), the leaf broth was reacted with $Cu^{+2}_{(aq)}$ to form

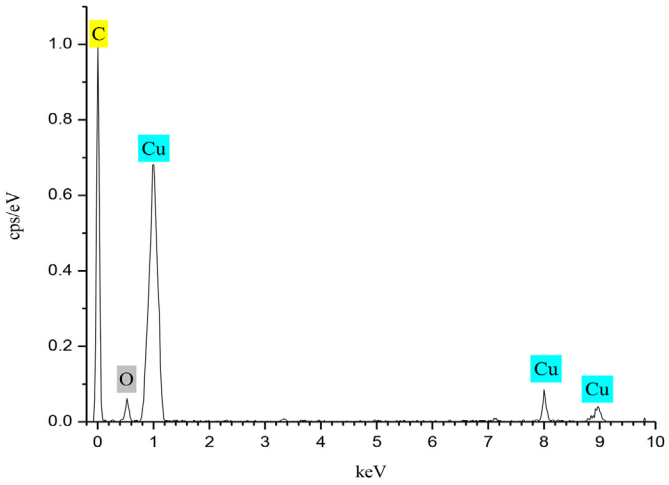

Fig. 5. EDS spectra of synthesized CuNPs.

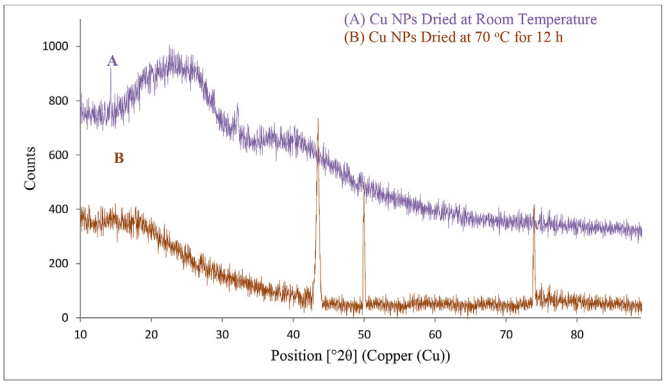

Fig. 6. XRD of biosynthesized Copper Nanoparticles (A) Dried at room temperature, (B) Vacuum dried at 70 °C for 12 h.

[Cu/*A. indica* leaf broth]$^{+2}$ complex, which further reacts with functional group of *A. indica* leaf broth to form [Cu/*A. indica* leaf broth] (Equation (2)).

UV-visible absorbance spectroscopy has been proved to be a very useful technique for the detection of synthesized metallic NPs because the peak position and shape of the spectra are sensitive to

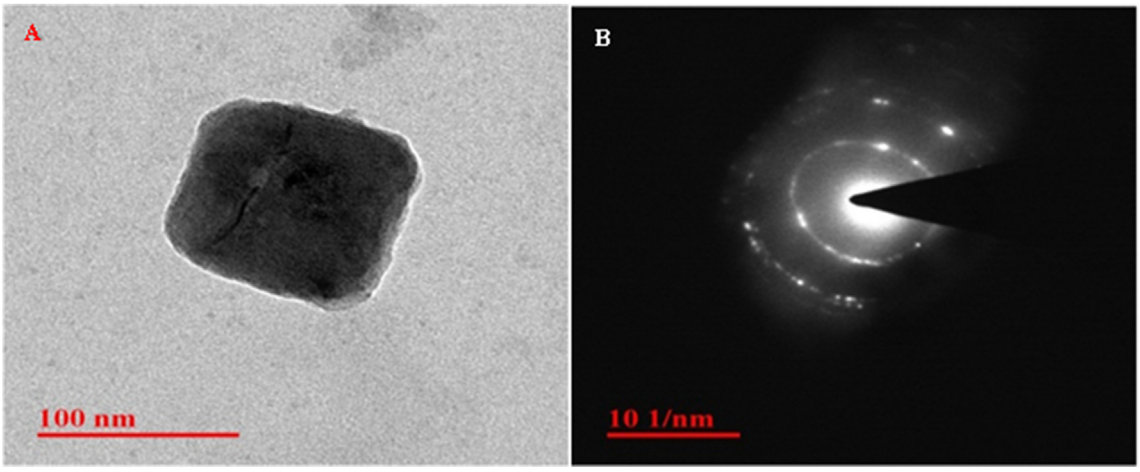

Fig. 4. (A) Tem image of synthesized Copper Nanoparticle, (B) SAED pattern of Copper Nanoparticles.

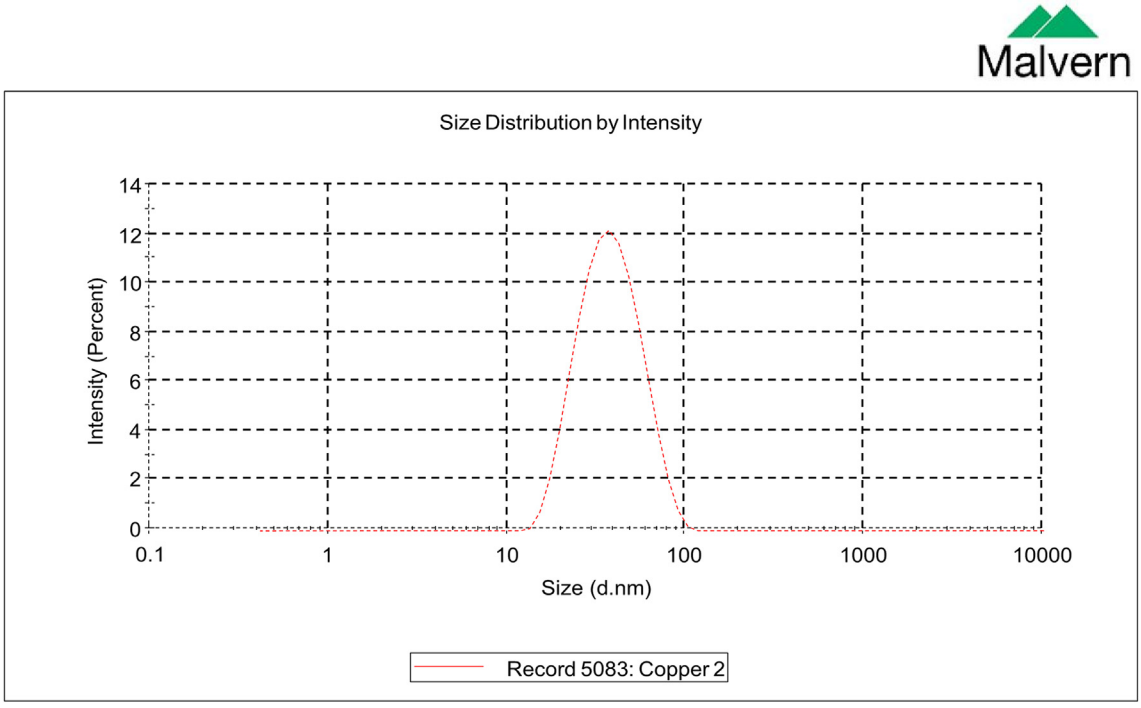

Fig. 7. Particles size distribution of synthesized Copper Nanoparticles.

the particle size. The UV-visible spectra of dispersion were recorded at different time intervals from the initiation of reaction (Fig. 3). The intensity of SPR peak increased as the passage of time, which indicated the continued reduction of copper ions into CuNPs. The absorption peak maximum at 560 nm, which can be confidently ascribed to the SPR of CuNPs formed [34]. The absorption band for CuNPs has been reported to be in the range of 500–600 nm [7]. The shape of synthesized CuNPs was cubical, confirmed by the TEM analysis [24] (Fig. 4A, S1) and TEM results shows the synthesized NPs are surrounded by a thin layer of capping organic material from neem leaf broth. The Selected Area Electron Diffraction (SAED) pattern recorded of CuNPs was a ring like a pattern shown synthesized CuNPs are highly crystalline (Fig. 4B) [18].

The EDS spectra of synthesized NPs give a clear indication regarding the elements of CuNPs. The strong signal of copper atom confirmed that CuNPs contain pure copper (Fig. 5). The element of Carbon and oxygen are contaminated all around the peaks, which must be due to phytochemicals present in plant extract [35]. Thus these elements as the evidence for the organic substance attached to the CuNPs. No other impurities were observed in EDS profile.

Fig. 6 A presents the XRD pattern of synthesized CuNPs dried at room temperature, observation shows the CuNPs capped by

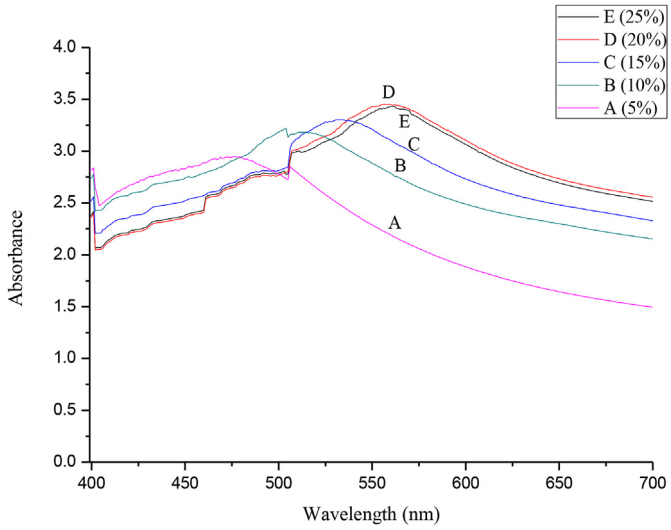

Fig. 8. UV-Visible absorption spectra of synthesized CuNPs recorded at various neem leaf broth percentage.

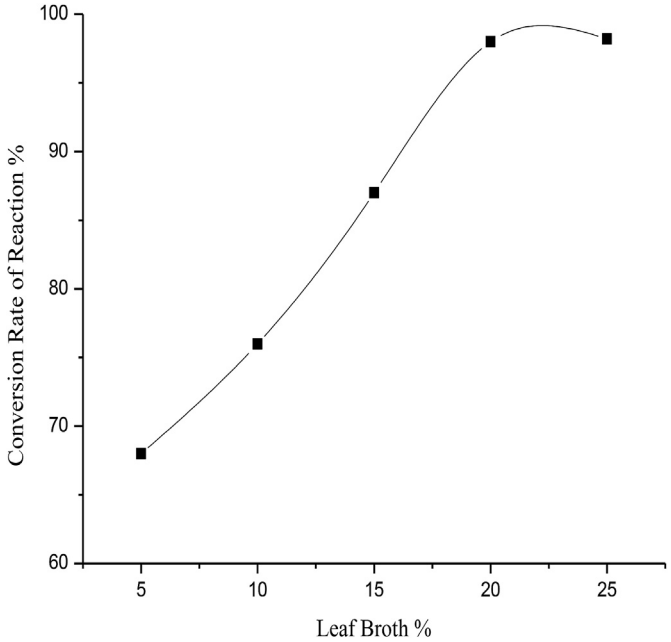

Fig. 9. Effect of various leaf broth percentage on the conversion rate of reaction at constant $[CuCl_2 \cdot 2H_2O] = 7.5 \times 10^{-3}$ M, pH = 6.6 and Temperature 85 °C.

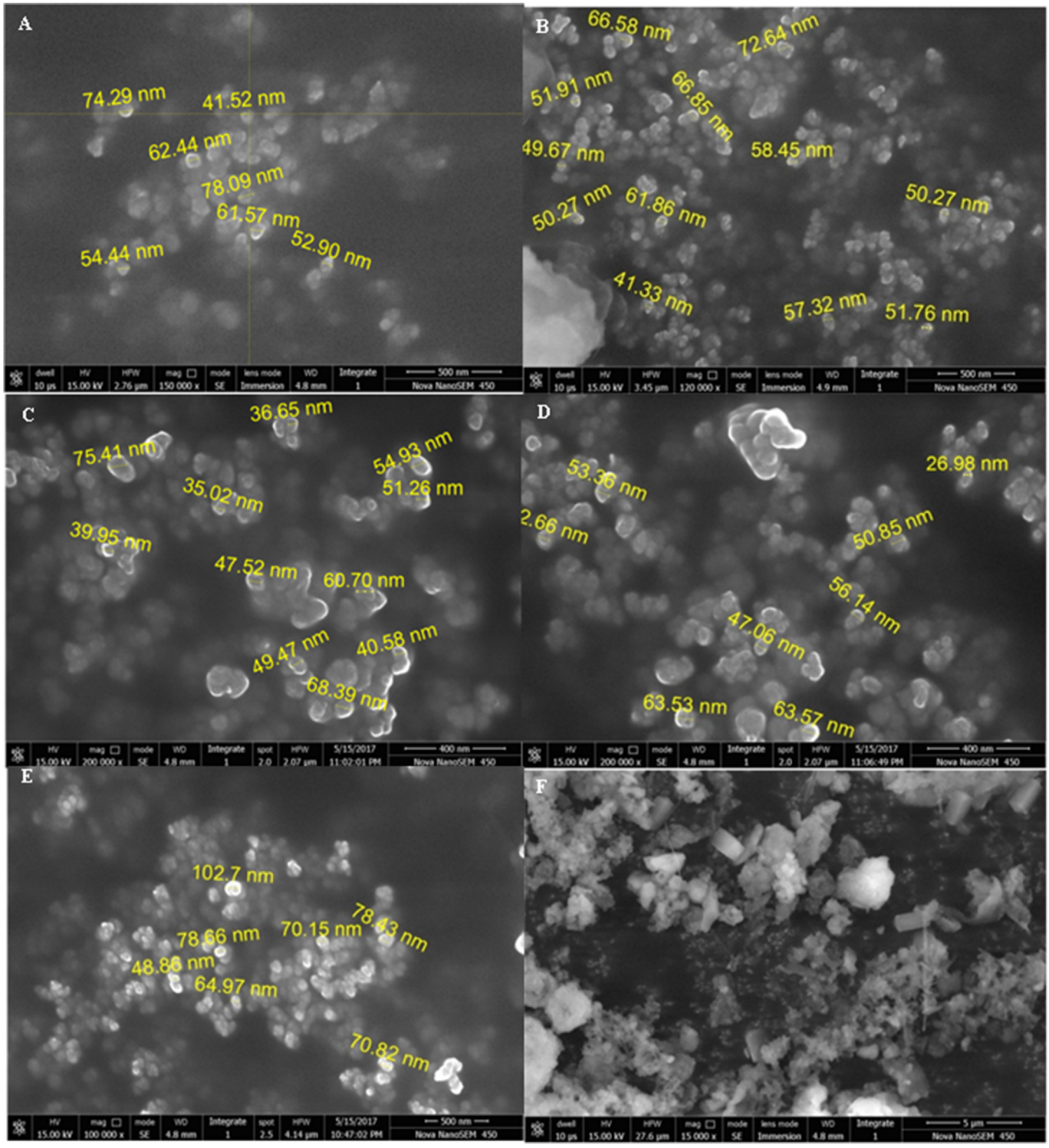

Fig. 10. SEM images of synthesized Copper nanoparticles at different initial concentration of $CuCl_2$ (A) 6×10^{-3} M, (B) 6.5×10^{-3} M, (C) 7×10^{-3} M, (D) 7.5×10^{-3} M, (E) 8×10^{-3} M, (F) 10×10^{-3} M.

biomolecules but not give proper information about crystalline nature. Whereas the CuNPs dried in vacuum at 70 °C for 12 h, gives a sharp peak at $2\theta = 43.5°$, 49.9° and 74.01° corresponding to (111), (200) and (220) representing a face-centered cubic (FCC) structure of copper. Which are closely matched with the values of FCC phase copper reported by S. Yallappa et al. Above all, it is encouraging to note that the 2θ values of the synthesized CuNPs are also matched with joint committee for powder diffraction standard (JCPDS). The Synthesized CuNPs were found to be pure without any impurities like CuO, Cu_2O, $Cu(OH)_2$ [36]. Furthermore, the average particle size of NPs was 48 nm was calculated by well-known Scherer equation.

Dynamic light scattering result gives the information about the size distribution of NPs. Fig. 7 indicates the size of CuNPs situated in

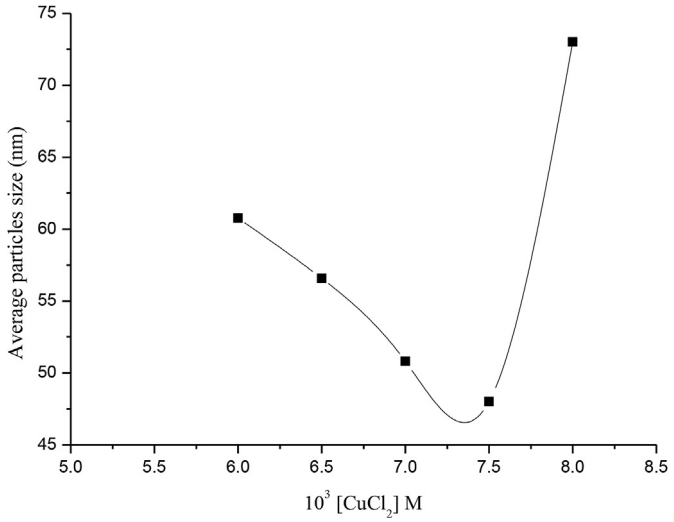

Fig. 11. Effect of different concentration of [$CuCl_2 \cdot 2H_2O$] on average particle size Copper nanoparticles at leaf broth = 20%, pH = 6.6 and Temperature 85 °C.

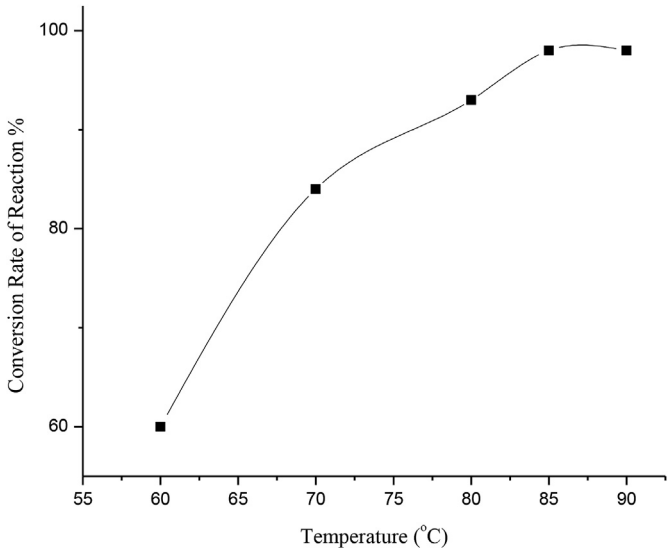

Fig. 12. Effect of Temperature on conversion rate of Copper Nanoparticles synthesis at [$CuCl_2 \cdot 2H_2O$] = 7.5×10^{-3} M, leaf broth = 20% and pH = 6.6.

between 35 and 102 nm range with an average particle size 48 nm of CuNPs.

3.1. Effect of leaf broth percentage

The effect of various leaf broth percentages on the synthesis process has been studied by UV-visible absorbance spectroscopy as shown in Fig. 8. The absorption peak is increasingly broadening with an increasing leaf broth percentage. At low percentage of leaf broth (5%) a weak absorption peak was observed at wavelength 506 nm, may be an insufficient reduction of copper ion. As the percentage of leaf broth increases up to 20% the intensity of SPR peak also increases. Such effect was also confirmed by a plot of the conversion rate of reaction versus different percentage of leaf broth (Fig. 9). The results illustrated that conversion rate of reaction increases with increases in leaf broth percentage up to 20% after that increasing trend not distinct, indicating the agglomeration of colloidal CuNPs at the higher percentage of leaf broth. It is due to the excess number of biomolecules present at the high percentage, secondary reduction process initiates on the surface of the perform nuclei, resultant growing the particle size. Therefore, the optimal leaf broth percentage is 20 for the synthesis of CuNPs [37]. These results are consistent with observed UV-visible spectra at different leaf broth percentage.

3.2. Effect of initial concentration of precursor salt

The effect of initial concentration of precursor salt on the formation of CuNPs studied at the concentration of precursor salt between 6×10^{-3} to 10×10^{-3} M. Formation of CuNPs in the dispersion occurs in two stages, the first stage is to generate copper nuclei and the second stage is the growth of copper. So it is important to optimize the initial concentration of procures salt to copper nuclei must generate faster and grows up slower [34]. The results of SEM images shows synthesized CuNPs with the particle size in the range of 48.01–78.51 nm [38] (Fig. 10). The green synthesized CuNPs size is highly depending on the concentration of precursor salt. It was confirmed that the concentration of $CuCl_2$ increased from 6×10^{-3} M to 7.5×10^{-3} M, the particle size of NPs decreases after that increase in the concentration of salt, particles size increased (Fig. 11). It can be seen that an increase in the concentration of precursor salt, the copper nuclei rises and smaller particles size are obtained correspondingly. But an excess number of nuclei will be generated at high reactant concentration so results in the agglomeration of the nuclei and growth of particles size. Similarly, aggregation of Nanoparticles was earlier reported by G. Annadurai et al. by using the leaf extract of *Morinda tinctoria* in the reduction of silver ions [39]. So the optimal concentration of precursor salt is 7.5×10^{-3} M for the synthesis of CuNPs.

3.3. Effect of temperature

The effect of temperature on the synthesis of CuNPs was studied by the conversion rate of a process at an optimal concentration of reactants. The reduction of Cu^{2+} ions was not completed at 60 °C temperature due to insufficient for the reaction. It can be seen from Fig. 12 that conversion rate of Cu^{2+} ions considerable increases when the temperature goes up (60–85 °C), but the synthesis rate is too high when increasing to a certain temperature. In the reaction system, the effect on the nucleation rate by temperature is greater than that the growth rate, therefore the nucleation rate is faster than growth rate when the temperature increases. But the nuclei surface activity is enhanced when the temperature is too high, which promotes the nuclei to colloid and agglomerated. Therefore the optimal reaction temperature is 85 °C.

3.4. Effect of pH

pH of the reaction dispersion is another important parameter for the synthesis of NPs. Variation in pH affects the synthesis rate and morphology of NPs. Capping and stabilizing ability is dependent on the charge of biomolecules, which might affect by pH. It

Table 1
Effect of pH on average particles size at [$CuCl_2 \cdot 2H_2O$] = 7.5×10^{-3} M, leaf broth = 20% and Temperature 85 °C.

S. No.	pH	Average Particle Size
1	4.7	CuNPs were not formed
2	6.0	56 nm
3	6.6	48 nm
4	8.4	60 nm
5	9.3	73 nm

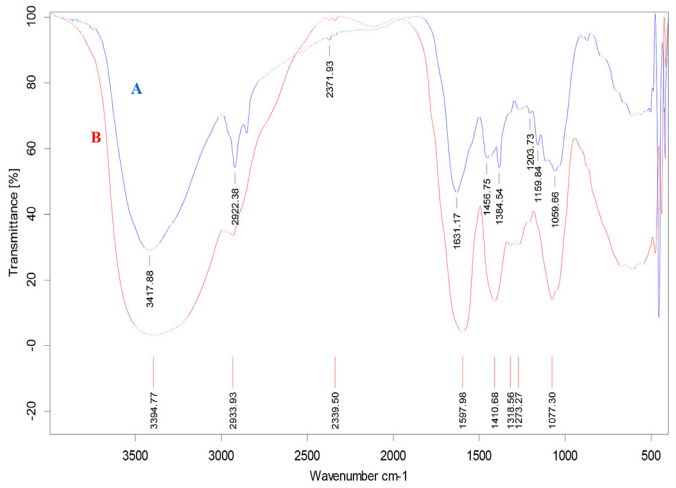

Fig. 13. Comparative FTIR spectra of (A) synthesized CuNPs and (B) Neem leaf broth.

was observed that in acidic pH, NPs were not formed. It indicates acidic pH suppresses the NPs synthesis. Under the acidic condition, such biomolecules are likely to be inactivated so that NPs synthesis could not occur at pH 4.7. At higher pH (6–6.6) however, more number of small-sized NPs were synthesized due to the availability of functional group for copper binding (Table 1). Interestingly, even high pH was also found to efficient in producing NPs, but they agglomerated and formed large size NPs. Therefore the pH 6.6 is favorable for the biosynthesis of CuNPs. It has been also observed that during synthesis process the pH of the medium decreases due to release of H^+ ions by the species of leaf broth at their oxidation in presence of Cu^{2+} ions [7].

3.5. The stability of synthesized copper nanoparticles

The stability of NPs is a very important key factor for their application [34]. The NPs are generally stabilized with capping agents such as polymers, surfactant etc [40,41]. Here, we report the synthesized CuNPs are stable for 2 months at 4 °C by the bio capping of leaf broth, which was confirmed by the comparative FTIR spectra of pure neem and bio-reduced synthesized CuNPs (Fig. 13). Synthesized CuNPs exhibits major peaks at 2922 cm^{-1} (O-H stretching of phenolic group), 2371 cm^{-1} (C-N stretching of aromatic amine), 1631 cm^{-1} (C=O stretching), 1456 cm^{-1} (C=C stretching), 1384 cm^{-1} (aldehydic C-H stretching) correspond to the neem leaf broth, suggests the presence of flavonoids, terpenoids and polyphenols, that may be responsible for reduction and stabilization process [24,42]. Also, the band observed at around 1077 cm^{-1} was attributed to the C-O stretching, which is characteristic of ether functional moiety. S. S. Shankar et al. reported that these biomolecules bounded on the surface of *Azadirachta indica* leaf extract mediated synthesized AgNPs [29].

Further, the stability of synthesized CuNPs was determined by zeta potential value. The value of zeta potential gives the degree of electrostatic repulsion between adjacent, similarly charged particles in the dispersion. The high magnitude of zeta potential value shows the great stability of NPs [43,44]. The result of the zeta potential of synthesized CuNPs has been found as a sharp peak at −17.5 mV (Fig. 14) suggests that biosynthesized NPs are highly stable.

4. Conclusion

We have synthesized CuNPs by the *A. indica* leaf broth by a novel biological synthesis technique which is simple and environmentally benign. It is an easy, cost-effective and doesn't involve any

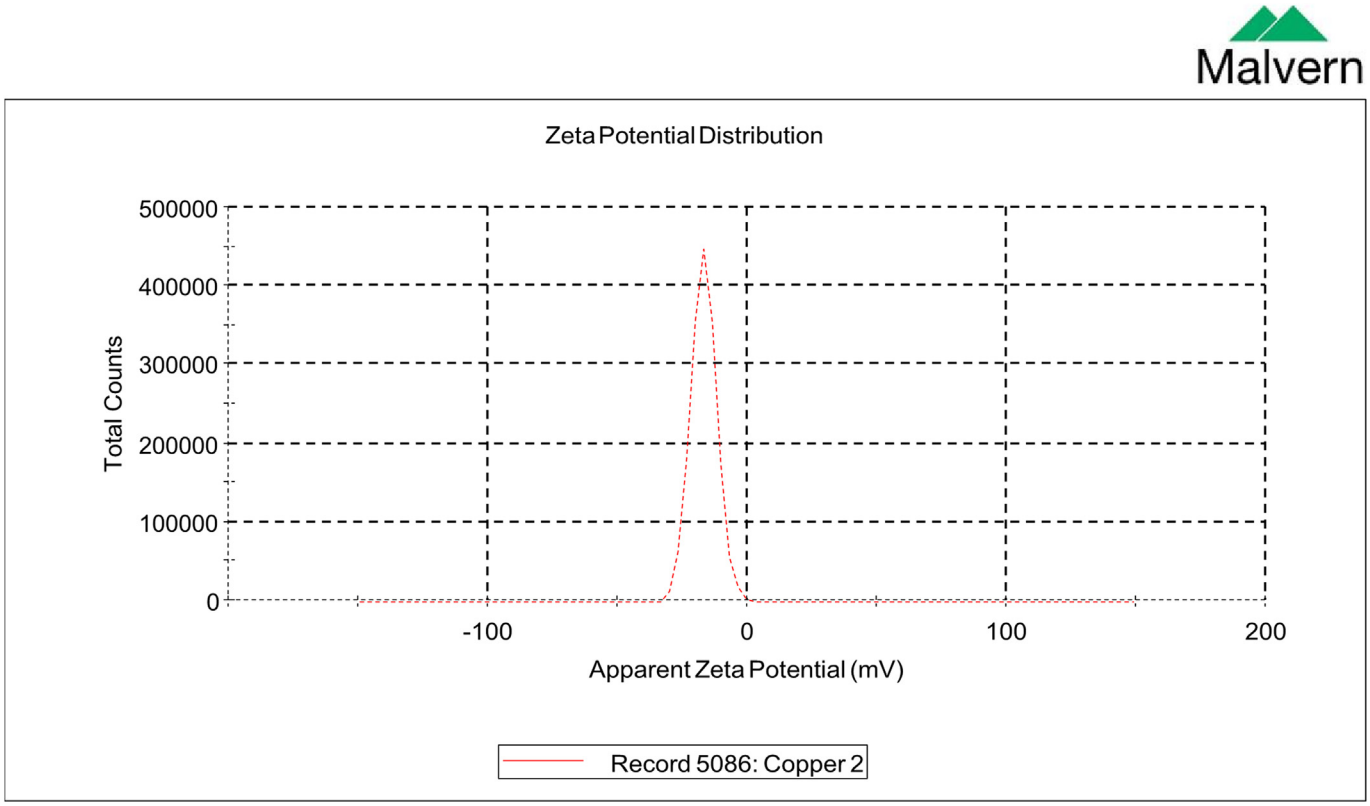

Fig. 14. Zeta potential of synthesized CuNPs.

harmful and toxic chemicals. The biomolecules present in the leaf broth not only reduce the metal ions and also stabilize the metal NPs. Different reaction conditions were analyzed by the different instrumental techniques in the synthesis process. Synthesized CuNPs are highly crystalline, cubical in shape with an average size 48 nm and stable for 2 months at 4 °C due to high zeta potential (−17.5 mV) under optimum conditions. The rate of reduction of metal ions by neem leaf broth is much faster than earlier reported studies using micro-organisms, highlighting that nanoparticle biological synthesis methodologies will achieve the rate of synthesis comparable to those of chemical methods.

Acknowledgment

This work was supported in part by Department of Science and Technology sponsored FIST Laboratory (SR/FST/CSI-172/2008 Dated 10/11/2009) of our institution for experimental work and University Grants Commission for financial support as JRF (Ref. No: 22/12/2013(ii) EU-V Dated 01/07/2014). We are grateful to SAIF Panjab University Chandigarh and MNIT, Jaipur for characterization techniques.

Appendix A. Supplementary data

Supplementary data related to this article can be found at https://doi.org/10.1016/j.matchemphys.2018.04.007.

References

[1] M.S. Niasari, Z. Fereshteh, F. Davar, Synthesis of oleylamine capped copper nanocrystal via thermal reduction of a new precursor, Polyhedron 28 (1) (2009) 126–130.
[2] M.S. Niasari, F. Davar, Synthesis of copper and copper (I) oxide nanoparticles by thermal Decomposition of A New precursor, Mater. Lett. 63 (3–4) (2009) 441–443.
[3] Q.-L. Zhang, Z.-M. Yang, B.-J. Ding, X.-Z. Lan, Y.-J. Guo, Preparation of copper nanoparticles by chemical reduction method using potassium borohydride, Trans. Nonferrous Met. Soc. China 20 (2010) 240–244.
[4] P. Pulkkinen, J. Shan, K. Leppanen, A. Kansakoshi, A. Laiho, M. Jarn, H. Tenhu, Poly(Ethylene imine) and tetraethylenepentamines as protecting agents for metallic copper nanoparticles, Appl. Mater. Interfaces 1 (2) (2009) 519–525.
[5] V. Sivanandam, M. Purushothaman, M. Karunanithi, Green synthesis of silver nanoparticles using plant leaf extract and evaluation of their antibacterial and in vitro antioxidant activity, Asian. Pac. J. Trop. Biomed 1 (2012) 1–8.
[6] A. Verma, M.S. Mehata, Controllable synthesis of silver nanoparticles using Neem leaves and their antimicrobial activity, J. Radiat. Res. Appl. Sci. 9 (1) (2016) 109–115.
[7] S. Yallappa, J. Manjanna, M.A. Sindhe, N.D. Satyanarayan, S.N. Pramod, K. Nagaraja, Microwave assisted rapid synthesis and biological evaluation of stable copper nanoparticles using T. arjuna bark extract, Spectrochem. Acta A Mol. Biomol. Spectrosc 110 (2013) 108–115.
[8] D.K. Sobha, K. Surendranath, V. Meena, K.T. Jwala, N. Swetha, K.S.M. Latha, Emerging trends in nanobiotechnology, J. Biotech. Mol. Bio. Rev. 5 (1) (2010) 001–012.
[9] K. Sahayaraj, S. Rajesh, Bionanoparticles synthesis and antimicrobial applications, in: A. Méndez-Vilas (Ed.), Science against Microbial Pathogens: Communicating Current Research and Technological Advances, 2011, pp. 228–244.
[10] N. Krithiga, A. Jayachitra, A. Rajalakshmi, Synthesis, characterization and analysis of the effect of copper oxide nanoparticles in biological systems, An Ind. J. NanoSci. 1 (1) (2013) 6–15.
[11] N. Nagar, S. Jain, P. Kachhawah, V. Devra, Synthesis and characterization of silver nanoparticles via green route, Korean J. Chem. Eng 33 (10) (2016) 2990–2997.
[12] P. Banerjee, M. Satapathy, A. Mukhopahayay, P. Das, Leaf extract mediated green synthesis of silver nanoparticles from widely available Indian plants: synthesis, characterization, antimicrobial property and toxicity analysis, Bioresourc. Bioprocess 1 (3) (2014) 1–10.
[13] D. Philip, C. Unni, S.A. Aromal, V.K. Vidhu, Murraya koenigii leaf-assisted rapid green synthesis of silver and gold nanoparticles, Spectrochem. Acta A Mol. Biomol. Spectrosc 78 (2) (2011) 899–904.
[14] S. Iravani, Green synthesis of metal nanoparticles using plants, Green Chem. 13 (2011) 2638–2650.
[15] O.V. Kharissova, H.V.R. Dias, B.I. Kharisov, B.O. Pérez, V.M. Jiménez Pérez, The greener synthesis of nanoparticles, Trends Biotechnol. 31 (2013) 240–248.
[16] A.K. Mittal, Y. Chisti, U.C. Banerjee, Synthesis of metallic nanoparticles using plant extracts, Biotechnol. Adv. 31 (2013) 346–356.
[17] A. Umer, S. Naveed, N. Ramzan, M.S. Rafiqui, Selection of a suitable method for the synthesis of Copper nanoparticles, Nano 7 (5) (2012), 1230005-1-1230005-18.
[18] S. Jain, A. Jain, P. Kachhawah, V. Devra, Synthesis and size control of copper nanoparticles and their catalytic application, Trans. Nonferrous Met. Soc. China 25 (2015) 3995–4000.
[19] M. Tiwari, P. Jain, R.C. Hariharapura, K. Narayanan, B.K. Udaya, N. Udupa, J.V. Rao, Biosynthesis of copper nanoparticles using copper-resistant Bacillus cereus, a soil isolate, Process Biochem. 51 (2016) 1348–1356.
[20] V. Trisaksri, S. Wongwises, Critical review of heat transfer characteristics of nanofluids, Renew. Sust. Energ. Rev. 11 (2007) 512–523.
[21] E.K. Athanassiou, R.N. Grass, W.J. Stark, Large-scale production of carbon-coated copper nanoparticles for sensor applications, Nanotechnology 17 (6) (2006) 1668–1673.
[22] Y. Abboud, T. Saffaj, A. Chagraoui, A.E. Bouari, K. Brouzi, O. Tanane, B. Ihssane, Biosynthesis, characterization and antimicrobial activity of copper oxide nanoparticles (CONPs) produced using brown alga extract (Bifurcaria bifurcata), Appl. Nanosci. 4 (5) (2013) 571–576.
[23] A. Nasirian, Synthesis and characterization of Cu nanoparticles and studying of their catalytic properties, Int. J. Nano. Dimens 2 (2012) 159–164.
[24] K. Saranyaadevi, V. Subha, R.S.E. Ravindran, S. Renganathan, Synthesis and characterization of copper nanoparticle using Capparis zeylanica leaf extract, Int. J. Chem. Tech. Res. 6 (10) (2014) 4533–4541.
[25] V.D. Kulkarni, P.S. Kulkarni, Green synthesis of copper nanoparticles using Ocimum sanctum leaf extract, Int. J. Chem. Studies 1 (3) (2013) 1–4.
[26] B.H. Patel, M.Z. Channiwala, S.B. Chaudhari, A.A. Mandot, Biosynthesis of copper nanoparticles; its characterization and efficacy against human pathogenic bacterium, Journal of Envionrmental Chemical Engineering (JECE) 4 (2016) 2163–2169.
[27] I. Subhankari, P.L. Nayak, Synthesis of copper nanoparticles using Syzygium aromaticum (cloves) aqueous extract by using Green chemistry, World J. Nano Sci. Technol 2 (1) (2013) 14–17.
[28] J.K.V.M. Angrasan, R. Subbaiya, Biosynthesis of copper nanoparticles by Vitis vinifera leaf aqueous extract and its antibacterial activity, Int. J. Curr. Microbiol. App. Sci. 3 (9) (2014) 768–774.
[29] S.S. Shankar, A. Rai, A. Ahmad, M. Sastry, Rapid synthesis of Au, Ag, and bimetallic Au core–Ag shell nanoparticles using Neem (Azadirachta indica) leaf broth, J. Colloid Interface Sci. 275 (2) (2004) 496–502.
[30] K. Mukunthan, S. Balaji, Cashew apple juice (Anacardium occidentale L.) speeds up the synthesis of silver nanoparticles, Int. J. Green Nanotechnol. 4 (2) (2012) 71–79.
[31] H.S. Garg, D.S. Bhakuni, An isoprenylated flavanone from leaves of Azadirachta Indica, Phytochemistry 23 (9) (1984) 2115–2118.
[32] M. Dubey, S. Bhadauria, B. Kushwah, Green synthesis of nanosilver particles from extract of Eucalyptus hybrida (safeda) leaf, Dig. J. Nanomater Biostruct 4 (2009) 537–543.
[33] J.L. Huang, Q.B. Li, D.H. Sun, Y.H. Lu, Y.B. Su, X. Yang, H. Wang, Y. Wang, W. Shao, N. He, J. Hong, C. Chen, Biosynthesis of silver and gold nanoparticles by novel sundried Cinnamomum camphora leaf, Nanotechnology 18 (2007), 105104–1-105104-11.
[34] S. Jain, A. Jain, V. Devra, Experimental investigation on the synthesis of copper nanoparticles by chemical reduction method, Int. J. Sci. Eng. Res. 5 (11) (2014) 973–978.
[35] M. Valodkar, R.N. Jadeja, M.C. Thounaojam, R.V. Devkar, S. Thakore, Biocompatible synthesis of peptide capped copper nanoparticles and their biological effect on tumor cells, Mater. Chem. Phys. 128 (1–2) (2011) 83–89.
[36] W. Yu, H. Xie, L. Chen, Y. Li, C. Zhang, Synthesis and characterization of monodispersed copper colloids in polar solvents, Nanoscale Res. Lett. 4 (5) (2009) 465–470.
[37] J.Y. Song, B.S. Kim, Rapid biological synthesis of silver nanoparticles using plant leaf extracts, Bioprocess. Biosyst. Eng 32 (2009) 79–84.
[38] H.–J. Lee, G. Lee, N.R. Jang, J.H. Yun, J.Y. Song, B.S. Kim, Biological synthesis of copper nanoparticles using plant extract, NSTI- Nanotech 1 (2011) 371–374.
[39] M. Vanaja, K. Paulkumar, M. Baburaja, S. Rajeshkumar, G. Gnanajobitha, C. Malarkodi, M. Sivakavinesan, G. Annadurai, Degradation of methylene blue using biologically synthesized silver nanoparticle, Bioinorg. Chem. Appl. 2014 (2014) 742346–742354.
[40] T.M.D. Dang, T.T.T. Le, E.F. ourg-Blanc, M.C. Dang, The influence of solvents and surfactants on the preparation of copper nanoparticles by a chemical reduction method, Adv. Nat. Sci. Nanosci. Nanotechnol. 2 (2011) 025004–025010.
[41] A.P. Reverberi, M. Salerno, S. Lauciello, B. Fabiano, Synthesis of copper nanoparticles in ethylene glycol by chemical reduction with vanadium (+2) salts, Materials 9 (2016) 809–819.
[42] P. Velmurugan, K. Anbalagan, M. Manosathyadevan, K.-J. Lee, M. Cho, S.-M. Lee, J.-H. Park, S.-G. Oh, K.-S. Bang, B.-T. Oh, Green synthesis of silver and gold nanoparticles using Zingiber officinale root extract and antibacterial activity of silver nanoparticles against food pathogens, Bioprocess. Biosyst. Eng 37 (2014) 1935–1943.
[43] S. Raja, V. Ramesh, V. Thivaharan, Antibacterial and anticoagulant activity of silver nanoparticles synthesised from a novel source–pods of Peltophorum pterocarpum, J. Ind. Eng. Chem. 29 (2015) 257–264.
[44] T. Varadavenkatesan, R. Selvaraj, R. Vinayagam, Phyto-synthesis of silver nanoparticles fromMussaenda erythrophylla leaf extract and their application in catalytic degradation of methyl orange dye, J. Mol. Liq. 221 (2016) 1063–1070.